RENEWAL OF INTESTINAL STEM CELLS LACKING INTRINSIC SURVIVAL PROGRAM REQUIRES MICROBIOME AND IMMUNE SIGNALING INPUT

by

XIAO ZHANG

A Dissertation submitted to the

Graduate School-Newark

Rutgers, The State University of New Jersey

In partial fulfillment of the requirements

For the degree of

Doctor of Philosophy

Graduate Program in Biological Sciences

Written under the direction of

Nan Gao

And approved by

_____

_____

_____

_____

Newark, New Jersey

May 2020

ABSTRACT OF THE DISSERTATION

RENEWAL OF INTESTINAL STEM CELLS LACKING INTRINSIC SURVIVAL PROGRAM REQUIRES MICROBIOME AND IMMUNE SIGNALING INPUT

By XIAO ZHANG

Dissertation Director:

Nan Gao, Ph.D.

Being one important part of the digestive system, the intestine is responsible for nutrient uptake and for establishing a critical barrier against luminal insults from harsh chemicals or pathogens. Both functions are vital for the survival of the host. Strictly defined architecture of intestinal epithelial cells and the gradient of signaling cues along the villus-crypt axis ensure the maintenance of adult intestinal stem cells, as well as proper regeneration and differentiation of all intestinal epithelial cell types. The Rho family small GTPase Cdc42 controls the proper division of intestinal stem cells and affects subsequent fate-determination of the progenitor cells. How the intestinal epithelium maintains homeostasis and regenerative capacity during constant exposure to genotoxic and pathogenic insults is unclear. We found that *ex vivo* survival and clonogenicity of intestinal stem cells (ISCs)

strictly required Cdc42-mediated response, and Cdc42-deficient enteroids underwent rapid apoptosis. Mechanistically, Cdc42 engaged EGFR and enabled MAPK signaling. Accordingly, mice engineered to have boosted Cdc42-MAPK signaling in ISCs showed enhanced regeneration and were protected from epithelial injury. However, mice with *Cdc42*-deficient epithelium were viable and maintained functional homeostasis. An *ex vivo* screen uncovered that a number of inflammatory cytokines restored growth of *Cdc42*-deficient enteroids. Indeed, intestinal regeneration in mice lacking epithelial Cdc42 was compromised when cytokine-signaling or microbiota sensing was abolished. Antibiotic treatment, IL-22 deficiency, or Stat3 blockage compromised epithelial survival and injury-induced regeneration in mice lacking epithelial Cdc42. Data from this thesis shed lights on how ISC-intrinsic survival programs collaborate with signals from immune and microbiome compartments to provide non-redundant layers of protection for epithelial integrity. We conclude that signaling inputs from microbiome and lamina propria lymphocytes facilitate survival of ISCs with defective survival program. These results suggest that activation of specific epithelial extrinsic signals may benefit intestinal mucosal regeneration in hosts with diminished survival program such as during severe genotoxic or pathogenic injuries.

ACKNOWLEDGEMENTS

I would like to express my greatest gratitude to Dr. Nan Gao, my thesis advisor, who has been giving me tremendous help during my PhD. He is a brilliant leader and researcher who is doing cutting edge study in the biology field and also a role model of mine when I pursue the research career. He advised me with both detailed instructions and farseeing guidance, leading to production of multiple papers being published. He also always encourages me to become an independent researcher by supporting me to attend conferences and instruct me on how to write grant proposals. I would like to thank him for supporting me when I had a hard time with family issues, for taking care of the difficulty I encountered in my experiments, and for doing everything he could to give me the training I needed to achieve my PhD degree.

My sincere acknowledgment also goes to my committee members: I want to thank Dr. Edward M. Bonder, for advising me all along my PhD study, easing all the administrative hassles, and supporting me with sophisticated and honest suggestions without which I wouldn't be able to land on my scientific career. I would also like to thank Dr. Wilma Friedman at whose lab I did my first laboratory rotation. Helps from Dr. Friedman and people in her lab including Juan and Laura made sure I started my first semester without any problems. And I would like to thank Dr. Haesun Kim, whose lecture is my favorite among all that I have ever had. Dr. Kim has been my committee member since I had my qualifying exam. I am very grateful for what she had taught me and for being approachable and patient with me. Also, I appreciate so much for the generous support that Dr. Ronaldo P. Ferraris has

ever given to me. Thank you for the collaboration and sharing samples and materials I needed for the projects.

I thank all former and present members in Gao Lab, Ryo, Soumya, Richard, Connie, Juan, Sayantani, Iyshwarya, Sheila, Ivor, Yue and Rajbir, for their constant support and all their helpful recommendations during laboratory meetings. I am so grateful that I am able to work with them during these years. Thanks to all the colleagues at Life Science Center for your understanding and cooperation. I thank all the collaborators of my projects.

I thank the Facility of Genome Editing of Rutgers Cancer Institute of New Jersey (P30CA072720) for developing Cdc42 $V2^{Tg}$ mice. This work was made possible by support from the Graduate School of Rutgers Newark, NIH (R21CA178599, R01DK102934, R01AT010243, R01DK119198), ACS Scholar Award (RSG-15-060-01-TBE), NSF/BIO/IDBR (1353890), and a Rutgers IMRT award to N.G.;

Lastly, I would like to thank my family for their unconditional love.

TABLE OF CONTENTS

LIST OF FIGURES

CHAPTER 1

INTRODUCTION

Information included in this chapter was partially taken from and had been published in

Zhang et al., Small GTPases. 2016 Apr-Jun; 7(2): 59–64.

1.1 The structure and composition of intestinal epithelium

The mammalian intestinal mucosa is composed of the epithelium, luminal microbiota, and underlying lamina propria that consists of resident immune cells and a variety of mesenchymal cells. The epithelial cells make direct contact with nutrients and microbiota and are responsible for nutrient uptake and for establishing a critical barrier against luminal insults from harsh chemicals or pathogens. Both functions are vital for the survival of the host (Okumura and Takeda, 2017).

Architecture of the intestine epithelium

The intestinal tract is covered by a single sheet of epithelial cells that is folded into millions of finger-like protrusions, known as the villi, facing towards the lumen. At the root of each villus, there is an invaginated crypt compartment embedded and surrounded by the lamina propria cells. The villus epithelial cells are composed of mature cell types with the majority being enterocytes, cells that are responsible for nutrient absorption. Additional villus epithelial cell types include goblet cells, enteroendocrine cells, and tuft cells. All these mature villus epithelial cells are progenies of transient amplifying (TA) cells that migrate upwards out from crypt and move upwards to villus where they undergo several rounds of division before terminally differentiating and moving into the villus. These TA cells are direct descendants of the crypt based columnar (CBC) stem cells. In contrast to villus-localized mature epithelial cells, Paneth cells are uniquely situated at the base of the crypts, where they immediately juxtaposed to intestinal stem cells (ISCs).

Intestinal homeostasis

The intestine epithelium is the most rapidly renewed tissue in the body of adult mammals. The entire epithelial sheet is replaced every 3-5 days. There is a constant loss of mature epithelial cells at the villus tip. This massive cell loss is efficiently balanced by daily cell regeneration from the crypt-localized ISCs. At steady state, such robust capacity of regeneration of intestinal epithelia ensures an intact barrier function that separates luminal microbiota and host tissue (Peterson and Artis, 2014). This feature also allows the intestinal epithelia to rapidly respond to injuries (e.g., mechanical, pathogenic, chemical, etc.), by launching reparative activities to the damaged tissues. Under certain pathological conditions, when cell regeneration cannot compensate cell loss, the intestinal barrier function is impaired leading to bacterial endotoxin leaking across the epithelium into blood stream causing systemic inflammation or sepsis (Chelakkot et al., 2018). Alternatively, when excessive stem cell proliferation fails to be balanced by proper differentiation and cell death, intestinal tumors arise. Thus, it became increasingly appreciated that a proper functioning of intestinal epithelial cells (IECs) relies on a signaling network that sustains a balanced cell production and differentiation (van der Heijden and Vermeulen, 2019). The intra-cellular machinery and inter-cellular signaling pathways that maintain this crucial balance remains to be an active field of investigation and also the central theme of this thesis.

Enterocytes

Enterocytes are specialized epithelial cells with millions of microvilli densely packed at the apical side of the plasma membrane. Enterocytes have three major functions corresponding to their cellular structural features: nutrient absorption, barrier function and antigen uptake (Snoeck et al., 2005). The so-called brush border structure in enterocyte is built with actin bundles at the core of each microvillus, whose assembly is assisted by actin-interacting proteins Villin, Espin and Fimbrin (Crawley et al., 2014). The stabilization of apical membrane with microvilli is achieved by unconventional myosins (e.g., myosin1, 6) and ERM (ezrin, radixin, moesin) family proteins, which anchor the plasma membrane to the underlying actin cytoskeleton (Crawley et al., 2014). During the process of cytoskeletal assembly and membrane polarizations, small GTPases of the Rho subfamily are indispensable (Crawley et al., 2014). The purpose of having microvilli is to maximize the surface area where the enterocytes can be in contact with luminal contents.

Genetic abnormalities that impair the proper formation of microvilli have been associated with severe malabsorptive intestinal disorders (Muller et al., 2008; Wiegerinck et al., 2014a). One of these disorders, known as Microvillus Inclusion Disease (MVID), has received increasingly intense attentions in recent years due to the identifications of several disease-related mutations. MVIDs are rare yet serious congenital intestinal enteropathy characterized by a severe loss of apical microvilli, accumulation of intracellular vesicles and microvillus inclusion bodies, as well as a mis-localization of apical and basolateral proteins. Patients of MVIDs

completely lose the ability to absorb nutrients in the intestine (Cutz et al., 1989; Davidson et al., 1978). Two genetic mutations have so far been isolated from MVID patients: *MYO5B* (Erickson et al., 2008; Muller et al., 2008), encoding a motor protein MYOSIN 5B, and *STX3* (Wiegerinck et al., 2014a), encoding an apical SNARE protein SYNTAXIN 3. However, long before the isolation of MYO5B mutations, the potential link of a Rab small GTPase, Rab8a, to MVID pathogenesis had been suspected owing to the observation that Rab8a homozygous knockout mice developed typical microvillus inclusion bodies in the cytoplasm of affected enterocytes, although no *RAB8A* mutation has been isolated from MVID patients to date (Sato et al., 2007). This first MVID mouse model developed by Harada group illustrated clear defects of apical cargo transport in Rab8a-deficient enterocytes (Sato et al., 2007). Prior to identification of *MYO5B* mutation, it had also been demonstrated that MYO5B interacts with both RAB8A and RAB11A to facilitate the apical transport of cargos along cytoskeleton tracks to plasma membrane (Knowles et al., 2014; Roland et al., 2011). These studies collectively suggest that essential apical transport cellular machinery consisting RAB8A, RAB11A and MYO5B may contribute to the proper microvillus morphogenesis, whereas improper functioning of this machinery may cause defective delivery of apical cargos, such as STX3, leading to abnormal microvillus formation and function. This model has received further support from additional mouse genetic studies, in which intestinal epithelial cell specific ablation of either Myosin 5b (Carton-Garcia et al., 2015; Schneeberger et al., 2015) or Rab11a (Knowles et al., 2015 ; Sobajima et al., 2014) leads to defective Syntaxin 3 trafficking and MVID-

like phenotypes in mutant enterocytes. A recent study demonstrated Myo5B and Stx3 coordinates with Rab8 and Rab11 during apical cargo exocytosis by using CRISPR editing to introduce a Myo5B patient mutation in a human epithelial cell line (Vogel et al., 2015).

Paneth cells

Paneth cells are specialized secretory epithelial cells that first migrate into the transit amplifying zone and the during differentiation migrate back into crypts. This unique crypt-positioning appeared to be controlled by signals involving Ephrin/EphB at the cell membrane. Being a fully mature epithelial cell type, Paneth cells produce a number of growth factors, antimicrobial peptides, cytokines, and chemokines. Paneth cells execute important functionalities to not only support intestinal stem cells (ISC), but defend against pathogens and potentially regulate the mucosal immune responses (Clevers and Bevins, 2013). For example, Paneth cells produce key stem cell niche factors including EGF, Wnt3, and the Notch ligand. Delta-like 4 (Dll4) (Sato et al., 2011b). Among the many antimicrobial proteins that are produced by Paneth cells, defensins are a family of bactericidal small peptides secreted into the lumen to regulate the microbiota community. Because of the crucial role of Paneth cells in regulating gut microbiota and intestinal mucosal immune responses, misfunctioning of these processes were considered to be related to the pathogenesis of Crohn's disease, a devastating form of inflammatory bowel disease (IBD) (Bevins and Salzman, 2011). In addition, a C-type lysozyme is another important anti-microbial product of Paneth cells.

Abnormal secretion of Paneth cell specific lysozyme, the product of Lyz1 gene in mice, was linked to a changed gut microbiota landscape and an altered susceptibility to experimental colitis in mice (Yu et al., 2017).

Tuft cells

Tuft cells are also known as brush cells. They are found mostly in the respiratory and digestive systems (Sbarbati and Osculati, 2005). Tuft cells constitute 0.4% of the entire intestinal epithelial cell population, and can be morphologically distinguished by their long and blunt microvilli with prominent actin rootlets and tubulovesicular system in the supranuclear cytoplasm (Sato, 2007). Tuft cells have high expression levels of cytokeratin18, tubulin, and ankyrin indicating a possible mechanical sensing role by these cells (Hofer and Drenckhahn, 1996). Doublecortin-like Kinase 1 (Dclk1) is a specific marker for Tuft cells (Gerbe et al., 2009; Leppanen et al., 2016), and was proposed to coordinate protein trafficking along microtubules (Gerbe et al., 2011; Lipka et al., 2016). Studies focusing on Tuft cell fate commitment reached controversial opinions regarding whether or not Tuft cell differentiation required Atonal Homolog 1 (Atoh1) (Bjerknes et al., 2012; Gerbe et al., 2011), a transcription factor that is responsible for the fate commitment between absorptive and secretory lineages in the intestinal epithelium. In one study, upon induced Atoh1 deletion by gavages of tamoxifen, Tuft cells remained (Bjerknes et al., 2012). In another study, deletion of Atoh1 in intestinal epithelia cells (IECs) via intraperitoneal injection of tamoxifen impaired the differentiation of all 3 major secretory cell types including Tuft cells (Shroyer et al., 2007).

Delta/Notch signaling promotes differentiation of the absorptive lineage by suppressing Atoh1 in undifferentiated precursor cells (VanDussen et al., 2012). However, whether Cdc42 modulates Atoh1 expression or Delta/Notch signaling to affect secretory cell differentiation, especially Tuft cell differentiation is unknown. Tuft cells are also involved in intestinal carcinogenesis (Carstens et al., 1976), and were detected in the human colorectal cancer cell line LIM1863 (Barkla et al., 1988).

Goblet cells

Goblet cells are another secretory cell type primarily residing in villus epithelium. They are also considered as an essential part of epithelial defense mechanism against luminal pathogens. When Notch signaling was blocked by γ-secretase inhibitors, the Notch cytoplasmic component no longer entered the nucleus, resulting in an enhanced secretory lineage differentiation at the expense of enterocyte production (Clevers, 2013a). Mature goblet cells are the primary producers of intestinal mucus, which is made from the MUC2, FCGBP, CLCA1, ZG16, and AGR2, etc (Birchenough et al., 2015). Goblet cell derived mucin serve as the frontline of anti-pathogen firewall that diminishes any unwanted microbial invasion towards the epithelium (Birchenough et al., 2015). Under certain microbial insults, goblet cells respond by undergoing expansion as exemplified in parasitic helminth infections. In this scenario, IL-4Rα and IL13Rα1 receptors on goblet cell surface sense and transmit type 2 cytokine signals (e.g., IL-4 and IL-13) in response to infection, leading to massive goblet cell propagation (Marillier et al.,

2008) (Oeser et al., 2015) (Steenwinckel et al., 2009). Another example of how goblet cells may coordinate with mucosal immune signaling was the demonstration that Th17 cells produced IL-22 to regulate goblet cell differentiation and mucin production by synergizing the hyperplasia effect induced by type 2 cytokines (Turner et al., 2013). These studies placed the goblet cell population as participating in integration/interpretation of multiple important immune cell derived signaling cues.

Enteroendocrine cells

Being only 1% of intestinal epithelium, enteroendocrine cells are differentiated from the common secretory precursors when a transient expression of Neurogenin3 (Neurog3) is switched on (Jenny et al., 2002), along with micro-RNA-375 (Knudsen et al., 2015), followed by a variety of transcription factors, including Neurogenic differentiation 1 (Neurod1), Paired box (Pax) 4/6, Insulin gene enhancer protein (Isl1), pancreatic and duodenal homeobox 1 (Pdx1), Nkx6-1, and Nkx2-2. Enteroendocrine cells further mature into distinct subgroups (Worthington et al., 2018), depending on their expression of distinct transcription factors such as Pdx1, caudal type homeobox 2 (Cdx-2), Gata4, Gata-5, Gata6, Hepatocyte nuclear factor-1α (Hnf-1α), Hnf-1β, or CCAAT-displacement protein (Cdp). Although enteroendocrine cells represent a tiny fraction of epithelium, these cells have indispensable functions in hormone-producing, metabolite-sensing, and bowel movement (Gribble and Reimann, 2019). In addition, enteroendocrine cells are also considered a part of the entirety of mucosal immune system as they not only

produce cytokines or cytokine-like peptides but communicate with immune cells about the gut microbial status. Using toll-like receptors (TLRs), enteroendocrine cells were shown to sense microbial stimuli, resulting in activated NF-κβ and MAPK signaling, as well as increased Ca2+ flux that promoted the release of TNFα, TGFβ, macrophage inflammatory protein-2, CXCL1/3, IL32, etc (Bogunovic et al., 2007; Palazzo et al., 2007) (Selleri et al., 2008).

1.2 Biology of ISCs

The fast-cycling ISCs reside in the crypt bottom, self-renew on a daily basis, and give rise to all mature epithelial cell types described above. The ISC "niche" refers to the crypt cells and the stromal cells that are surrounding the ISCs. In the crypt, Paneth cells intermingle with ISCs, and were proposed to be crucial for ISC renewal through chemical and mechanical support to the ISCs (van der Flier and Clevers, 2009). Canonical Wnt and EGF signaling are two major growth pathways for intestinal stem cell (ISC) survival and renewal (Basak et al., 2017; Gregorieff and Clevers, 2005; Krausova and Korinek, 2014; Schepers and Clevers, 2012), while BMP pathway drives formation of differentiated villus epithelia (He et al., 2004; Qi et al., 2017).

Canonical Wnt signaling and ISC homeostasis

Canonical Wnt signaling is one of the master regulatory pathways for embryo development and is engaged in the maintenance of adult intestinal homeostasis (Clevers, 2006). In the intestine, Wnt ligands are produced and secreted mostly by

Paneth cells and subepithelial mesenchymal cells, providing a gradient of Wnt ligand along the villus-crypt axis. High Wnt abundance at crypt maintains a high cellular proliferation activity while reduced Wnt abundance at the villus-crypt boundary allows terminal differentiation to occur. Wnt signaling promotes the expression of a network of target genes through stabilizing beta-catenin from the APC/Axin/CK1/GSK3 destructing machinery and transcriptional activation via TCF factors (Schuijers et al., 2014). Knockout of mouse TCF4 resulted in a deformation of crypt structure as well as a loss of stem cells in neonatal mice (van Es et al., 2012) (Korinek et al., 1998). On the other hand, transgenic expression of Dkk-1, an endogenous inhibitor of Wnt signaling in adult mice led to complete disruption of crypts (Pinto et al., 2003).

R-Spondins (RSPOs) potentiate Wnt signaling (Kim et al., 2005) by binding to leucine-rich repeat containing, G protein-coupled receptors 4, 5 and 6 (LGR4/5/6), leading to removal of two cell surface E3 ubiquitin ligases RNF43 and ZNRF3, which target Wnt receptors for degradation (Nagano, 2019). The synergistic effect of Wnt and R-Spondin on beta-catenin activation and ISC homeostasis were best illustrated by the *ex vivo* model of intestinal organoid culture. With Wnt proteins only, the transcription activity of beta-catenin was increased 4-fold compared to untreated organoids; adding both Wnt and R-Spondin increased this activation by 400 times. However, binding of R-Spondin to its membrane receptor Lgr5 (Peng et al., 2013) was also proposed to potentiate TGF-β signaling (Zhou et al., 2017). Given the prompt and strong pro-survival and pro-proliferation effects of Wnt signaling, aberrant regulation of this pathway as exemplified by APC loss-of-

function represented the major cause of colorectal cancers (Clevers, 2006).

Paneth cells are component of ISC niche compartment

Paneth cells produce Wnt3, EGF and TGFα, and were proposed to be an indispensable niche component for stem cell renewal (Sato et al., 2011b). The fate of intestinal stem cells is determined at least in part by their relative localization to Paneth cells. This was illustrated in a model of natural competition among stem cells that can either remain as stem cell or adopt a TA cell fate thereby contributing to differentiated lineages (Snippert et al., 2010). Thus, various ISC niche growth factors including EGF, TGFα, Wnt3, Notch ligands Dll1 and Dll4 (Paneth cell products), and HGF (from mesenchymal cells) coordinate to regulate ISC homeostasis (Barker et al., 2010). It becomes increasingly appreciated that a synthetic interplay of these pathways ensure a homeostasis, where crypt-based ISCs self-renew and produce various lineages of progenitors that, upon transit amplification, differentiate into mature IECs to offset programmed cell death (Clevers, 2013b; Gehart and Clevers, 2019).

Markers of ISCs

Widely considered as the maker of rapid cycling stem cells in multiple organs (Barker et al., 2010), Leucine-rich repeat-containing G-protein coupled receptor 5 (Lgr5) is the well-studied ISC marker (Barker and Clevers, 2007). Lgr5 was also identified as one of the target genes of canonical Wnt signaling (Van der Flier et al., 2007). Lgr5 is a co-receptor of R-Spondin that enhances canonical Wnt

signaling (Schuijers and Clevers, 2012). In addition to serving as ISC marker in normal intestinal epithelium, Lgr5 also marks the colorectal cancer stem cells (Hirsch et al., 2014)}. When mutant APC was introduced to intestinal Lgr5+ cells, adenoma formed in a short period of time in these mice, arguing that Lgr5+ cells acted as cell-of-origin of colon cancer (Barker et al., 2009). Other markers for active proliferating stem cells include Olfm4 (van der Flier et al., 2009), Ascl2 (Schuijers et al., 2015), ALCAM (Levin et al., 2010) MSI1 (O'Brien et al., 2007) etc. The so-called “quiescent stem cells” or ”label retention stem cells” have been proposed to be reserve stem cells when Lgr5+ stem cells are lost, and these cells are marked by Bmi1 (Yan et al., 2012), Hopx (Takeda et al., 2011), Tert1 (Suh et al., 2017), DCLK1 (May et al., 2008), and Lrig1 (Powell et al., 2012).

Enteroid model and clonogenicity of ISC

The intestinal enteroid culture model developed by Sato et al. (2009a) has greatly contributed to the ISC research field. The original report showed that a single Lgr5 stem cell isolated from mouse intestines could be cultured in a specially formulated medium and develop into a mini-gut structure containing all known intestinal epithelial cell types. Such culture could be indefinitely maintained and passaged for numerous generations with few or no mutations acquired in the cells. Specifically, in this culture system, mouse small intestinal crypts were isolated and embedded in Matrigel as a 3D organotypic culture in DMEM/F12 media that was supplemented by EGF, Noggin and R-Spondin (also known as ENR) (Sato et al., 2009a). Through this culture system, indispensability of Wnt, EGF, and BMP

pathways for ISC function was unequivocally demonstrated: the indefinite ISC renewal and proliferation were sustained by Wnt and EGF agonists, while the differentiation was suppressed by BMP pathway inhibitor, Noggin (Barker et al., 2010; Radtke and Clevers, 2005; Sato et al., 2009b).

Similar organoid methods were then modified and developed to culture human colon, adenoma, adenocarcinoma, and Barrett's epithelium, etc (Sato et al., 2011a). The absolute requirement of "ENR" was later tested by replacement of Wnt pathway activators and BMP pathway inhibitors, further supporting the necessity of previously demonstrated ISC niche signaling (Li et al., 2018). To date, intestinal organoid culture has been modified and utilized in settings to meet the requirement and demand of investigating intricate ISC regulatory mechanisms across various disciplines including dietary metabolites, gut microbiota, immune and stromal cell signaling, in the context of both physiology and disease (Nigro et al., 2019) (Min et al., 2020). From a translational perspective, since the organoid culture method now allowed a rapid and efficient expansion of primary tissues, this technique opened a door for high throughput drug screening and precision medicine for the search of cure of certain diseases such as IBD and cancer (Liebau et al., 2019; Schulte et al., 2019).

Injury-induced ISC regeneration

Although the intestinal epithelium constantly encounters environmental challenges, severe insultations caused by pathogens, chemicals, or irradiation may lead to drastic epithelial damages. For example, ionizing radiation, which some cancer

patients have to go through, specifically targets proliferating cells for rapid apoptosis. One to two days after radiation, there is a drastic decline in numbers of Lgr5+ ISCs and TA cells. This quantitative loss of ISCs was postulated to activate the so-called “quiescent” ISCs, in mechanism still poorly understood, to replace the lost ISCs and contribute to epithelial repopulation after injury (Kim et al., 2017b). Work in the recent decade documented the remarkable plasticity of intestinal epithelia in intact animals. A body of literature demonstrated the injury-induced stemness acquisition by not only quiescent ISCs, but by mature cell types in response to ISC loss (Basak et al., 2017; Gerbe et al., 2009; May et al., 2014; Schmitt et al., 2018; Sei et al., 2018; Tetteh et al., 2016; Westphalen et al., 2014; Yan et al., 2017; Yi et al., 2018; Yu et al., 2018) (Yu, 2013). The interactive complexity of intrinsic and non-intrinsic epithelial signaling that confers remarkable tissue plasticity remains poorly defined and is an important area of exploration by this thesis work through biomedical and genetic approaches.

1.3 Cdc42 and intestinal homeostasis

How small GTPases works?

Rho GTPases belong to the Ras superfamily, with the primary family members being Cdc42, Rho and Rac. As usually occurring to all small GTPases, a guanine nucleotide exchange factor (GEF) binds to the GDP-bound Rho GTPases through Dbl homology-pleckstrin homology (DH-PH) domain or Dock homology region-1 (DHR1) domain, stimulating the replacement of GDP by GTP. GTPase-activating proteins (GAPs) binds to GTP-bond GTPases and activates GTPase activity that

hydrolyzes GTP into GDP, resulting in an “inactive” GTPase. Sometimes, GEFs may also bind to the GTP form of GTPases to promote the positive feedback signal (Sinha and Yang, 2008). Inactive forms of GEFs can be due to the autoinhibitory binding between their PH and DH domains, which blocks binding between GEF and GTPases. In order to activate a GEF, the following conditions need to be met: the GEF is in close proximity with a GTPase; the GEF is released from its auto-inhibitory conformation; and there is an induction of allosteric changes in the catalytic domain (Bos et al., 2007). Rho GTPases usually exert their functions through downstream effector proteins. The effectors of Rho-GTPases are proteins that typically contain a Cdc42-Rac interactive binding (CRIB), p21-binding domain (PBD), or GTPase-binding domain (GBD) domains.

Cdc42 is a small GTPase of the Rho subfamily

Cdc42, as a Rho subfamily small GTPase, is activated by extracellular growth factors, cytokines, as well as signals emitted from integrin, proteoglycans and G-protein coupled receptor (GPCR) ligands. The activity of Cdc42 is controlled by its GTP/GDP-binding states as well as by its anchorage at distinct intracellular membrane compartments (e.g., plasma membrane or golgi apparatus). In order to recruit its downstream effectors, Cdc42 needs to be localized to the plasma membrane, where Cdc42-specific GEFs or effectors accumulate in response to the upstream stimuli. Specific binding between GEFs and Cdc42 was dependent on agonist stimulations (Calvo et al., 2011). For example, the PH domain of Vav1 interacts with two lipid products of phosphatidylinositol 3-kinase (PI3K) to further

regulate Vav1. Phosphatidylinositol 4,5-biphosphosphate (PIP2) inhibits Vav1 activation while phosphatidylinositol facilitates activation, suggesting that the particular upstream stimulating cues are determinants for the specificity and perhaps amplitude of subsequent signaling pathways.

Cdc42 is involved in a wide variety of cellular functions such as polarity establishment, vesicular trafficking, cell cycle, and even transcriptional dynamics in the nucleus (Johnson and Pringle, 1990) (Hall, 2012). Using affinity chromatography and yeast two-hybrid system, studies had identified at least 23 proteins as potential Cdc42 effectors. A partial list includes p70-S6K; MLK2/3; MEKK1/4; PAK1/2/3/4; MRCKα/β; ACK1/2; PI3K; PLD; PLCbeta2; WASP, N-WASP; MSE55 and BORGs; IQGAP1/2; and CIP-4 etc. (Bishop and Hall, 2000). The functional categories of these effectors range from protein kinases, lipid kinases, hydrolases, phosphatases, actin-binding proteins, vesicle coating proteins, to adaptor proteins. However, with regard to Cdc42, the effectors have similar binding affinity to it, and they can be activated without bias if there is no specific direction from upstream signaling. Overexpression or hyperactivation of Rho-family small GTPase was a hallmark of multiple cancer types, including colorectal cancer (CRC), leukemia, breast cancer, prostate cancer, etc (Karlsson et al., 2009).

Splicing variants of Cdc42

Cdc42 has two alternative mRNA splicing variants. Variant 1, referred to as Cdc42-V1, is universally expressed, and Variant 2, or Cdc42-V2 had initially

reported to be brain enriched (Wirth et al., 2013). The major distinction between the two variants are the last ten amino acids at the C-terminus. Cdc42-V1 carries a single Cysteine at 188 that can be lipid-modified as prenylation, whereas Cdc42-V2 harbors two Cysteines at a.a. 188 and 199 that can be prenylated and palmitoylated, respectively (Wirth et al., 2013b; Yap et al., 2016) (Nishimura and Linder, 2013) (Mukai et al., 2015) (Kang et al., 2008) (Lee et al., 2018a). The differential and dynamic localizations of Cdc42 is believed to be controlled by lipidation status (palmitoylation and/or prenylation) of its C-terminal domain (Johnson et al., 2012; Wirth et al., 2013b). Palmitoylation was reported to prevent Cdc42 from binding with RhoGDI, a Cdc42 inhibitor that sequesters Cdc42 from membrane while stabilizing the cytoplasm-localized Cdc42 (Nomanbhoy et al., 1999) (Nishimura and Linder, 2013). Whether palmitoylated Cdc42 has a strong signaling capacity and how it may influence stem cell behavior in vivo are currently unknown, due to a lack of a model dedicated to the variant of Cdc42-V2.

Cdc42 maintains intestinal epithelial homeostasis

Our laboratory has extensively documented the essential contribution of Cdc42 to intestinal homeostasis and the progression of incipient intestinal tumor cells. Using IEC-specific Cdc42 knockout (KO) mice, we and others had reported that mouse intestinal epithelium lacking Cdc42 developed a typical phenotype resembling the human MVID (Michaux et al., 2016; Sakamori et al., 2012b; Zhang and Gao, 2016). MVID is rare, yet devastating congenital enteropathy characterized by a severe loss of apical microvilli in enterocytes, accumulation of

intracellular vesicles, development of typical microvillus inclusion bodies, as well as mis-localization of apical and basolateral proteins (Ruemmele et al., 2006).

In addition to enterocyte, loss of Cdc42 also impacted the proper division of ISCs and localization of Paneth cells (Akcora et al., 2013; Melendez et al., 2013; Sakamori et al., 2012b; Zhang and Gao, 2016). When Cdc42 was specifically deleted from ISCs in $Cdc42^{fl/fl}$; $Lgr5^{EGFP\text{-}IRES\text{-}CreER}$ mice, Cdc42-deficient ISCs exhibited an impaired division and lineage-tracing into villus compartment, suggesting that Cdc42 is required for ISC homeostasis (Sakamori et al., 2012). Increased Cdc42 levels may participate in intestinal tissue repair in damaged mucosa induced by mesenteric ischemia/reperfusion in the small intestine and by dextran sulfate sodium in the colon. (Liu et al., 2017). In aggregate, these *in vitro* and *in vivo* studies clearly demonstrated the impact of Cdc42 on epithelial cell barrier function (Schlegel et al., 2011), survival and proliferation (Sakamori et al., 2012; Sakamori et al., 2014), differentiation (Bruurs et al., 2017), and migration (Babbin et al., 2007; Lowe and Moseley, 2013; Melendez et al., 2013). In other tissue sites, Cdc42 was reported to control the balance of aging and rejuvenation of hematopoietic stem cells (Florian et al., 2012). However, it remained unclear how Cdc42 regulates pro-survival pathways at a mechanistic level that contribute to stem cell homeostasis and regeneration.

Cdc42 and Colorectal Cancer

Elevated Cdc42 levels had been reported in human CRCs (Al-Tassan et al., 2015; Cardoso et al., 2014), and most importantly was proposed as an indicator

for highly metastatic CRCs (Stengel and Zheng, 2011). GWAS and meta-analysis with 1000 Genomes found Cdc42 gene implicated in the inherited genetic susceptibility to CRC (Al-Tassan et al., 2015). In mice, genetic or pharmacological inhibition of Cdc42 suppressed the progression of intestinal tumorigenesis (Humphreys et al., 2014; Ke et al., 2014; Sakamori et al., 2014b).

Along the same line, downstream effectors of Cdc42, such as IQGAP and PAK, were found highly expressed in CRC tissues and correlated with higher malignancy (Carter et al., 2004) (Gong et al., 2009) (White et al., 2009). Ectopic overexpression of a constitutively active Cdc42(Q61L) in human colorectal cancer SW480 cells enhanced cell migration and invasion (Gao et al., 2013). Furthermore, fast cycling Cdc42 mutant F28L augmented the pro-survival signaling and transformation of NIH3T3 cells (Lin et al., 2003) . Taken together, literature robustly supported a pro-survival and -growth role of Cdc42 in the intestinal tissues, yet the specific pathways mediating these phenotypes are less well understood.

1.4 EGF-EGFR-MAPK pathway

Epidermal growth factor (EGF) is an indispensable ISC niche factor

EGF superfamily of growth factors include EGF, transforming growth factor-α (TGF-α), Amphiregulin (AR), Epiregulin (EPR), Epigen, Betacellulin (BTC), Neuregulins, etc. The EGF-EGFR-MAPK pathway is one of the most versatile pathways in regulating cellular functions. EGF family proteins bind to ErbB family receptors (ErbB2/HER-2, ErbB3/HER-3, and ErbB4/HER-4) of the Receptor Tyrosine Kinase superfamily. EGF ligands bind the extracellular domain of EGFR

causing a dimerization between the cell surface receptors. The dimerization triggers an autophosphorylation of tyrosine residues within the C-terminal of the receptor proteins (Hubbard, 2005). Cytoplasmic proteins containing Src Homology 2 (SH2) domains are then recruited to ErbB receptors leading to a signaling cascade involving Ras/Raf/mitogen-activated protein kinase pathway (MAPK), Phosphatidylinositol 3-kinase (PI3K)/AKT pathway, Phospholipase C pathway, Signal Transducers and Activators of Transcription (STAT) pathway, Src kinase pathways, etc (Yarden and Sliwkowski, 2001). In terms of activation of MAPK pathway, adaptor proteins Grb2, Shc and Sos bind to the phosphorylated tyrosine cites on ErbB (Batzer et al., 1994), resulting in the recruitment and activation of Ras that in turn activates Raf-1 and MAPK cascade (Hallberg et al., 1994). EGF is one of the indispensable components that define the “ENR” media used in enteroid culture, indicating the crucial role of the pathway in ISC survival and differentiation.

EGFR and ISC Homeostasis

ISC proliferation and regeneration support not only the development and maturation of the tissue, but also the life-long maintenance of this homeostasis after tissue injuries caused by pathogens, chemicals, and genotoxic damages. EGF signaling is one of the most conserved pathways that critically regulate the survival and regeneration of ISCs (Cordero et al., 2014; Liang et al., 2017; Suzuki et al., 2010; Yang et al., 2017). In *Drosophila*, EGFR signaling controls gut development and adult midgut progenitor proliferation (Buchon et al., 2010; Jiang and Edgar, 2009; Jiang et al., 2011; Jiang et al., 2016; Jin et al., 2015; Pyo et al.,

2018; Xu et al., 2011). These functions of EGFR signaling in gastrointestinal tract are conserved in other species (Mytych et al., 2018; Satora et al., 2018). In addition, proper localizations of EGFR within epithelial cells appeared to determine cell type specific functions (Ungewiss et al., 2018). Consistent with a largely pro-proliferation activity, elevated expression of phosphorylated EGFR positively correlated with mouse and human adenocarcinomas (Cordero et al., 2012; Wang et al., 2015a; Wang et al., 2015b). The total EGFR level was also linked to intestinal epithelial aging and development of CRC (Levi et al., 2009; Nautiyal et al., 2012; Patel et al., 2009). Moreover, the significance of EGFR signaling was particularly highlighted in studies of injury-induced epithelial regeneration and YAP-driven carcinogenesis (Gregorieff et al., 2015; Ren et al., 2010).

MAPK and intestinal epithelial homeostasis

In mice, the EGFR-MAPK pathway was required to keep Lgr5+ ISCs constitutively active in the intestine (Basak et al., 2017). This pathway was also shown to prevent cell shedding from intestinal epithelium (Miguel et al., 2017). Together, the EGF-EGFR-MAPK signaling plays a central role in the maintenance of ISC and the homeostasis of the intestinal epithelium. p38 mediates intestinal stem cell aging downstream of mTOR (He et al., 2020). In *Drosophila*, Jun N-terminal kinase (JNK) pathway promotes ISC proliferation in response to stress (Biteau and Jasper, 2011), while p38 mediates age related ISC homeostasis (Park et al., 2009). Shp2/ERK signaling controls goblet/paneth cell fate decisions by regulating Wnt/β-catenin signaling on the posttranslational level in the intestine

(Heuberger et al., 2014a). Interestingly, Wnt signaling suppresses the ERK pathway to maintain crypt base ISCs (Kabiri et al., 2018).

1.5 Components of intestinal lamina propria

Intestinal lamina propria refers to the underlying mucosal tissue layer that joins the epithelium with the outer wall of muscularis. In addition to mesenchymal cells, including myofibroblasts, fibroblasts, mural cells (pericytes) of the vasculature, bone marrow–derived stromal stem cells, smooth muscle of the muscularis mucosae, and smooth muscle surrounding the lymphatic lacteals (Powell et al., 2011). Lamina propria also contains a variety of professional and innate immune cells, such as innate lymphocytes (ILCs), macrophages, neutrophils, and dendritic cells, etc. The lamina propria also plays a role in supporting the villus structure and in holding numerous capillaries and lacteals towards the villus tip. Part of the lamina propria cell population may serve as the ISC niche by providing signaling factors such as Wnts (Gregorieff et al., 2005), BMPs (Zhang and Li, 2005), RSPO (Chen et al., 2017), and epimorphin (Shaker et al., 2010). Stromal cells (myofibroblasts, fibroblasts, and probably pericytes) were also shown to secrete chemokines under pathological or other types of insults (Pinchuk et al., 2007) (Vogel et al., 2004). Some myofibroblasts and fibroblasts express TLRs and may serve as antigen presenting cells to mediate responses of professional immune cells (Otte et al., 2003) (Walton et al., 2009). Innate lymphocytes express pattern recognition receptors (PRR) to recognize microbial-associated molecular patterns (MAMP), and to respond through secreting pro-inflammatory cytokines or

producing anti-pathogen molecules. Macrophages and dendritic cells may sense pathogens and present antigens to professional T cells. Lastly, activated T cells differentiate into specific subsets, including Th1, Th2, Th17, or Treg to regulate local and systemic inflammation.

Lamina propria derived cytokines and ISC homeostasis

The mucosal resident immune cells not only take actions on pathogens, but also closely modulate epithelial homeostasis and functionality through distinct cytokine signaling. The aforementioned expansions of Tuft and goblet cells upon parasitic infection, epithelial cells express surface receptors for specific cytokines that mediate the crosstalk between immune cells and IECs (Onyiah and Colgan, 2016). Cytokines such as IFNγ, TNFα, IL-1β, IL-10, IL-6, IL-22, IL-4, IL-13, IL-25 and IL-8 may regulate epithelial barrier function, leucocyte recruitment, antigen presentation, proinflammatory response, and metabolite transportation, etc (Andrews et al., 2018). Interestingly, recent studies suggested that ISCs may rely on distinct immune cell signals for renewal and differentiation. Some innate immune cells were shown to promote epithelial regeneration (Lindemans et al., 2015) (Saha et al., 2016). T cytotoxic cells eliminated Lgr5+ ISCs via MHC class I (Agudo et al., 2018), while following infection, ISCs interacted with T helper cells via MHCII machinery for their fate decision. Specifically, IL10 secreted from T-Reg cells promoted ISC renewal whereas IFNγ, IL-17, and IL-13 from T helper cells induced ISC differentiation into mature lineages (Biton et al., 2018b).

IL22-STAT3 and ISC biology

IL22 belongs to the IL10 superfamily of cytokine, is constantly produced in intestinal mucosa, and maintains epithelial barrier function and regeneration. IL22 was also shown to modulate inflammatory response during the pathogenesis of several gastrointestinal diseases, including graft-versus-host disease (GVHD) (Munneke et al., 2014), Crohn's disease (Schmechel et al., 2008), ulcerative colitis, the experimental colitis in mice (Sugimoto et al., 2008), as well as acute sepsis (Weber et al., 2007).

Various immune cell types express IL22, including T helper cells (Th1, Th17 and Th22) (Trifari et al., 2009), intraepithelial lymphocytes (IEL), in particular the γδ T cells (Mabuchi et al., 2011), ILCs (Eberl et al., 2015), and Natural Killer T (NKT) cells (Raifer et al., 2012). Of particular interest is ILCs that sense and respond to invading pathogen or pathogenic molecules leak across the epithelium. There are three groups of ILCs: 1) ILC1 cells express the transcription factor T-bet and are characterized by secretion of IFNγ; 2) ILC2 cells are GATA3+ and secrete IL-5 and IL-13; 3) ILC3 cells express RORγt, and secrete IL17 and IL22 (Geremia and Arancibia-Carcamo, 2017). As the primary producers of IL22, ILC3 cells can be activated by cytokines such as IL23 and IL1-beta.

IL-22 binds to the heterodimer of IL22RA1 and IL-10R2 on receiving cells (Kotenko et al., 2001), triggers activation of Janus kinase 1 (Jak1) and non-receptor protein tyrosine kinase 2 (Tyk2), leading to activation of STAT3. Although STAT1, STAT5 and MAPK pathways may also be activated by IL22 (Sekikawa et al., 2010) (Lejeune et al., 2002). IL22RA1 is absent from Immune cells including T

cells, B cells, monocytes, NK cells, etc. (Wolk et al., 2004). Instead in the epithelium, only primarily expressed in subgroups of ISCs and TA cells (Zwarycz et al., 2019), indicating IL22 signaling is considered essential to ISCs. Activities of STAT3 are usually induced by cytokines and growth factors to engage the target cells in damage repair, pathogen defense, and cell differentiation/proliferation (Schindler and Darnell, 1995) (Zhong et al., 1994). STAT3 activity was considered absolutely required for the ISC survival (Matthews et al., 2011), as deletion of Stat3 in mouse CBC cells or long-term label-retaining cells increased ISC apoptosis and rapid clearance from the crypts. During tissue regeneration after irradiation, STAT3 was also shown to be indispensable, yet STAT3 did not appear to take part in Wnt-driven intestinal tumorigenesis (Oshima et al., 2019). Rather, STAT3 may play a role in preventing tumor progression (Musteanu et al., 2010).

Role of Prolactin in the intestine

Prolactin is a polypeptide hormone found in anterior pituitary gland that promotes lactation. However, prolactin is also expressed in central nervous system, the immune system, the uterus, the mammary gland, skin and the sweat gland (Ben-Jonathan et al., 1996). The release of prolactin from the nervous system can be induced by various kind of stimuli, such as light, audition, olfaction, and stress. In human, prolactin transcript first is translated into a prohormone of 227 amino acids and matures into prolactin of 199 amino acids by cleaving the signal peptide. Prolactin belongs to the prolactin/growth hormone/placental lactogen family. Inhibition of circulating prolactin resulted in immune dysfunction and death (Nagy

and Berczi, 1991).

Prolactin (Prl) binds to the Prl receptor (Prlr) on the resoinding cells. Depending on the tissue specificity, prolactin may function in autocrine or paracrine manners, as growth factor, neurotransmitter, or immunomodulator (Bole-Feysot et al., 1998). Prlr belongs to class 1 cytokine receptor superfamily that includes receptors for a number of interleukins, granulocyte-colony stimulating factor (G-CSF), granulocyte macrophage-colony stimulating factor (GM-CSF), leukemia inhibitory factor (LIF), Oncostatin M (OM), erythropoietin (EPO), thrombopoietin (TPO), gp130, and leptin, etc (Wells and de Vos, 1996).

The Prl/Prlr signaling may be influenced by JAK-STAT , Ras/MAPK, PI3K, PLCγ or G-proteins (Radhakrishnan et al., 2012) to control reproduction, water/electrolyte balance, body growth, tissue development, endocrinology and metabolism, immune-responses, and neurological behaviors. PRL also induces immune response. Specifically, it may up-regulate immunity in target immune cells and organs by promoting lymphocyte proliferation, cytokine production, receptor expression, etc. (Freeman et al., 2000). Interestingly, with regards to IL22/STAT3 signaling, Prolactin showed a positive regulatory effect in the skin (Hau et al., 2014) but a negative effect in the bone (Ledesma-Colunga et al., 2017).

PRLR is expressed in cells along the entire gastrointestinal track in rat (Ouhtit et al., 1994). The fact that either lactating or injecting prolactin caused an increase in mucosa mass and intestinal length in rats suggested a potential role of prolactin in regulating IEC cell production (Bates et al., 1963; Muller and Dowling, 1981) (Elias and Dowling, 1976). Other studies suggested that prolactin promoted

calcium absorption and ion transport in the intestine with unclear mechanism (Charoenphandhu and Krishnamra, 2007) (Seale et al., 2014) (Ferlazzo et al., 2012). Nonetheless, how prolactin orchestrates intestinal mucosal homeostasis is unknown.

1.6 Intestinal microbiome in regulating epithelial stem cells

Bacterial molecular patterns regulate ISCs via pattern recognition receptors and MyD88

The intestinal microbiome contains a spectrum of micro-organisms including bacteria, archaea, fungi, protozoa, and viruses. A broad variety of host physiologies, e.g., tissue metabolism, epithelial homeostasis, immune response, disease pathogenesis, and systematic neuro-behavioral process etc., are directly or indirectly influenced by the gut microbial composition and activity (Shreiner et al., 2015). Usually Toll-like receptors (TLRs) and NOD (nucleotide-binding oligomerization domains)-like receptors (NLRs) of epithelium sense pathogens to induce immune responses (Bäumler and Sperandio, 2016; Fukata et al., 2009; Moossavi et al., 2013; Nigro et al., 2014). Activated TLRs recruit cytosolic Myd88 adaptor protein to convey signal for immune responses against infection (Blasius and Beutler, 2010). In the *Drosophila* midgut, response to both infectious and indigenous bacteria, enterocytes produce cytokines which activate the JAK-STAT pathway in stem cells thus promotes proliferation (Buchon et al., 2009) (Jiang et al., 2009). In mouse, TLR2/4 and Myd88 mediated microbiota sensing is essential for protecting intestinal homeostasis against DSS-induced injury (Rakoff-Nahoum

et al., 2004). A recent study showed that Paneth cells in germ-free and conventionally raised mice had different features that were not dependent on ISCs (Schoenborn et al., 2018). Intriguingly, non-pathogenic E. coli invoked host cell tumorigenic stemness (Sahu et al., 2017). Another in vitro study suggested commensals induced p-ERK signaling in host cells via generation of reactive oxygen species (ROS) (Wentworth et al., 2011; Wentworth et al., 2010). This interplay between the intestinal epithelium and microbiome (Jones, 2016; Wang and Huycke, 2015) suggested currently unknown mechanisms underlying microbiome mediated stem cell regulation and tissue homeostasis.

Bacterial metabolites regulate ISC homeostasis

Bacterial metabolites can be sensed by the mucosa and lead to regulation of both epithelium and immune cells. Muramyl-dipeptide (MDP), a peptidoglycan motif common to all bacteria, stimulates Nod2 and protects stem cell from oxidative stress-mediated cell death (Nigro et al., 2014). Other commonly found metabolites are the short-chain fatty acids (SCFAs), produced primarily in the colon through the fermentation of dietary fibers. SCFA butyrate suppressed colonic stem cell proliferation through regulating transcription factor Foxo3, while nicotinic acid have promotes proliferation of colonic stem cells (Kaiko et al., 2016).

CHAPTER 2

MATERIALS AND METHODS

Cell lines and cell culture

Culture of Hela, HEK293T and Caco2 cell lines have been described previously (Sakamori et al., 2012a; Sun et al., 2017). Briefly, cells were grown in a Dulbecco's Modification of Eagle's Medium (DMEM, Fisher, MT10013CM) containing 10 % fetal bovine serum (Sigma, F2442) and 1 % Penicillin/Streptomycin solution (Gibco,15070063), and were passaged with Trypsin-Ethylene-Diamine-Tetra-acetic-Acid (Trypsin-EDTA, Gibco™ Fisher 25-200-072) digestion every three days. 1×10^6 cells were then seeded into a 60 mm cell culture dish (Thermo Scientific Nunc, Catalog No. 12-565-97) containing 4 mL of fresh complete culture medium and were grown overnight to a complete confluent monolayer. All cell culture experiments have been repeated for at least 3 times unless specified otherwise in the figure legend.

Small molecular chemicals and growth factors

The sources and working concentrations of chemical and growth factors used in this study are: Dynasore (Sigma, D7693) at 80 μg/mL, and Ciliobrevin (Tocris 4529) at 100 μM, Filipin (Sigma, F4767) at 2 μg/mL, Chlorpromazine hydrochloride (Sigma, C8138) at 50 μg/mL, MβCD (Sigma, C4555) at 5 mM, EGF (Life Technologies, PMG8043) at 100 ng/mL, and recombinant mouse Wnt3a (R&D Systems) at 100 ng/mL, CHIR99021 (Sigma, SML1046-5MG) at 5 μM, Stattic (Santa Cruz, sc-202818) and WP1066 (Santa Cruz, sc-203282) IL1RN (Novus Biologicals, NBP2-35105) at 1 μg/ml, Prolactin (Novus Biologicals, NBP2-35120) at 500 ng/ml, CXCL1(Peprotech, 250-11) at 500 ng/ml, CXCL2 (Peprotech, 250-

15) at 500 ng/ml, IL33 (Peprotech, 210-33) at 100 ng/ml.

Plasmids

Plasmid from Addgene include: pcDNA6A-EGFR WT (#42665), pcDNA6A-EGFR ICD (645-1186) (#42667), pcDNA6A-EGFR ECD (1-644) (#42666), and CAG-lox-CAT-lox-unique Bam cloning site-bGH polyA (Clone 17) (#53959). Plasmid CAG-3×Flag-Cdc42 V2 for developing the transgenic mice was constructed by inserting the 3xFlag-V2 DNA into the CAG-lox-CAT-lox-unique Bam cloning site-bGH polyA (Clone 17) vector at the BamHI site. DNA for three copies of Flag sequence (DYKDDDDK) were inserted into the NotI/AgeI sites of pQCXIP vector (Clontech) as N-terminal tags, referred to as pQCXIP-3×Flag vectors. PQCXIP-3×Flag-Cdc42V1, PQCXIP-3×Flag-Cdc42V2, PQCXIP-3×Flag-Cdc42V2-K185R were constructed by inserting DNA of 3XFlag-Cdc42V1, 3×Flag-Cdc42V2, or 3×Flag-Cdc42V2-K185R into the NotI/EcoRI sites. Human V2-K185R mutant DNA was obtained from human colorectal cancer cell line LIM1215.

Cdc42 GLISA assay

Caco2 cells were serum starved overnight and then treated with EGF (50 ng/ml, #315-09 B, Peprotech), Wnt3a (100 ng/ml, #315-20, Peprotech), TGFα (50 ng/ml, #T7924, Sigma), Noggin (100 ng/ml, #250-38, Peprotech), and R-Spondin (1 μg/ml, #3474-RS-050, R&D Systems), respectively. CDC42 activity was determined before and after treatment by CDC42-specific GLISA assay (#BK127, Cytoskeleton) performed according to the manufacturer's instructions.

Lentivirus-mediated Cdc42 knockdown

To stably knockdown Cdc42 in Caco2 cells, human Cdc42-specific lentiviral transduction particles (#TRCN0000047628, Sigma-Aldrich) was added to cells at 1/5 multiplicity of infection with 8 μg/ml Polybrene. Cells infected by non-Target shRNA Control Transduction Particles (#SHC203V, Sigma-Aldrich) were used as control. Infected cells were selected by 10 μg/ml puromycin for 2 weeks. To induce MAPK activation, 100 ng/ml human EGF or 100 ng/ml mouse recombinant Wnt3a was added to serum starved (12 hrs) cells for indicated time before cells were harvested for pErk1/2 detection.

Atomic force microscope (AFM) analysis

A commercial atomic force microscope system (Dimension ICON, by Bruker-Nano Inc., Santa Barbara, CA) was used to measure all the cellular surface plasma membrane properties. As previously published (Zhang et al., 2018), a MLCT-C cantilever was used to measure the Young's modulus of cells, with a spring constant at 0.01 N/m calibrated via the thermal tune method (Bruker-Nano Inc.). To avoid the substrate effect and keep consistency of the measurement conditions, all of the measurements were performed at the top of the cell over the cell nucleus. The probe radius was calibrated by using a tip-radius calibration sample, and a silicon sample was used as the hard reference sample for all the indentation measurements. To minimize the cantilever drift due to the temperature fluctuation caused by the heating of the laser, the system was thermally equilibrated at 37°C

for 40 min before the measurements.

Transfection of HEK293 cells

HEK293 cells were prepared to reach 70–90% confluent at the time of transfection. 2 μg plasmid DNA was transfected using Lipofectamin 3000 (#L3000008, Invitrogen). Forty-eight hours after transfection, cell lysate was made for further experiments.

Proteomic analysis with mass spectrometry

HEK293T cells were transfected with empty pQCXIP-3×Flag vector, pQCXIP-3×Flag-Cdc42-V1 or pQCXIP-3×Flag-Cdc42-V2. Cell lysates were subjected to immunoprecipitation using a Flag antibody (FLAGIPT1, Sigma-Aldrich). Immuno-precipitates were resolved by NuPAGE™ 4-12% Bis-Tris Protein Gels (NP0335, Thermo Scientific), fixed for 1 hour with fixative containing 50% methanol and 10% acetic acid. After staining with Ruby Red, protein bands were cut for mass spectrometry analysis at Center for Advanced Proteomics Research of Rutgers University. Data was analyzed with Scaffold 4 software, DAVID Bioinformatics Resources 6.8, Excel 3D Scatter Plot v2.1, and esyN (Bean et al., 2014)

Phospho-kinase array analysis

Lysates from HEK293T cells transfected with empty vector, Cdc42-V1 or Cdc42-V2 were subjected to a kinase array analysis using the Proteome Profiler Human Phospho-Kinase Array (#ARY003B, R&D Systems) according to the

manufacturer's instructions.

Optiprep gradient cellular fractionation

HEK293T cells were lysed with buffer composed of 150 mM NaCl, 50 mM Tris-HCl pH 8.0, 5 mM EDTA and 0.5% Triton-X100, supplemented with protease and phosphatase inhibitors. After solubilization for 20 min at 4°C, 300 µl of lysates were combined with 600 µl of 60% Optiprep solution to yield a 900 µl 40% Optiprep-Lysate mixture. After loading this mixture to the bottom of a Beckman ultracentrifuge tube, 3 ml of 30% Optiprep solution (in lysis buffer) and 750 µl of 15% Optiprep solution was overlaid sequentially, followed by 500 µl of pure lysis buffer on the top. Samples were centrifuged at 50,000 rpm for 3.5 hrs in rotor SW41Ti at 4°C. After taking two 800 µl fractions from the top, seven 0.5 ml fractions were collected until the bottom of the tube and used for western blot. Lysates collected at the interface of 15% and 30% were referred to as detergent-resistant fraction (or lipid raft). The rest of fractions were referred to as detergent soluble.

Western blots

Cells or fresh intestinal tissue lysates were prepared in lysis buffer containing 50 mM Tris (pH 7.5), 150 mM NaCl, 10 mM EDTA, 0.02% NaN3, 50 mM NaF, 1 mM Na3VO4, 1% NP40, 1 mM PMSF, and protease inhibitors (Sigma). Lysates were heated at 95°C for 5 min in 1× LDS buffer (Invitrogen) and loaded on 8% or 10% SDS-PAGE (Invitrogen). Proteins were transferred to PVDF membranes (Invitrogen). Primary antibodies were added to the membrane for overnight

incubation at 4°C and washed 3 times 5min each with PBS. Secondary antibody was incubated at room temperature for 1-2 hours before development. Membranes were stripped in western stripping buffer (Pierce) and re-probed sequentially with corresponding antibodies.

Dextran uptake assay, immunofluorescence, and confocal microscopy

For dextran uptake, cells with or without treatment were incubated with 100 μg/mL Dextran-568, or Dextran-488 (10,000 MW, Anionic, Fixable, ThermoFisher Scientific) for 30 min at 37°C. After washing with PBS, cells were fixed with 4% paraformaldehyde (PFA), washed with PBS, and stained for actin with Phalloidin-488 (ThermoFisher Scientific, A12379), for 20 min at room temperature. After washing with PBS for three times, cells were dried in dark, and mounted with ProLong® Gold Antifade Mountant (ThermoFisher, P36930) before imaging with Zeiss LSM confocal microscope.

Immunofluorescent analysis has been previously described by us (Das et al., 2015; Yu et al., 2014a; Yu et al., 2014b). Briefly, cells with or without treatment were washed with PBS twice and fixed with 4% PFA at room temperature for 15 min. Cells were then washed with PBS and blocked with 10% donkey serum in PBS with 0.1% Triton X-100 for 1 hr at room temperature. Cells were incubated with EEA1 antibody (Cell Signaling, #3288), at 1:200 dilution in blocking buffer over-night at 4°C. Cells were washed with PBS and incubated with Alexa-555 conjugated anti-rabbit secondary antibody (1:500) and Phalloidin-Alexa-488 (1:3000) at room temperature for 1 hr before washing and mounting.

Mice

The Cdc42 flox (Wu et al., 2006), emEGFR (Yang et al., 2017), IL22Cre knock-out/in (Ahlfors et al., 2014), Myd88 flox (Hou et al., 2008), Villin-Cre (Madison et al., 2002), Villin-CreER (El Marjou et al., 2004), Lgr5EGFP-IRES-CreER (Barker et al., 2007), and Rosa26R-ZsGreen mice (Madisen et al., 2010) have been previously described.

A conditional Cdc42-V2^{Tg} mouse allele was established by inserting the 3XFlag-Cdc42-V2 coding sequence downstream of a chick actin (CAG) promoter and a lox-CAT-lox cassette, at the unique BamH1 restriction site, followed by a bGH poly-A sequence. All mice were maintained on a 12-hour light/dark cycle and provided with food and water ad libitum in individually ventilated cages under specific-pathogen-free (SPF) conditions at Rutgers University-Newark animal facility. Experimental procedures in this study were approved by the Institutional Animal Care and Use Committee of Rutgers University. Experimental comparisons were strictly made among littermates. All mouse analysis in this thesis were repeated with at least 3 mice of each genotype in every experimental condition, otherwise will be specified in figure legends.

Tamoxifen administration

1 mg tamoxifen in corn oil was injected to mice of 8-12 weeks of age intraperitoneally on certain days determined by the experimental scheme. Usually 7 days after tamoxifen administration, intestinal tissues were collected for analysis.

Enteroid culture, 4-OH-Tamoxifen administration, propidium iodide staining, and cell titer-Glo 3D cell viability assay

Enteroid cultures from Cdc42-deficient or Cdc42-WT mice were conducted based on previously described method (Gregorieff and Clevers, 2010). After dissecting out the small intestinal tissue, it was cut open longitudinally and then into fragments (about 2cm). Small intestinal fragments were washed with cold PBS until the supernatant was clear. Then the tissue fragments were incubated in 2 mmol/L EDTA/PBS buffer for 40 minutes on ice. Next, tissue fragments were vigorously shaken in cold EDTA/PBS buffer in a 50mL tube to isolate intestinal crypts. The supernatant was filtered using 70μm cell strainer. The flow-through containing crypts were collected in 50 mL Falcon tube and centrifuged with 300 g for 5 mins at 4°C. After discarding the supernatant, crypts were washed with cold PBS buffer, and centrifuged again. After counting the number of crypts for each sample, they were seeded into 48well plate by mixing with Matrigel and supplied with “ENR” crypt culture media. To induce Cdc42 deletion in iKO enteroids, 100-200 wild type or Cdc42-iKO crypts were seeded in Matrigel with ENR media and allowed to develop for 3 days. On day 4, 500 nM 4-OHT was added to the enteroids for 24 hrs. Viable enteroids were counted under a bright field microscope 1-7 days after 4-OHT treatment. For propidium iodide staining, enteroids were incubated with 500 nM propidium iodide (P4170, Sigma) in PBS solution at 37°C for 10 min and washed with PBS before imaging. For 3D cell viability assay, 100 organoids were seeded in each well on a 96 well-plate and cultured in ENR media for 4 days

before addition of 4-OHT. Cell viability was determined typically at time points indicated in each figure after 4-OHT treatment using the Cell Titer-Glo 3D Cell Viability Assay (G9681, Promega) by Glomax system (E9032, Promega).

Enteroid growth rescuing assay

Cdc42 iKO crypts were seeded at a concentration of 100/well in 96-well plate and allowed to develop for 3 days. The following recombinant cytokines or growth factors were individually added to enteroids at the time when 4-OHT was added: murine cytokines including IL33 (100 ng/ml, Peprotech), IL22 (50 ng/ml, Peprotech), IL12 (50 ng/ml, Peprotech), Cxcl1 (50 ng/ml, Peprotech), Cxcl2 (100 ng/ml, Peprotech), Cxcl6 (50 ng/ml, Peprotech) and growth factors including Wnt3a (100 ng/ml, PeproTech), TGFα (50 ng/ml, Sigma), HGF (50 ng/ml, Sigma) and Amphiregulin (100 ng/ml, R&D). Viable or dead enteroids were counted using bright field microscope, propidium iodide staining, and 3D cell viability assays. Duplicates were carried out for each condition in each experiment, and independent experiments were repeated using different Cdc42 iKO animals.

Embedding enteroids for histological analysis

To dissolve Matrigel containing enteroids, medium was removed from wells and treated with 500 µl of Corning Recovery Solution (354253, Corning) on ice for 10 minutes. A p1000 pipette was then used to dissolve remaining Matrigel. Two to three wells of enteroids were combined in a microcentrifuge tube and centrifuged at 200 × g for 5 minutes. Ice cold PBS was used to wash the pellet. After a 2-minute

centrifugation at 200 × g, PBS was removed, and enteroids were resuspended in 4% paraformaldehyde for 10-15 minutes. After fixation, enteroids were centrifuged at 200 × g for 5 minutes and washed 3 times in cold PBS. After removing the last PBS wash, 10-20 µl of Matrigel was added to form clump of enteroids and left at 37°C to solidify. Once solid, 70% ethanol was added and stored at 4°C until paraffin embedding at the Histology Core of Rutgers New Jersey Medical School.

Total-body γ irradiation

Animals were subjected to total body irradiation using a Caesium-137 irradiator calibrated to a dose of 12 Gy. All procedures follow the biosafety guidelines of Rutgers-New Jersey Medical School.

Antibiotic treatment

Mice were administrated with antibiotic cocktail (1 mg/ml of Ampicillin, Vancomycin, Neomycin, Cefoperazone, and Metronidazole in autoclaved water) for 7 days for most experiments. Depending on experimental schemes, mice were provided with regular sterile water afterwards or continued on antibiotic water.

Administration of EGF to mice

Recombinant mEGF (315-09 B, Peprotech) was injected intraperitoneally at a concentration of 1 µg per gram body weight, 30 mins prior to tissue collection.

Administration of STAT3 inhibitors to mice

Stattic and WP1066 were dissolved in PBS containing 10% DMSO and 10% Tween 20 to a final concentration of 5 mg/ml. Inhibitors were intraperitoneally injected to mice at 20 μg/g of body weight every other day for a total 3 injections. In irradiation experiments, WP1066 were injected for two sequential days after irradiation.

EdU and BrdU incorporation in mice

Mice were intraperitoneally injected with BrdU labeling reagent (00-0103, Invitrogen) at 10 μl/g body weight 30 mins before tissue collection. EdU was injected intraperitoneally into mice at 100 mg/kg for 2, 6 or 24 hrs before tissue collection. Intestinal tissue was embedded in either paraffin or OTC for sectioning. BrdU was detected by BrdU antibody and secondary fluorescent anti-Rat antibody. EdU was detected by a Click-iT EdU Imaging Kit (C10338, Invitrogen).

Immunofluorescence and immunohistochemistry

Intestinal tissues were collected and fixed in 4% paraformaldehyde or 10% neutral formalin buffer and embedded in paraffin. 5 μm sections were sliced, dewaxed, and subjected to antigen retrieval (0.1 M citric acid, pH 6.0 for most of the antibodies except phospho-STAT3 using DAKO Target Retrieval Solution and Signal Stain EDTA Unmasking Solution respectively). Slides were immersed into antigen retrieval buffer at a sub-boiling temperature for 15 minutes. After incubation with 3% H2O2 in methanol for 10 minutes, sections were then blocked in PBS containing 0.1% Triton-X100, 2% BSA and 2% normal serum for at least one hour

at room temperature, and then probed with indicated antibodies at 4 °C overnight. Next morning, slides were washed in PBS three times and probed with biotinylated secondary antibody (for IHC) or fluorescence-conjugated secondary antibodies (for immunofluorescence). After one-hour incubation at room temperature, slides were washed three times. For IHC, slides were incubated with streptavidin-conjugated horseradish peroxidase (HRP) for an hour at room temperature. DAB HRP substrate kit was used for development. For immunofluorescence, slides were washed with PBS three times and subsequently subjected to DAPI counter-staining, before being air-dried and mounted with Prolong Gold antifade medium. Immunofluorescent images were collected by LSM 510 Laser Scanning Microscope and analyzed by AIM software (version 4.2) or Fiji software (https://fiji.sc).

Realtime PCR

Total mRNAs were extracted using QIAGEN RNeasy mini Kit from scraped epithelia. cDNA synthesis was performed using Thermo Scientific Maxima H Minus First Strand cDNA Synthesis Kit. Real-Time PCR reactions were assembled using the SYBR Green Real-Time PCR Master Mixes (Thermo Fisher). Reactions were run in replicates by a Roche Light cycler 480. The PCR cycling conditions were 10 min pre-heating at 95°C followed by 45 cycles of denaturing (95°C for 10 s), annealing (60°C for 10 s) and extension (72°C for 10 s). Fluorescent signal was acquired during the extension phase. Melting curves were analyzed to ensure PCR specificities. House-keeping genes (such as HPRT) were used as internal

references.

Bulk RNA-sequencing and gene set enrichment analysis (GSEA)

RNA seq data was deposited at NCBI BioProject with access number GSE124848. GSEA (Mootha et al., 2003; Subramanian et al., 2005), pre-ranked files of differentially expressed genes calculated by the rank metric = -log (p-value) * SIGN (logFC) (Jia et al., 2015). GSEA was performed on intestinal stem cell gene signatures (Munoz et al., 2012). Normalized enrichment scores (NES) and p-values were documented (K-S Test). Heatmaps of select EGF receptor and cytokine genes were generated by plotting z-scores of fpkm normalized RNA-Seq data of individual replicates.

16S fecal DNA sequencing

Mouse fecal samples were longitudinally collected before and 7, 8, 9 and 10 days after antibiotics treatment. Fresh samples were snap frozen. From all samples, DNA was extracted using DNeasy PowerSoil Kit (Qiagen) according to the manufacturer's protocol. The hypervariable V4 region of the 16S rRNA gene was amplified using 515 forward primer and 806 reverse barcoded primer (Caporaso et al., 2010) with MyFi Bioline DNA polymerase Master Mix in the final volume of 40 μL. Amplicons were quantified using Quant-It PicoGreen dsDNA Assay kit (Invitrogen) according to the manufacturer's protocol. 240ng of amplicons from each sample were pooled and cleaned using UltraClean PCR Clean-Up Kit (MoBio). Pooled amplicons were diluted, denatured and 7nM of the

pooled library was sequenced on MiSeq platform (Illumina) using custom primers (Caporaso et al., 2010). Due to the limited sequence diversity among 16S rRNA amplicons, 5% of the PhiX control library (Illumina) made from phiX174, was added to the run. The pooled 16S rRNA library was subjected to paired-end sequencing using 2 x 150bp MiSeq Reagent Kit V2 (Illumina), fastq files were generated, and Qiime2 (www.qiime2.org) pipeline was employed for data analysis. Denoising was done using dada2 plug-in (Callahan et al., 2016) and richness (alpha diversity) was calculated as a measure of antibiotic efficacy. For all groups (pairwise) stats were calculated.

Intestinal epithelial cell isolation, lamina propria cell isolation and IL22 measurement by ELISA

Mouse distal ileum was harvested and placed on an ice-cold petri dish with commercial 1X PBS. Then the tissue was cut open longitudinally to clear the luminal contents, followed by cutting the tissue into sections of smaller pieces (2-3 cm) and washing the pieces by inverting 10-15 times in a falcon tube with 30mL ice-cold PBS. After repeating the washing for 3 times, the intestine pieces were added to 30mL of crypt isolation buffer and shaken in a 37˚C incubator for 15 mins, followed by vortexing and passing the solution through a tea mesh. The flow through contains IECs and IELs. Repeat shaking the tissues in 30ml crypt isolation buffer for another 15 mins at 37˚C, vortex and discard the solution. Then incubate the tissues in 40ml DMEM/ RPMI-1640 for 10 mins at 37 ˚C on a shaker. After discarding the solution, the intestine was minced to smaller pieces and shaken at

225rpm in 8ml of digestion buffer at 37˚C for 30 mins. Digested cells were spin down at 200g for 5 mins. The isolated cells were washed once with PBS and then transferred to RPMI-1640 with 10%FBS, P/S, and 20mM HEPES.

IL-22 level in LP cells with or without chemokine treatments (IL1RN-1ug/ml, Prolactin-500ng/ml, CXCL1-500ng/ml, CXCL2-500ng/ml, IL33-100ng/ml) were measured using commercially available enzyme-linked immunosorbent assay (ELISA) kits (BioLegend) according to the manufacturer's instructions.

QUANTIFICATION AND STATISTICAL ANALYSES

Statistical and graphic data analysis was conducted using Prism GraphPad 7.04 (https://www.graphpad.com) and Microsoft Excel 2016. The data were presented as mean ± S.E.M. in bar graphs or in box-whiskers plots. The histology and immunostaining results were reported from 3 to 20 sections of a total of at least 3 mice in each experiment unless stated differently. To quantify immunostaining results, Image J (1.6.0_24 version) IHC toolbox package (https://imagej.nih.gov/ij/plugins /ihc-toolbox/index.html), was used to determine signals within a crypt or a crypt-villus unit depending on the specific antigen and experiment elaborated in figure legends. At least 20 crypt or villus units were analyzed from each section. Animal numbers used in each experiment were detailed in figure legend. Paired student t-test was used for most analysis unless stated otherwise.

CHAPTER 3

ELEVATING INTESTINAL STEM CELL EGFR-MAPK PROGRAM BY A NON-CONVENTIONAL CDC42 ENHANCED REGENERATION

INTRODUCTION

The intestinal epithelia are essential for nutrient absorption and survival of the host. Proper functioning of intestinal epithelial cells (IECs) relies on a signaling network that sustains continued cell production while simultaneously maintaining tissue integrity and retaining the crucial balance among progenitor and differentiated cell populations. Canonical Wnt and EGF signaling are two major growth pathways for intestinal stem cell (ISC) survival and renewal (Basak et al., 2017; Gregorieff and Clevers, 2005; Krausova and Korinek, 2014; Schepers and Clevers, 2012), while BMP pathway drives formation of differentiated villus epithelia (He et al., 2004; Qi et al., 2017). It becomes increasingly evident that synthetic interplay of these pathways ensure a homeostasis balance, where crypt-based ISCs self-renew and produce various lineages of progenitors that, upon transit amplification, differentiate into mature IECs to offset programmed cell death (Clevers, 2013b; Gehart and Clevers, 2019). Indispensability of Wnt, EGF, and BMP pathways for ISC function are unequivocally demonstrated in enteroid culture system, in which an indefinite ISC renewal is sustained by Wnt and EGF pathway agonists along with BMP pathway inhibitor, Noggin (Barker et al., 2010; Radtke and Clevers, 2005; Sato et al., 2009b). Surprisingly, in contrast to enteroid models, intestinal epithelia in intact animals demonstrate remarkable plasticity displayed by stemness acquisition by quiescent and mature cell populations in response to injury-induced ISC loss (Basak et al., 2017; Gerbe et al., 2009; May et al., 2014; Schmitt et al., 2018; Sei et al., 2018; Tetteh et al., 2016; Westphalen et al., 2014; Yan et al., 2017; Yi et al., 2018; Yu et al., 2018) (Yu, 2013). The interactive

complexity of intrinsic and non-intrinsic epithelial signaling that confers remarkable tissue plasticity remains both poorly defined and is of important biomedical impact.

The cell division control 42 (Cdc42) is an important Rho subfamily small GTPase with pleiotropic functions in cytoskeleton organization, cell polarity, and cell migration across eukaryotic species (Al-Tassan et al., 2015; Cardoso et al., 2014; Johnson, 1999b). Previously, we reported that elevated Cdc42 level was observed in human and mouse intestinal tumors (Sakamori et al., 2014b). Genome wide association study identified a single nucleotide polymorphism in *CDC42* linked to *Irritable Bowel Syndrome* (Wouters et al., 2014). Genetic ablation of *Cdc42* in mouse IECs resulted in enteropathy resembling a lethal form of the pediatric disorder, *Microvillus Inclusion Disease* (Michaux et al., 2016; Sakamori et al., 2012b; Wiegerinck et al., 2014b; Zhang and Gao, 2016). The initial link between Cdc42 and ISC homeostasis was made based on the observation of abnormal organization of intestinal crypts in mice lacking epithelial Cdc42 (Sakamori et al., 2012b). It remains unclear how Cdc42 controls ISC renewal and regeneration, and whether modulating Cdc42 program may enhance ISC function.

Using proteomics and kinase assay screening, we identified the involvement of Cdc42 in endocytosis associated EGF-EGFR-MAPK signaling. Elimination of Cdc42 in enteroids resulted in rapid apoptosis, coincident with lost EGF-stimulated EGFR vesicular traffic. We found that a native Cdc42 splice variant 2 (V2) (Kang et al., 2008; Lee et al., 2018a; Mukai et al., 2015; Nishimura and Linder, 2013; Wirth et al., 2013a; Yap et al., 2016) has enhanced EGFR engagement and MAPK-activating capacity. Mice engineered to produce Cdc42-V2 in intestinal epithelia

exhibited robust regenerative capability and mitigated injury-induced damage. These results shed fresh lights on the role of epithelial intrinsic survival program in mediating protection from stem cell injury.

RESULTS

Cdc42 is indispensable for enteroid survival

Cdc42$^{Fl/Fl}$*;Villin-Cre* (*Cdc42*$^{\Delta IEC}$) mice with constitutive IEC-specific *Cdc42* ablation via *Villin-Cre* were viable but developmentally retarded (Sakamori et al., 2012b). Histological analysis of Cdc42-defiicent intestine epithelium revealed a dramatic dislocation of Paneth cells from crypts to villi **(Fig. 1A)**. This epithelial defect was accompanied by an increase in apoptotic cells in the crypts as illustrated by TUNEL staining **(Fig. 1B).**

Although *Cdc42*$^{\Delta IEC}$ mice were viable and the overall intestinal crypt-villus structures were maintained, crypts isolated from *Cdc42*$^{\Delta IEC}$ mice failed to develop into enteroids in EGF, Noggin, and R-Spondin (ENR)-containing medium. Within 24 hrs after seeding, all *Cdc42*$^{\Delta IEC}$ crypts were growth-arrested **(Fig. 2A)**. As this growth deficit could be secondary to abnormal development by *Cdc42*$^{\Delta IEC}$ intestinal epithelia, we used *Villin-CreER* to delete *Cdc42* from mature *Cdc42*$^{Fl/Fl}$*; Villin-CreER* (*Cdc42*^{iKO}) enteroids. Forty-eight hours after *4*-hydroxytamoxifen (4-OHT) addition, the epithelial buds in over 60% of *Cdc42*^{iKO} enteroids regressed with cell death and cellular debris **(Fig. 2B)**. After 72 hrs, 95% of *Cdc42-iKO* enteroids accumulated significant amounts of propidium iodide indicative of massive cell death **(Fig. 2C, D)**, which was further corroborated by elevated numbers of cleaved

caspase 3-positive cells **(Fig. 2E)** and a loss of over 90% live enteroid cells quantified by the cell titer-Glo 3D viability assay **(Fig. 2F)**. Viable enteroid were not detected at 5 days after *Cdc42* deletion and the growth of *wild type (WT)* enteroids was not affected by 4-OHT over this time period **(Fig. 2D)**. Thus, maintenance of enteroid growth in ENR medium absolutely was dependent upon Cdc42 expression.

Cdc42 is required for and sufficient to promote EGF-MAPK signaling ex vivo

As Cdc42 was required for enteroid survival that requires EGF, Wnt/R-Spondin, and Noggin, we tested Cdc42 activity in response to these growth factors in vitro. Treating serum-starved-human Caco2 cells with EGF ligands (EGF and TGFα), canonical Wnt ligand (Wnt3a), or Noggin all increased Cdc42 GTPase activity within minutes **(Fig. 3A)**, suggesting that these ISC growth factors might act through Cdc42.

When we used a GSK3-beta inhibitor (CHIR99021) to enhance Wnt signaling in Cdc42-deficient enteroids ex vivo, we did not detect a rescuing effect on enteroid survival **(Fig. 3B)**, suggesting that loss of Cdc42 might not primarily affect the canonical Wnt signaling. We thus conducted an unbiased proteomic search for Cdc42-regulated survival signaling. Parallel mass spectrometry was done on canonical Cdc42 (V1) and its splicing variant (V2), both of which were 3xFlag-tagged and transfected to HEK293 cells. Proteomic analysis of Cdc42 V1- and V2 immuno-precipitates identified an overlapped interactome of 910 proteins, where the 5 top functional clusters mapped to cell cycle, cell division, clathrin-coated

endocytosis, mitosis, and MAPK cascade components ($p<0.001$, **Fig. 4A, B)**. Notably, the proteins found to mediate clathrin endocytosis, regulate actin organization, and affect MAPK signaling **(Fig. 4C)** are essential components for EGFR signalosomes.

The identification of a clathrin and MAPK interactome components suggested that Cdc42 may control MAPK activation through clathrin-dependent endocytic EGF receptor signaling (Goh et al., 2010; Henriksen et al., 2013; Huang et al., 2004; Sigismund et al., 2008; Vehlow et al., 2013). EGF stimulates rapid receptor-mediated endocytosis that generates changes in plasma membrane elasticity measurable by atomic force microscope (Zhang et al., 2018) (Detailed in Chapter 5). Within 30 seconds of EGF loading, there was a robust increase in nanomechanical stiffness on the surface of control Caco2 cells (blue line, **Fig. 5A**). This response was abolished in cells pretreated with the endocytosis inhibitor dynasore (green line, **Fig. 5A**) (Macia et al., 2006). *Cdc42*-knockdown cells produced a much diminished (89% reduction in stiffness) and a delayed (by 10 mins) response to EGF ligands (pink line, **Fig. 5A**). This impaired nanomechanical response to EGF coincided with reduced intracellular pERK1/2 levels in *Cdc42*-knockdown cells **(Fig. 5B)**, illustrating Cdc42's requirement for EGF-MAPK activation.

To further dissect signaling cascades downstream of Cdc42, we examined 43 major intracellular kinase targets **(Fig. 6A)** in HEK293 cells overexpressing either Cdc42 V1 or V2 **(Fig. 6B)**. Compared with cells expressing empty vector, phosphorylation levels of 3 major MAPK components, ERK1/2, c-Jun, and p38,

were elevated in Cdc42-overexpressing cells, especially in V2-overexpressing cells **(Fig. 6C)**.

We validated this above finding in a time course experiment, in which overexpressing Cdc42 in HEK293 cells resulted in a 5-fold increase in pERK1/2 (V2 shown in **Fig. 7A**). In addition to EGFs, canonical Wnt has also been shown to trans-activate ERK (Yun et al., 2005). In the presence of Wnt3a, an ISC growth factor, Cdc42-V2 robustly elevated pERK1/2 (**Fig. 7A)**. A side-by-side comparison of ERK-activating capabilities of the two variants showed that V2's strength was 230% of V1 **(Fig. 7B)**.

Cdc42 V1 and V2 differ in the last 10 amino acids. Mutation of V2-specific lysine 185 (K185R) within the C-terminus poly-lysine region reported to be essential for membrane attachment (Davis et al., 1998; Johnson, 1999a; Johnson et al., 2012), led to a markedly reduction in pERK1/2 levels **(Fig. 7C)**, suggesting that Cdc42's MAPK-stimulating activity requires membrane association. The stronger MAPK-activating capabilities by V2 were not due to different binding to the Cdc42 effector PAK1, which equally associated to both variants **(Fig. 7D)**.

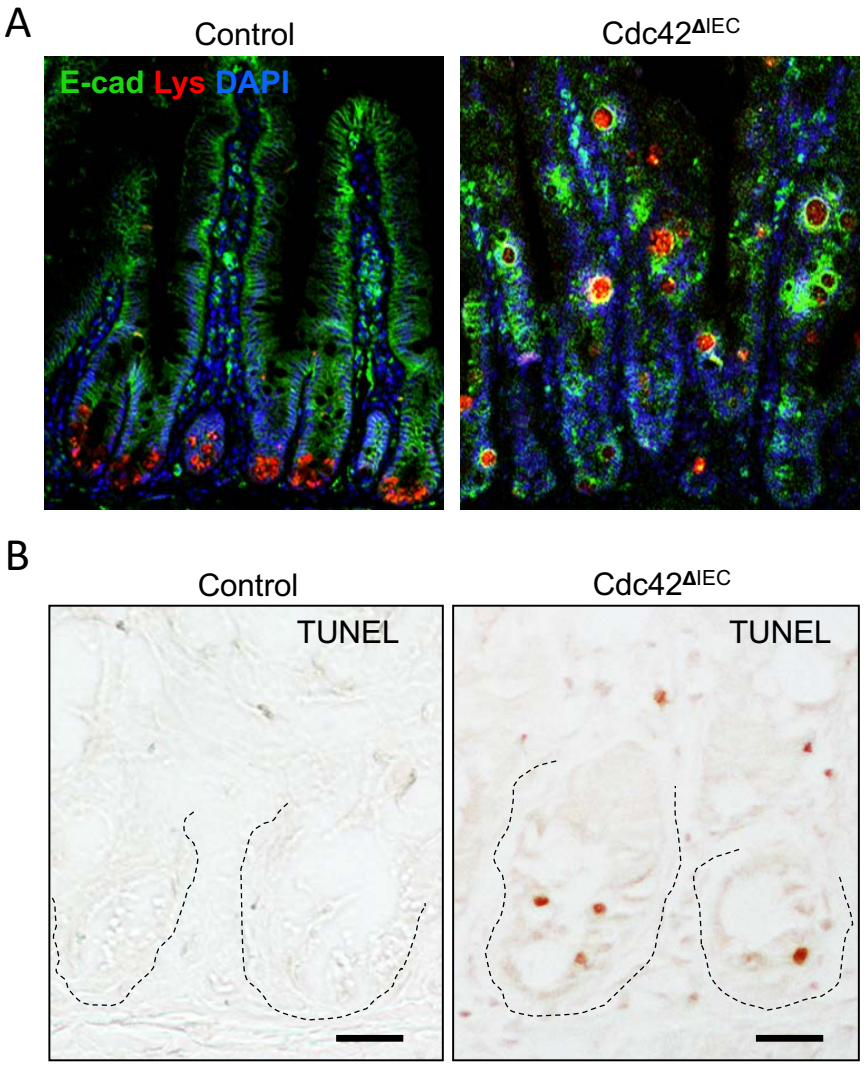

Figure 1. Deletion of Cdc42 in mouse intestine epithelium causes changes in the crypt (Sakamori et al., 2012b) .

(A) Immunofluorescence staining for lysozyme (red) and E-cadherin (green). Nuclei were labeled with DAPI (blue). (B) TUNEL staining. Crypts are indicated by dotted lines.

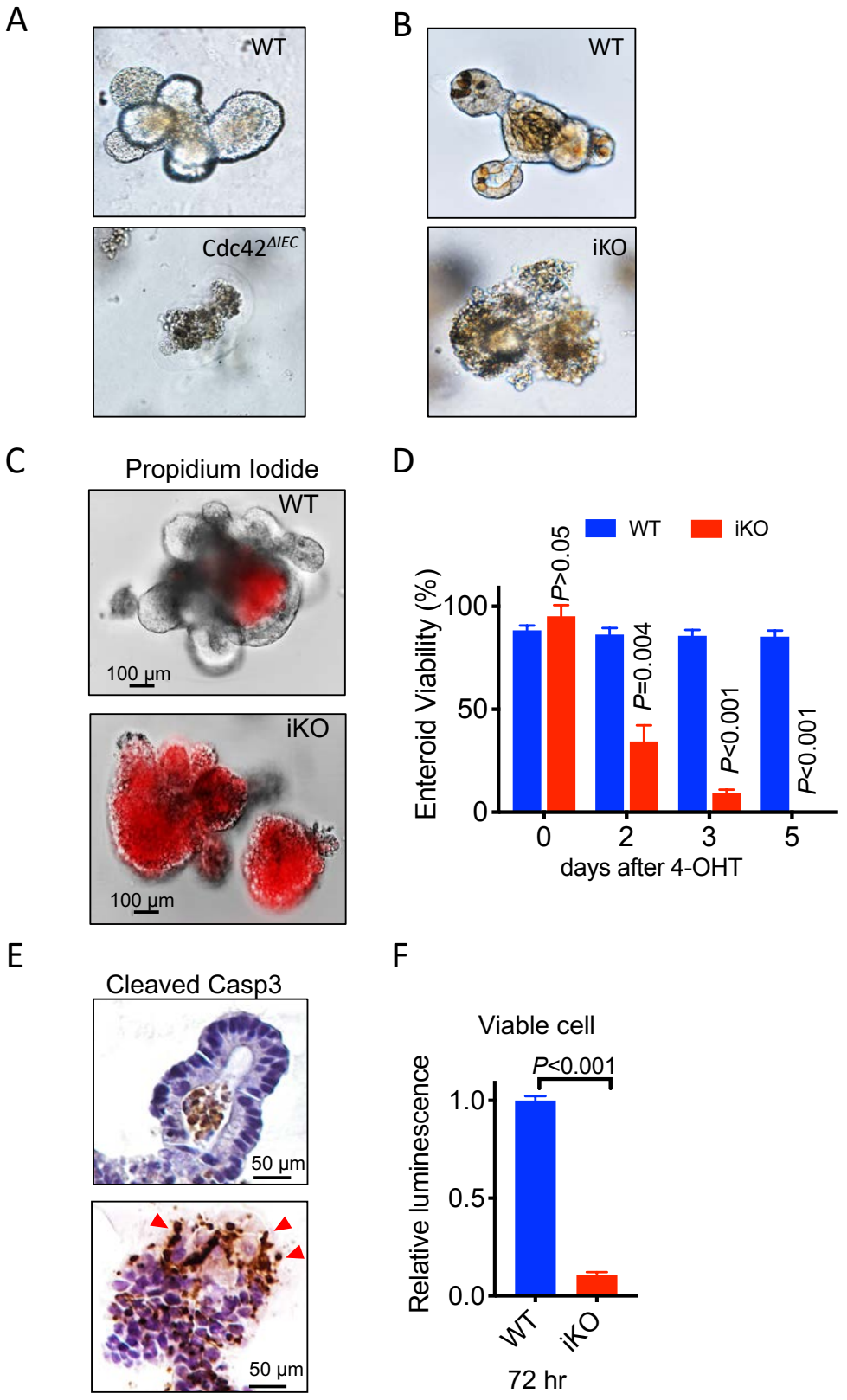
A
WT
Cdc42ΔIEC
B
WT
iKO
C
Propidium Iodide
WT
100 μm
iKO
100 μm
D
WT
iKO
P>0.05
P=0.004
P<0.001
P<0.001
Enteroid Viability (%)
100
50
0
0
2
3
5
days after 4-OHT
E
Cleaved Casp3
50 μm
50 μm
F
Viable cell
P<0.001
Relative luminescence
1.0
0.5
0.0
WT
iKO
72 hr

Figure 2. Loss of Cdc42 causes cell death in enteroid culture.

(A) Bright field images of representative of *WT* and *Cdc42*$^{\Delta IEC}$ enteroids of 5 days' culture. (B) Bright field images of representative of *WT* and *Cdc42*-iKO enteroids 48hrs after 4-OHT addition. (C) Propidium iodide staining showed massive cell death 72 hrs after 4-OHT treatment in *Cdc42-iKO* enteroids. (D) Viable enteroids were counted 2, 3 and 5 days after 4-OHT treatment. The data represents 3 independent experiments each containing 2 replicates per genotype. (E) Cleaved Caspase 3 staining for enteroid sections detected increased apoptosis in 4-OHT treated iKO. Images shown were enteroids 72 hrs after treatment. (F) Quantification of cell viability by 3D-Glo luminescent assays showed significant reduction of live iKO enteroid cells 72 hrs after 4-OHT treatment. Data represents two independent experiments each containing 2 replicates per genotype.

A

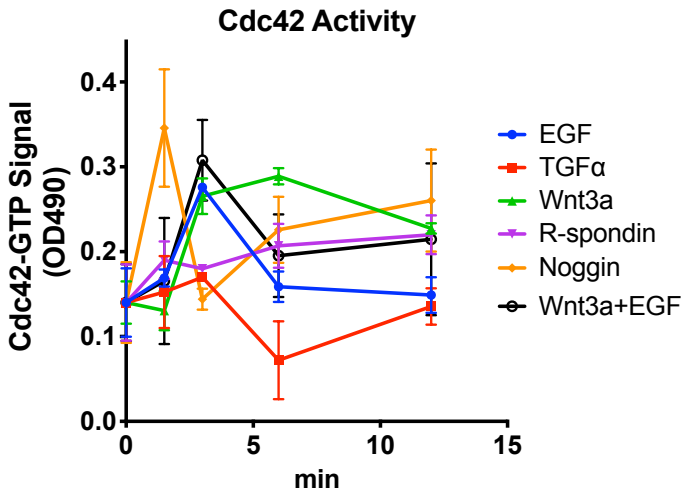

B

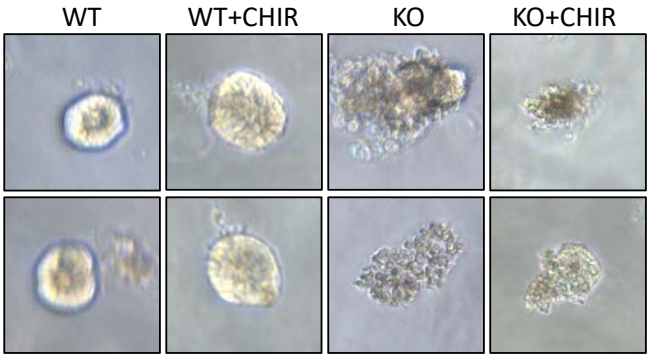

Figure 3. Although Cdc42 is activated by niche factors in vitro, inhibition of GSK3beta does not rescue cell death in *Cdc42*$^{\Delta IEC}$ enteroids

(A) Cdc42 GLISA assay based on OD490 luminescence showed that Cdc42 activity was increased with different intensities in serum starved Caco2 cells by EGF, TGFα, Wnt3a, Noggin, R-spondin, or a combination of Wnt3a and EGF. Reading of OD490 were collected at 0 min (without growth factors), 1.5 min, 3 min, 6 min and 12 min after addition of growth factor. **(B)** Representative bright field images of day1 WT and *Cdc42*$^{\Delta IEC}$ enteroids in culture with or without GSK3beta inhibitor, CHIR99021.

A

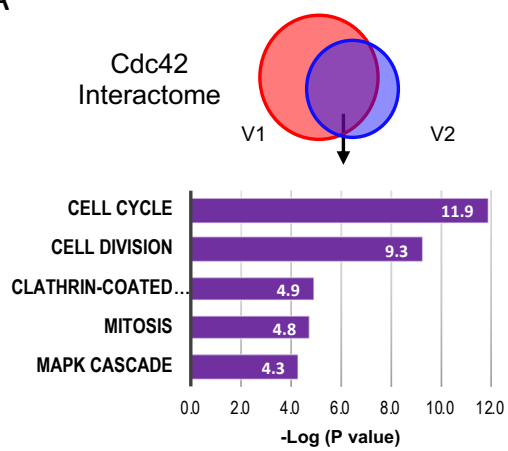

B

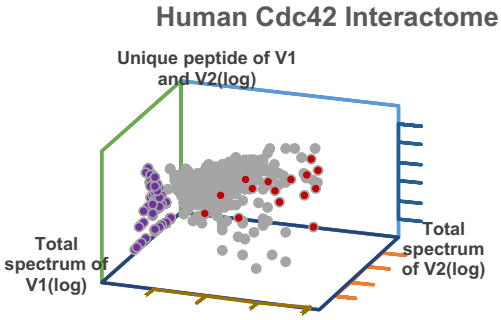

C

Function Clusters	Identified Proteins (275)	Spectra counts (Cdc42V1)	Spectra counts (Cdc42V2)
Cdc42	Cell division control protein 42 homolog	30	12
Formation of Clathrin-dependent endosomes	AP-2 complex subunit alpha-1	3	1
	AP-2 complex subunit beta	2	1
	AP-2 complex subunit sigma	1	0
	Clathrin heavy chain 1	14	7
	ADP-ribosylation factor 6	1	1
Regulation of Actin filament	Myosin light polypeptide 6	10	3
	Myosin regulatory light chain 12A	4	1
	Myosin-10	8	2
	Myosin-9	32	13
	Actin-related protein 2/3 complex subunit 2	3	1
	Actin-related protein 2/3 complex subunit 3	1	1
	Actin-related protein 2/3 complex subunit 4	3	1
	Actin, cytoplasmic 1	89	49
	Actin, cytoplasmic 2	89	49
	Actin-related protein 3	1	1
Components of MAPK endocytic signalosome	Ras-related protein Rab-5C	5	1
	Dynactin subunit 1	2	2
	Dynactin subunit 2	4	3
	Serine/threonine-protein kinase PAK 4	4	1
	Growth factor receptor-bound protein 2	4	1
	Mitogen-activated protein kinase 1	7	3
	Mitogen-activated protein kinase kinase kinase 7	17	8

Figure 4. Mass spectrometry analysis of Flag-Cdc42 immuno-precipitates.

(A) HEK293 cells were transfected with Flag-tagged Cdc42 V1 or V2. Mass spectrometry analysis of Flag-Cdc42 immuno-precipitates identified variant-specific interactome. Venn diagram reveals 910 shared interactors. Functional annotation identified 5 most enriched clusters ranked by p value by NIH DAVID. (B) 3D representation of Flag-Cdc42 V1 and V2 interactomes identified in the proteomic analysis. Purple and red dots represent V1- and V2-specific interactor, while gray dots are proteins associated with both. Note that a single dot might represent multiple proteins having identical numbers of peptide spectrum. (C) List of Cdc42-assocated proteins, detected by proteomic analysis, which are known to mediate clathrin endocytosis, regulate actin organization, and affect MAPK signaling.

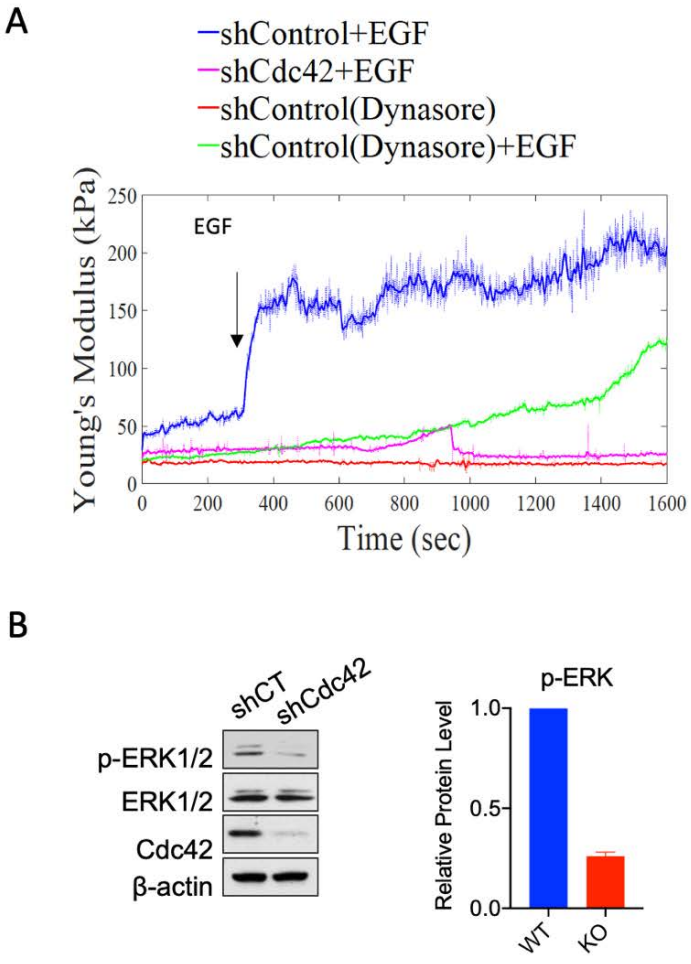

Figure 5. Cdc42 is required in both EGFR response to EGF and activation of ERK.

(A) Serum-starved Caco2 control and Cdc42 knockdown cells were analyzed by atomic force microscope. EGF was added to cells 300 sec after recording of each sample. Young's modulus (kPa) indicated EGF-induced nanomechanical changes on control Caco2 cell surface, diminished responses in control cells pre-incubated with dynasore or in Cdc42 knockdown cells. Graphs are representative of 4 independent experiments. (B) Western blots showed decreased p-ERK1/2 levels in Cdc42 knockdown Caco2 cells compared to controls. Data were quantified from 2 independent experiments.

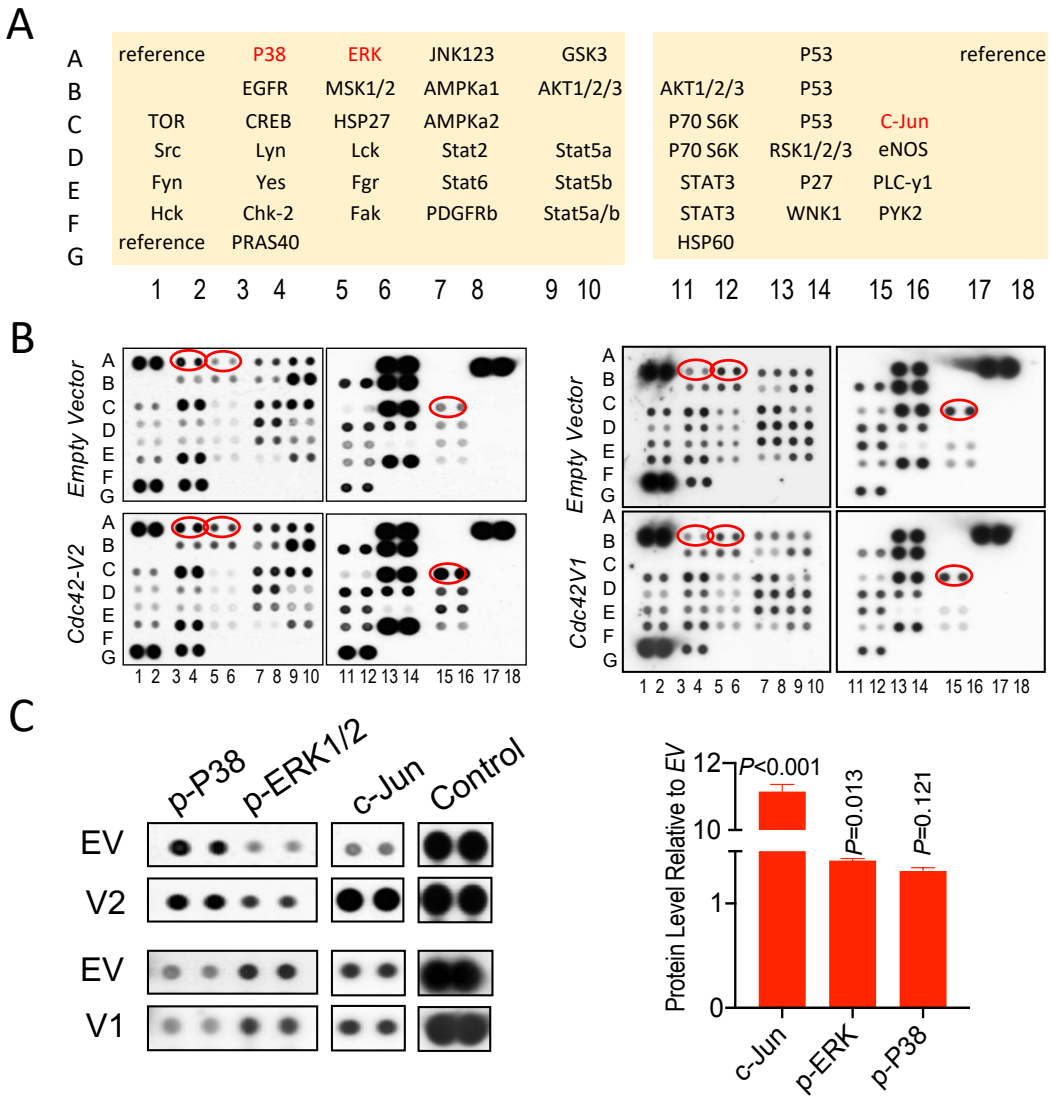

Figure 6. Phospho-kinase array was used to search for functional pathways downstream of Cdc42.

(A) Position and name of 43 kinase targets in the phospho-kinase array analysis (B) Expression level of 43 kinase targets in Cdc42-V1 or V2 overexpressing HEK293T cells compared to empty vector transfected cells. (C) Among 43 kinase targets, overexpressing Cdc42 in HEK293 cells increased levels of phosphorylated ERK1/2, p38 and c-Jun, especially in V2-expressing cells compared to empty vector controls. Graph shows the mean values from 2 replicates.

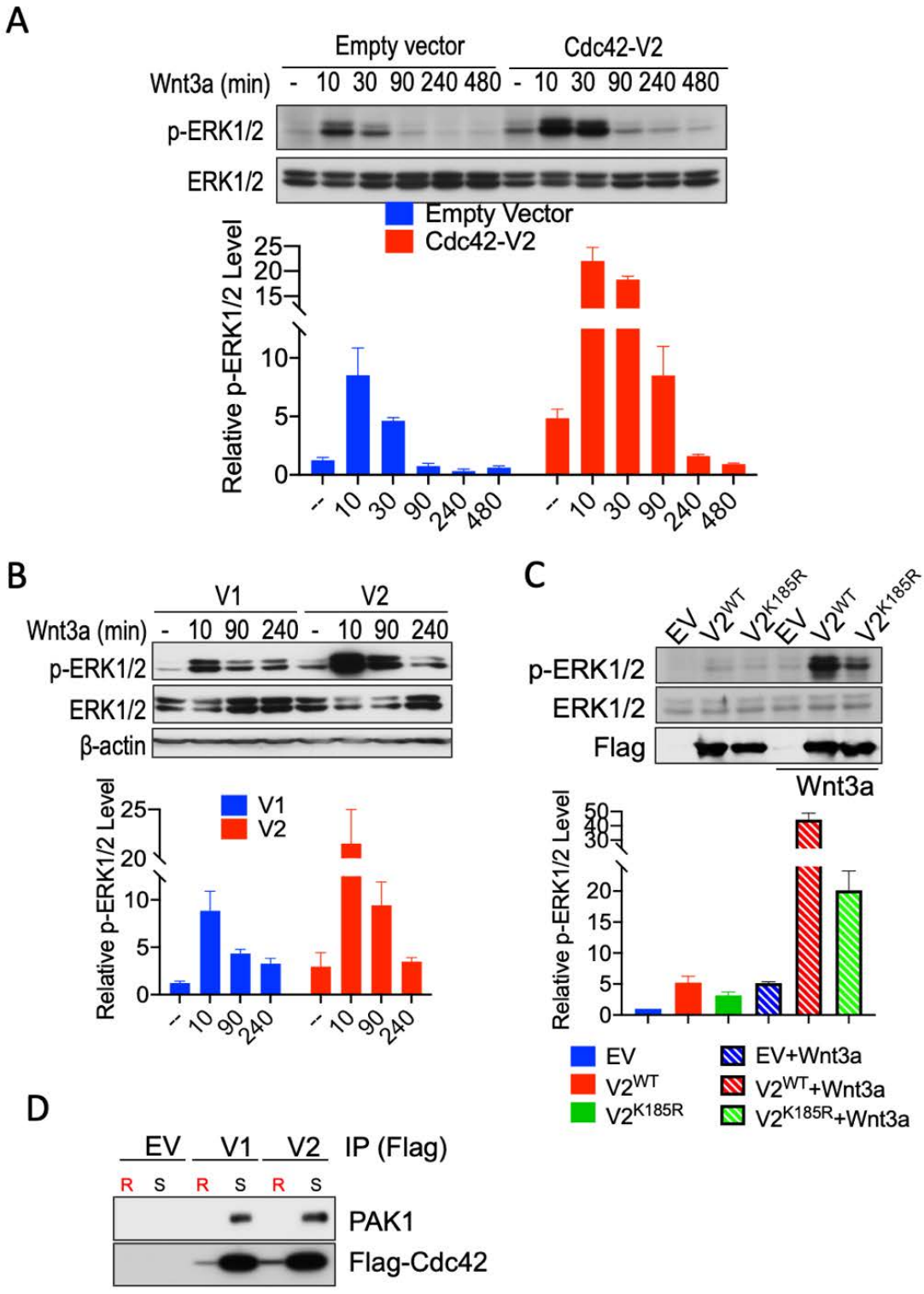
A
Empty vector
Cdc42-V2
Wnt3a (min) - 10 30 90 240 480 - 10 30 90 240 480
p-ERK1/2
ERK1/2
Empty Vector
Cdc42-V2
Relative p-ERK1/2 Level
B
V1
V2
Wnt3a (min) - 10 90 240 - 10 90 240
p-ERK1/2
ERK1/2
β-actin
Relative p-ERK1/2 Level
C
EV
V2WT
V2K185R
p-ERK1/2
ERK1/2
Flag
Wnt3a
Relative p-ERK1/2 Level
EV
V2WT
V2K185R
EV+Wnt3a
V2WT+Wnt3a
V2K185R+Wnt3a
D
EV
V1
V2
IP (Flag)
R S R S R S
PAK1
Flag-Cdc42

Figure 7. Time course activation of ERK by overexpression of Cdc42

(A) Time course experiments were used to determine change of p-ERK1/2 levels in serum-starved control and Cdc42-V2 expressing cells, following the addition of Wnt3a (100ng/ml), an ISC niche factor shown to activate MAPK. (B) A side-by-side comparison of V1 vs. V2 showed stronger MAPK-activating capabilities by V2 shown by western blot of p-ERK. (C) Mutant $V2^{K185R}$ showed a reduced MAPK-activating capability compared to WT V2 by western blot. (D) Co immunoprecipitation using HEK293T cell lysates overexpressing empty vector, Flag-V1 or Flag-V2 showed that PAK1 bound equally to both Cdc42 variants in soluble cellular fractions. R, detergent-resistant; S, soluble.

Cdc42 engages EGF receptor and facilitates MAPK signaling

To examine the intrinsic impact of loss of Cdc42 on EGFR endocytic signalosome in the intestinal epithelium, *Cdc42* was inducibly knocked-out in mature Cdc42^{iKO} enteroids. Cells with delocalized EGFR appeared as early as 8 hrs following 4-OHT treatment, a time point before any apoptosis occurred **(Fig. 8A).** At 40 hrs, more cells with delocalized EGFR appeared along with apoptosis **(Fig. 8B)**. At 48 hrs, Cdc42^{iKO} enteroid cells showed a noticeable loss of polarized intracellular EGFR distribution and a reduction in pHH3^{+} mitotic activity **(Fig. 8C)**.

To directly visualize EGFR vesicular trafficking *in vivo*, Cdc42^{iKO} mice were crossed to a CRISPR-CAS9 engineered emEGFR mouse allele (Yang et al., 2017). Administration of a pulse of EGF to WT mice elicited a marked induction, within 30 mins, of emEGFR vesicles as well as emEGFR-EEA^{+} endocytic vesicles, which were diminished in Cdc42^{iKO} crypt cells **(Fig. 9A).** This reduction of EGF-stimulated "signalosomes" in Cdc42^{iKO} crypt cells echoed a slight decrease in levels of pErbB1(Y1068) and pErbB2 (Y1221/1222), active forms of major EGF receptors in Cdc42^{iKO} IECs **(Fig. 9B)**. Of note, total levels of both receptors were increased and there were residual amounts of pErbB1, pErbB2, pERK1/2 in Cdc42^{iKO} IECs **(Fig. 9B)**. These data suggested a major change of EGFR compartmentalization and activation in Cdc42^{iKO} IECs in vivo.

Co-immunoprecipitation (co-IP) analysis indicated that both V1 and V2 associated with EGFR through binding to the receptor's intracellular domain (ICD) **(Fig. 10A,** see IP Flag panel). Ligand-stimulated EGF receptors are associated with lipid rafts that are internalized to transduce MAPK signaling (Hofman et al.,

2008; Irwin et al., 2011; Patra, 2008; Pike et al., 2005; Puri et al., 2005). When lipid rafts were extracted from V2-overexpressing cells using Optiprep gradient cellular fractionation (Bruckner et al., 1999), a pool of V2 co-sedimented with the lipid raft proteins Flotillin (Salzer and Prohaska, 2001) and Caveolin-1 (Rothberg et al., 1992) along with, EGFR, tyrosine receptor Fyn (Pereira and Chao, 2007), Phosphoinositide 3-kinases (PI3K) (Gao et al., 2011), and Wnt-activated pLrp6 (Bilic et al., 2007; Yamamoto et al., 2006) **(Fig. 10B)**. This suggests the possibility that Cdc42V2 is actively involved in the signaling hubs at lipid rafts together with membrane receptors. The interaction of Cdc42 with EGFR was further validated for endogenous EGFR and Cdc42 variants **(Fig. 10C)**. Compared to Cdc42 V1, the V2-variant exhibited a stronger association towards both EGFR and clathrin **(Fig. 10C)**, consistent with V2's demonstrated stronger MAPK-activating capability **(Fig. 7B)**. A further examination of Cdc42 interactomes showed numerous structural and signaling components reported to be involved in EGFR endocytosis and MAPK cascade **(**see the proposed model in **Fig. 11A;** network view of these proteins in **Fig. 11B).** Thus, Cdc42 directly engaged EGFR-MAPK signaling.

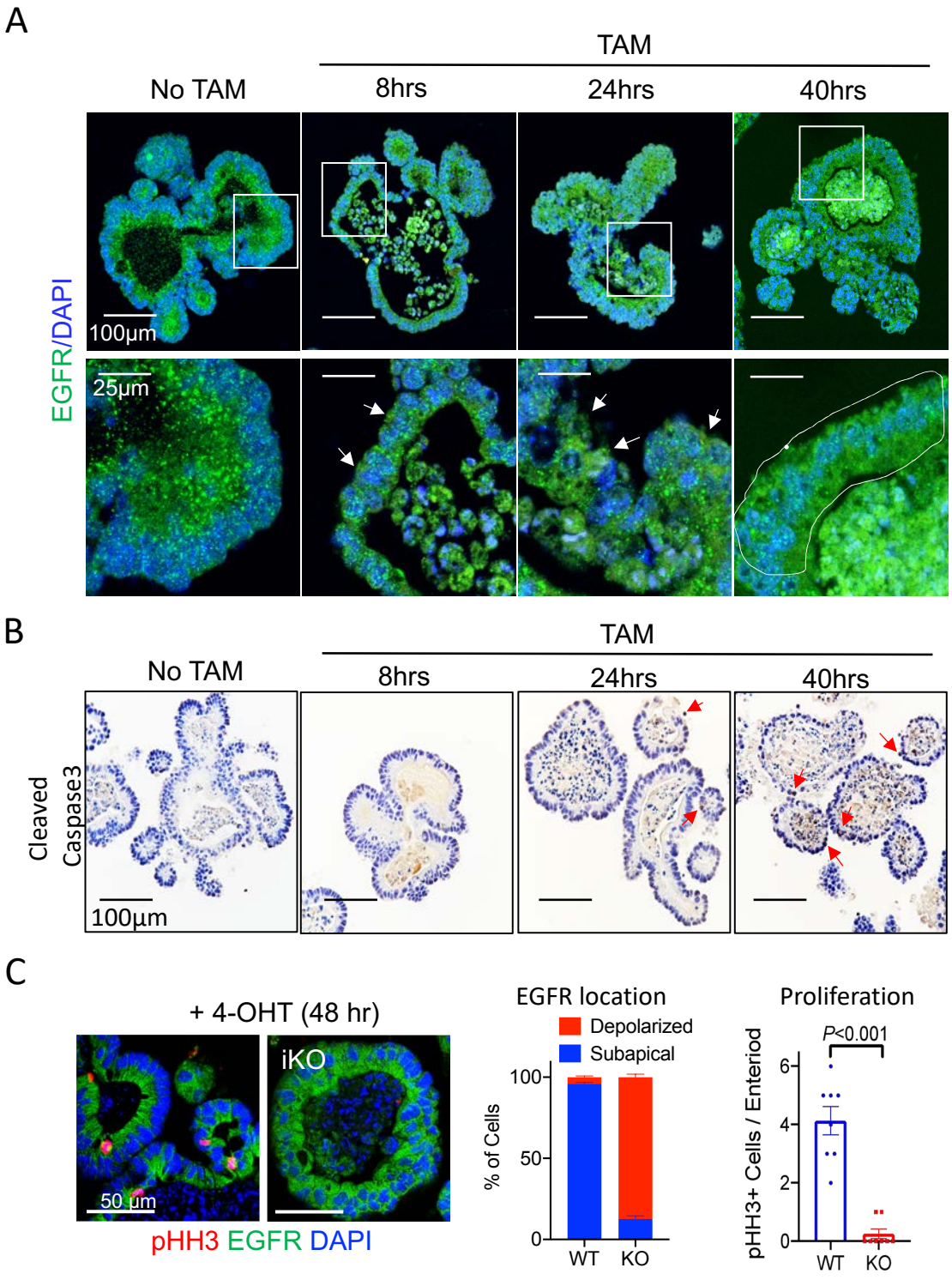
A
TAM
No TAM
8hrs
24hrs
40hrs
EGFR/DAPI
100μm
25μm
B
TAM
No TAM
8hrs
24hrs
40hrs
Cleaved Caspase3
100μm
C
+ 4-OHT (48 hr)
iKO
50 μm
pHH3 EGFR DAPI
EGFR location
Depolarized
Subapical
% of Cells
100
50
0
WT
KO
Proliferation
P<0.001
pHH3+ Cells / Enteriod
6
4
2
0
WT
KO

Figure 8. Cdc42 is required for EGFR localization.

(A) Immunofluorescence staining of EGFR in enteroid sections after 4-OHT treatment. White arrows pointing at delocalized EGFR. (B) Immunohistochemistry staining of cleaved-caspase3 in enteroid sections after 4-OHT treatment. Red arrow pointing at cleaved-caspase3+ cells. (C) Immunofluorescence staining showed the primarily apical localization of EGFR observed in WT enteroid cells was clearly altered in iKO cells 48 hrs after 4-OHT treatment. pHH3+ cell number was diminished in iKO organoids.

A

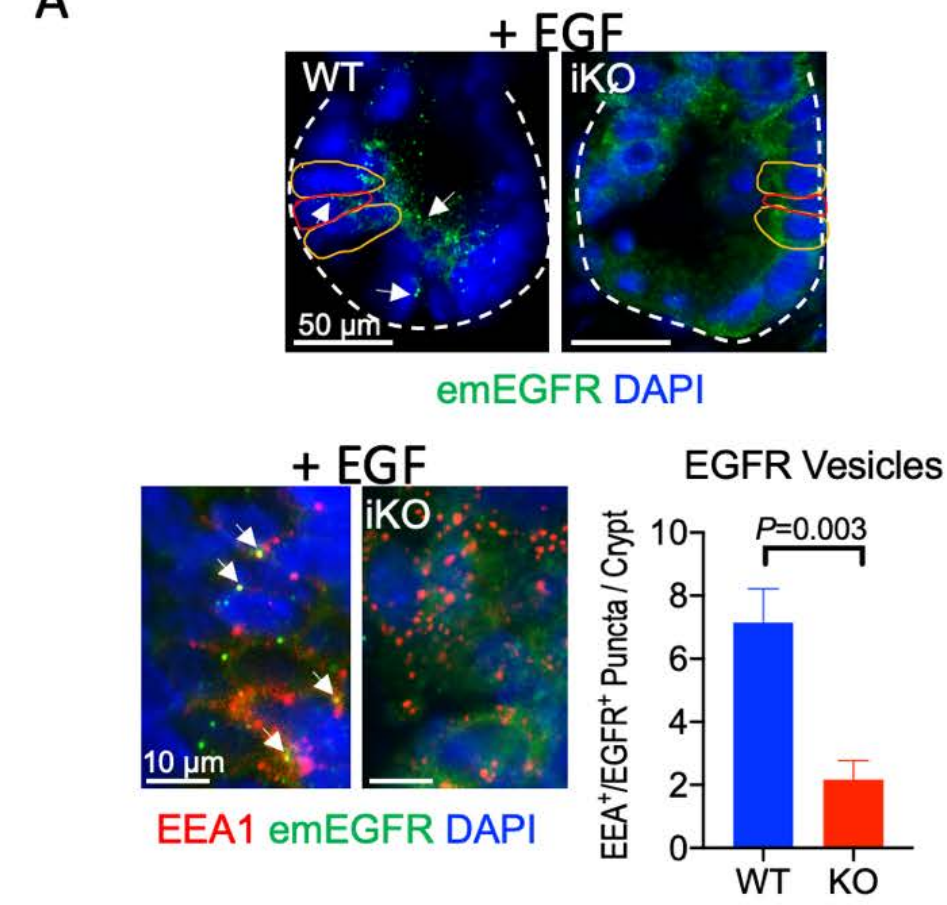
+ EGF
WT
iKO
50 μm
emEGFR DAPI
+ EGF
iKO
10 μm
EEA1 emEGFR DAPI
EGFR Vesicles
P=0.003
EEA+/EGFR+ Puncta / Crypt
10
8
6
4
2
0
WT
KO

B

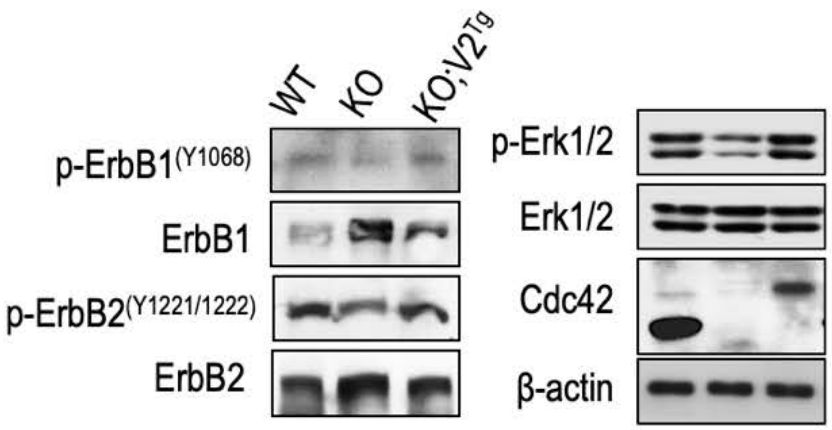
WT
KO
KO;V2Tg
p-ErbB1(Y1068)
ErbB1
p-ErbB2(Y1221/1222)
ErbB2
p-Erk1/2
Erk1/2
Cdc42
β-actin

Figure 9. Loss of Cdc42 impaired EGF-stimulated EGFR endocytic vesicles EGFR.

(A) Cdc42^{iKO} mice were crossed to a CRISPR-CAS9 engineered emEGFR mouse allele to visualize EGF-induced EGFR vesicular trafficking. 30-min after EGF injection, Emerald-EGFR vesicles (green, white arrows) were seen in Cdc42-WT mouse crypt cells, whereas barely detected in iKO crypt cells. Paneth cells are circled by yellow lines while CBCs are by red lines. Double fluorescent analysis for EEA1 (red) and emerald-EGFR (green) detected endocytic EGFR in WT crypt cells but not Cdc42^{iKO} cells 30 min after EGF injection. EEA1+/EGFR+ puncta per crypt were quantified from 4 mice in 2 independent experiments. (B) Western blots showed slight reductions in Cdc42 KO IECs of endogenous pErbB1 (Y1068), pErbB2 (Y1221/1222), and p-ERK1/2, which were restored to WT levels in Cdc42 KO; V2Tg mice. Note total ErbB1 and ErbB2 levels were increased in KOs.

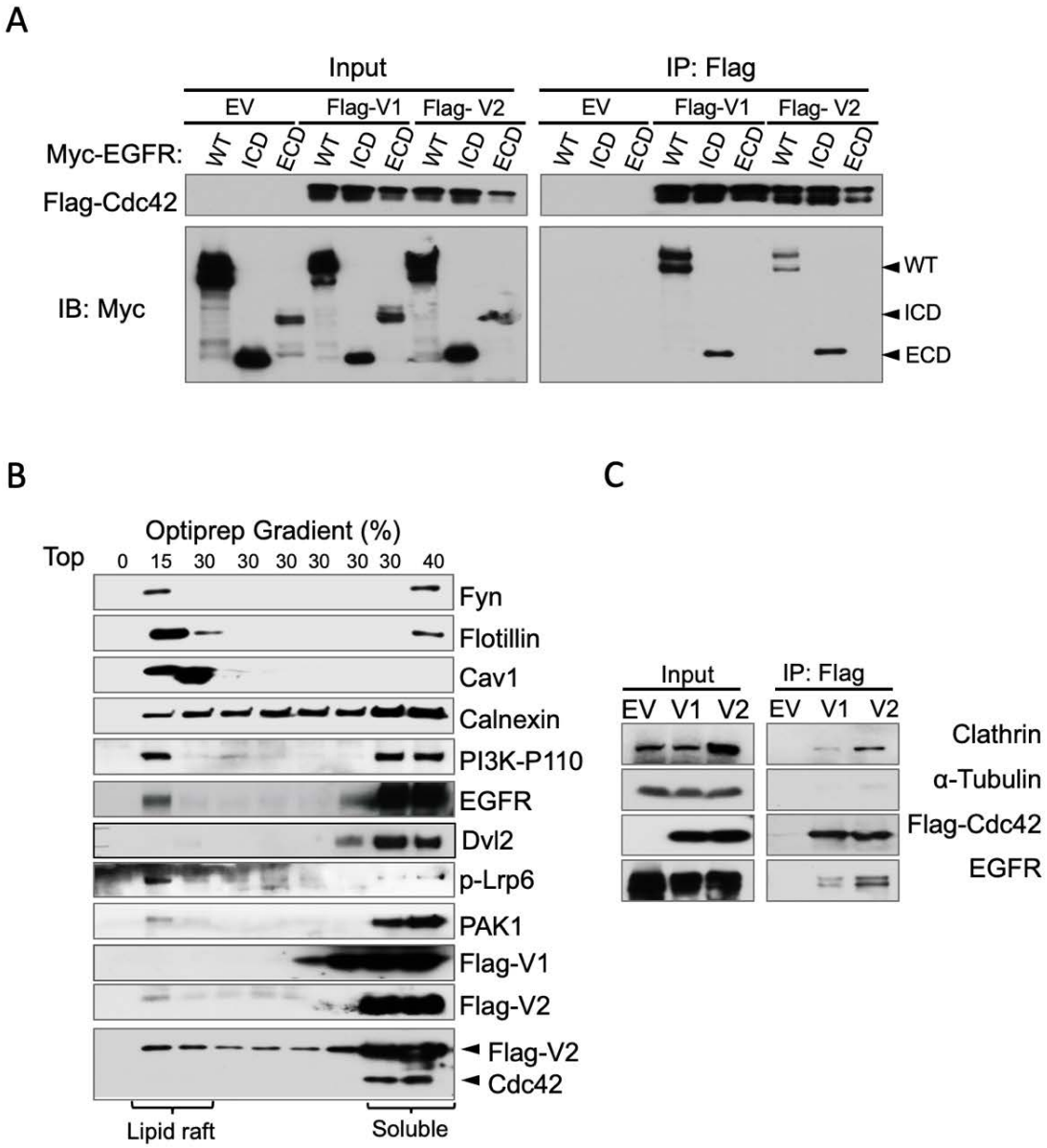
A
Input
IP: Flag
EV
Flag-V1
Flag- V2
Myc-EGFR:
WT
ICD
ECD
Flag-Cdc42
IB: Myc
WT
ICD
ECD
B
Optiprep Gradient (%)
Top
0 15 30 30 30 30 30 30 40
Fyn
Flotillin
Cav1
Calnexin
PI3K-P110
EGFR
Dvl2
p-Lrp6
PAK1
Flag-V1
Flag-V2
Flag-V2
Cdc42
Lipid raft
Soluble
C
Input
IP: Flag
EV V1 V2
EV V1 V2
Clathrin
α-Tubulin
Flag-Cdc42
EGFR

Figure 10. Cdc42 V2 co-fractionations with EGFR at lipid rafts, and associates with EGFR and Clathrin stronger than V1

(A) Flag-tagged Cdc42 variants showed co-immunoprecipitation with full length EGFR and the receptor's intracellular domain (ICD), but not the extracellular domain (ECD) in HEK293 cells. (B) Optiprep gradient cellular fractionation of HEK293 cells showed co-sedimentation of Cdc42-V2 with EGFR, p-LRP6, and PI3K-P110 in lipid raft fractions marked Fyn, Cav1, and Flotillin. Calnexin is an ER marker. Data represents 3 independent experiments (C) A side-by-side comparison of V1 and V2 showed stronger V2 interactions with endogenous EGFR and clathrin in HEK293 cells by immunoprecipitation.

A

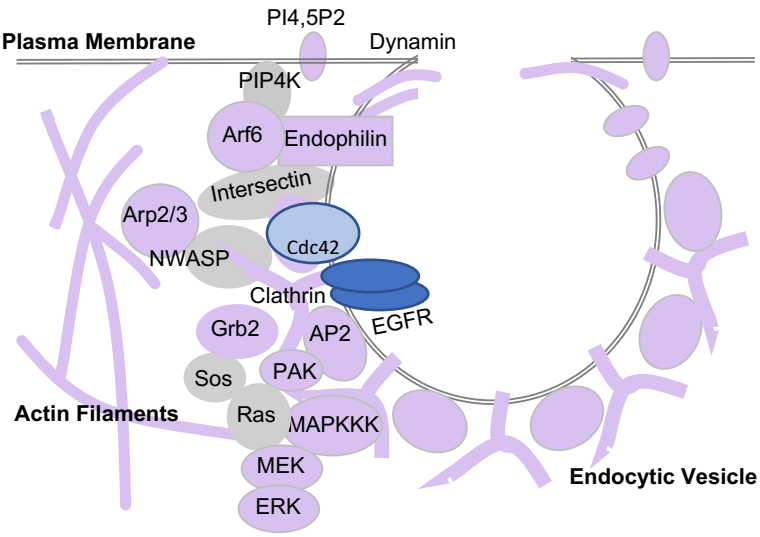

Actin	MAPKKK7	MYL6	MAPK1	Rab5C	DCTN2	Grb2	EHD4	MAPK3	AP-2b	SH3GLB1	DCTN1	DNM1L	AP-2S	ARF6	MYL2	Arp3/6
Myo9	CLTC	Myo10	Myo4/6	MYL12A	PAK 4	AP-2a-1	Arp2/3-2	Arp2/3-4	PIP4K-2a	MYL1/3	MAPK9	DNM3	CLINT1	SH3GL1	Arp2/3-3	Dynein

90 1

B

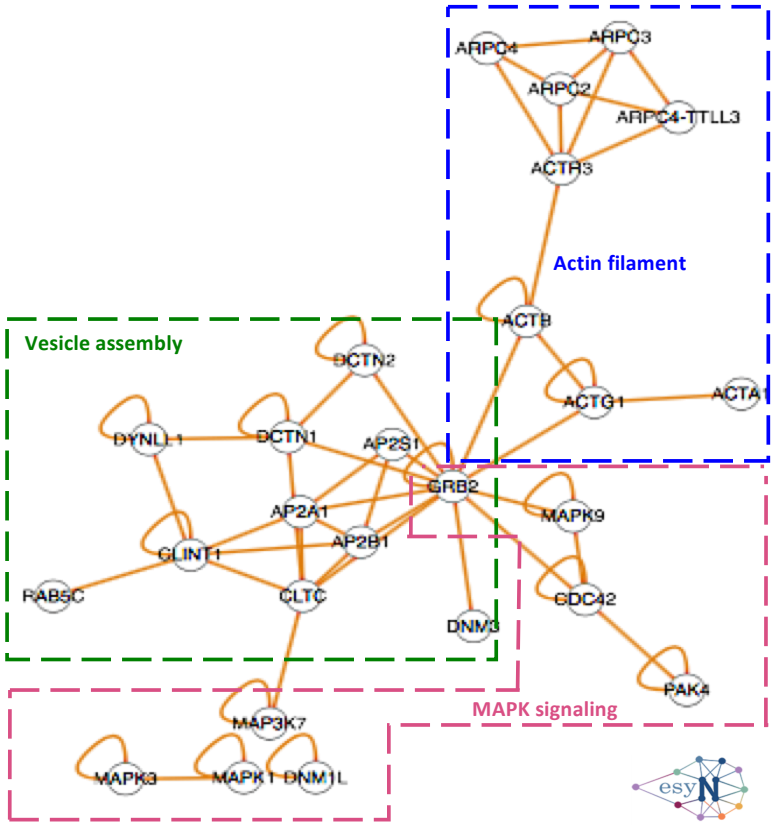

Figure 11 Schematic diagram proposing Cdc42 engagement in EGFR signalosome.

(A) A diagram illustrates structural and functional protein components identified in Cdc42 proteomics (**identified Cdc42 interacting proteins are in violet;** with peptide counts from 90 to 1) that were known to involve in clathrin-mediated trafficking, EGFR endocytosis, and MAPK cascade. Full data list shown in the **APPENDIX.** (B) EasN analysis of Cdc42 interactomes showed protein networks known to involve in EGFR endocytosis and MAPK signaling.

IEC specific Cdc42-V2 expression impacts epithelial differentiation in Cdc42$^{\Delta IEC}$ mice

To date, study of Cdc42 has been hampered by the absence of a gain-of-function *in vivo* model. We found that, in contrast to the ubiquitous expression of Cdc42 V1, expression of V2 could be detected in mouse enteroids **(Fig. 12A)** and fetal intestines, while its level was reduced in adult intestines **(Fig. 12B)**. V2 mRNA is also higher expressed in patient tumor tissue compared with adjacent non-tumor tissue **(Fig. 12C)**.

Based on V2's stronger MAPK-activating capacity, we sought to determine if elevating Cdc42 activity in adult IECs by overexpressing V2-variant (a naturally expressed protein) might enhance ISC function *in vivo*. We thus established an inducible mouse allele (referred to as *V2^{Tg}*), which allowed a Cre-activated cell-specific production of a Flag-tagged Cdc42-V2 **(Fig. 13A)**. We validated IEC-specific Cdc42-V2 production in small intestinal and colonic epithelia of independent *V2^{Tg}* founders crossed to *Villin-Cre* or *Villin-CreER* drivers by western blot **(Fig. 13B)** and by immunohistochemistry **(Fig. 13C)**. A *V2^{Tg}* founder producing V2 at approximately 40% of endogenous Cdc42 was selected for further experiments **(Fig. 13D)**. *Villin-Cre; V2^{Tg}* intestines (referred to as *V2^{Tg}* mice hereafter) had longer villi, more crypts **(Fig. 13E)**.

Examination of IEC cell types revealed that *V2^{Tg}* intestine had a reduction of Tuft cells by 80% while *Cdc42$^{\Delta IEC}$* intestines showed a complete loss of Tuft cells **(Fig. 14A, B)**. *V2^{Tg}* intestine showed no change in goblet cells **(Fig. 14C)**, while *Cdc42$^{\Delta IEC}$* intestines had an 30% increase in goblet cells **(Fig. 14C**. Interestingly,

expressing *V2*^{Tg} in *Cdc42*$^{\Delta IEC}$ intestinal epithelium significantly restored the Paneth cell defect **(Fig. 15A, B)** and microvillus inclusion phenotype **(Fig. 15C, D)** previously reported in *Cdc42*$^{\Delta IEC}$ intestines (Sakamori et al., 2012b). These data functionally validated this newly developed *V2*^{Tg} mouse allele and revealed an unknown impact of Cdc42-V2 on Tuft cell differentiation.

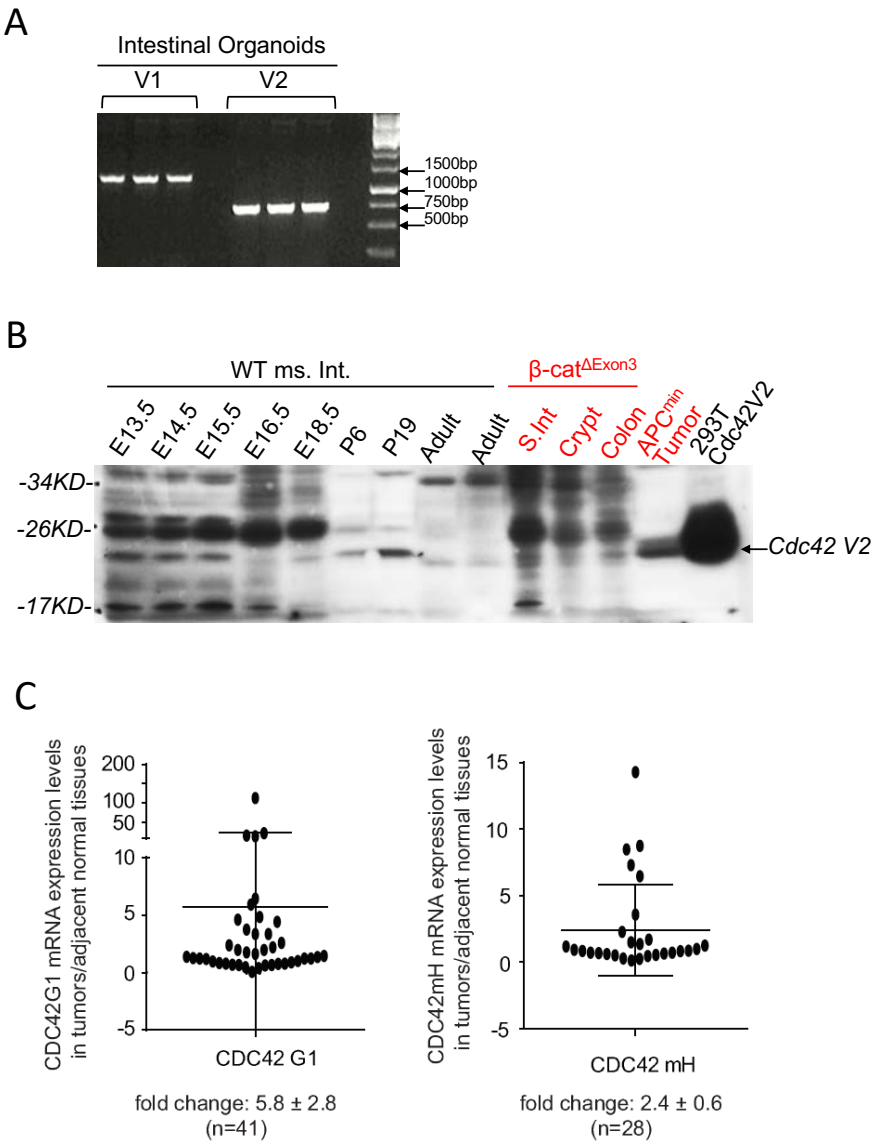

Figure 12. Cdc42 V2 is expressed in developing mouse intestine and enteroids, as well as in human colorectal cancer.

(A) RT-PCR detection of mRNAs of both Cdc42 variants in mouse enteroids. (B) Cdc42 V2 specific antibody detected V2 expression in fetal mouse intestines. The expression level reduced in adult intestinal tissue. HEK239T cells overexpressing V2 was used as a positive control. **(C)** Level of Cdc42 V1 and V2 mRNA in patient tumor tissue and adjacent non-tumor tissue detected by real-time PCR.

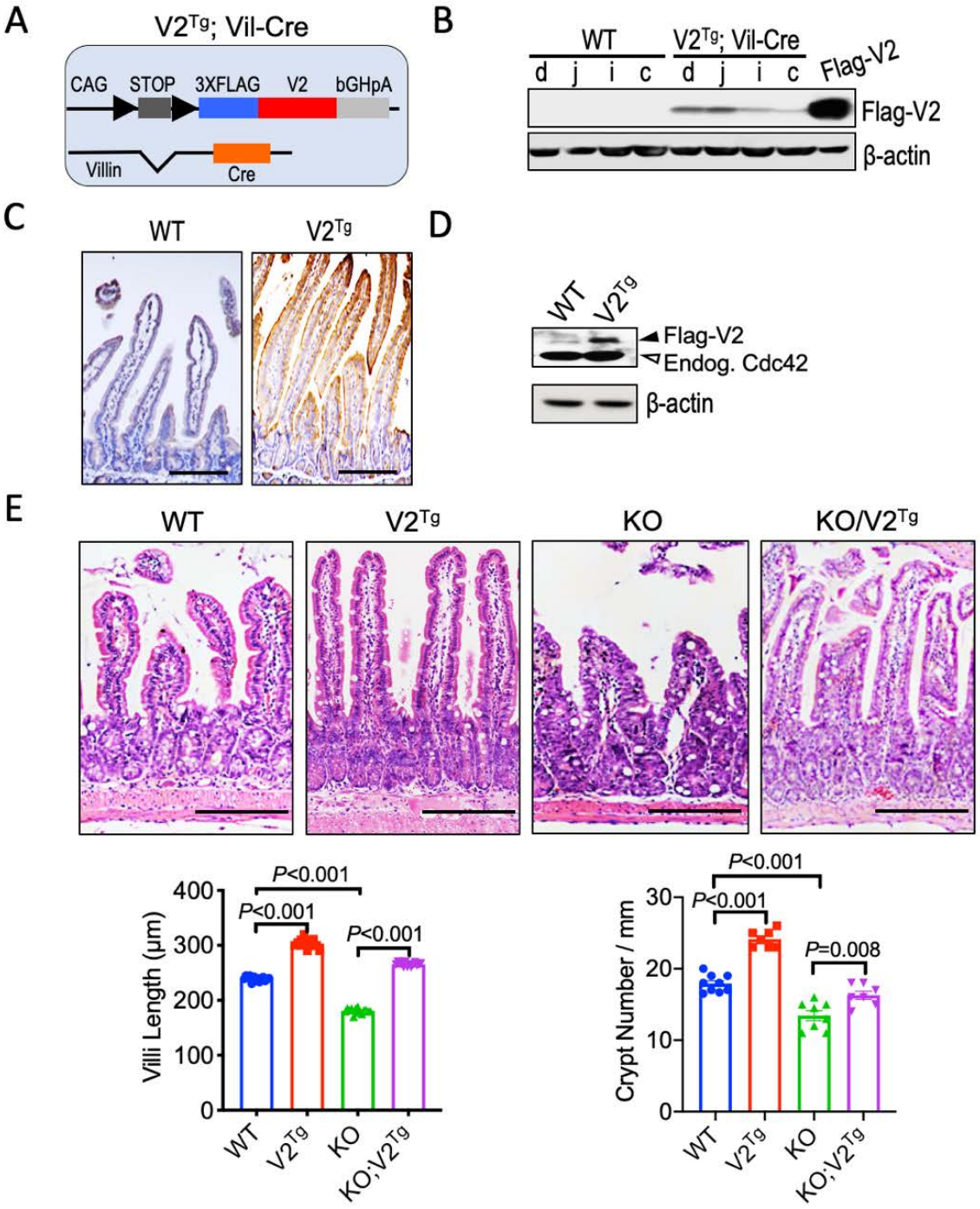
A
V2Tg; Vil-Cre
CAG
STOP
3XFLAG
V2
bGHpA
Villin
Cre
B
WT
V2Tg; Vil-Cre
d j i c d j i c
Flag-V2
Flag-V2
β-actin
C
WT
V2Tg
D
WT
V2Tg
Flag-V2
Endog. Cdc42
β-actin
E
WT
V2Tg
KO
KO/V2Tg
Villi Length (μm)
400
300
200
100
0
P<0.001
P<0.001
P<0.001
WT
V2Tg
KO
KO;V2Tg
Crypt Number / mm
30
20
10
0
P<0.001
P<0.001
P=0.008
WT
V2Tg
KO
KO;V2Tg

Figure 13. Overexpressing Cdc42 V2 in mouse intestinal epithelium.

(A) A schematic diagram shows the development of a new Cdc42 gain-of-function mouse model *V2^{Tg}*, which expresses a Flag-tagged V2 in Cre-dependent manner. A loxP-stop-loxP-3xFlag-V2-bGHpolyA cassette was inserted downstream of a CAG promoter. (B) Western blots detected Flag-V2 expression in duodenum, jejunum, ileum, and colon of *V2^{Tg}* driven by VilCre. HEK293 cells expressing Flag-V2 was used as positive control. (C) Immunohistochemistry detected Flag expression in *V2^{Tg}* mouse IECs. Images are representative of 3 independent mice per genotype. (D) Cdc42 antibody detected both V2 expression (upper band) at the level of approximately 40% of endogenous Cdc42 (empty arrowhead) in *V2^{Tg}* mice. (E) H&E staining of mouse intestine. *V2^{Tg}* small intestines showed longer villi and more crypts; KO showed blunted villi as well as fewer crypts.

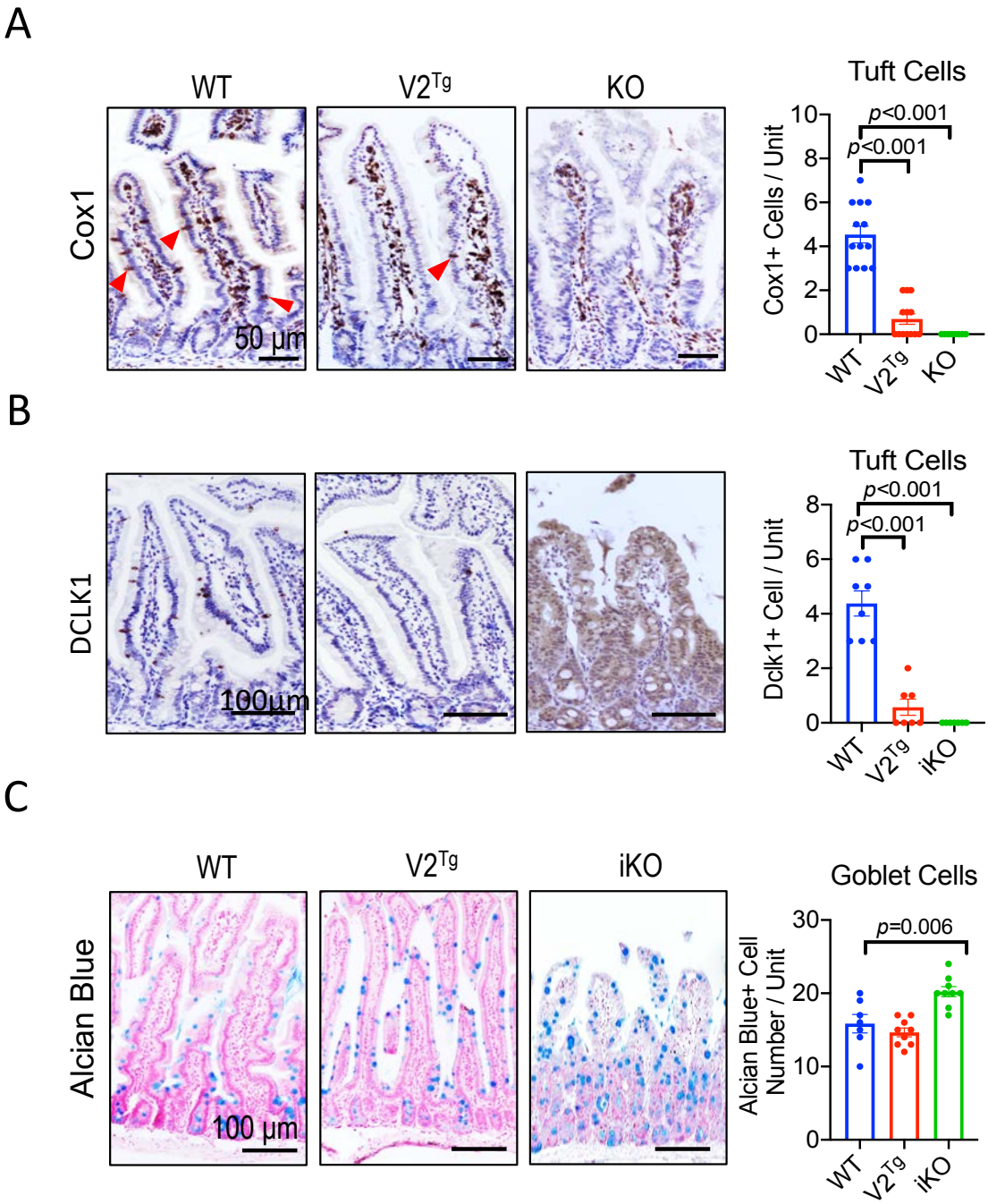
A
WT
V2Tg
KO
Cox1
50 μm
Tuft Cells
p<0.001
p<0.001
Cox1+ Cells / Unit
10
8
6
4
2
0
WT
V2Tg
KO
B
DCLK1
100μm
Tuft Cells
p<0.001
p<0.001
Dclk1+ Cell / Unit
8
6
4
2
0
WT
V2Tg
iKO
C
WT
V2Tg
iKO
Alcian Blue
100 μm
Goblet Cells
p=0.006
Alcian Blue+ Cell Number / Unit
30
20
10
0
WT
V2Tg
iKO

Figure 14. Examination of differentiated linages in *V2^{Tg}* mice.

(A) Immuno-histochemistry of Cox1+ cells, with red arrowhead pointing at Cox1+ cells; quantification of Cox1+ cell number per crypt-villus unit. (B) Immunohistochemistry for DCLK1+ Tuft cells and quantification from 3 animals per genotype. Quantification of intestinal villus length and crypt number from 3 animals per genotype. (C) Alcian Blue staining and quantification of Goblet cells.

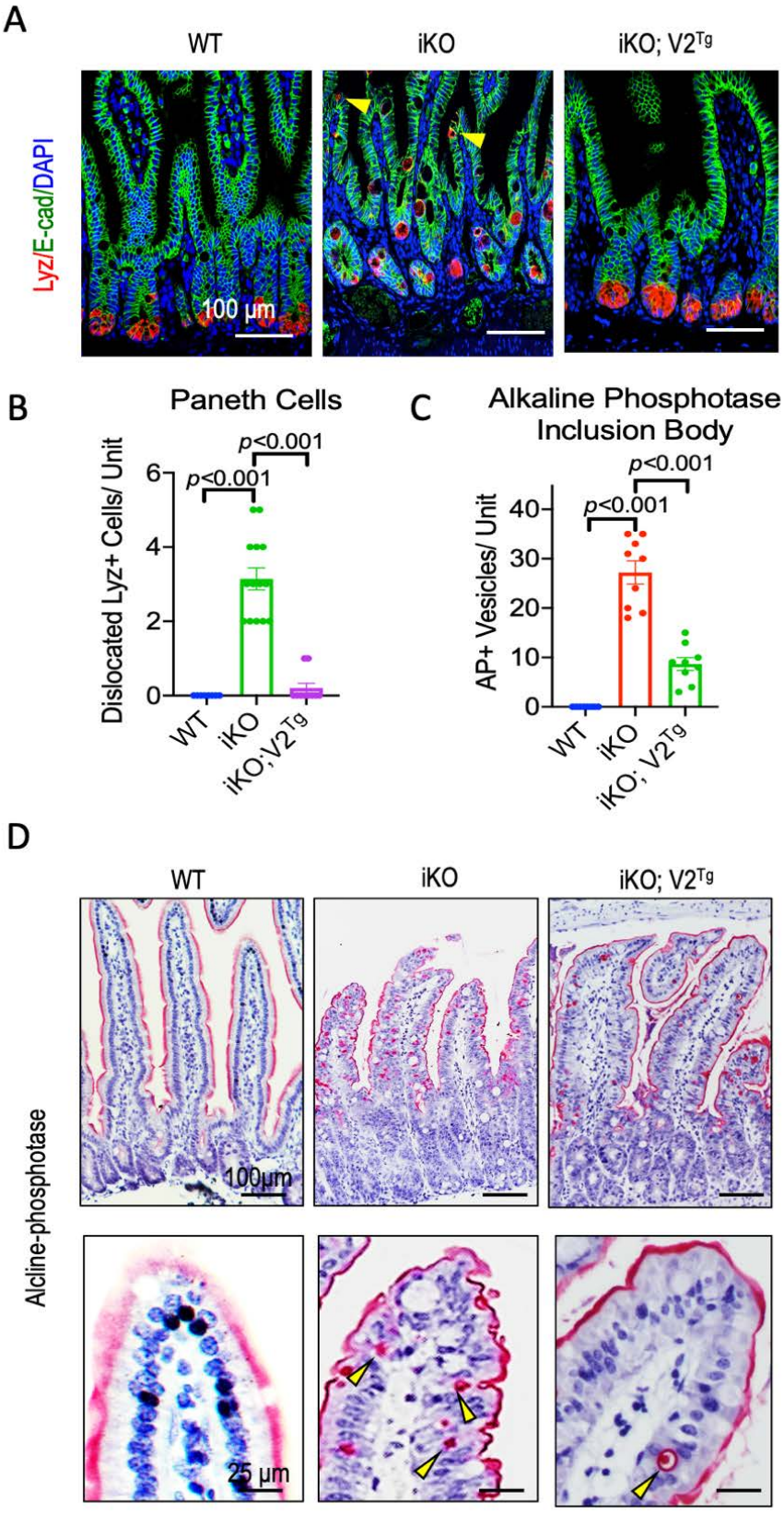
A
WT
iKO
iKO; V2Tg
Lyz/E-cad/DAPI
100 μm
B
Paneth Cells
Dislocated Lyz+ Cells/ Unit
p<0.001
p<0.001
WT
iKO
iKO;V2Tg
C
Alkaline Phosphotase Inclusion Body
AP+ Vesicles/ Unit
p<0.001
p<0.001
WT
iKO
iKO; V2Tg
D
WT
iKO
iKO; V2Tg
Alcline-phosphotase
100μm
25 μm

Figure 15. Re-expressing V2 in Cdc42 iKO epithelium mitigates Paneth cell dislocation and AP+ inclusion.

(A) Immunofluorescent staining for Lyz1+ Paneth cells (red), E-cad (green), and DAPI (blue). (B) Quantification of mis-localized Paneth cells. (C) Quantification of AP+ inclusion bodies showed a rescue by V2 expression in iKO IECs. (D) Alkaline phosphatase (AP) staining showed representative AP+ inclusion bodies (arrows) in iKO IECs.

Cdc42-V2 robustly elevates ISC function in vivo

Inhibition of MAPK by EGFR inhibitor in enteroid culture was shown to promote Tuft cell differentiation (Basak et al., 2017). The observed loss of Tuft cell differentiation in both gain- and loss-of-Cdc42 function prompted us to examine the impact of Cdc42 on ISC functions. Quantitative RT-PCR detected a 5-fold increase in *Cdc42* mRNA level in ISC-enriched enteroids treated with CHIR99021 and valproic acid (Kishida et al., 2017; Yin et al., 2014) as compared to enteroids typically grown in ENR medium **(Fig. 16A)**. Bulk RNA-seq of $Cdc42^{\Delta IEC}$ intestines affirmed a transcriptomic reduction of Lgr5 ISC gene signature (p=0.007, **Fig. 16B**).

Intestinal length was shown to positively correlate with ISC function (Riehl et al., 2012; Weaver et al., 1991). $Cdc42^{\Delta IEC}$ mice had shorter intestines (73% of WT littermates, **Fig. 17A**), while *Villin-Cre;*$V2^{Tg}$ mice with elevated Cdc42-V2 in IECs had longer intestines, 112% of WT mice **(Fig. 17A)**,. $V2^{Tg}$ intestines had increased levels of Olfm4, an ISC marker, in crypts **(Fig. 17B)**, along with elevated levels of markers of both fast-cycling and “quiescent” ISCs, in particular Bmi1 **(Fig. 17C)**.

Importantly, we observed a pronounced expansion of pERK1/2^{+} active cell population to the villus region in $V2^{Tg}$ intestines **(Fig. 18A)**. By contrast, pERK1/2^{+} cells in WT mice were restricted to crypt and transit amplifying compartments as previously reported (Geske et al., 2008; Heuberger et al., 2014b). Scattered pERK1/2^{+} cells were present throughout $Cdc42^{\Delta IEC}$ villus epithelium. We also detected elevated a beta-catenin level in $V2^{Tg}$ intestine **(Fig. 18B)**, in overall agreement with an enhanced ISC function in homeostasis. We established $Cdc42^{\Delta IEC}$*;* $V2^{Tg}$ mice where deletion of endogenous Cdc42 and production of the

V2 transgene were driven by Cre in same IECs. *Cdc42*$^{\Delta IEC}$; V2^{Tg} mice showed largely restored IEC phenotypes compared to *Cdc42*$^{\Delta IEC}$ mice **(Fig. 17-18)**. These phenotypic restorations were accompanied by restoration of pErbB1, pErbB2, and pERK1/2 levels in *Cdc42*$^{\Delta IEC}$*; V2*^{Tg} mouse intestines **(Fig. 9B)**.

Ex vivo, *V2*^{Tg} enteroids exhibited a much more robust epithelial budding **(Fig. 18C, D)**, larger sizes **(Fig. 18C, D)**, and increased proliferation activities **(Fig.18E).** Thus, elevating epithelial Cdc42-V2 autonomously enhanced ISC function at steady state.

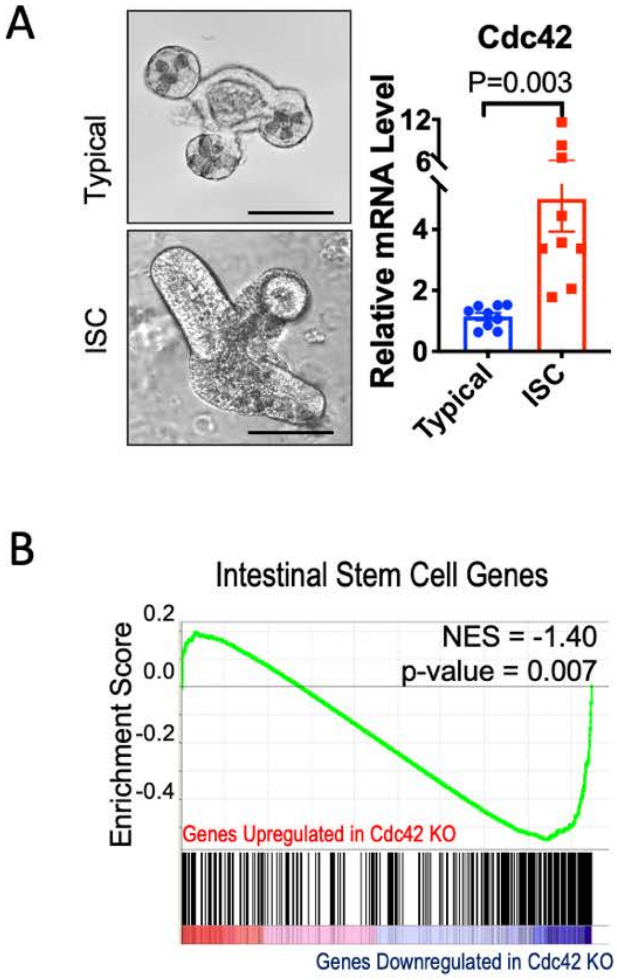

Figure 16. Enrichment of Cdc42 expression in ISCs coordinates with reduced ISC marker level in Cdc42 KO intestine.

(A) Bright field images of a typical and an ISC enriched enteroid treated by CHIR99021 and valproic acid. Quantification RT-PCR detected higher Cdc42 mRNA in ISC enteroids. (B) Gene set enrichment analysis (GSEA) of bulk RNA-seq showed a significantly reduced Lgr5 ISC gene signature (p=0.007) in iKO compared to WT IECs.


A
WT
V2Tg
KO
KO/V2Tg
Intestine length
P<0.001
P=0.004
P=0.003
Relative to WT
1.2
1.0
0.8
0.6
WT
V2TG
KO
KO;V2Tg

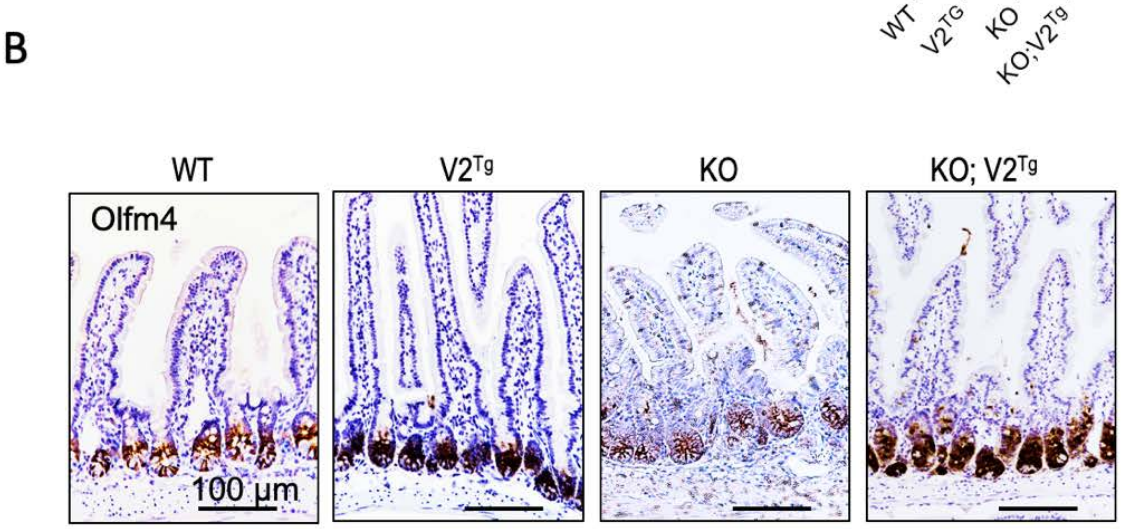
B
WT
V2Tg
KO
KO; V2Tg
Olfm4
100 μm

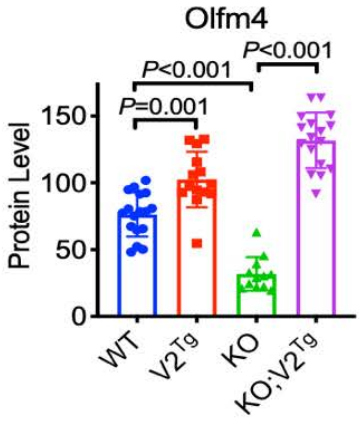
Olfm4
P<0.001
P<0.001
P=0.001
Protein Level
150
100
50
0
WT
V2Tg
KO
KO;V2Tg

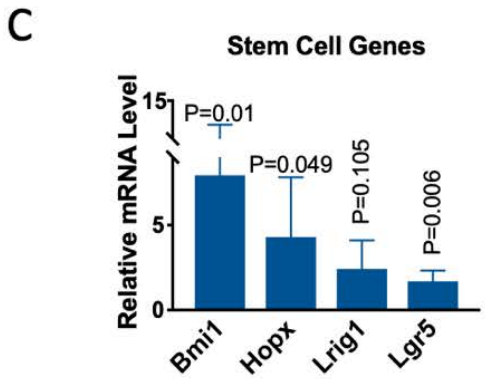
C
Stem Cell Genes
Relative mRNA Level
15
5
0
P=0.01
P=0.049
P=0.105
P=0.006
Bmi1
Hopx
Lrig1
Lgr5

Figure 17. Intestine gross morphology and Evaluation of stem cells in $V2^{Tg}$ mice.

(A) Representative gross morphology of *WT, $V2^{Tg}$, KO* and *KO; $V2^{Tg}$* mouse intestines. Note *$V2^{Tg}$* intestine is noticeably longer than littermate WT. (B) Immunohistochemistry for Olfm4 showed increased crypt base ISCs in *$V2^{Tg}$* intestines and decreased ISCs in KO intestines. Average Olfm4 protein level within crypt were quantified from multiple intestinal sections of a total of 3 animals per genotype. (C) qRT-PCR for ISC markers in *$V2^{Tg}$* mice relative to WT mice showed significant increase of Bmi1, Hopx and Lgr5. N=3 for each genotype.

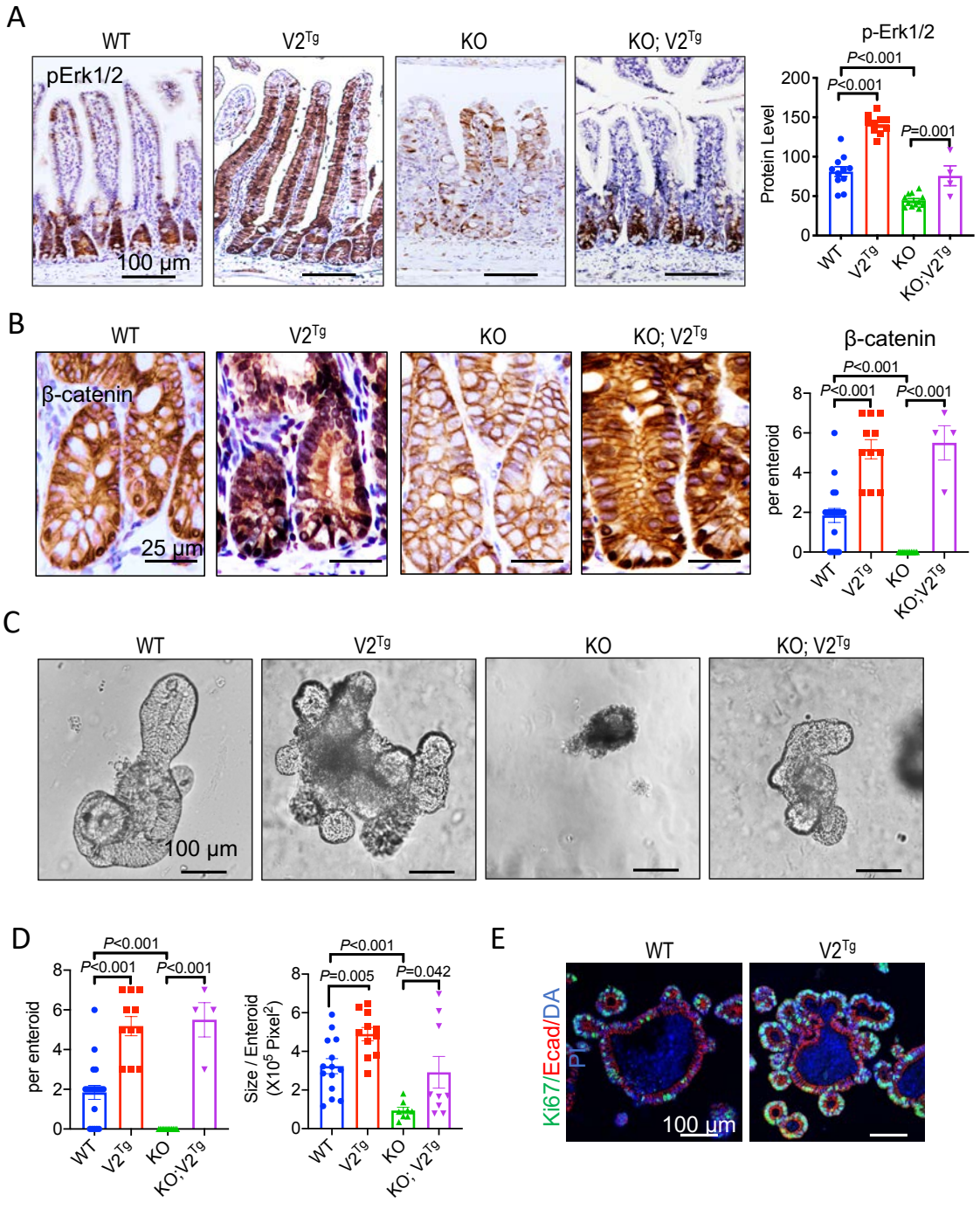
A
WT
V2Tg
KO
KO; V2Tg
pErk1/2
100 μm
p-Erk1/2
P<0.001
P<0.001
P=0.001
Protein Level
200
150
100
50
0
WT
V2Tg
KO
KO;V2Tg
B
WT
V2Tg
KO
KO; V2Tg
β-catenin
25 μm
β-catenin
P<0.001
P<0.001
P<0.001
per enteroid
8
6
4
2
0
WT
V2Tg
KO
KO;V2Tg
C
WT
V2Tg
KO
KO; V2Tg
100 μm
D
P<0.001
P<0.001
P<0.001
per enteroid
8
6
4
2
0
WT
V2Tg
KO
KO;V2Tg
P<0.001
P=0.005
P=0.042
Size / Enteroid (X10^5 Pixel^2)
8
6
4
2
0
WT
V2Tg
KO
KO; V2Tg
E
WT
V2Tg
Ki67/Ecad/DA
PI
100 μm

Figure 18. Increased pERK and β-catenin level in *V2^{Tg}* mice; Enhanced growth of enteroids from *V2^{Tg}* mice

(A) Compared to WT mice, pERK1/2+ cells were expanded in *V2^{Tg}* intestines and became scattered in KO intestines. Average pERK1/2 level within a crypt-villus unit were quantified from multiple intestinal sections of a total of 3 animals per genotype. (B) Immunohistochemistry for β-catenin showed increased nuclear β-catenin in *V2^{Tg}* crypt cells. N=2 for each genotype. (C) Representative enteriods of designated genotypes. (D) The average number of epithelial buds per enteroid and the average size of enteroid were quantified from 3 animals per genotype. (E) Immunofluorescent staining of enteroid sections showed increased Ki67+ cells in epithelial buds of *V2^{Tg}* enteroids.

Cdc42-V2 mitigates injury-induced epithelial damage

Prompted by above results, the impact of V2 expression on epithelial regeneration after injury was examined. ISCs are sensitive to irradiation (Potten, 1977) with fast-cycling ISCs dying within 2 days after irradiation (Gong et al., 2016; Kim et al., 2017a; Metcalfe et al., 2014). Mice were exposed to 12 Gy total-body irradiation **(Fig. 19A).** Compared to WT littermates, *Cdc42*$^{\Delta IEC}$ mice lost nearly 25% of body weight 4 days after irradiation **(**green line, **Fig. 19B)**. This was accompanied by declining body conditions and 25% post-irradiation mortality of *Cdc42*$^{\Delta IEC}$ mice within a week. All *WT, V2*^{Tg}, and *Cdc42*$^{\Delta IEC}$*; V2*^{Tg} mice survived the experimental duration. *V2*^{Tg} mice were resistant to body weight loss and exhibited an earlier weight recovery **(**red line, **Fig. 19B)**, while *Cdc42*$^{\Delta IEC}$*; V2*^{Tg} mice showed improved body weight and health condition compared to *Cdc42*$^{\Delta IEC}$ mice **(**purple line, **Fig. 19B)**. Examination of intestines revealed that *Cdc42*$^{\Delta IEC}$ intestines were 24% shorter than *WT*s **(Fig. 19C)**, with reduced numbers of regenerative crypts **(Fig. 19D)**.

At mRNA level, both proliferating and quiescent stem cell genes Olfm4 and HopX were elevated in *V2*^{Tg} mice post irradiation **(Fig. 20A)**. Consistent with the elevation of stem cell marker mRNA level, more Olfm4^{+} crypts were detected in *V2*^{Tg} mice **(Fig. 20B)**.

Furthermore, 24-hr EdU labeling (red) followed by a 30-min BrdU labeling (green) before sacrifice **(Fig. 19A)** indicated that *Cdc42*$^{\Delta IEC}$ mice had reduced cycling cells as well as cell-cycle re-entry indicated by EdU^{+}/BrdU^{+} cells **(Fig. 21A, B).** *Cdc42*$^{\Delta IEC}$ mice also had reduced numbers of cells migrating into villus epithelia

(arrows in **Fig. 21A, C)**. V2 expression enhanced IEC proliferation, migration and restored above-illustrated phenotypic defects in *Cdc42$^{\Delta IEC}$; V2^{Tg}* mice **(Fig. 21A-C).**

Elevating ISC-specific Cdc42 enhances regeneration after irradiation-induced injury.

The above experiments used pan-IEC Cre drivers and thus limited insights about role of Cdc42 specific to ISCs. To offset this limitation, *V2^{Tg}* was specifically targeted to Lgr5 ISCs and tested to determine if this would be sufficient to enhance their regeneration after injury. Lineage-tracing of Lgr5^{+} ISCs was conducted in 12 Gy irradiated *Lgr5$^{CreER\text{-}IRES\text{-}EGFP}$; R26R^{zsGreen}; V2^{Tg}* mice, where V2 production was restricted to Lgr5 ISCs. Compared to Cdc42-WT mice, *Lgr5$^{CreER\text{-}IRES\text{-}EGFP}$; R26R^{zsGreen}; V2^{Tg}* mice showed significantly more lineage tracing events (illustrated by ratio of green stripes / green crypts) with elevated mitosis in traced crypts **(Fig. 21D-F)**. In contrast, *Cdc42$^{Fl/FL}$; Lgr5$^{CreER\text{-}IRES\text{-}EGFP}$; R26R^{zsGreen}* mice lacking Cdc42 in ISCs showed drastically reduced lineage tracing events accompanied by reduced mitosis **(Fig. 21D-F).** Thus, Cdc42 is an ISC-autonomous machinery and elevating Cdc42-V2 was sufficient to mitigate epithelial damage after injury.

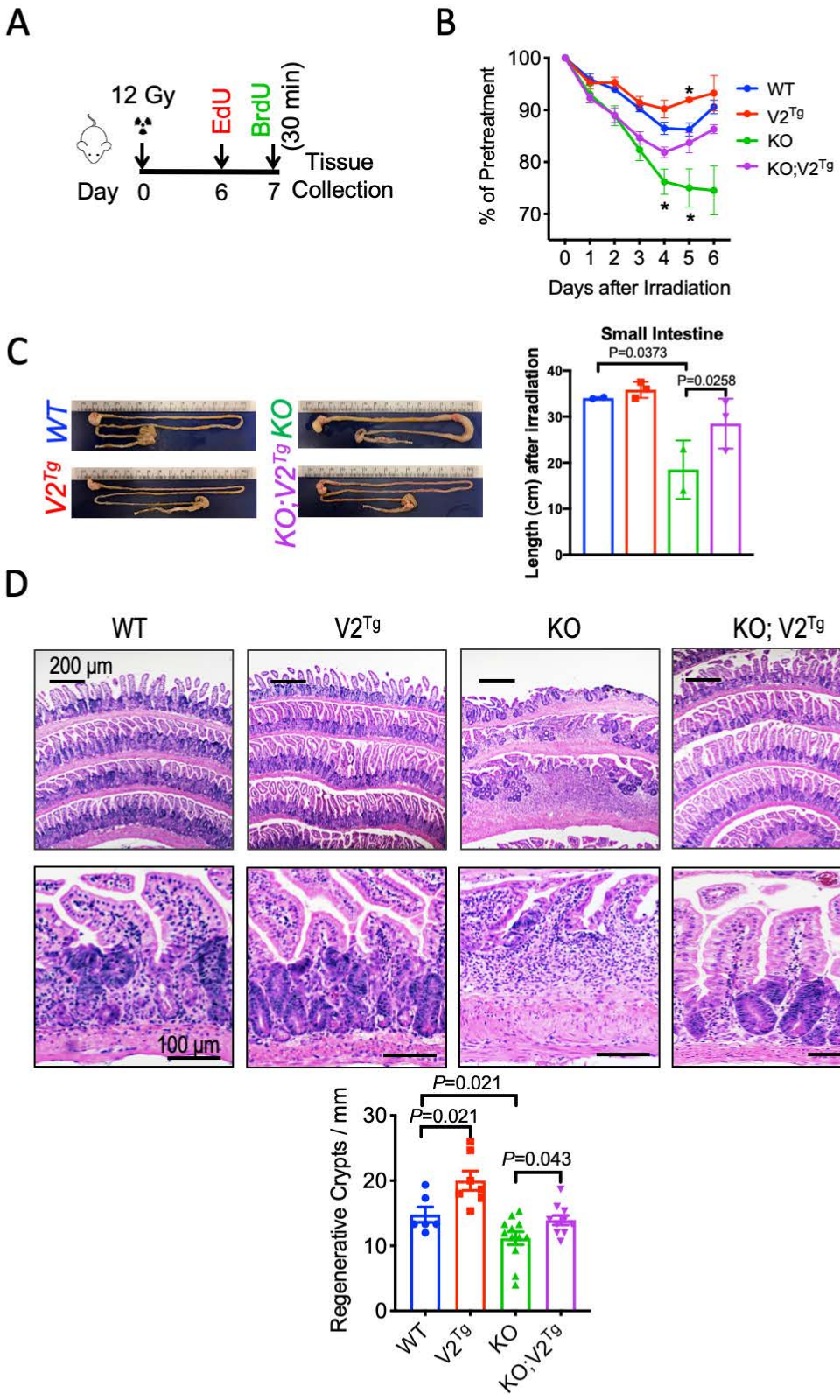
A
12 Gy
EdU
BrdU
(30 min)
Tissue Collection
Day 0 6 7
B
% of Pretreatment
Days after Irradiation
WT
V2Tg
KO
KO;V2Tg
C
WT
V2Tg
KO
KO;V2Tg
Small Intestine
P=0.0373
P=0.0258
Length (cm) after irradiation
D
WT
V2Tg
KO
KO; V2Tg
200 µm
100 µm
P=0.021
P=0.021
P=0.043
Regenerative Crypts / mm

Figure 19. Elevating epithelial Cdc42 reduces body weight loss, increases gut length and mitigates mucosal damage.

A) Schematic diagram shows that mice received 12 Gy total body irradiation and were sacrificed 7 days after irradiation. Labeling of cycling IECs that re-entered cell-cycle was accomplished by sequential injection of EdU (1 day) and BrdU (30 min) before sacrifice. (B) Body weight changes after irradiation are presented as percentage of initial body weight of individual mice. Eight mice per genotype were subjected to irradiation. Note there was a loss of KO animals during the experiment following irradiation. (C) Representative images and quantifications showing the gross intestinal morphology of designated genotypes 7 days after irradiation. Note a clear elongation of $V2^{Tg}$ gut length and a severe shortening of KO gut. (D) Images of post-irradiation ileal sections of designated genotypes 3 days after irradiation. Average numbers of regenerative crypts per mm were quantified from multiple ileal sections of 2 post-irradiation animals per genotype. They were increased in $V2^{Tg}$ intestines and decreased in KO intestines.

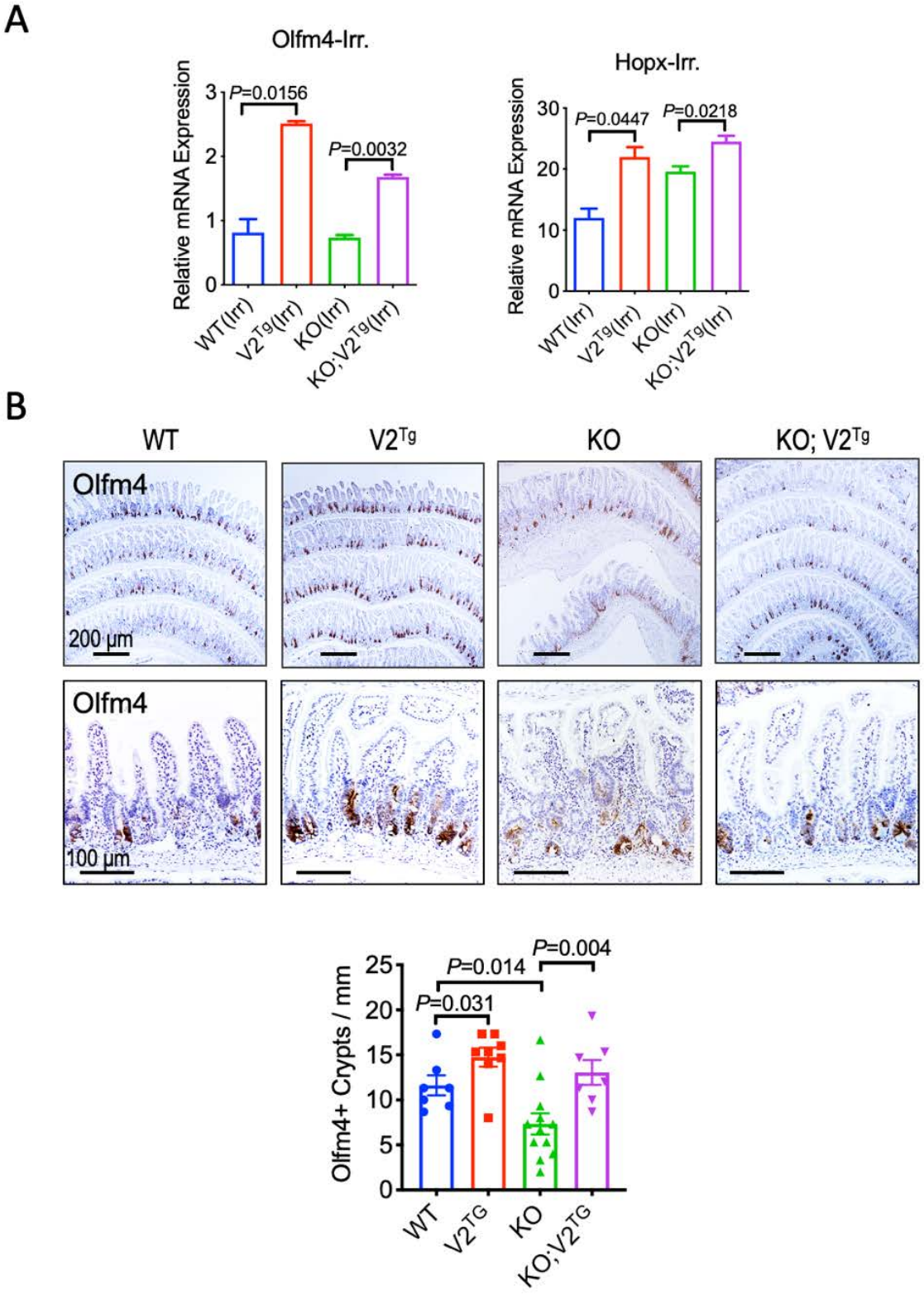
A
Olfm4-Irr.
Relative mRNA Expression
P=0.0156
P=0.0032
WT(Irr)
V2Tg(Irr)
KO(Irr)
KO;V2Tg(Irr)
Hopx-Irr.
P=0.0447
P=0.0218
B
WT
V2Tg
KO
KO; V2Tg
Olfm4
200 μm
100 μm
Olfm4+ Crypts / mm
P=0.031
P=0.014
P=0.004
WT
V2TG
KO
KO;V2TG

Figure 20. Elevating epithelial Cdc42 increases Olfm4 expression during injury-induced repair.

(A) qRT-PCR for ISC markers in *V2*^{Tg} mice relative to WT mice showed significant increase of Olfm4 and Hopx after irradiation. N=3 for each genotype. (B) Representative images of crypts containing Olfm4+ cells. Quantified from multiple ileal sections of 2 post-irradiation animals per genotype.

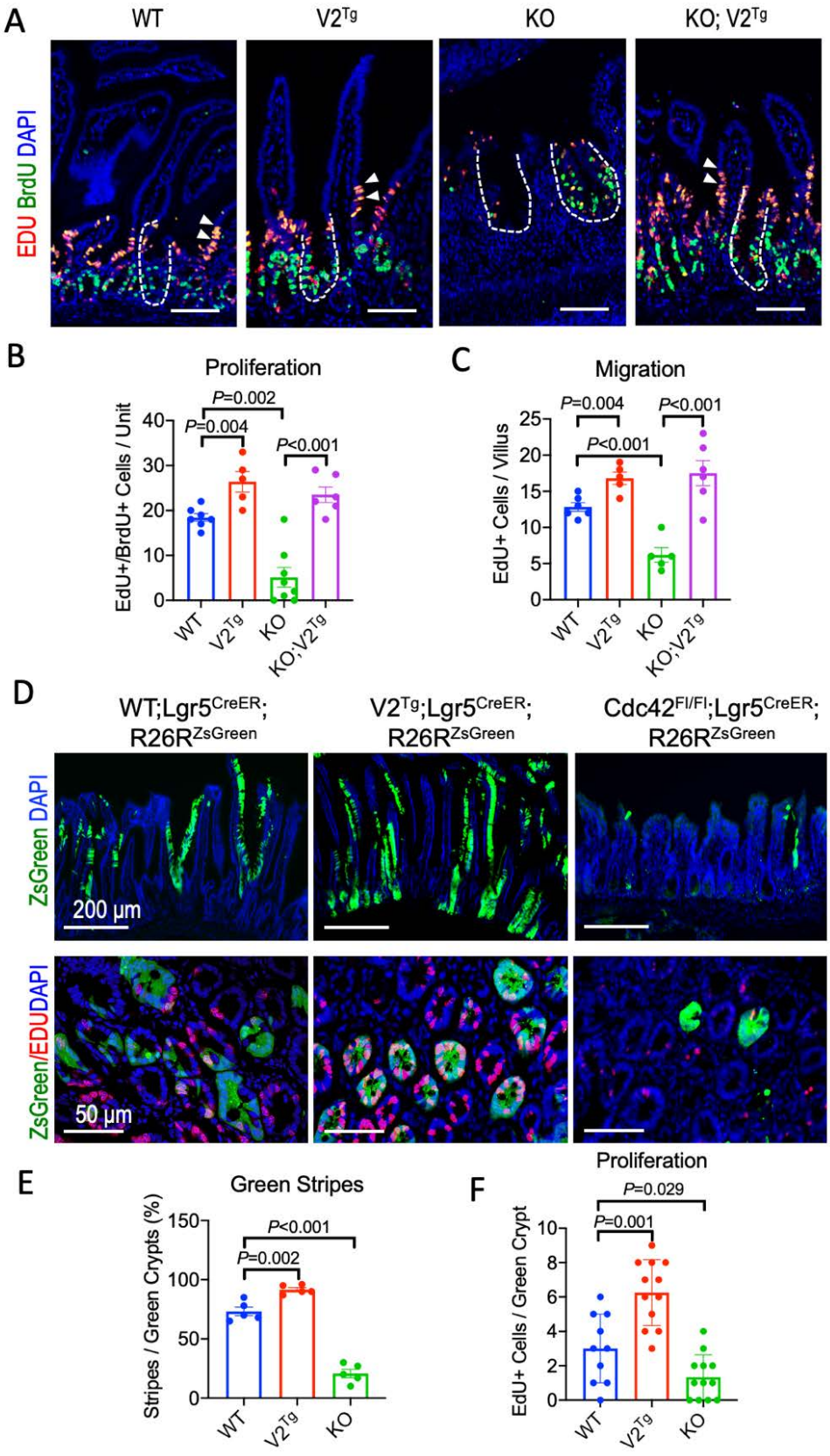
A
WT
V2Tg
KO
KO; V2Tg
EDU BrdU DAPI
B
Proliferation
EdU+/BrdU+ Cells / Unit
P=0.002
P=0.004
P<0.001
WT
V2Tg
KO
KO;V2Tg
C
Migration
EdU+ Cells / Villus
P=0.004
P<0.001
P<0.001
D
WT;Lgr5CreER; R26RZsGreen
V2Tg;Lgr5CreER; R26RZsGreen
Cdc42Fl/Fl;Lgr5CreER; R26RZsGreen
ZsGreen DAPI
200 μm
ZsGreen/EDUDAPI
50 μm
E
Green Stripes
Stripes / Green Crypts (%)
P<0.001
P=0.002
F
Proliferation
EdU+ Cells / Green Crypt
P=0.029
P=0.001

Figure 21. Elevating epithelial Cdc42 enhances proliferation, migration and ISC lineage tracing after irradiation.

(A) EdU (Red) and BrdU (Green) staining of mouse intestines 3 days after irradiation. Dashed lines indicate crypts; white arrows point to EdU+/BrdU+ IECs migrating to villi. Nucleus is counterstained with DAPI (Blue). (B) Average numbers of EdU or/and BrdU labeled IECs per crypt-villus unit were quantified from multiple sections of 3 post-irradiation animals per genotype. (C) Average numbers of only EdU-labeled IECs in upper crypt and villus region were quantified from multiple sections of 3 post-irradiation animals per genotype. (D) Lineage tracing of Lgr5 ISCs of distinct (Cdc42-*WT, V2*^{Tg}, or *KO*) genotypes 7 days after irradiation using a R26RZsGreen reporter. EdU was injected 6 hrs before sacrifice to identify cycling ISC descendants. (E) Lineage tracing events are presented as percentage of observed green stripes out of total number of green crypts within the same field. Data represent multiple sections of 2 post-irradiation animals. Note that *V2*^{Tg} and *KO* ISCs showed increased and diminished lineage tracing events. (F) The average numbers of EdU+ cells per green crypt were quantified from multiple sections of 2 post-irradiation animals.

DISCUSSION

Current data provides molecular, genetic, and cell biological insight into underlying mechanism that provide intestinal epithelial tissue with extraordinary regenerative capacity in response to injury. Our molecular and genetic experiments produced new insights into how exactly Cdc42 regulates MAPK and potentially other signaling pathways related to ISC survival. Based on atomic force microscopic study, proteomics, and kinase array analysis, we demonstrated at molecular and nanomechanical levels that Cdc42 is required for ligand-stimulated EGFR endocytosis and MAPK signaling. Cdc42-deficient IECs lost responses to both EGF and Wnt ligands that activate MAPK.

EGFR signaling possesses a foundationally conserved role in regulating gut development and cell proliferation in lower (Buchon et al., 2010; Jiang and Edgar, 2009; Jiang et al., 2011; Jiang et al., 2016; Jin et al., 2015; Pyo et al., 2018; Xu et al., 2011) and higher eukaryotic species (Mytych et al., 2018; Satora et al., 2018). The requirement of EGF initiated signaling for epithelial survival and renewal is extensively documented (Cordero et al., 2014; Liang et al., 2017; Suzuki et al., 2010; Takeda and Kiyokawa, 2017; Yang et al., 2017), and is proposed to keep $Lgr5^{+}$ ISCs in a constitutively active state (Basak et al., 2017). EGFR-MAPK signaling may enhance intestinal epithelial survival by preventing cell shedding (Miguel et al., 2017). Proper intraepithelial EGFR localization has also been shown to define cell-type specific functions (Ungewiss et al., 2018). These studies and the reported contribution of EGFR signaling to injury-induced tissue regeneration (Gregorieff et al., 2015; Ren et al., 2010) were consistent with our observed impact

of Cdc42 on EGFR-MAPK cascade and cell survival *in vitro* and *in vivo*.

Cdc42 has 2 physiologically transcribed isoforms with one being universally expressed (V1) while the other (V2) was initially found to be enriched in neuronal tissues. The major distinction between them was a selective splicing into a distinct last exon that encodes for the very C-terminal 10 amino acids. While both variants can be prenylated, only V2 can be palmitoylated at a unique C-terminal cysteine residue that was absent from the conventional Cdc42 (V1) (Nishimura and Linder, 2013). Studies in neuronal cells had suggested Cdc42-V2's stronger incorporation into lipid rafts (Kang et al., 2008; Kim et al., 2014; Moutin et al., 2017; Mukai et al., 2008; Nishimura and Linder, 2013; Wirth et al., 2013a), which was proposed as a potential mechanism for its greater traffic and concentration in the dendritic spines (Mukai et al., 2015; Wirth et al., 2013a) . It was postulated that Cdc42-V2 acted to promote the formation of subcellular post-synaptic structures, leading to a greater synaptic plasticity during brain activity (Kang et al., 2008),, whereas the canonical Cdc42 aided axonogenesis (Lee et al., 2018a; Yap et al., 2016). Our data suggested that the stronger MAPK-activating capability by Cdc42-V2 was likely mediated by its enhanced affiliation with lipid compartments.

MAPK signaling plays multiple roles in the intestinal epithelia. Other than maintaining intestinal stem cells, it also engages in the differentiation of mature cell types (Tong et al., 2017): deficient MAPK signaling through blocking the Shp2-Mek1 pathway promotes Paneth cell differentiation while activating MAPK expands the Goblet cell population (Heuberger et al., 2014a). In contrast to these in vivo results, study with Caco2 cells suggested activation of the MAPK pathway by

FGFR-3 is required for Paneth cell differentiation (Brodrick et al., 2011).

The newly engineered *Cdc42 V2^{Tg}* mice allowed a direct demonstration of a robust impact of Cdc42 gain-of-function on MAPK activation and ISC regeneration. The Cdc42 splice variant V2, which is physiologically expressed in intestinal cells at lower levels, provided a molecular tool to enhance Cdc42 function and target MAPK activity. Our data suggested the stronger MAPK-activating capability by Cdc42-V2 was likely mediated by its enhanced affiliation with lipid compartments. Indeed, this splicing variant possesses a unique C-terminal cysteine residue (C189) that was absent from the conventional Cdc42 (V1). Studies in neuronal cells had suggested Cdc42-V2's stronger incorporation into lipid rafts (Kang et al., 2008; Kim et al., 2014; Moutin et al., 2017; Mukai et al., 2008; Nishimura and Linder, 2013; Wirth et al., 2013a). The cell-autonomous effects of Cdc42-V2 on epithelial regeneration have important implication for mitigating gastrointestinal pathologies that require an enhanced tissue repair program.

As Cdc42 also associates other signaling components that utilize the endocytic pathways, such as Wnt and PI3K cascades, loss or gain of Cdc42 is likely to impact non-EGF-MAPK pathways as well. For example, within the lipid raft compartment, we also detected the presence of the active form of Wnt receptor, the phosphorylated Lrp6, as well as PI3K **(Fig. 10).** These data suggest that Cdc42 is likely exerting a pleiotropic influence on multiple pro-survival signaling for intestinal stem cell survival. Nevertheless, our data supported a more consistent impact of Cdc42 on MAPK signaling rather than other pathways. However, current study cannot rule out Cdc42's collateral effects on major stem cell signaling especially

Wnt-catetin pathway.

Our studies heavily certered around stem cell survival signaling pathways. Given Cdc42's function in regulating general cell polarity and cytoskeleton, it is almost certain that Cdc42-mediated cellular structural regulations are strongly associated with cellular responses to extracellular signals such as EGF. First, Cdc42 deletion could disrupt apical and basolateral cell polarity leading to misallocalization of membrane proteins, such as EGFR. Second, Cdc42 abnormality could affect intercellular junctions thereby impacting Hippo signaling, whose activation relies on junctional integrity. Third, our study implied an impact of Cdc42 on the juxtocrine Ephrin-EphB3 signaling that has been shown to regulate Paneth cell positioning at crypts. Furthermore, the formation of microvillus inclusion in Cdc42-deficient enterocytes reflect a robust dysregulation of cortical actins in these cells. Thus, these defects demonstrate a structure-dependent signaling activity regulated by the epithelial intrinsic Cdc42 machinery.

The exact physiological function of V2 in intestinal epithelium has not been resolved at this moment. When comparing Cdc42 V1 and V2 in promoting intracellular kinases, we noticed some fundamental distinctions between the two variants in a non-neuronal cells. For example, WNK1 phosphorylation was down regulated in Hek293T cells overexpressing Cdc42 V1, while WNK1 was upregulated in V2 overexpressing cells. Future studies are needed to investigate the mechanism of such completely opposite signaling efficacy by the two Cdc42 variants. In particular, we speculate that activation of WNK1 may require a palmitoylated Cdc42 V2 that mediates better association with plasma membrane.

Future studies are necessary to further delineate the spatial and temporal expression or activation of Cdc42 V2 under physiological and pathological conditions, such as during aging, pathogen infection, injury, and tumor progression.

SUMMARY OF CHAPTER 3

How the intestinal epithelium maintains homeostasis and regenerative capacity during constant exposure to environmental insults are unclear. *Ex vivo* survival and clonogenicity of intestinal stem cells (ISCs) strictly required Cdc42-mediated response and Cdc42-deficient enteroids underwent rapid apoptosis. Mechanistically, Cdc42 engaged EGFR, was required for EGF-stimulated receptor endocytosis and sufficient to promote MAPK signaling. Proteomics and kinase analysis revealed that a physiological but non-conventionally spliced Cdc42 variant exhibited stronger MAPK-activating capability. Accordingly, mice engineered to express this Cdc42 variant showed elevated MAPK signaling, enhanced epithelial regeneration, and a mitigated mucosal damage in response to injury induced ISC attrition. Furthermore, boosting Cdc42-MAPK program specifically in mouse ISCs enhanced intestinal regeneration following epithelial injury. Thus, the ISC intrinsic Cdc42-MAPK program is required for intestinal epithelial regeneration while elevating this signaling cascade mediates a protection from genotoxic injury.

CHAPTER 4

GUT MICROBIOTA AND LAMINA PROPRIA IL22-STAT3 INTERSECT EPITHELIAL CDC42-MAPK SIGNALING FOR STEM CELL SURVIVAL

INTRODUCTION

Increasing evidences suggest that intestinal epithelium is under constant regulation from the gut microbiome and the lamina propria cells. Goblet cells in both small intestine and colon produce mucus to separate the epithelium from commensal bacteria and pathogens (Birchenough et al., 2015). Nonetheless, communication between the microbiome and epithelium appears to be constant, as microbial metabolites can get through the mucus. In addition, some microbes such as the segmented filamentous bacterium (SFB) are able to directly attach to epithelium (Ivanov et al., 2009). Intestinal mucosal-microbial interaction led to signaling cascades initiated by numerous sensors, such as microbial pattern receptors, on the apical membrane of the epithelial cells (Bäumler and Sperandio, 2016; Fukata et al., 2009; Moossavi et al., 2013; Nigro et al., 2014). Activation of these pathways change the behaviors of epithelial cells, including the most well characterized alteration of epithelial secretions of antimicrobial peptides, hormones, chemokines or cytokines (Blasius and Beutler, 2010). Some of the microbial antigens may be presented by epithelial cells towards immune cells from the basal side of the epithelium in the lamina propria. At steady state, healthy mucosal immune system tolerates the commensal bacteria and their production of antigen.

Innate immune response represents the frontline reaction to microbial signals through detection of microbial-associated molecular patterns (MAMP) by pattern recognition receptors (PRR) on innate lymphocytes (ILC). ILCs secret antimicrobial cytokines or protective cytokines to regulate mucosal homeostasis.

On the other hand, epithelial cells together with myofibroblasts and fibroblasts can also present microbial antigens to professional immune cells (Otte et al., 2003) (Walton et al., 2009) to initiate adaptive immune response.

Immune cells especially tissue resident innate immune cells orchestrate the mucosa health through a variety of cytokines. Among these ILCs, ILC1 cells resemble T helper type 1 (Th1) cells with a weaker cytotoxic ability; ILC2 cells can be activated by IL25 or IL33 that are usually secreted by epithelium during Helminths infection; and ILC3 cells are non-cytotoxic cells, which secret IL22 and IL17 under homeostasis or pathological conditions (Spits and Cupedo, 2012).

IL22 can be secreted by several types of immune cells in the intestine tissue in addition to ILC3 cells, for example cells expressing natural killer cell cytotoxicity receptor Nkp44+, CD4+/CD8+αβ T-cells (Dumoutier et al., 2000) (Liu et al., 2011; Wolk et al., 2002), γδ T-cells (Ness-Schwickerath and Morita, 2011), NKT cells (Moreira-Teixeira et al., 2011), NK cells (Kumar et al., 2013), Mast cells (Mashiko et al., 2015), and Neutrophils (Zindl et al., 2013). Despite of differential cell types, some IL22 producing cells share the feature of expressing RORγT(Montaldo et al., 2014). The expression of IL22 receptor, IL22RA1, in subgroups of ISCs and TA cells (Zwarycz et al., 2019) suggested that the IL22 signaling may affect biology of ISCs.

Our study in Chapter 3 demonstrated the indispensability of Cdc42 for enteroid survival ex vivo; however the intact mice lacking Cdc42 in IECs were viable, suggesting the existence of compensatory signals in the intact intestinal mucosa. As intestinal epithelium communicates with luminal microbiome as well as the

lamina propria cells, our next overarching goal is to identify the how Cdc42-deficient intestinal epithelia survive in vivo in the absence of such an important intrinsic factor. We specifically investigated the potential cytokine signals from immune cells as well as microbial signals in Cdc42 KO mice. Our data identified specific cytokine signaling cascade, IL22-Stat3, which was originated from immune cells and contributed to the survival of Cdc42-deficient IECs by intersecting MAPK signaling. In addition, our studies suggested that the Cdc42-deficient IECs may communicate to lamina propria cells through production of prolactin, and that the microbiota in Cdc42 KO mice also played a role in supporting epithelial survival.

RESULTS

Cdc42-deficent IECs receive survival signals from immune compartment in vivo

While we observed strong ISC dependence on Cdc42 expression for survival and renewal ex vivo, it was noted that *Cdc42*$^{\Delta IEC}$ intestines maintained IEC homeostasis in intact mice. Bulk RNA-seq of *Cdc42*$^{\Delta IEC}$ intestines revealed transcriptional upregulations of EGFR as well as several EGF ligands (Areg, TGFα, Ereg) **(Fig. 22A)**, in agreement with elevated EGFR levels detected by Western blots in CHAPTER 3 **(Fig. 9B)**. Thus, ISC defects were not due to lack of either EGF or EGFR components. Interestingly, we also noted a robust alteration of mucosal immune system, exemplified by alterations of cytokine signaling network genes **(Fig. 22B, C).** And gene ontology analysis suggested significant activations

of pathways related with inflammation, cytokine stimulus, leukocyte migration, and JAK-STAT cascade (p<0.001, **Fig. 22D**).

Paracrine cytokines were recently shown to affect ISC function (Biton et al., 2018a). We postulated that paracrine cytokines secreted from non-epithelial tissue, such as immune compartments, which were absent in enteroid culture, might have promoted *Cdc42*$^{\Delta IEC}$ epithelial survival *in vivo*. To test if particular paracrine cytokines indicated in transcriptomic analysis may contribute to *Cdc42*$^{\Delta IEC}$ cell survival, we performed an unbiased growth rescue screening assay using *Cdc42*^{iKO} enteroids in ENR medium supplemented with distinct recombinant proteins **(Fig. 23A)**. Surprisingly, IL22, IL12, IL34, CXCL1, or CXCL2, when applied individually, were able to noticeably restore *Cdc42*^{iKO} enteroid growth **(Fig. 23B)**, while canonical Wnts, EGF ligands (Areg, TGFα), and a number of other cytokines had no detectable effect (**Fig. 23C, E)**. Among the cytokines tested, IL22 consistently showed the strongest pro-survival and anti-apoptotic effects **(Fig. 23B, D, F)**.

IL22 signals through STAT3 for transcriptional regulation of its targets (Nagalakshmi et al., 2004; Radaeva et al., 2004). Chemical inhibitors of STAT3, Stattic (Schust et al., 2006) or WP1066 (Horiguchi et al., 2010) suppressed the rescuing effects of IL22 and several other cytokines **(Fig. 24)**. These data suggested that STAT3 axis might be employed by several paracrine cytokines in *Cdc42*$^{\Delta IEC}$ mucosa as a compensatory survival pathway.

String analysis of upregulated genes indicated enhanced IL22-STAT3 and Tlr4 signaling **(Fig. 25A).** Quantitative RT-PCR detected significant elevations of *IL22*

and STAT3 pathway targets in *Cdc42*$^{\Delta IEC}$ intestines, most notably c-Myc, a pro-survival factor of transit amplifying cells **(Fig. 25B).** Immunohistochemistry revealed more pSTAT3^{+} cells in *Cdc42*$^{\Delta IEC}$ intestines at homeostasis **(Fig. 26A)** and upon irradiation **(Fig. 26B).**

Loss of Cdc42 in enteroids recapitulated the in vivo observation that ERK pathway was blocked without Cdc42 **(Fig. 27A)**. In order to test whether IL22 may activate MAPK to promote stem cell survival in *Cdc42*^{iKO} epithelium, we add U0126, a specific MEK inhibitor, to *Cdc42*^{iKO} enteroid with the presence of IL22. Inhibition of MEK abolished the effect of IL22 on enteroid survival **(Fig. 27B-C)**, reflected by loss of pERK **(Fig. 27D).** This suggested that IL22 signaling promoted cell survival in *Cdc42*^{iKO} enteroids through ERK activation.

A

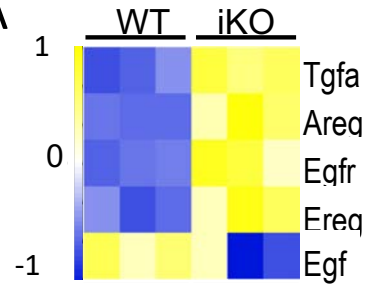

B

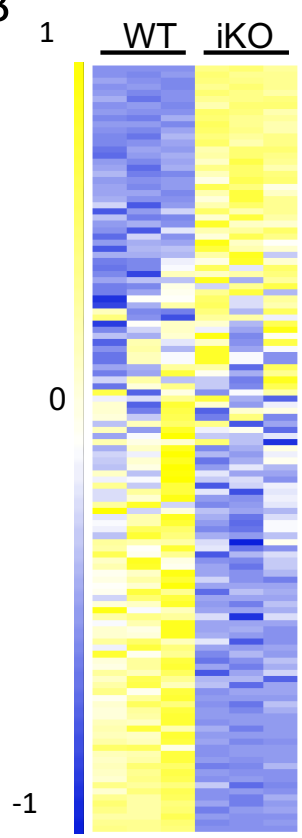

C

	FC	*P* value
Prl2c2	**129.1**	8.5E-08
Cxcl5	**98.4**	2.2E-11
Il1rn	**62.6**	3.5E-170
Il1f6	**30.8**	7.2E-04
Cxcl3	**29.6**	7.5E-19
Prl2c5	**29.5**	6.6E-03
Tnfsf18	**28.6**	8.3E-03
Cxcl1	**25.5**	3.9E-10
Tnfrsf11b	**14.6**	2.0E-38
Cxcl2	**14.1**	4.9E-05
Il12a	**10.4**	1.9E-01
Il33	**8.9**	5.2E-54
Tnfrsf12a	**8.9**	5.8E-42
Prl2c3	**6.6**	4.4E-01
Tnfrsf23	**5.9**	7.5E-25
Tnfsf9	**5.5**	4.8E-22
Il1f8	**5.5**	3.5E-06
Prl2a1	**5.3**	5.3E-01
Il22	**5.0**	1.5E-01
Ngf	**5.0**	5.5E-01

D

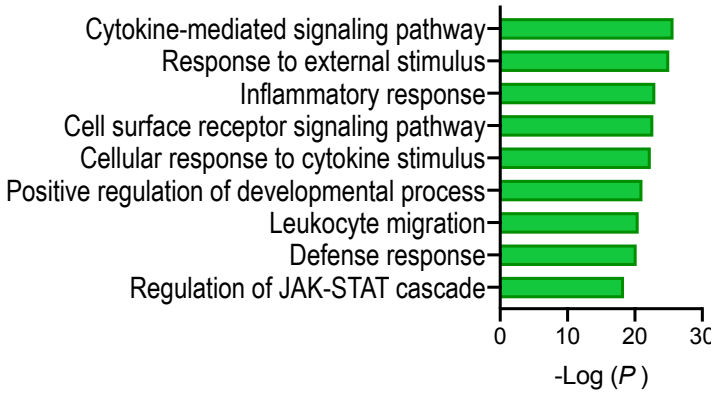

Figure 22. Bulk RNA-seq analysis of *Cdc42*^{iKO} mucosa

(A) Heatmap shows multiple EGF ligands and EGFR were increased in *Cdc42*^{iKO}. (B) Meanwhile, cytokine and their receptor signaling networks were altered in *Cdc42*^{iKO} mucosa. (C) List of selected cytokines/chemokines upregulated in *Cdc42*^{iKO} mucosa, with fold change and *P* value. (D) ShinyGo analysis of upregulated transcriptome in *Cdc42*^{iKO} mucosa showed enrichment of gene sets related to inflammatory, defense, cytokine responses, etc.

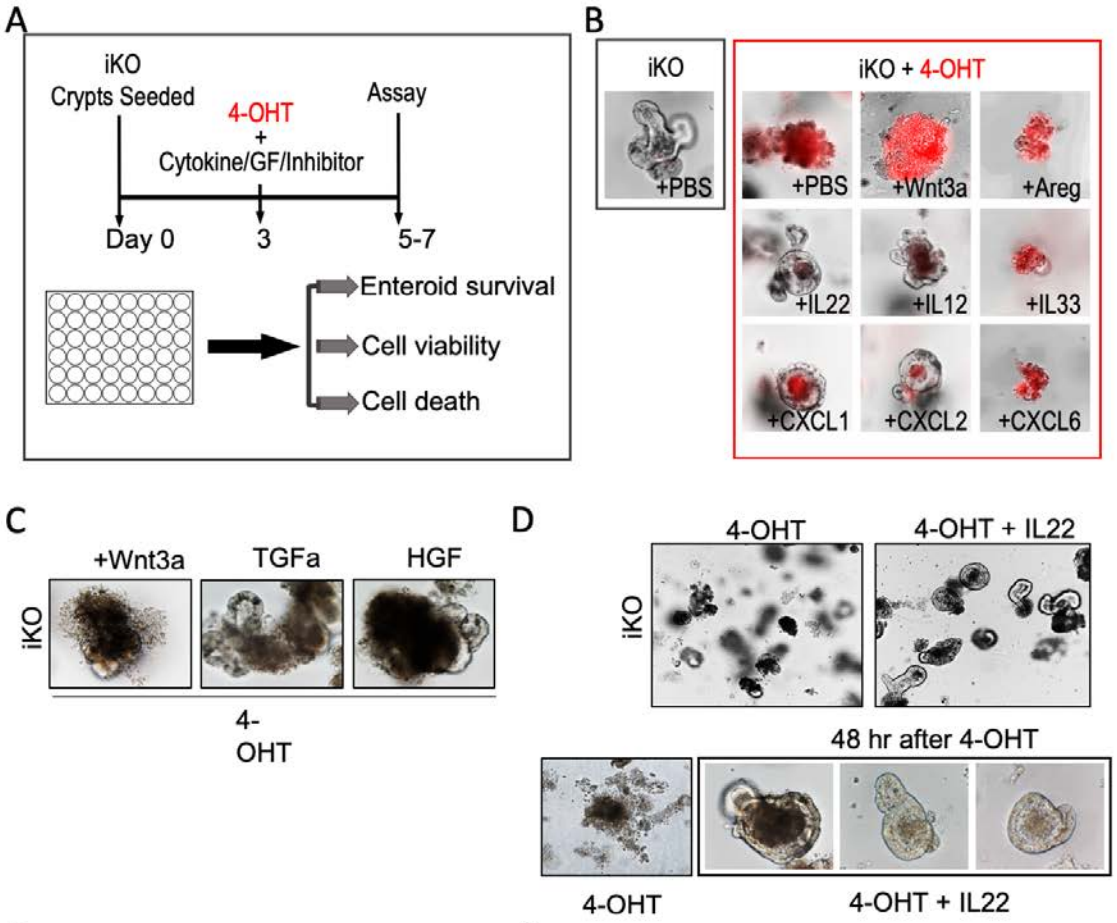
A
iKO
Crypts Seeded
4-OHT
+
Cytokine/GF/Inhibitor
Assay
Day 0
3
5-7
Enteroid survival
Cell viability
Cell death
B
iKO
+PBS
iKO + 4-OHT
+PBS
+Wnt3a
+Areg
+IL22
+IL12
+IL33
+CXCL1
+CXCL2
+CXCL6
C
+Wnt3a
TGFa
HGF
iKO
4-
OHT
D
4-OHT
4-OHT + IL22
iKO
48 hr after 4-OHT
4-OHT
4-OHT + IL22
E
Enteroid Viability (%)
20
15
10
5
0
P>0.05
iKO
Vehicle
Areg
HGF
TGFa
Wnt3a
F
Enteroid Viability (%)
40
30
20
10
0
P>0.05
P>0.05
P=0.016
P=0.022
P=0.01
P<0.001
iKO
Vehicle
IL33
CXCL6
CXCL1
IL12
CXCL2
IL22

Figure 23. Effect of selected cytokines on *Cdc42^{iKO}* enteroids

(A) Schematic diagram shows strategy of *Cdc42^{iKO}* enteroid rescuing experiments using various recombinant cytokines, growth factors, and pathway inhibitors. (B) Representative propidium iodide-stained *Cdc42^{iKO}* enteroids in the presence of exogenous cytokines or growth factors. IL22, IL12, Cxcl1 and Cxcl2 rescued growth of *Cdc42^{iKO}* enteroids, while Wnt3a, Areg, Cxcl6 or IL33 failed. (C) Bright field images of *Cdc42^{iKO}* enteroids after addition of 4-OHT with Wnt3a, HGF, or TGFα. No growth restoration was found. (D) Representative bright field images of enteroids of *Cdc42^{iKO}* enteroids with or without IL22 48 hrs after 4-OHT treatment. Images represent two independent experiments with replicates of each condition. (E-F) Percentages of viable enteroids were analyzed from 2 independent experiments with 2 replicates per condition in each experiment.

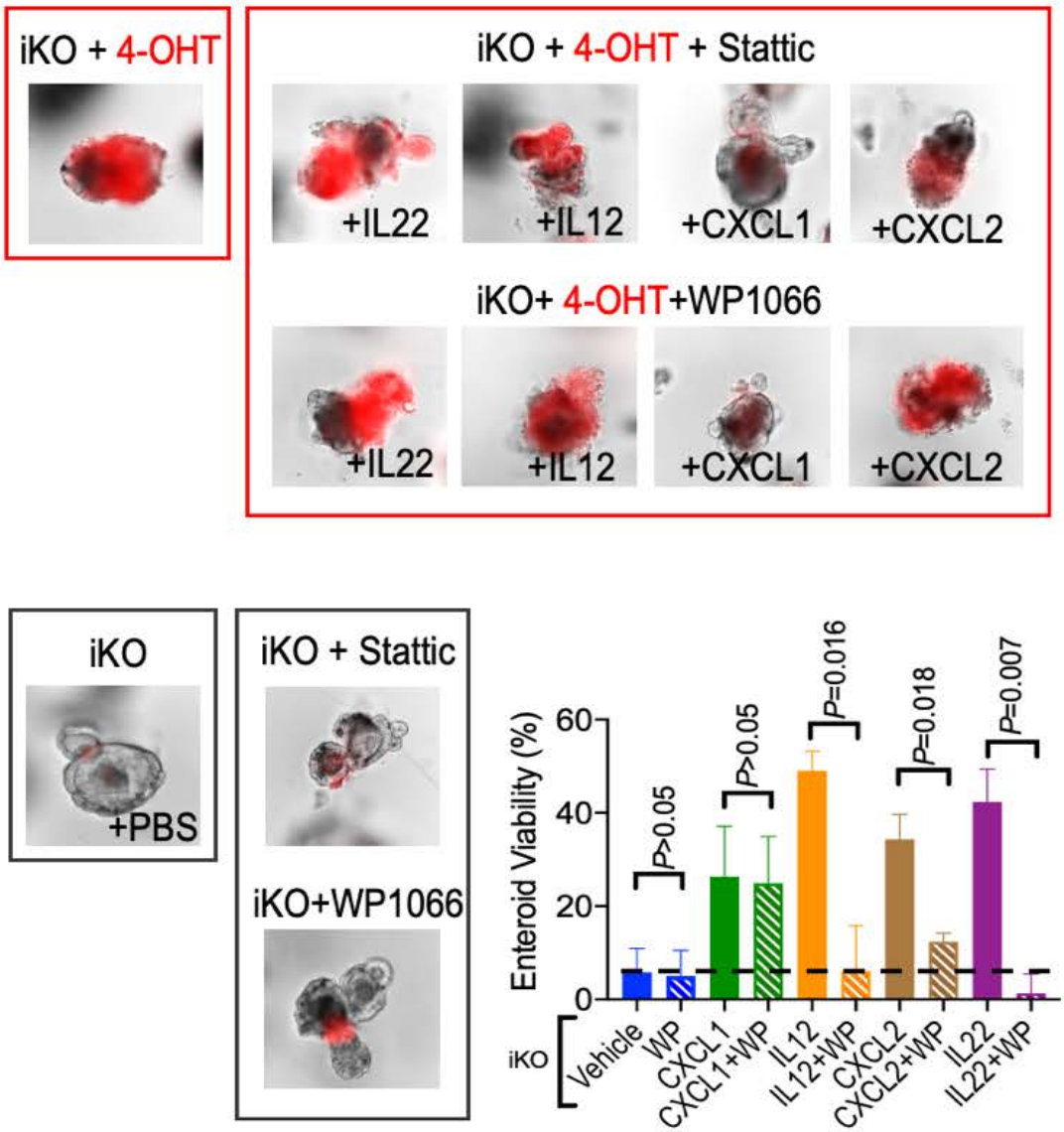

Figure 24. Inhibition of STAT3 activity disrupts effect of cytokines in promoting the survival of *Cdc42*^{iKO} enteroids.

PI staining showed the rescuing effects by IL22, IL22, and CXCL2 were abolished by STAT3 inhibitors (Stattic or WP1066), which did not inhibit enteroid growth on their own before 4-OHT addition. Data represent 2 replicates for each condition.

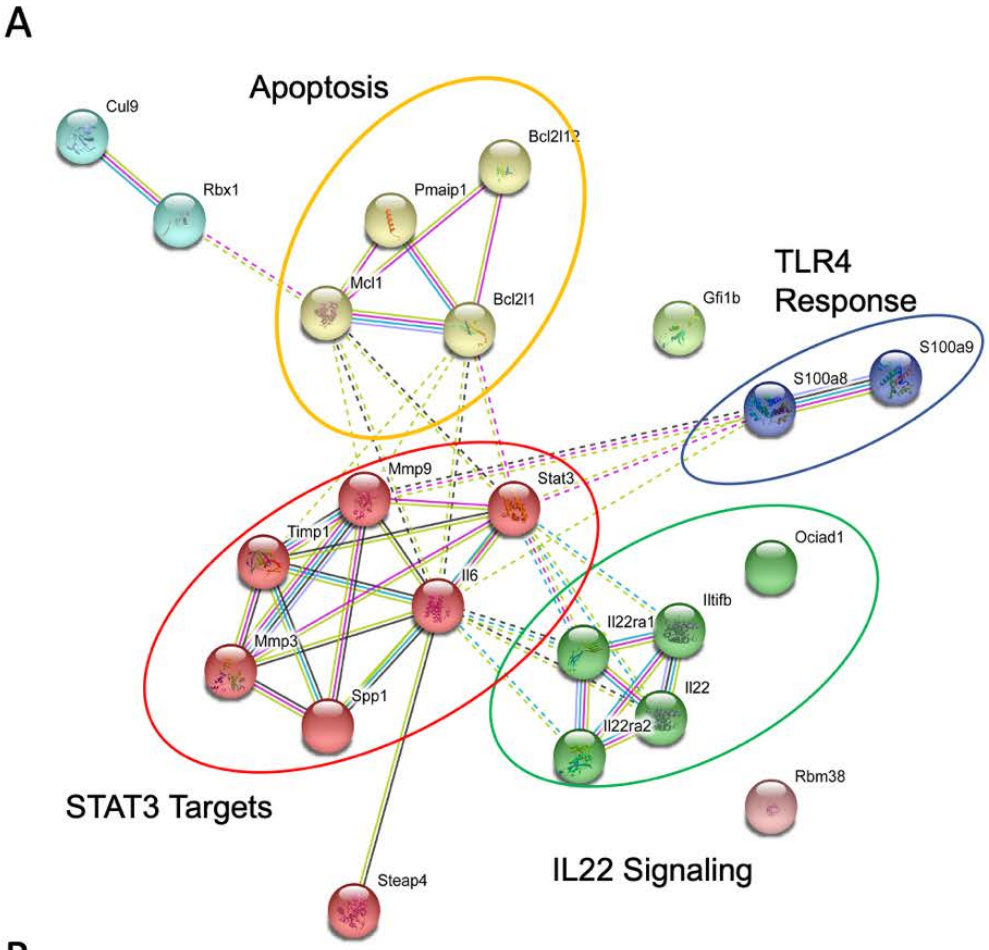
A
Apoptosis
Cul9
Rbx1
Bcl2l12
Pmaip1
Mcl1
Bcl2l1
TLR4
Response
Gfi1b
S100a9
S100a8
Mmp9
Stat3
Timp1
Il6
Mmp3
Spp1
Ociad1
Iltifb
Il22ra1
Il22
Il22ra2
Rbm38
STAT3 Targets
IL22 Signaling
Steap4

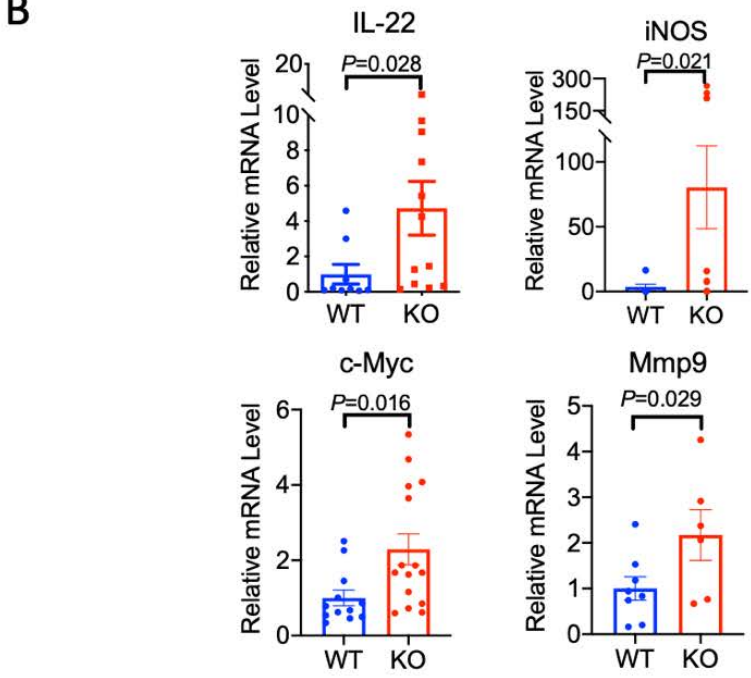
B
IL-22
P=0.028
Relative mRNA Level
WT
KO
iNOS
P=0.021
c-Myc
P=0.016
Mmp9
P=0.029

Figure 25. IL22/STAT3 genes are upregulated in *Cdc42*^{iKO} mucosa.

(A) String analysis suggested enhanced signaling pathways of TLR4 related immune response, IL22 signaling, STAT3 pathway in *Cdc42*^{iKO} intestines. (B) Relative mRNA levels of IL22, and IL22-STAT3 targets iNOS, c-Myc and Mmp9 were increased in *Cdc42*$^{\Delta IEC}$ intestinal mucosa compared to WT detected by realtime-PCR. Data were plotted 4-6 animals per genotype including technical replicates.

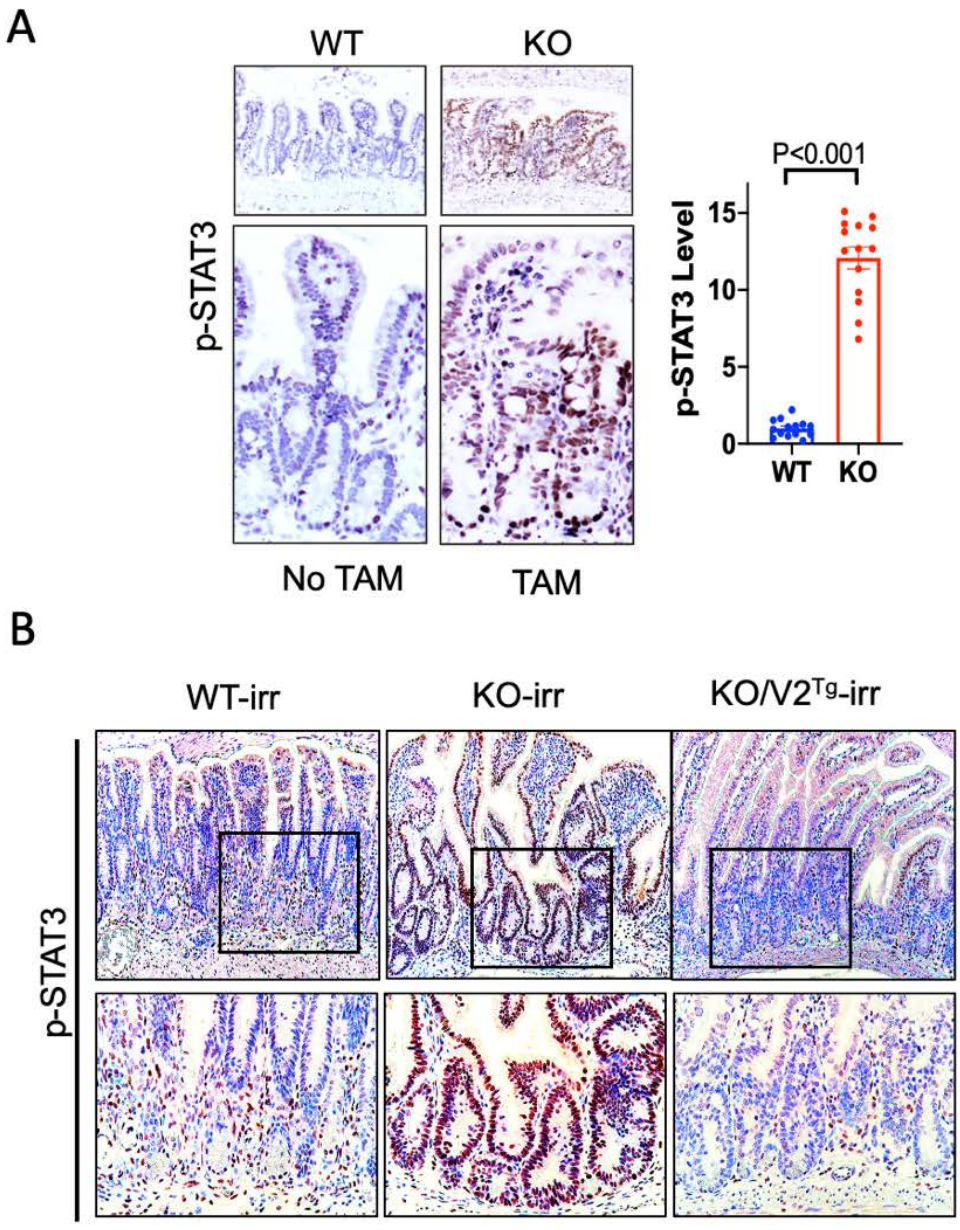

Figure 26. STAT3 activation in *Cdc42*$^{\Delta IEC}$ mice.

(A) Immunohistochemistry showed increased pSTAT3+ cells in KO intestines in homeostasis. (B) Immunohistochemistry showed increased pSTAT3+ cells in KO, but not in KO; V2^{Tg} mouse intestines 7 days after irradiation.

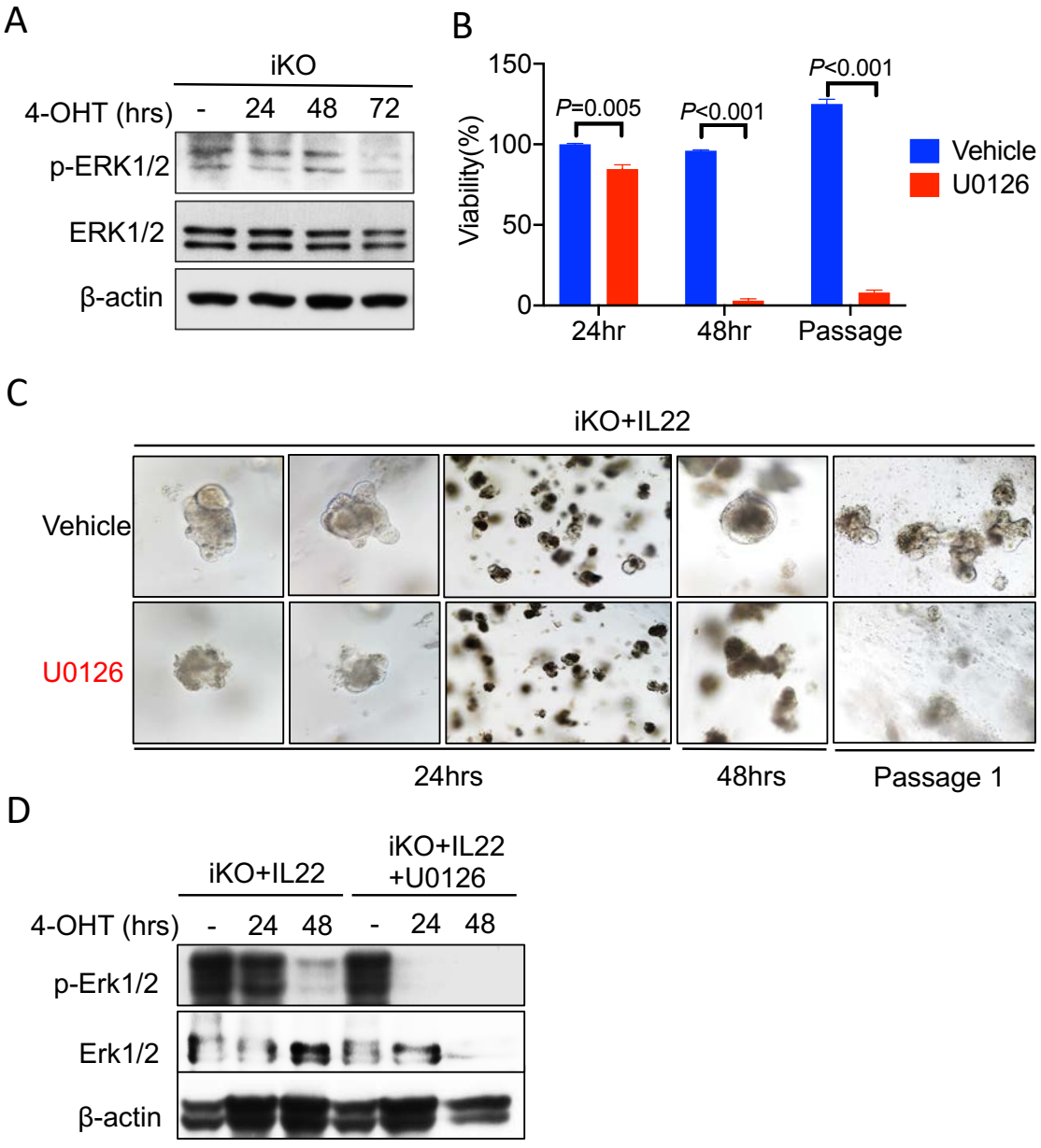
A
iKO
4-OHT (hrs) - 24 48 72
p-ERK1/2
ERK1/2
β-actin
B
150
100
50
0
Viability(%)
P=0.005
P<0.001
P<0.001
Vehicle
U0126
24hr
48hr
Passage
C
iKO+IL22
Vehicle
U0126
24hrs
48hrs
Passage 1
D
iKO+IL22
iKO+IL22 +U0126
4-OHT (hrs) - 24 48 - 24 48
p-Erk1/2
Erk1/2
β-actin

Figure 27. IL22 signaling promotes cell survival in *Cdc42^{iKO}* enteroids through ERK activation.

(A) Western blot of lysates from *Cdc42^{iKO}* enteroid before and after 4-OHT treatment showed progressive loss of p-ERK. (B-C) IL22 supplement in *Cdc42^{iKO}* enteroid was not able to support cell survival when U0126 was added to inhibit MAPK activity. 95% loss of live cells was observed 48hrs after U0126 addition. Passaged clones from these enteroids showed continued effect. Data represent 2 replicates for each condition. (D) Detection of p-ERK in enteroid lysate from IL22 treated *Cdc42^{iKO}* with or without U0126 by western blot. ERK activity sustained in *Cdc42^{iKO}* by IL22 at 24 and 48hrs after 4-OHT treatment was abolished by U0126.

Lamina propria immune cell IL22/STAT3/MAPK signal is essential for Cdc42$^{\Delta IEC}$ epithelial survival

Enteroid experiments indicated that the IL22-STAT3/MAPK pathway can promote *Cdc42^{iKO}* cell survival **(Fig. 24, 27)**. To examine the *in vivo* contribution of this pathway, we genetically ablated IL22 in *Cdc42^{iKO}* mice. We firstly tested *Cdc42^{iKO}* as we found it difficult to obtain viable double knockouts using Vil-Cre driver. Remarkably, upon tamoxifen administration, *IL22$^{-/-}$; Cdc42^{iKO}* mice, showed a more pronounced body weight loss compared to single knockout (*Cdc42^{iKO}* or *IL22$^{-/-}$*) littermates **(Fig. 28A)**. Strikingly, tamoxifen administration, within 10 days, induced a 15% reduction in intestinal lengths in *IL22$^{-/-}$; Cdc42^{iKO}* mice compared to *Cdc42^{iKO}* mice **(Fig. 28B)**, with further reduction in crypt base ISCs **(Fig. 28C)**, pERK1/2 **(Fig. 28D)**, and *Survivin* **(Fig. 28E)**. When we finally got the VilCre driven *IL22$^{-/-}$*; *Cdc42$^{\Delta IEC}$*, we found removing IL22 from *Cdc42$^{\Delta IEC}$* mice lead to death as early as at 2-month-old **(Fig. 29A)**. In the alive DKO mice, reduced Olfm4 and pERK level were also observed **(Fig. 29B)**.

More importantly, *IL22$^{-/-}$* mice did not show higher susceptibility to irradiation compared to *WT* littermates, indicating redundancy of ligands/pathways within the animal to ensure the commitment of pro-survival programs post injury. However, IL22 showed strong indispensability for *Cdc42*-deficient IECs when compared to WT. Exacerbated body weight loss **(Fig. 30A, B)** and epithelial damages **(Fig. 30C)** were exhibited in *IL22$^{-/-}$; Cdc42^{iKO}* (DKO) mice. There was a 42% reduction of Olfm4^{+} crypt ISCs in DKO mice following irradiation **(Fig. 30D)**.

STAT3 inhibitor (WP-1066), when administrated to *Cdc42$^{\Delta IEC}$* mice, led to an

even more pronounced intestinal shortening up to 20% **(Fig. 31A)**, and reduction of Olfm4 and pERK1/2 levels **(Fig. 31B)** Thus, enhanced signaling from immune cells were critical to maintain a level of homeostasis in *Cdc42*$^{\Delta IEC}$ IECs. Above results suggest that STAT3 blockage possibly impinged on signal inputs from multiple cytokines including but not limited to IL22, consistent with reports that several cytokines co-stimulate STAT3 and MAPK pathways (Fukui et al., 2014; Lejeune et al., 2002; Lindemans et al., 2015; Sugimoto et al., 2008)

Similar to steady state, WP-1066 induced shortening of the intestinal length compared to control *Cdc42*^{iKO} mice 3 days after irradiation **(Fig. 32A-B).** Further, *Cdc42*^{iKO} mice pre-treated with WP-1066 exhibited the most severe post-irradiation epithelial damage, with 45% reduction in regenerating crypts and Olfm4^{+} crypt cells compared to vehicle-treated *Cdc42*^{iKO} mice **(Fig. 32C-D).** Importantly, neither IL22 loss nor WP1066 had noticeable impact on mice carrying intact Cdc42 (**Fig. 28-32**). Thus, the protective effects IL22-STAT3 signaling were especially pronounced in hosts lacking IEC intrinsic Cdc42 survival program.

.

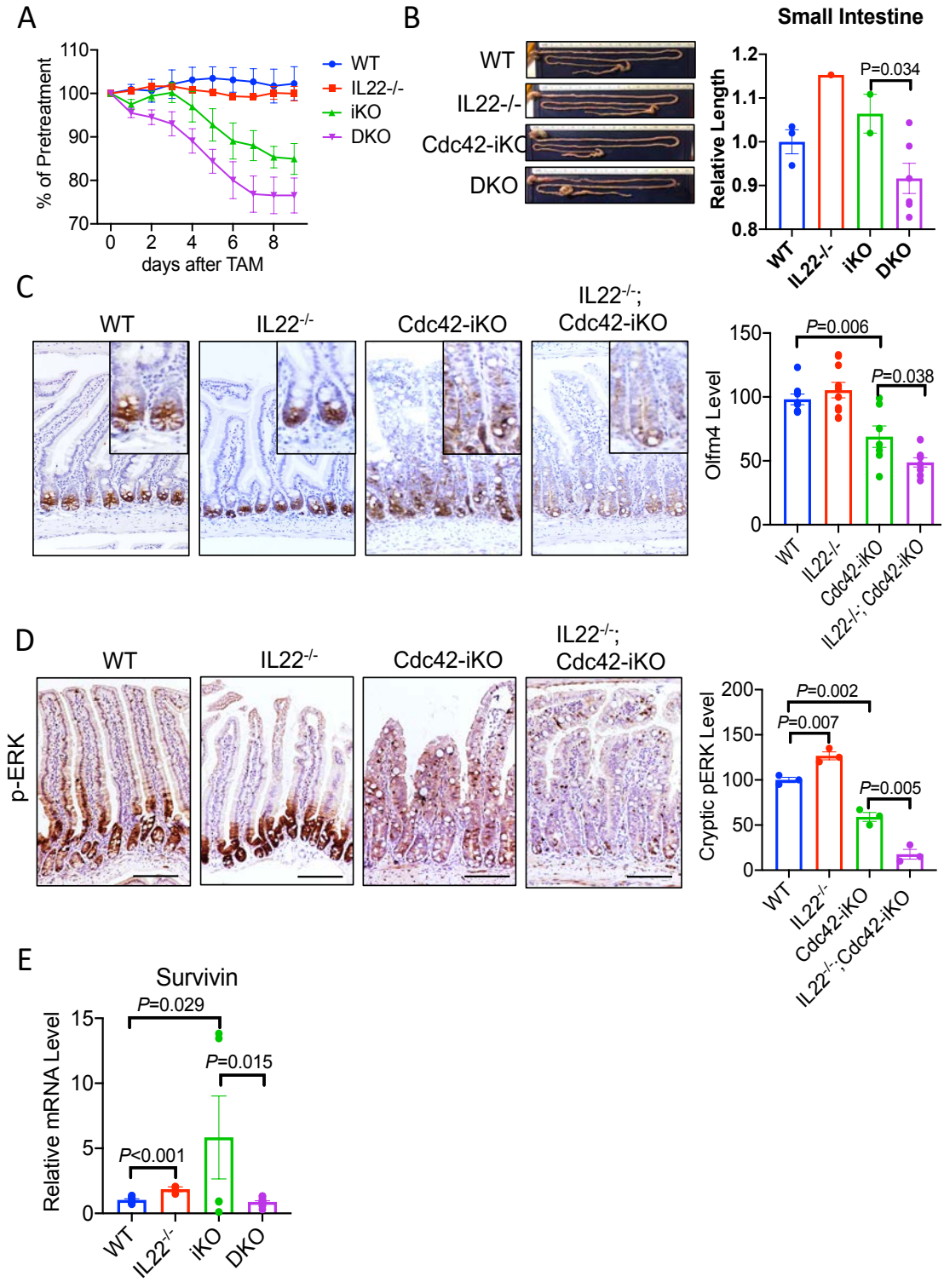
A
% of Pretreatment
days after TAM
WT
IL22-/-
iKO
DKO
B
Small Intestine
Relative Length
P=0.034
C
WT
IL22-/-
Cdc42-iKO
IL22-/-; Cdc42-iKO
Olfm4 Level
P=0.006
P=0.038
D
p-ERK
Cryptic pERK Level
P=0.002
P=0.007
P=0.005
E
Survivin
Relative mRNA Level
P=0.029
P=0.015
P<0.001

Figure 28. IL22-Stat3 signaling mediate IEC survival in *Cdc42^{iKO}* intestines

(A) Body weight changes were measured daily for *WT* (n=2), *IL22$^{-/-}$* (n=2), *Cdc42^{iKO}* (n=3) and *IL22$^{-/-}$; Cdc42^{iKO}* (n=8) mice after tamoxifen injection. (B) Representative images and quantification of intestinal length of *WT, IL22$^{-/-}$, Cdc42^{iKO}* and *IL22$^{-/-}$; Cdc42^{iKO}* mice. (C) Representative images of Olfm4 immunohistochemistry on ileal epithelia of designated genotype and treatment. Average levels of Olfm4 within a crypt were quantified from multiple sections of 2-3 animals per genotype in 2 independent experiments. (D) Immunohistochemistry for pERK1/2 in *WT, IL22$^{-/-}$, Cdc42^{iKO}* and *IL22$^{-/-}$; Cdc42^{iKO}* small intestines. Average levels of pERK within a crypt were quantified from multiple sections of 2-3 animals per genotype in 2 independent experiments. (E) Relative mRNA expression of *Survivin* in *WT*, *IL22$^{-/-}$, Cdc42^{iKO}* and *IL22$^{-/-}$; Cdc42^{iKO}* small intestines was detected by realtime-PCR.

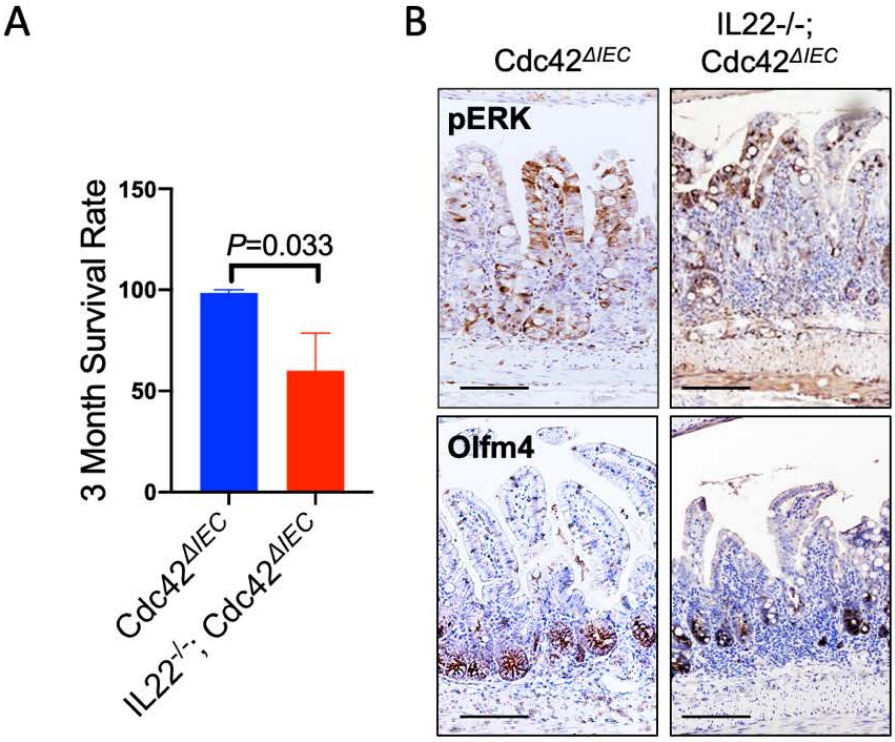

Figure 29. Removing IL22 from *Cdc42*$^{\Delta IEC}$ mice further lead to death and reduced Olfm4 and pERK level.

(A) Survival rate evaluated based on a threshhold of 3 month. 40% of *IL22*$^{-/-}$*; Cdc42*$^{\Delta IEC}$ mice die with in 3 month. (B) Immunohistochemistry for pERK1/2 and Olfm4 in *Cdc42*$^{\Delta IEC}$ and *IL22*$^{-/-}$*; Cdc42*$^{\Delta IEC}$ small intestines. Average levels of pERK and Olfm4 within a crypt were quantified from multiple sections of 2-3 animals per genotype in 2 independent experiments.

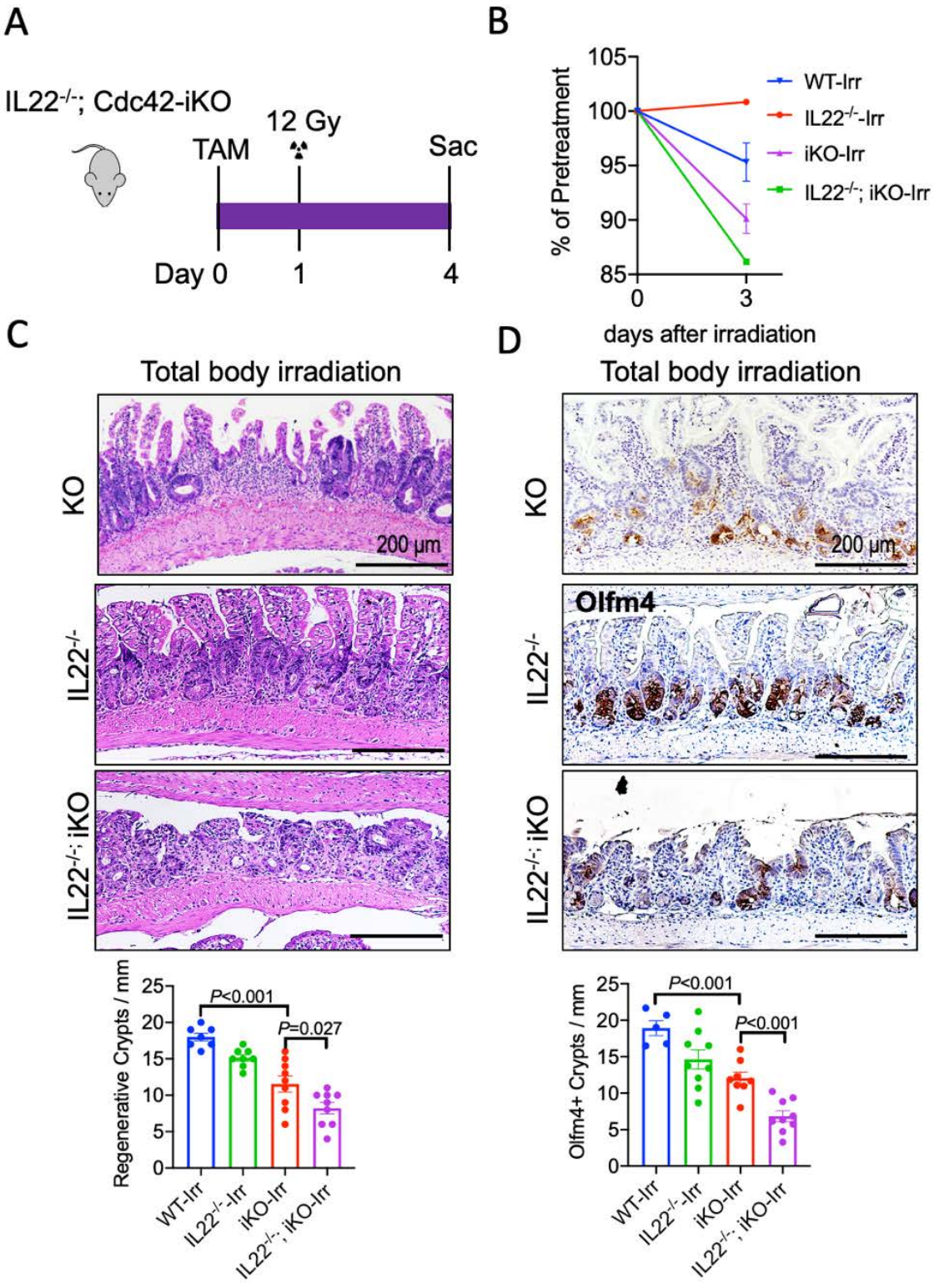
A
IL22-/-; Cdc42-iKO
12 Gy
TAM
Sac
Day 0
1
4
B
% of Pretreatment
105
100
95
90
85
0
3
days after irradiation
WT-Irr
IL22-/--Irr
iKO-Irr
IL22-/-; iKO-Irr
C
Total body irradiation
KO
IL22-/-
IL22-/-; iKO
200 μm
Regenerative Crypts / mm
P<0.001
P=0.027
WT-Irr
IL22-/- -Irr
iKO-Irr
IL22-/-; iKO-Irr
D
Total body irradiation
KO
IL22-/-
IL22-/-; iKO
200 μm
Olfm4
Olfm4+ Crypts / mm
P<0.001
P<0.001
WT-Irr
IL22-/- -Irr
iKO-Irr
IL22-/-; iKO-Irr

Figure 30. Evaluation of *IL22-/-; Cdc42^{iKO}* mice under irradiation.

(A) Schematic showing of WT, *IL22$^{-/-}$, Cdc42^{iKO}*, and *IL22$^{-/-}$; Cdc42^{iKO}* mice that were subjected to 12 Gy total body irradiation 1 day after tamoxifen administration. (B) Body weight changes before and 3 days after irradiation suggested a protection by IL22 for mice lacking Cdc42 in IECs. (C) H&E staining showed in *IL22$^{-/-}$; Cdc42^{iKO}* mice there was further reduced number of regenerative crypts in response to irradiation. (D) Immunohistochemistry for Olfm4 showed in *IL22$^{-/-}$; Cdc42^{iKO}* intestine further reduced numbers of Olfm4 crypts.

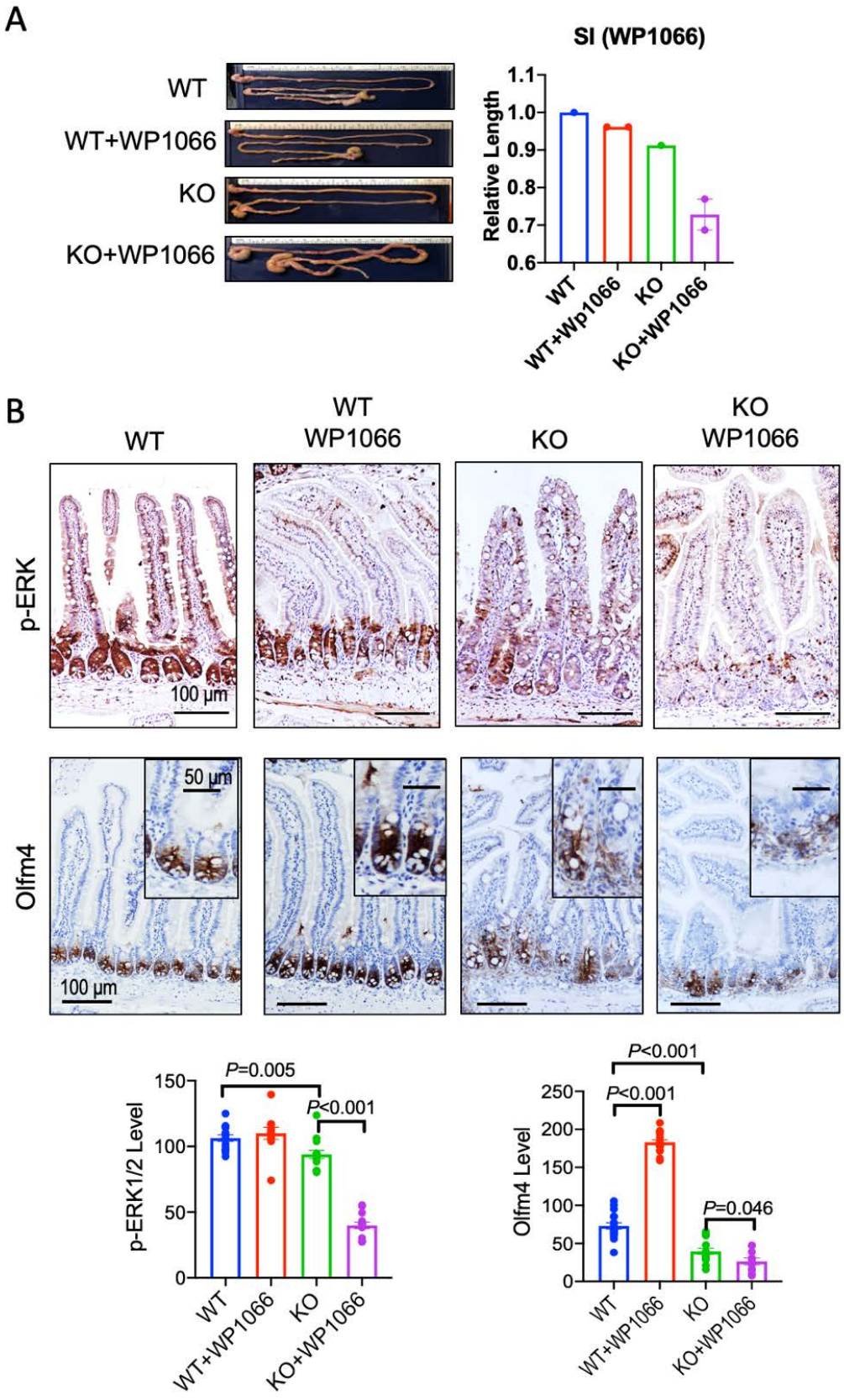
A
WT
WT+WP1066
KO
KO+WP1066
SI (WP1066)
Relative Length
1.1
1.0
0.9
0.8
0.7
0.6
WT
WT+Wp1066
KO
KO+WP1066
B
WT
WT
WP1066
KO
KO
WP1066
p-ERK
100 μm
Olfm4
50 μm
100 μm
p-ERK1/2 Level
P=0.005
P<0.001
150
100
50
0
WT
WT+WP1066
KO
KO+WP1066
Olfm4 Level
P<0.001
P<0.001
P=0.046
250
200
150
100
50
0
WT
WT+WP1066
KO
KO+WP1066

Figure 31. Inhibition of STAT3 activity shortens the intestine and further reduces pERK and Olfm4 in *Cdc42*$^{\Delta IEC}$ mice.

(A) Representative images and quantification of intestinal lengths WT and *Cdc42*$^{\Delta IEC}$ mice with or without WP1066 treatment. (B) Immunohistochemistry for pERK1/2 and Olfm4 in WT and *Cdc42*$^{\Delta IEC}$ mice with or without WP1066 treatment. Average levels of p-ERK and Olfm4 within a crypt were quantified from multiple sections of WT (n=2), WP1066-treated WT (n=3), KO (n=3), and WP1066-treated KO mice (n=2).

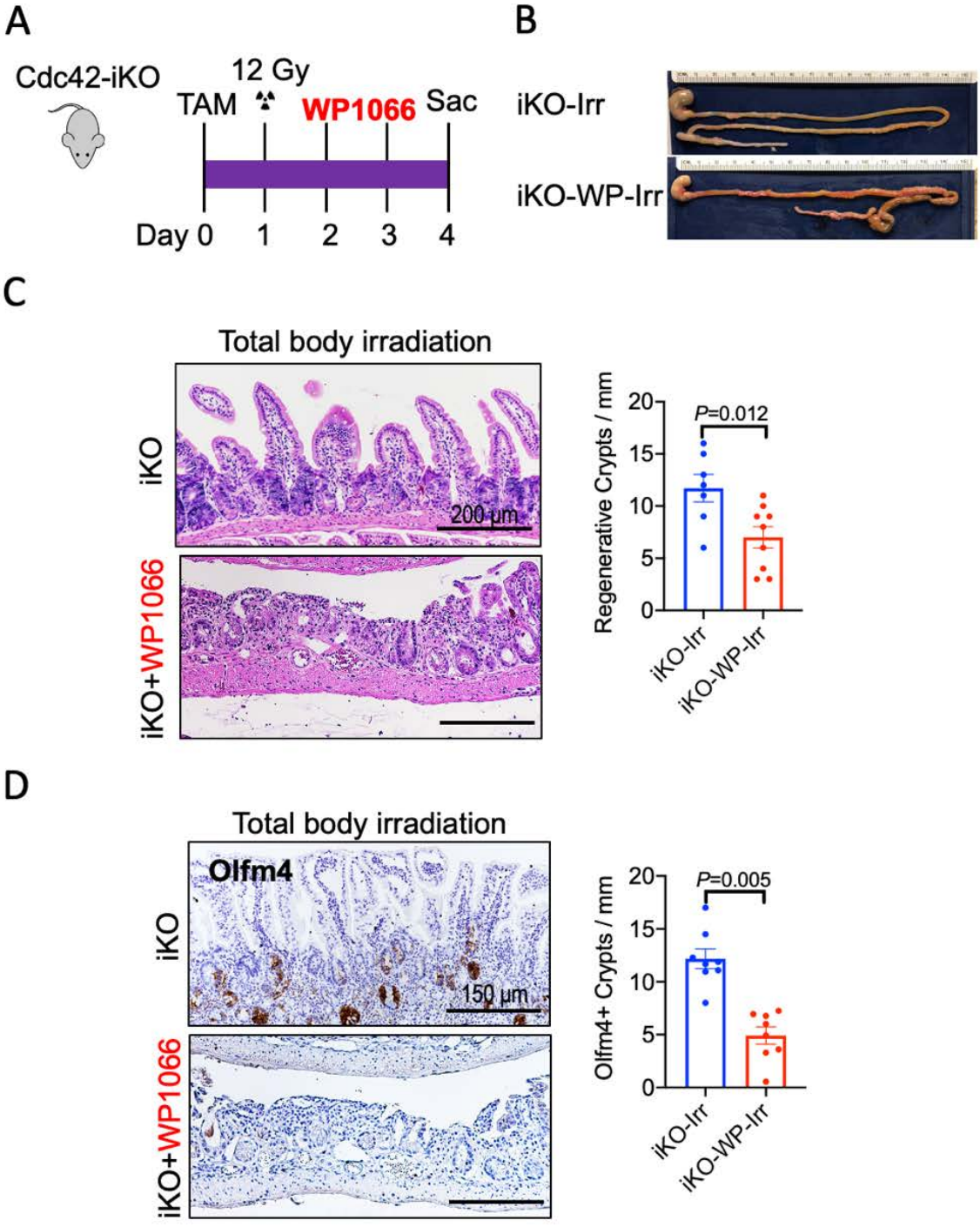
A
Cdc42-iKO
12 Gy
TAM
WP1066
Sac
Day 0
1
2
3
4
B
iKO-Irr
iKO-WP-Irr
C
Total body irradiation
iKO
iKO+WP1066
200 μm
Regenerative Crypts / mm
P=0.012
iKO-Irr
iKO-WP-Irr
D
Total body irradiation
Olfm4
iKO
iKO+WP1066
150 μm
Olfm4+ Crypts / mm
P=0.005
iKO-Irr
iKO-WP-Irr

Figure 32. Inhibition of STAT3 activity further reduces regenerative crypts and Olfm4 level in *Cdc42^{iKO}* mice after irradiation.

(A) Schematic showing of *Cdc42^{iKO}* mice that were subjected to 12 Gy total body irradiation 1 day after tamoxifen administration. Half of the mice received WP1066 injections on day 1 and 2 after irradiation. (B) Representative images of intestines of *Cdc42^{iKO}* mice with or without WP1066 treatment 3 days after irradiation. (C-D) Representative ileal histology and Olfm4 immunohistochemistry images of irradiated *Cdc42^{iKO}* mice with or without WP1066 treatment. In response to irradiation, WP1066 injected *Cdc42^{iKO}* mice showed further reduction of regenerative crypts and Olfm4 crypt cells compared to untreated *Cdc42^{iKO}* mice.

Prolactin produced by Cdc42$^{\Delta IEC}$ epithelium induces IL22 release from LP cells

Production of chemokines and cytokines are elevated in *Cdc42$^{\Delta IEC}$* mucosa. Some of them were increased more than 100fold than that in WT. To better understand how LPLs sense and respond to epithelial genetic deficiency such as in *Cdc42$^{\Delta IEC}$* mice, we wonder are there chemokines and cytokines produced by the genetically deficient epithelium, and whether they work on IL22-secreting LPLs to promote survival signaling in *Cdc42$^{\Delta IEC}$* mucosa. Indeed, at Ileum where the mucosal immunity is the most active, elevated expression of Prl2c-2, Cxcl1/2/3/5, IL1rn, TNFrsf11b was observed **(Fig. 33)**, showing agreement with the Bulk RNA seq data on *Cdc42^{iKO}* mucosa **(Fig. 22B)**. To the contrast, cytokines known usually secreted by LPLs, IL12a and IL22 were only detected at low level in the overall epithelium samples. Even lower expression of these cytokines was observed in *Cdc42$^{\Delta IEC}$* epithelium as compared with WT epithelium **(Fig. 33)**. Unlike the lack of IL22 expression in the epithelium, IL22 produced by cultured *Cdc42$^{\Delta IEC}$* LP cells was as 4 times much as that in the WT LP cells **(Fig. 34A, B)**. Induction of IL22 by recombinant Prolactin is significant at 6hr from *Cdc42$^{\Delta IEC}$* LPLs, although the same trend is also seen in 20hrs and WT LPLs **(Fig. 34C)**. Collected LP cell supernatant was able to improve the viability of Cdc42 enteroids significantly **(Fig. 35A),** with the sustained pERK level **(Fig. 35B)**. Together, the data suggests epithelial factors such as Prolactin in response to the genetic deficiency is essential for epitheliual cells to communicate with immune cells and call for compensating survival signaling.

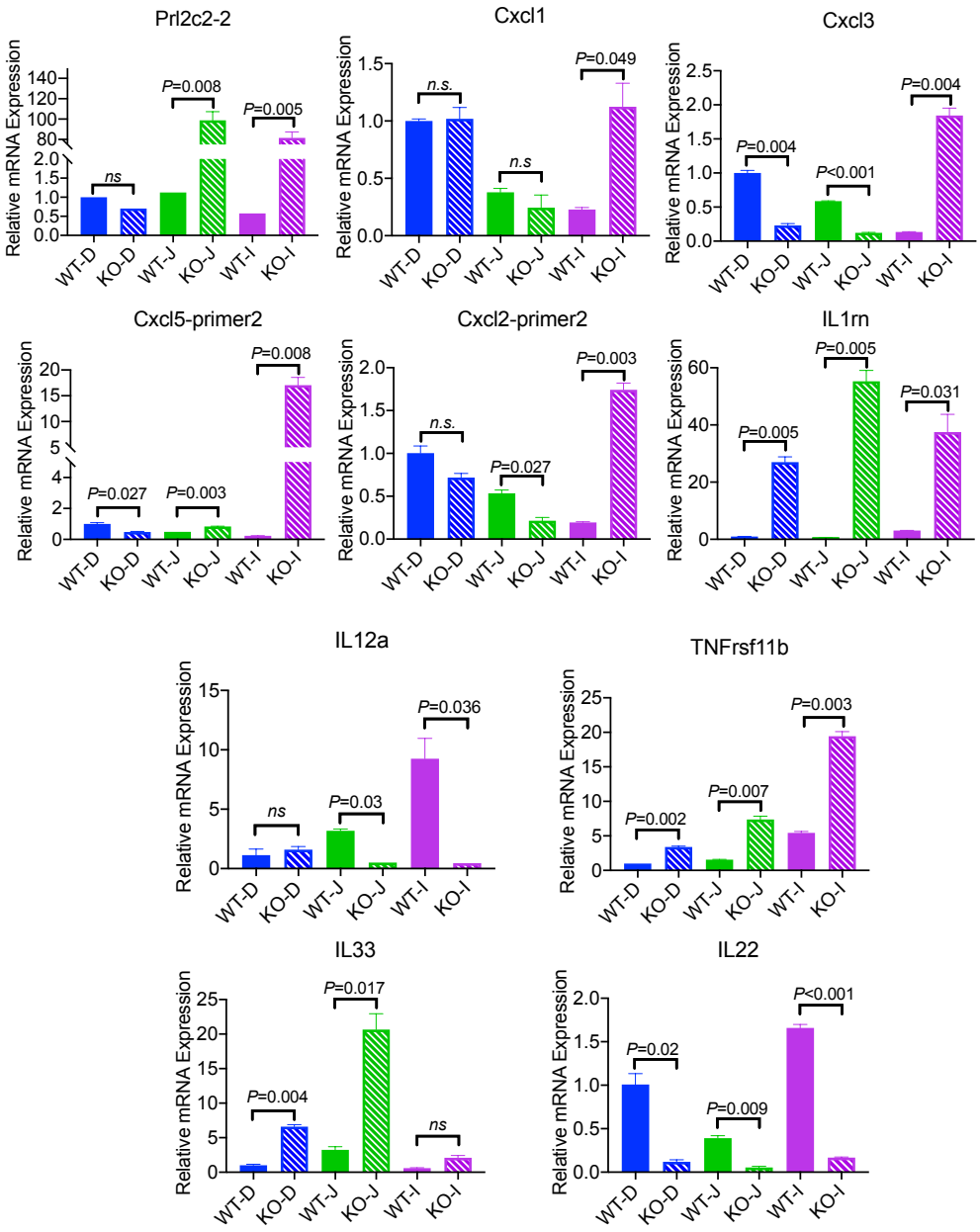

Figure 33. Loss of Cdc42 lead to production of gut hormones and chemokines from epithelium.

Realtime-PCR detected increased Prl2c-2, Cxcl1/2/3/5, IL1rn, TNFrsf11b mRNA level specially at the Ileum, no change of IL33 mRNA level and decreased IL22, IL12a level in isolated epithelial cells from *Cdc42*$^{\Delta IEC}$ mice.

A

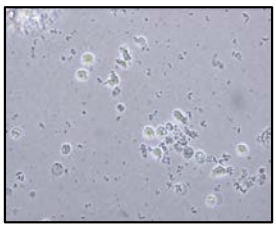
Cdc42ΔIEC LP cells

B

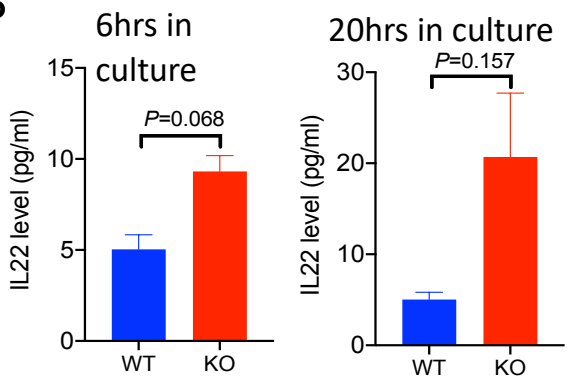
6hrs in culture
IL22 level (pg/ml)
P=0.068
WT
KO
20hrs in culture
IL22 level (pg/ml)
P=0.157
WT
KO

C

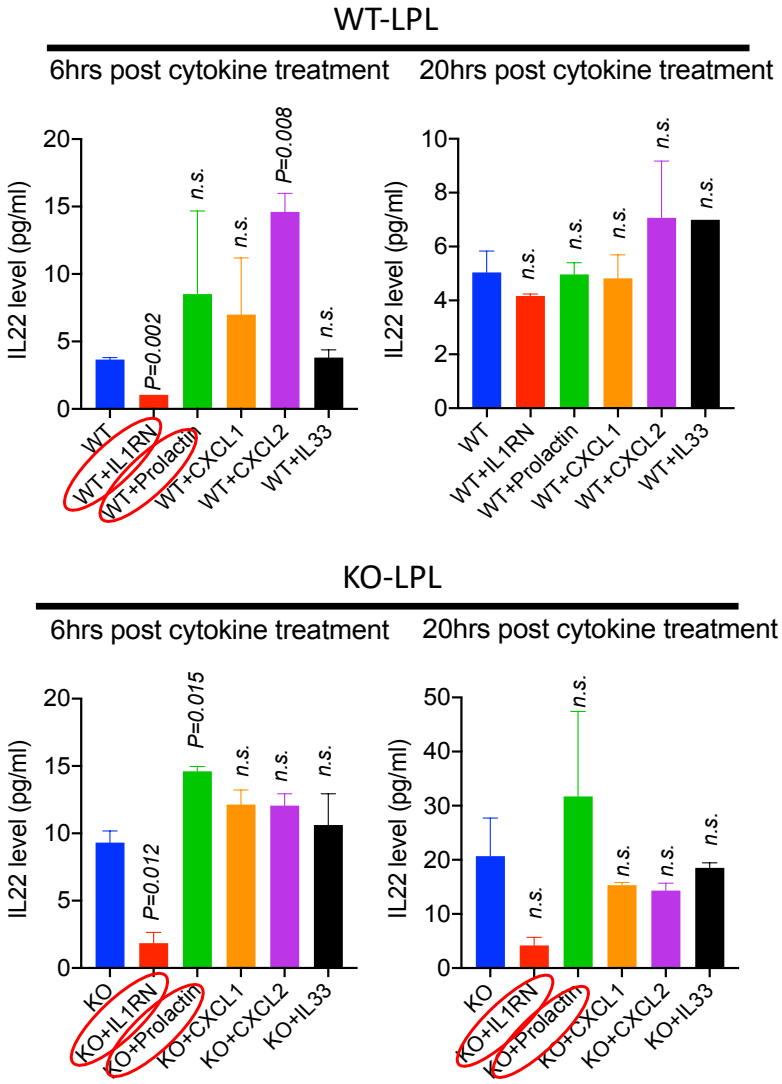
WT-LPL
6hrs post cytokine treatment
20hrs post cytokine treatment
IL22 level (pg/ml)
P=0.002
P=0.008
n.s.
WT
WT+IL1RN
WT+Prolactin
WT+CXCL1
WT+CXCL2
WT+IL33
KO-LPL
6hrs post cytokine treatment
20hrs post cytokine treatment
IL22 level (pg/ml)
P=0.012
P=0.015
n.s.
KO
KO+IL1RN
KO+Prolactin
KO+CXCL1
KO+CXCL2
KO+IL33

Figure 34. Prolactin induces production of IL22 from isolated mouse intestinal LPLs.

(A) Bright field image shows isolated LPL from *Cdc42*$^{\Delta IEC}$ mice. (B) ELISA of IL22 showed LPLs isolated from *Cdc42*$^{\Delta IEC}$ mice produced more IL22 at both a 6hrs or 20 hrs time period compared to WT LPLs. (C) ELISA detected that prolactin induced IL22 production in LPL isolated from *Cdc42*$^{\Delta IEC}$ mice after 6hrs stimulation but not in LPLs from WT mice; IL1RN suppressed IL22 production in both WT and *Cdc42*$^{\Delta IEC}$ LPLs at 6hrs.

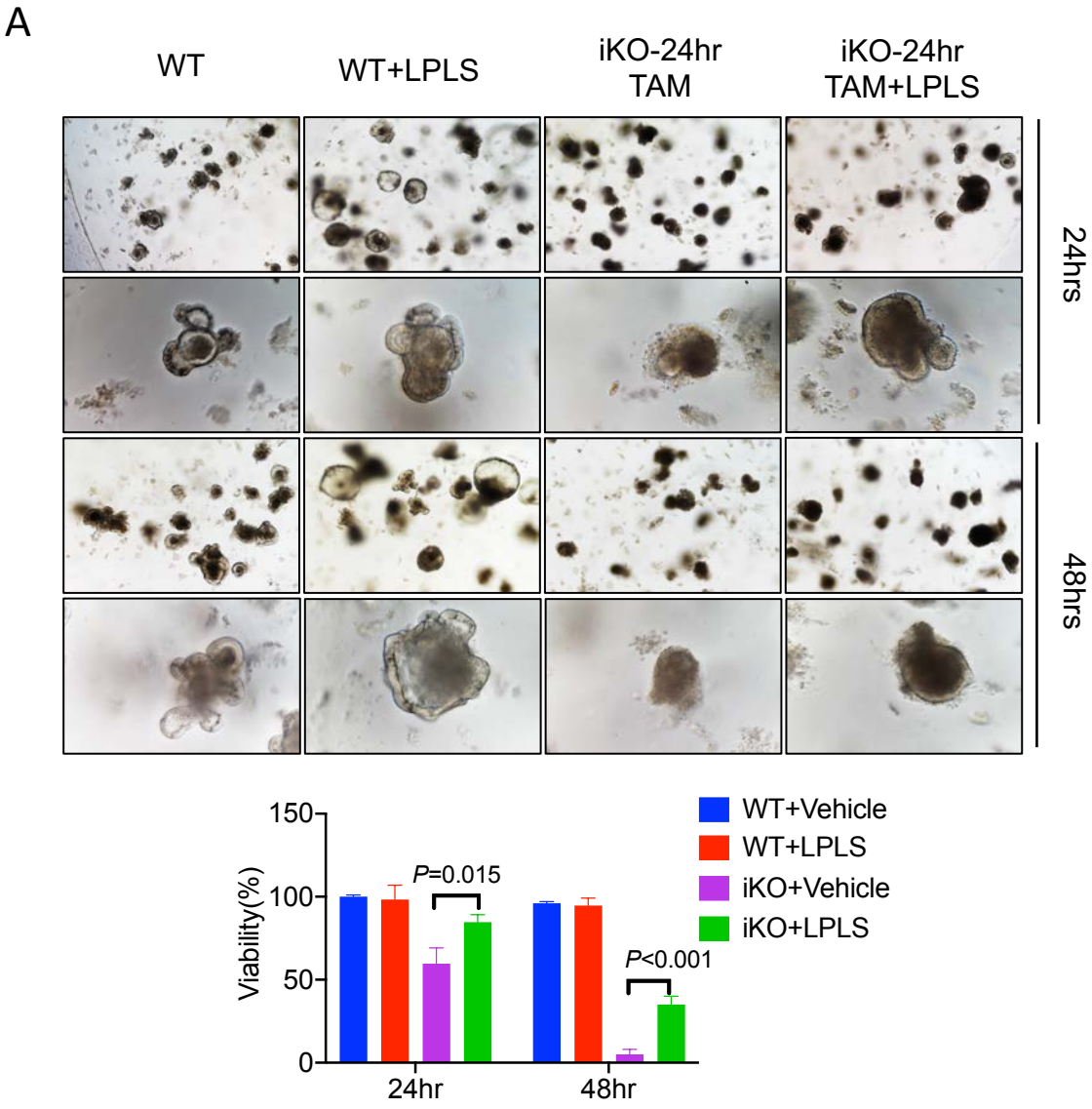
A
WT
WT+LPLS
iKO-24hr TAM
iKO-24hr TAM+LPLS
24hrs
48hrs
Viability(%)
150
100
50
0
P=0.015
P<0.001
24hr
48hr
WT+Vehicle
WT+LPLS
iKO+Vehicle
iKO+LPLS
B
iKO
iKO+LPLS
4-OHT (hrs)
-
24
48
72
-
24
48
p-ERK1/2
ERK1/2
β-actin

Figure 35. Cultured LPL supernatant enhances *Cdc42*^{iKO} enteroid viability and sustains the pERK level.

(A) Representative images of WT and *Cdc42*^{iKO} enteroids with or without LPL supernatant at 24 or 48 hrs after 4-OHT induced Cdc42 deletion. Quantification represents 2 replicates for each condition. (B) Western blot detected pERK1/2 in lysate from *Cdc42*^{iKO} enteroids supplemented without or with LPL supernatant for indicated time points.

Cdc42$^{\Delta IEC}$ epithelial survival requires a microbial component in homeostasis and after injury

Tlr4 agonists were known to activate IL22 and IL12 (Pickert et al., 2009; Tominaga et al., 2013) (Kobayashi et al., 2003), and transcriptomic analysis indicated a potential involvement of microbiome and bacterial sensing in *Cdc42$^{\Delta IEC}$* intestines **(Fig. 22).** To assess the contribution of microbiota, we administrated a drinking water cocktail of antibiotics (abx) (Rey et al., 2018) to *Cdc42$^{\Delta IEC}$* mice through drinking water. Surprisingly, *Cdc42$^{\Delta IEC}$* mice on abx drinking water displayed a pronounced loss of body weight (up to 30%) within 9 days, compared to *Cdc42$^{\Delta IEC}$* mice on regular water **(Fig. 36A)**. Because *Cdc42$^{\Delta IEC}$* mice develop epithelial defects due to loss-of-Cdc42 prior to adulthood, we examined the effect of microbial impact in adult *Cdc42^{iKO}* mice that were functionally wild type before tamoxifen administration **(Fig. 36B)**. Adult *Cdc42^{iKO}* mice were given abx for a week **(Fig. 36B)** followed by genomic sequencing of bacterial 16S DNA to validate microbial depletion in fecal samples **(Fig. 36C).** Abx had no effect on *Cdc42^{iKO}* mice before tamoxifen injection. However, upon tamoxifen administration, abx-treated *Cdc42^{iKO}* mice showed a pronounced body weight loss compared to *Cdc42^{iKO}* mice drinking regular water **(***p*=0.001, **Fig. 36B)**, with significant reductions in STAT3 signaling targets, c-*Myc, Mmp9* (**Fig. 36D**) compared to non-abx treated *Cdc42^{iKO}* mice.

Histopathological assessment of abx-treated *Cdc42^{iKO}* mice revealed severe villus blunting and loss of normal-appearing crypts **(Fig. 37A),** and reduced Olfm4^{+} **(Fig. 37B)** or pERK1/2^{+} IECs **(Fig. 37C)**. Meanwhile, *Survivin* an anti-apoptosis

protein and STAT3 downstream target, was further reduce too in abx-treated *Cdc42*^{iKO} mice **(Fig. 37D)**.

We further attempted to abrogate the major bacterial sensing adaptor Myd88 (downstream of Tlr4) in *Cdc42*$^{\Delta IEC}$ mice by establishing *Cdc42*$^{Fl/Fl}$*;Myd88*$^{Fl/Fl}$*;Villin-Cre* double knockouts. Only 3 double knockouts were obtained from over 100 progenies over 1-year of breeding indicating early lethality. The surviving *Cdc42*$^{Fl/Fl}$*; Myd88*$^{Fl/Fl}$*;Villin-Cre* pups showed early onset of rectal prolapse **(Fig. 38A)**, were runt with 40% less body weight **(Fig. 38B)**, and had distorted villi **(Fig. 38C)**, and reduced Olfm4^{+} cells at steady states **(Fig. 38C)**. Loss of Myd88 from *Cdc42*$^{\Delta IEC}$ mice shut down the production of CXCL2,3,5 but not IL1rn or TNFrsf11b **(Fig. 38D)**, suggesting CXCL expression is sensitively subject to the microbial cues, especially those signals sensed through the epithelial membrane where Myd88 is involved. These data suggested that intact gut microbiota and bacterial sensing by *Cdc42*-deficent IECs were protective for the hosts.

We next investigated, to what extend the microbial signals were protective against epithelial injury in the context of an intact versus Cdc42-deficient hosts. We found that abx treatment **(Fig. 39A**) further diminished injury-induced regenerative capacity in *Cdc42*$^{\Delta IEC}$ mice with regard to loss of regenerating crypts **(Fig. 39B)** and crypt base ISCs **(Fig. 39C)**.

In all, signaling inputs from microbiome and lamina propria lymphocytes compensated for the diminished canonical ISC signature and modified Cdc42-EGFR survival program leading to renewal and regeneration of intestinal epithelia. These results shed new light on the activation of epithelial extrinsic signals during

injury to promote epithelial survival and regeneration in hosts with diminished and/or defective survival program.

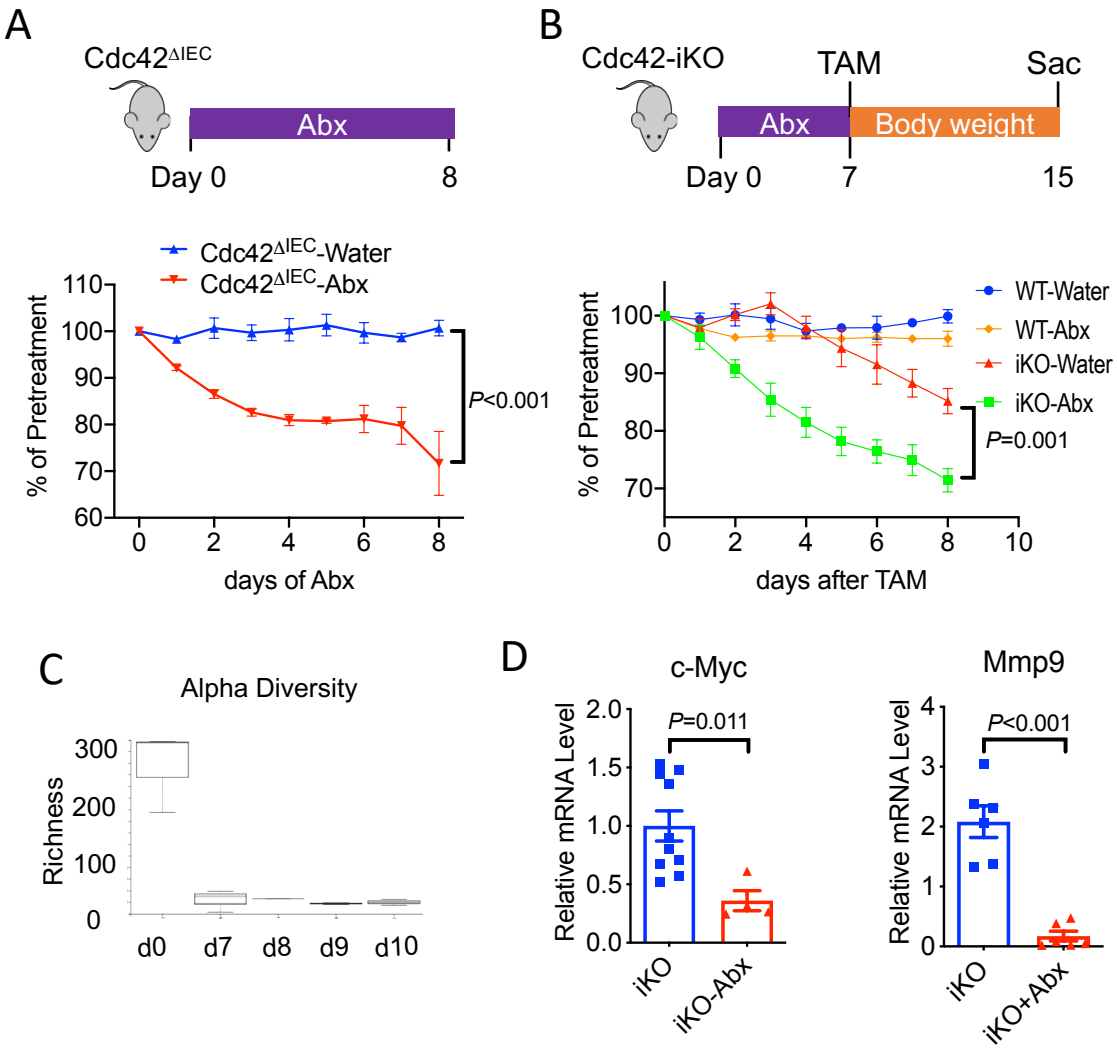
A
Cdc42ΔIEC
Abx
Day 0
8
Cdc42ΔIEC-Water
Cdc42ΔIEC-Abx
% of Pretreatment
110
100
90
80
70
60
0
2
4
6
8
days of Abx
P<0.001
B
Cdc42-iKO
TAM
Sac
Abx
Body weight
Day 0
7
15
WT-Water
WT-Abx
iKO-Water
iKO-Abx
% of Pretreatment
100
90
80
70
0
2
4
6
8
10
days after TAM
P=0.001
C
Alpha Diversity
Richness
300
200
100
0
d0
d7
d8
d9
d10
D
c-Myc
Relative mRNA Level
2.0
1.5
1.0
0.5
0.0
P=0.011
iKO
iKO-Abx
Mmp9
Relative mRNA Level
4
3
2
1
0
P<0.001
iKO
iKO+Abx

Figure 36. Ablation of microbiome caused significant body weight loss of *Cdc42*$^{\Delta IEC}$ and *Cdc42*^{iKO} mice.

(A) *Cdc42*$^{\Delta IEC}$ mice (n=5), treated by antibiotics in drinking water, showed a significant body weight loss compared to *Cdc42*$^{\Delta IEC}$ mice (n=2) on regular drinking water. (B) *Cdc42*^{iKO} mice, before tamoxifen injection, were treated with antibiotics for a week followed by tamoxifen injection. Body weight changes were measured daily after tamoxifen administration. Compared to *Cdc42*^{iKO} mice on regular water, *Cdc42*^{iKO} mice on antibiotics showed significant body weight loss (n=3 for each condition). (C) Alpha diversity analysis of the microbiome in *Cdc42*^{iKO} mice before and after antibiotic administration confirmed microbial ablation. (D) The elevated mRNA levels of c-Myc and Mmp9 in *Cdc42*^{iKO} mice were reduced in *Cdc42*^{iKO} mice treated by antibiotics, detected using real-time PCR. Data were plotted from 3 animals each group including technical replicates.

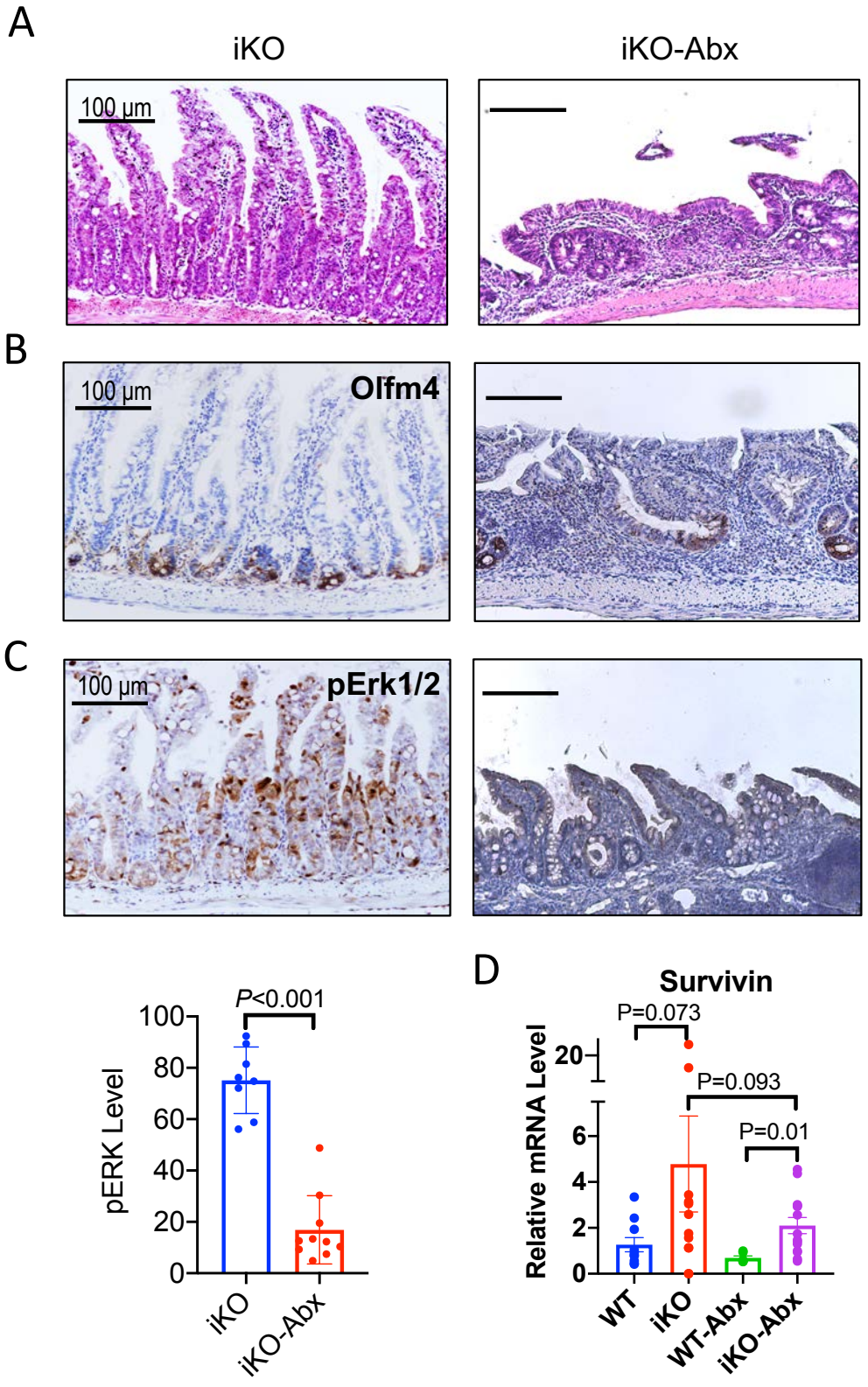
A
iKO
iKO-Abx
100 μm
B
100 μm
Olfm4
C
100 μm
pErk1/2
P<0.001
pERK Level
100
80
60
40
20
0
iKO
iKO-Abx
D
Survivin
P=0.073
P=0.093
P=0.01
Relative mRNA Level
20
6
4
2
0
WT
iKO
WT-Abx
iKO-Abx

Figure 37. Depletion of microbiota lead to further damage of mucosa in *Cdc42^{iKO}* mice and reduced STAT3 target gene expression.

(A) Representative ileal epithelia of *iKO* mice on regular water or antibiotics water. (B) Representative immunohistochemistry for Olfm4 and pERK1/2 in *Cdc42^{iKO}* mice on regular water versus on antibiotics. (C) Average p-ERK1/2 protein levels within a crypt-villus unit were quantified from multiple sections of 3 animals each condition. (D) qRT-PCR showed that the increased level of *Survivin*, an IL22-STAT3 target, in *Cdc42^{iKO}* intestines were decreased by antibiotics treatment.

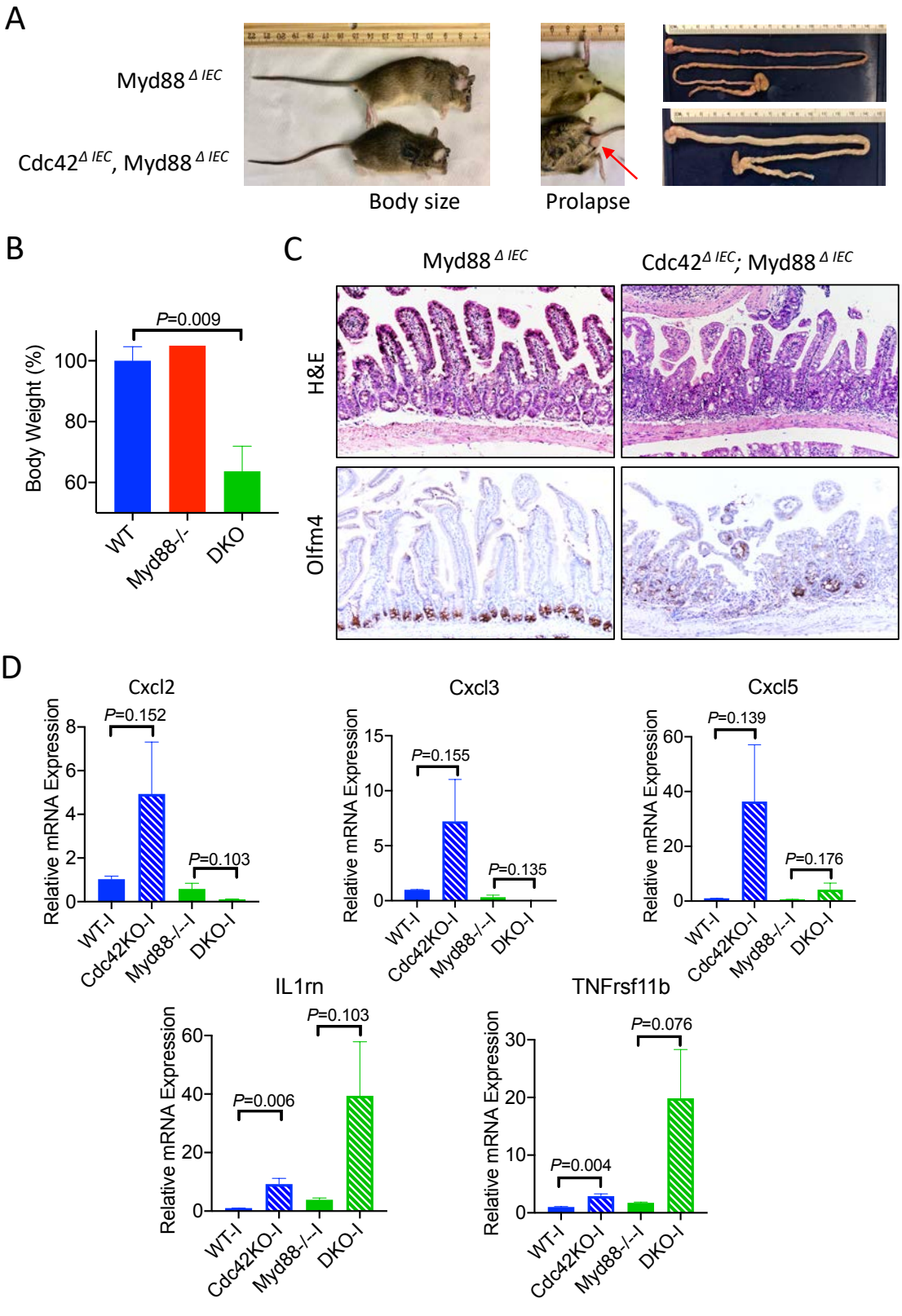
A
Myd88 Δ IEC
Cdc42Δ IEC, Myd88 Δ IEC
Body size
Prolapse
B
P=0.009
Body Weight (%)
100
80
60
WT
Myd88-/-
DKO
C
Myd88 Δ IEC
Cdc42Δ IEC; Myd88 Δ IEC
H&E
Olfm4
D
Cxcl2
P=0.152
P=0.103
Relative mRNA Expression
WT-I
Cdc42KO-I
Myd88-/--I
DKO-I
Cxcl3
P=0.155
P=0.135
Cxcl5
P=0.139
P=0.176
IL1rn
P=0.006
P=0.103
TNFrsf11b
P=0.004
P=0.076

Figure 38. Removal of Myd88 from Cdc42 KO mice further disrupted the homeostasis.

(A) Representative images of *Myd88Fl/Fl; Vil-Cre and Cdc42Fl/Fl; Myd88Fl/Fl; Vil-Cre* littermates. Note *Cdc42Fl/Fl; Myd88Fl/Fl; Vil-Cre* mice had early prolapse formation, and shortened intestine length. (B) Body weight percentage of *WT*(n=3), *Myd88Fl/Fl; Vil-Cre* (n=1) and *DKO* (n=2) mice. (C) Histology and Olfm4 staining of *Myd88Fl/Fl; Vil-Cre* and *Cdc42Fl/Fl; Myd88Fl/Fl; Vil-Cre* mouse intestines. (D) Realtime-PCR mRNA level of CXCL2,3,5, IL1RN, TNFrsf11b in isolated epithelial cells from the Ileum of *WT, Cdc42 KO, Myd88Fl/Fl; Vil-Cre* and *Cdc42Fl/Fl; Myd88Fl/Fl; Vil-Cre* mice.

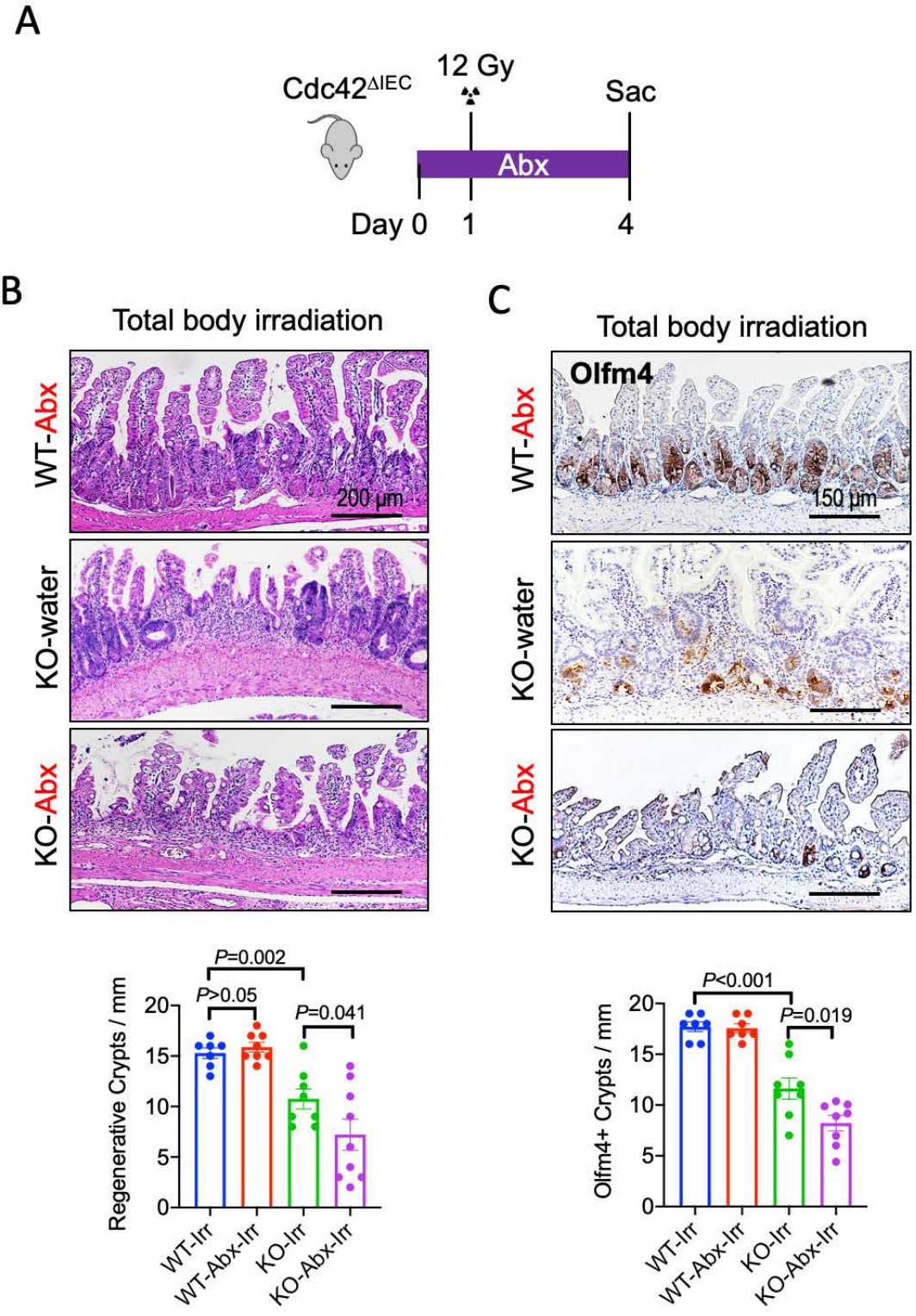
A
Cdc42ΔIEC
12 Gy
Sac
Abx
Day 0
1
4
B
Total body irradiation
WT-Abx
KO-water
KO-Abx
200 μm
C
Total body irradiation
Olfm4
WT-Abx
KO-water
KO-Abx
150 μm
P=0.002
P>0.05
P=0.041
Regenerative Crypts / mm
20
15
10
5
0
WT-Irr
WT-Abx-Irr
KO-Irr
KO-Abx-Irr
P<0.001
P=0.019
Olfm4+ Crypts / mm
20
15
10
5
0
WT-Irr
WT-Abx-Irr
KO-Irr
KO-Abx-Irr

Figure 39. Microbiome and immune cell signals are required for regeneration of Cdc42-deficient IECs.

(A) *Cdc42*$^{\Delta IEC}$ and littermate WT mice were treated with antibiotics for one day then subjected to 12 Gy total body irradiation. Mice remained on antibiotics and were sacrificed 3 days after irradiation. (B) Average numbers of regenerative crypts per mm and levels of Olfm4 within a crypt were quantified from multiple sections of *WT* (n=3) and *Cdc42*$^{\Delta IEC}$ (n=3) mice on regular water, *WT* (n=3) and *Cdc42*$^{\Delta IEC}$ (n=4) mice on antibiotics. (C) Representative ileal histology and Olfm4 immuno-histochemistry of mice with designated genotype and treatment. Note a further reduction of regenerating crypts and Olfm4+ crypt cells in antibiotics-treated *Cdc42*$^{\Delta IEC}$ mice.

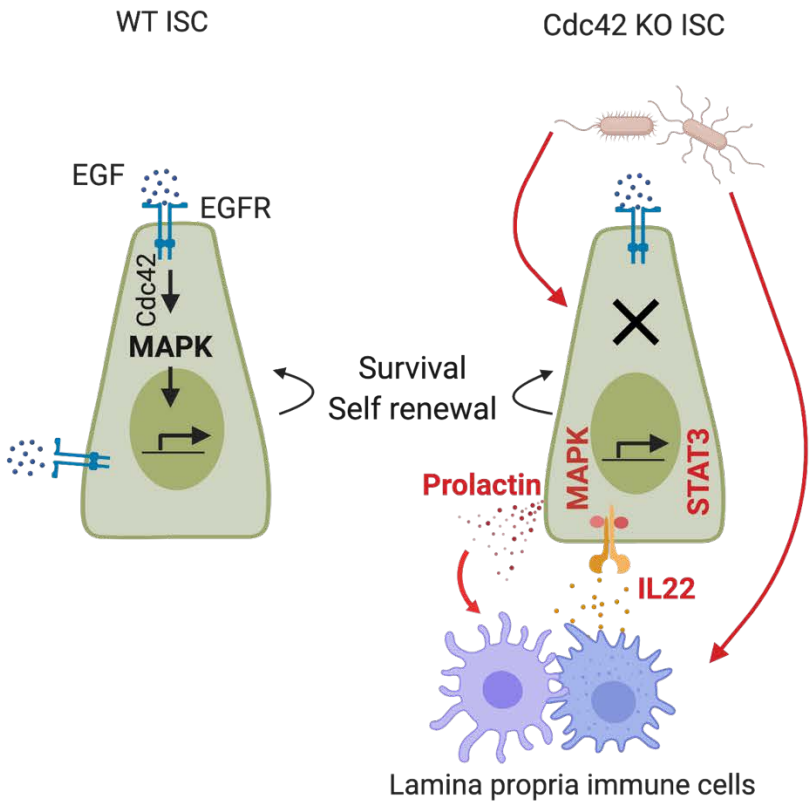

Figure 40. Graphic model.

A graphic model showing that microbiome and immune signals became essential for the renewal of ISCs lacking intrinsic Cdc42-MAPK survival program.

DISCUSSION

This chapter provides molecular, genetic, and cell biological insight into underlying mechanism that provide intestinal epithelial tissue with extraordinary regenerative capacity and cellular plasticity in response to injury. Additionally, when combined, the totality of the data provides a novel framework that links microbiome and immune cell derived paracrine signals into the regenerative and plasticity cascade of ISCs. In particular, extrinsic signals that appear dispensable in wild type hosts contribute critical functionality for tissue regeneration in hosts with intrinsic ISC defects **(Fig. 40)**. Together, this chapter provided evidence to support the essential involvement of extrinsic growth signals in hosts with an impaired ISC intrinsic survival program.

A provocative question initially arising with *Cdc42*$^{\Delta IEC}$ mice was how ISCs lacking Cdc42 were capable of sustaining a level of homeostasis *in vivo* whereas their clonogenicities were totally lost *ex vivo*. Since enteroids grow in an environment lacking microbiome and niche-supporting lamina propria components such as fibroblasts (Kabiri et al., 2014), telocytes (Aoki et al., 2016; Shoshkes-Carmel et al., 2018), and immune cells (Biton et al., 2018a), we searched for signals from extraepithelial sources that might have contributed to the regenerative activities in *Cdc42*$^{\Delta IEC}$ mice. Unbiased transcriptomic and enteroid rescue experiments uncovered, surprisingly, that multiple inflammatory cytokines were able to restore the growth of *Cdc42*-deficient enteroids, while canonical Wnt and EGF ligands failed to do so. Of note, IL22, IL12, IL34 and CXCL2 rescuing cytokines are primarily produced by innate or adaptive immune cells (Hasegawa et al., 2011;

Parks et al., 2016; Rigby et al., 2005), and *Cdc42*$^{\Delta IEC}$ intestinal mucosa produced elevated amounts of these cytokines. It is important to note in our study that abrogating IL22 did not impair ISC renewal or irradiation-induced regeneration in animals carrying wild type Cdc42. These data strongly support the notion that enhanced cytokine signaling from immune cells may be fundamental in supporting ISC functions especially in the context of reduced epithelial intrinsic survivability. Gronke and colleagues recently showed that IL22, produced by group 3 innate lymphoid cells and γδ T cells, is an important regulator of the DNA damage response machinery and protects intestinal epithelial stem cells against genotoxic stress (Gronke et al., 2019).

The identification of anatomically distinct mucosal cell populations that activate survival pathways and crosstalk (i.e., EGFR-MAPK vs. IL22-STAT/MAPK) is important for our understanding of how epithelial plasticity is both generated and maintained in response to injuries. Paracrine cytokines such as IL22 and others bind to cell surface receptors to recruit and activate Jak-Stat (Commins et al., 2008; Pickert et al., 2009). a mechanism that is initially distinct from EGF-induced receptor endocytosis and MAPK signaling. Importantly, mice with normal epithelial Cdc42-EGFR survival program appear tolerant to IL22 loss at steady states and after irradiation challenge. This suggest IL22/MAPK signal might be only allowed when EGFR/MAPK is compromised. As a result, removing IL22 or blocking STAT3 from hosts that lack Cdc42/EGFR/MAPK severely exacerbated disease manifestations in homeostasis and after injury. These results collectively suggest that the paracrine cytokines and STAT3 axis were protective for Cdc42-deficient

IECs probably as a compensatory survival mechanism.

Gut microbiome interact with the intestine tissue and induce epithelial responses as well as immune responses. The host also affects its own microbiome in many ways. Genetics, in addition to environmental factors such as diet and founder effect, determines and gardens microbiota of an individual (Goodrich et al., 2014) (Goodrich et al., 2017; Tierney et al., 2019). We mapped out stool microbiome changes at family level induced by Cdc42 deletion in the epithelium. The altered microbiome resulted from Cdc42 loss at the intestinal mucosa might be a corresponding reorganization of bacteria favored by current mucosa condition. After Cdc42 deletion, we have characterized a series of modified features of the intestinal tissue, including Paneth cell dislocation, stem cell reduction and dysfunction, increase of Goblet cells, delocalization of apical proteins, and abnormality of cell division, et al. Whether and how these changes in Cdc42 KO epithelium contribute to modification of the microbiota is not clear. Besides, Cdc42 has been shown to mediate the pathogen transfer of SFB through endocytosis in the intestinal epithelium, while Cdc42 deletion reduces Th17 cell differentiation (Ladinsky et al., 2019a). These indirect changes in immune cells might be potential mechanism for both microbiome gardening and stem cell maintenance regulated by Cdc42 as well.

SUMMARY OF CHAPTER4

How the intestinal epithelium maintains homeostasis and regenerative capacity during constant exposure to genotoxic and pathogenic insults is unclear. *Ex*

vivo survival and clonogenicity of ISCs strictly required Cdc42-mediated MAPK signaling and Cdc42-deficient enteroids underwent rapid apoptosis. However, mice with Cdc42-deficient epithelium were viable and maintained functional homeostasis. An *ex vivo* screen demonstrated that a number of inflammatory cytokines restored growth of *Cdc42*-deficient enteroids. Indeed, IL22 signal through both STAT3 and MAPK to support the survival of *Cdc42*-deficient enteroids. A special hormone Prolactin was secreted by Cdc42-deficient epithelium to activate IL22 production from lamina propria cells. Antibiotic treatment, IL-22 deficiency, or STAT3 blockage compromised epithelial survival and injury-induced regeneration in mice lacking epithelial Cdc42. Our results show that ISC-intrinsic survival programs and signals from immune and microbiome compartments provide non-redundant layers of protection for epithelial integrity.

CHAPTER 5

RECEPTOR-MEDIATED ENDOCYTOSIS GENERATES NANOMECHANICAL FORCE REFLECTIVE OF LIGAND IDENTITY AND CELLULAR PROPERTY

Information included in this chapter was partially taken from and had been published in

Zhang et al., Journal of Cellular Physiology (2017); 10.1002/jcp.26400

INTRODUCTION

The mammalian cell plasma membrane is a lipid bilayer separating extra- and intra-cellular components. It functionally transduces environmental signals via a diverse array of membrane-bound proteins. Chemical or thermal signals induce dynamic organization of lipids and proteins in the plasma membrane (Bernardino de la Serna et al., 2016). Whether these extracellular stimuli generate quantifiable, nanoscale, mechano-physical features in the plasma membrane has not been well studied. Specifically, it is not clear whether biochemical alterations in the plasma membrane will lead to substantial changes in the mechanical properties of the membrane. Assessment of such biophysical properties of the plasma membrane may provide important insights about the membrane evolutions at subcellular level, potentially shedding lights on key cellular events related to responding to environmental stimuli.

One of the fundamental cellular processes that involve active plasma membrane reorganization is endocytosis. During endocytosis, macromolecules are internalized by cells through small double-membrane vesicles emerged from plasma membrane. The formation of these endocytic vesicles employs strategies that most notably utilize clathrin- or caveolae-dependent pathways. In clathrin-dependent pathway, the coat protein clathrins are recruited to the cargo-concentrated membrane microdomains bound by clathrin adaptor proteins (APs) (Conner and Schmid, 2003) (Touz et al., 2004) (Gupta et al., 2006) (Kirchhausen et al., 2014) (Owen et al., 2004) (Traub and Bonifacino, 2013) (Kural et al., 2012). Clathrin-independent endocytic pathway is mediated by caveolin family proteins at

cholesterol and glycosphingolipid enriched membrane microdomains, also known as lipid rafts (Razani et al., 2002) (Lajoie and Nabi, 2010; Simons and Toomre, 2000) (Simons and Ehehalt, 2002). Insertion of caveolin into these microdomains drives the formation of flask-shaped membrane invaginations (Anderson, 1998) (Parton and Simons, 2007). In both pathways, the recruitment of a key small GTPase, dynamin, by a variety of accessory proteins, to the pinching site of the membrane enables scission and release of vesicles into the cell. This process exclusively depends on the hydrolysis of GTP by dynamin (Marsh and McMahon, 1999) (Praefcke and McMahon, 2004). Once internalized, the cargos travel to membrane-bound early endosomes, where they are further sorted to recycling endosome, late endosome, or lysosome for signaling or degradation (Sorkin and Von Zastrow, 2009) (Wolfe and Trejo, 2007). The trafficking of endocytic vesicles critically relies on a cytoplasmic ATPase motor, dynein, which dictates the retrograde vesicular movement along the microtubules. Small chemical molecules that inhibit dynamin or dynein activities are effective blockers of endocytosis (Firestone et al., 2012) (Roossien et al., 2015) (Kirchhausen et al., 2008) (Macia et al., 2006) (Hill et al., 2005). Likewise, small molecules that disrupt clathrin function or lipid raft organization have been shown to impact endocytosis (von Kleist et al., 2011) (Ros-Baro et al., 2001) (Auriac et al., 2010) (Allen et al., 2005) (Sarnataro et al., 2009) (Ares and Ortiz, 2012).

Ligand-induced receptor-mediated endocytosis is a particularly important cellular event initiated by extracellular ligands, such as growth factors, at plasma (Sorkin and Von Zastrow, 2009). During this process, ligand engagement of the

plasma membrane-localized receptors triggers an internalization of the ligand-receptor complex through clathrin-dependent or -independent pathways (Marsh and McMahon, 1999) (Rappoport, 2008). Key stem cell growth factors, such as the epidermal growth factor (EGF) and the Wnt proteins, have been demonstrated to induce receptor-mediated endocytosis to transduce, maintain, or terminate corresponding cellular signaling.

Atomic force microscope (AFM) technologies have been developed and utilized to interrogate and/or manipulate live cellular and subcellular structures in a biologically-friendly aqueous environment (Dufrene et al., 2017) (Kasas et al., 2017). Both morphological and/or mechanical properties of a live cell or subcellular compartment can be examined with nanoscale spatial and force resolutions. AFM measurement of mechanical properties (e.g., elasticity) of live cells (Butt et al., 2005), however, has been hampered by the difficulty in accounting for the effects of the cantilever motion and the associated hydrodynamic force on the mechanical measurement (Ren et al., 2013b). These challenges have been addressed in our recently developed control-based AFM nanomechanical measurement protocol (Ren et al., 2013b) (Cinar and Sahin, 2014). Our methods enabled a fast, noninvasive, broadband measurement of the real-time changes of plasma membrane elasticity in live mammalian cells (Ren et al., 2013a; Ren et al., 2013b) (Yu et al., 2015) (Yu et al., 2016)

Here, we utilized this nanomechanical protocol to monitor in real-time the variations of the elasticity in live mammalian cells. We hypothesize that the dynamic organization of plasma membrane during ligand-stimulated endocytosis,

e.g. processes such as the formation of membrane curvature, membrane invagination and fission, generates significant alternation in the mechanical behaviors of plasma membrane. We demonstrate that the changes of the plasma membrane elasticity in live cells sensitively correlate with the membrane status in response to thermal, chemical, and growth factor stimuli known to influence endocytosis. We further show that different ligands induce distinguishable nano-mechanical alterations, whereas cells with a single genetic manipulation produce distinct force signatures at plasma membrane in response to identical ligands.

RESULTS

Temperature alteration and endocytic inhibitors alter membrane elasticity at atomic level

Elasticity of cell membrane is one of the most fundamental and important mechanical characteristics of live mammalian cells. Using AFM, the elasticity of cell membrane can be quantified by applying an excitation force of known profile (amplitude as a function of time) from the cantilever probe to the cell **(Fig. 41 A, B)**, measuring the indentation generated, and then computing the Young's modulus (i.e., elastic modulus) from a chosen probe-sample contact mechanics model (Butt et al., 2005). Endocytosis is a temperature-dependent process (Punnonen et al., 1998) (Tomoda et al., 1989) (Weigel and Oka, 1981). We first assessed the Young's modulus of the plasma membrane of HeLa cells incubated at various temperatures. We detected a temperature-dependent difference in membrane elastic modulus, with an 11 (+/- 0.85) kPa Young's modulus at 37°C

compared to a 5 (+/- 0.3) kPa at 4°C **(Fig. 41C)**. Intermediate membrane elastic modulus was detected at 25°C. To monitor in real-time the evolution of the mechanical behavior (Young's modulus) of cell membrane in response to altered temperatures, we performed continuous measurement on Young's modulus in live cells that underwent a dynamic temperature alteration. As cells were gradually warmed up from 4°C to 25°C, we observed a steady increase in membrane tension, which stabilized around 10 (+/- 0.76) kPa when the temperature reached 25°C **(Fig. 41D)**. Conversely, when temperature was slowly decreased from 37°C to 25°C, cells exhibited a gradual reduction of Young's modulus, which ultimately stabilized around 10 kPa. Interestingly, we were able to detect a wider fluctuation in Young's modulus at higher temperatures (e.g., 25°C and 37°C) that were likely attributable to the enhanced membrane activities, as they were absent from cells at 4°C when only static membrane activity was observed (compare 1-200 s versus 800-1000 s, green line, **Fig. 41D**). Since endocytic rate normally reduces to negligible level below 10°C (Tomoda et al., 1989) , our results of plasma membrane mechano-physical properties suggested that the cell surface elasticity reflected as Young's modulus positively correlated with cellular endocytosis activity.

To examine the above correlation in a more specific manner, we tested plasma membrane elasticity in live cells in response to a potent endocytosis inhibitor dynasore. Dynasore is a membrane permeable reversible noncompetitive small molecular inhibitor for dynamin, which is required for membrane fission and vesicle release in both clathrin-dependent and caveolae-dependent endocytosis (Henley et al., 1999) (Henley et al., 1998). We used two cell biology methods, dextran

uptake and EEA1 staining, to assess endocytosis in parallel to AFM analysis on cells under treatment. Compared to vehicle-treated cells, cells pre-incubated in dynasore-containing medium for 2hrs demonstrated a reduced endocytic uptake of dextran **(Fig. 41F)** and a decreased number of early endosomes marked by EEA1 **(Fig. 41G)**. AFM examination of live cells that were pre-incubated with dynasore revealed a consistent reduction of Young's modulus **(Fig. 41D, E)**. The lowest detected elastic modulus dropped by over two folds to around 5 kPa **(Fig. 41D)**, a value similar to cells that were measured at 4°C. As dynasore was shown to block clathrin-dependent vesicle formation and endocytic pathway within seconds (Macia et al., 2006), we also examined the acute effect of dynasore on cellular membrane tension immediately following 80 μM of dynasore addition to the medium. Within 900 s, the Young's modulus decreased to approximately 5 kPa, strongly suggesting that the reduction of membrane indentation highly correlates with a reduced dynamin-mediated endocytosis **(Fig. 41H)**.

We then tested the effect of a different endocytosis inhibitor, ciliobrevin, which specifically blocks dynein-mediate retrograde movement of endocytic vesicles along microtubules **(Fig. 42A)** (Le Droguen et al., 2015) (Day et al., 2015). Cells pretreated with ciliobrevin A (CBVA) for 1 hr showed a slight reduction in dextran uptake and in the number of early endosomes **(Fig. 42B)**. AFM analysis of CBVA-treated live cells exhibited a drastically lower elastic modulus than vehicle-treated cells, suggesting that blockage of dynein-mediated retrograde transport of endocytic vesicles from the plasma membrane by CBVA reduced membrane elasticity, consistent with an inhibited endocytosis **(Fig. 42C)**.

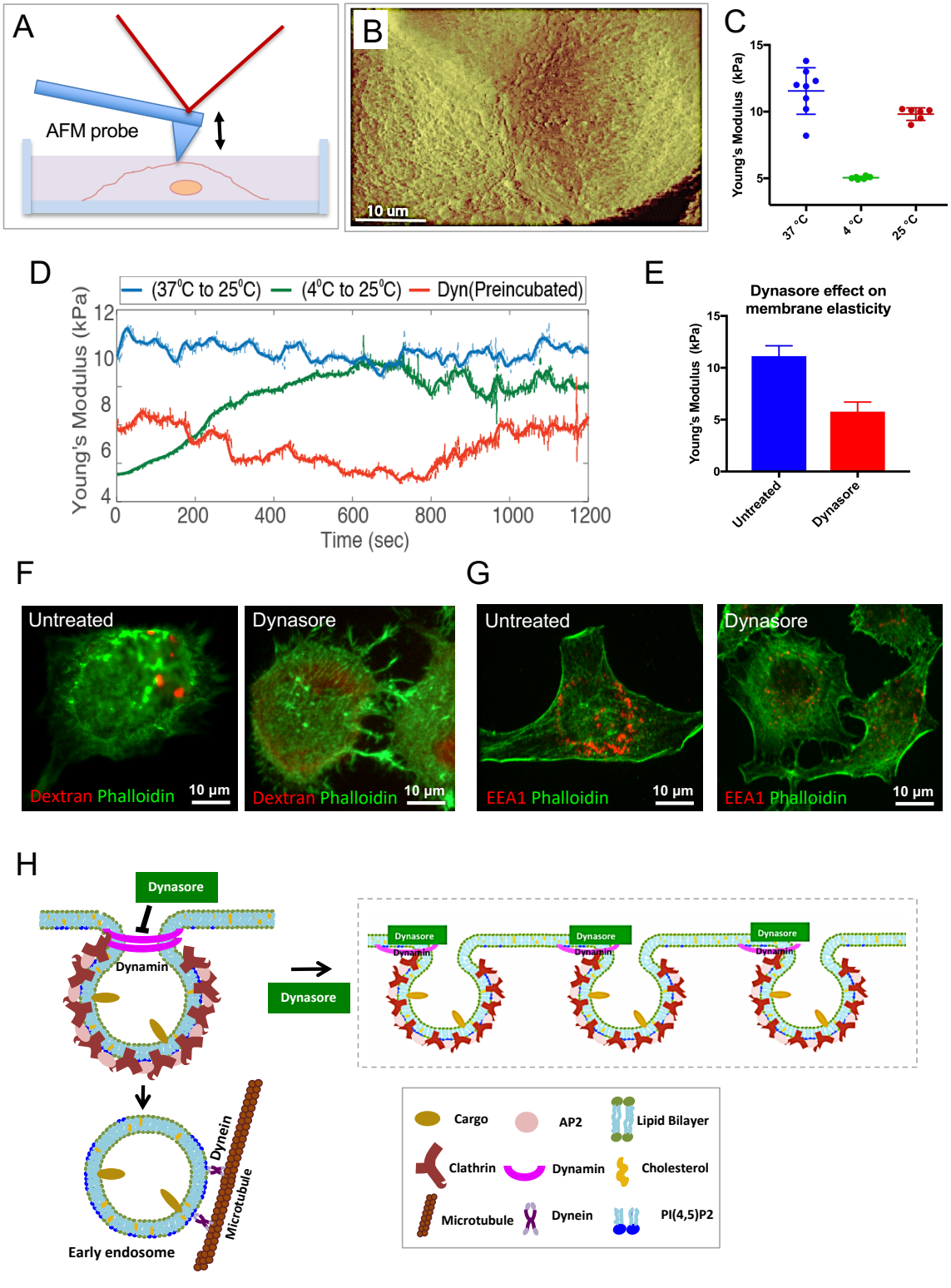
A
AFM probe
B
10 um
C
Young's Modulus (kPa)
15
10
5
37 °C
4 °C
25 °C
D
(37°C to 25°C)
(4°C to 25°C)
Dyn(Preincubated)
Young's Modulus (kPa)
12
10
8
6
4
0
200
400
600
800
1000
1200
Time (sec)
E
Dynasore effect on membrane elasticity
Young's Modulus (kPa)
15
10
5
0
Untreated
Dynasore
F
Untreated
Dextran Phalloidin
10 µm
Dynasore
Dextran Phalloidin
10 µm
G
Untreated
EEA1 Phalloidin
10 µm
Dynasore
EEA1 Phalloidin
10 µm
H
Dynasore
Dynamin
Dynasore
Dynasore
Dynamin
Dynasore
Dynamin
Dynasore
Dynamin
Dynein
Microtubule
Early endosome
Cargo
AP2
Lipid Bilayer
Clathrin
Dynamin
Cholesterol
Microtubule
Dynein
PI(4,5)P2

Figure 41. AFM detects thermal and chemical effects on nanomechanical membrane elasticity.

(A) Schematic diagram showing the setup of AFM and the vertical movement of the cell-contacting probe that applies force on plasma membrane of a live cell in medium. (B) An AFM scanning image of live HeLa cells. (C) AFM detected different Young's modulus of HeLa cells at 37 °C (blue), 4 °C (green), and 25 °C (red). (D) Real-time measurement by AFM on cells in medium with temperature changes from 4 °C to 25 °C (green) and from 25 °C to 4 °C (blue). Cells pre-treated with Dynasore showed an overall decreased Young's modulus (red line). (E) Dynasore pretreatment reduced membrane elasticity by half. (F and G) Dynasore treatment reduced dextran uptake and EEA1 positive early endosomes. (H) Schematic diagram illustrating the blockage of endocytosis by Dynasore may alter the plasma membrane mechanical property

The cell surface nanomechanical property reflects plasma membrane composition and organization.

We reasoned that as here the elasticity was measured by exerting an external force to the outer surface of cellular plasma membrane, the change of Young's modulus likely reflected the fluidity or rigidity of the membrane, which is often influenced by the composition and configuration of lipids. We then employed small molecules known to perturb the lipid bilayer composition or organization and asked whether they would induce detectable elastic alterations by AFM. Chlorpromazine (CPZ) usually inserts its hydrophobic cationic portion in the lipid bilayer of cell membrane by binding to poly-phosphoinositides **(Fig. 42A, E)**. By abrogating the $PI_{(4,5)}P_2$-dependent membrane recruitment of AP2 adaptor, CPZ has been shown to block clathrin-mediated endocytosis (Sofer and Futerman, 1995). The literature also suggested a tendency for CPZ to suppress clathrin-independent endocytosis (Vercauteren et al., 2010). Cells treated with CPZ for 2 hrs showed a reduced uptake of dextran into small vesicular puncta, which was accompanied by a clear reduction of EEA1 positive early endosomes **(Fig. 42D).** However, in contrast to the effects of dynasore and ciliobrevin, CPZ treatment almost doubled the elastic modulus in live HeLa cells up to 22 kPa **(**red line, **Fig. 42E)**, indicating that the Young's modulus here reflected an increased membrane rigidity upon CPZ anchoring to the lipid bilayer. This notion was also supported by treating cells with Filipin, a small molecule that binds with high affinity to cholesterols in plasma membranes, forms globular deposits, and disrupts the planar organization of the membrane **(Fig. 42H)**. Filipin-treated cells exhibited even stiffer membrane with

the Young's modulus quadrupled to nearly 50 kPa **(**yellow line, **Fig. 42E)**, an effect that was in agreement with the reported cellular plasma membrane viscosity and rigidity in Filipin-treated cells (Bonneau et al., 2010). Filipin treatment also inhibited dextran uptake into small vesicles as well as reduced the number of early endosome **(Fig. 42G)**, consistent with its reported blockage on non-coated endocytosis (Schnitzer et al., 1994) (Orlandi and Fishman, 1998). Thus, the increased membrane tension in CPZ- or Filipin-treated cells was not reflective of endocytic rate in these cells; instead it indicated the membrane rigidity.

We further tested the effects of MβCD, a small molecule that extracts cholesterol from cellular membranes (Vercauteren et al., 2010) **(Fig. 42J)**. Strikingly, addition of MβCD led to an initial fluctuation of membrane elasticity in the first 200 s, followed by a rapid decrease of elastic modulus around 300 s **(Fig. 42J)**. The Young's modulus became stabilized around 2 kPa that likely represented the minimal membrane elasticity in these cells. MβCD-treated cells showed a reduced dextran uptake and decreased number of early endosomes **(Fig. 42I)**, consistent with its reported inhibition on endocytosis in various cell lines (Vercauteren et al., 2010). Taken together, although CPZ, Filipin, and MβCD have similarly inhibitory effects on endocytosis, these pharmacological molecules elicited mechanistically distinct nanoscale elasticity profiles at plasma membrane, which should reflect their different actions on membrane configuration and composition.

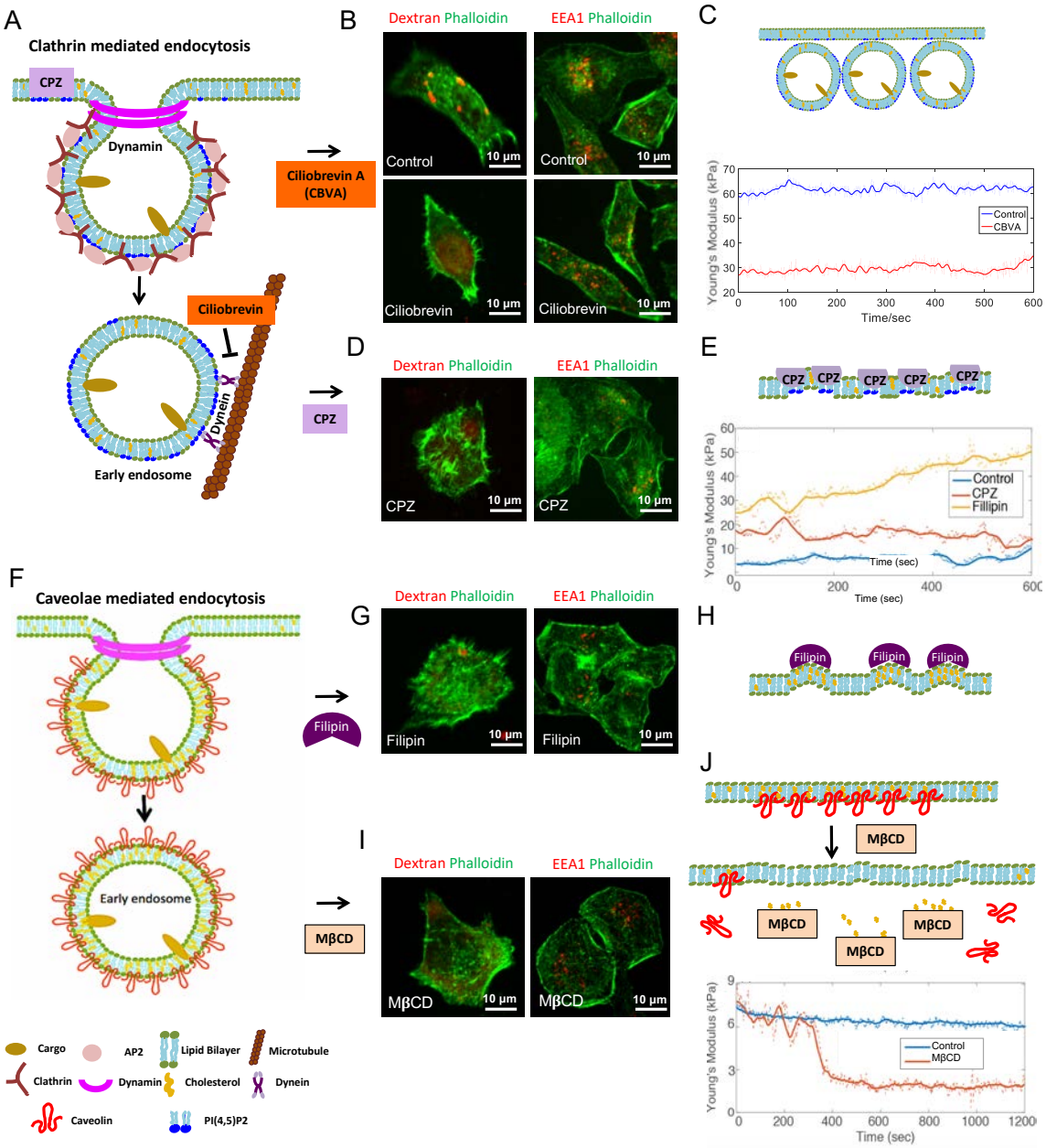
A
Clathrin mediated endocytosis
CPZ
Dynamin
Ciliobrevin A (CBVA)
Ciliobrevin
Dynein
Early endosome
B
Dextran Phalloidin
EEA1 Phalloidin
Control
Ciliobrevin
10 μm
C
Young's Modulus (kPa)
Time/sec
Control
CBVA
D
CPZ
E
Control
CPZ
Fillipin
Time (sec)
F
Caveolae mediated endocytosis
Early endosome
G
Filipin
H
I
MβCD
J
Cargo
AP2
Lipid Bilayer
Microtubule
Clathrin
Dynamin
Cholesterol
Dynein
Caveolin
PI(4,5)P2

Figure 42. The AFM elasticity property reflects the composition and organization of plasma membrane.

(A) Schematic diagram illustrating clathrin-mediated endocytosis and the molecular targets of Ciliobrevin A (CVBA) and CPZ. (B) CVBA treatment reduced dextran uptake and EEA1 endosome. (C) AFM detected a clear decrease in Young's modulus in CVBA-treated cells. The diagram above illustrates the blocked Dynein-dependent retrograde movement of vesicles. (D) CPZ treatment inhibited dextran uptake and EEA1 endosome. The diagram illustrates that CPZ binding to PI4,5P2 lipids on membrane potentially rigidifies the membrane. (E) AFM detected increased Young's modulus in CPZ- and Filipin-treated cells. (F) A diagram illustrating caveolae mediated endocytosis. (G) Filipin treatment decreased dextran uptake and EEA1 endosomes. (H) A diagram illustrating that anchoring of Filipin to cholesterol bends and stiffens the membrane. (I) MβCD treatment of cells reduced dextran uptake and EEA1 endosomes. (J) AFM detected a rapid decrease of elasticity following an initial fluctuation of modulus in response to addition of MβCD. A diagram above shows the extraction of cholesterol from cellular plasma membrane, potentially contributing to the decreased membrane stiffness.

AFM detects ligand-dependent nanomechanical profiles during receptor-mediated endocytosis

Above chemical molecules are potent membrane disruptors, the effects of which are not physiologically relevant for normal cellular activities. We next asked whether our AFM analysis could detect mechanical alterations in receptor-mediated endocytosis triggered by endogenously expressed ligands. EGF has been well studied for its effect on receptor-mediated clathrin-dependent endocytosis (Vieira et al., 1996). HeLa cells that were serum-starved for 30 mins showed an enhanced uptake of dextran at 2 hrs after EGF addition. This effect was blocked by dynasore **(Fig. 43A, B)**, consistent with the notion that EGF stimulates receptor endocytosis. We performed AFM measurement on serum-starved live cells receiving a single addition of EGF. Remarkably, AFM detected an almost immediate surge of the Young's modulus upon EGF addition to the culture medium **(**red line in **Fig. 43C)**. It took less than 60 s for the Young's modulus to reach the peak, which was followed by a wide range of oscillation between 14 and 17.5 kPa in the next 10 mins. The modulus returned to baseline after approximately 15 mins, reflecting an overall rapid but transient EGF effect on the plasma membrane elasticity. This robust EGF-induced surge of Young's modulus was blocked by pre-incubating cells with dynasore for 2 hrs **(**green line in **Fig. 43C)**, strongly suggesting that the detected EGF-triggered membrane tension was endocytosis-related. Interestingly, cells treated with dynasore alone, starting at 0 sec, showed a gradual decline of Young's modulus, whereas EGF treatment (in the presence of dynasore) appeared to antagonize the inhibitory effect of dynasore (compare

green versus purple lines, **Fig. 43C**). These results suggested that EGF rapidly stimulated receptor-mediated endocytosis, which was blocked by dynasore. In the presence of dynasore, there remained some EGF-receptor engagements at cell surface.

We then postulated whether the AFM-detected EGF effects could be seen for other growth factors that also stimulate receptor endocytosis. We thus tested the effect of Wnt3a, which represents another important extracellular factor required for stem cell renewal and adult tissue homeostasis. Wnt binds its receptor Frizzled and co-receptor LRP6 on plasma membrane. The formation of Wnt/Frizzled/LRP6 tertiary complex triggers an endocytic internalization via clathrin- or caveolae-mediated pathways (Feng and Gao, 2015). Similar to EGF treatment, Wnt3a addition to live serum-starved HeLa cells increased Young's modulus to a peak value around 17 kPa **(**yellow line in **Fig. 43D)**. Interestingly, even though both Wnt3a and EGF elicited similar maximal amplitudes **(Fig. 43E)**, in comparison to EGF, the effect of Wnt3a was almost five times slower lasted over two times longer **(Fig. 43D, F, G)**. It took an approximately 300 s to reach maximal Young's modulus upon Wnt3a addition **(Fig. 43D, F)**, as opposed to less than 60 s for EGF **(Fig. 43C, F).** However, Wnt3a-induced oscillation of membrane elasticity at an elevated modulus was sustained for more than 30 min. Just like EGF, the detected membrane effect of Wnt3a was reflective of receptor endocytosis as it was blunted by either dynasore treatment **(**orange line in **Fig. 43D),** or by lowering the cellular temperature to 4°C **(**purple line in **Fig. 43D)**. When cells gradually warmed up from 4°C to 25°C, this inhibitory effect was released, revealing the membrane effect

elicited by Wnt3a (1200-1600 s, purple line in **Fig. 43D**). These results collectively suggested that Young's modulus was capable not only to detect receptor endocytosis but also to reveal distinct membrane effects elicited by different ligands.

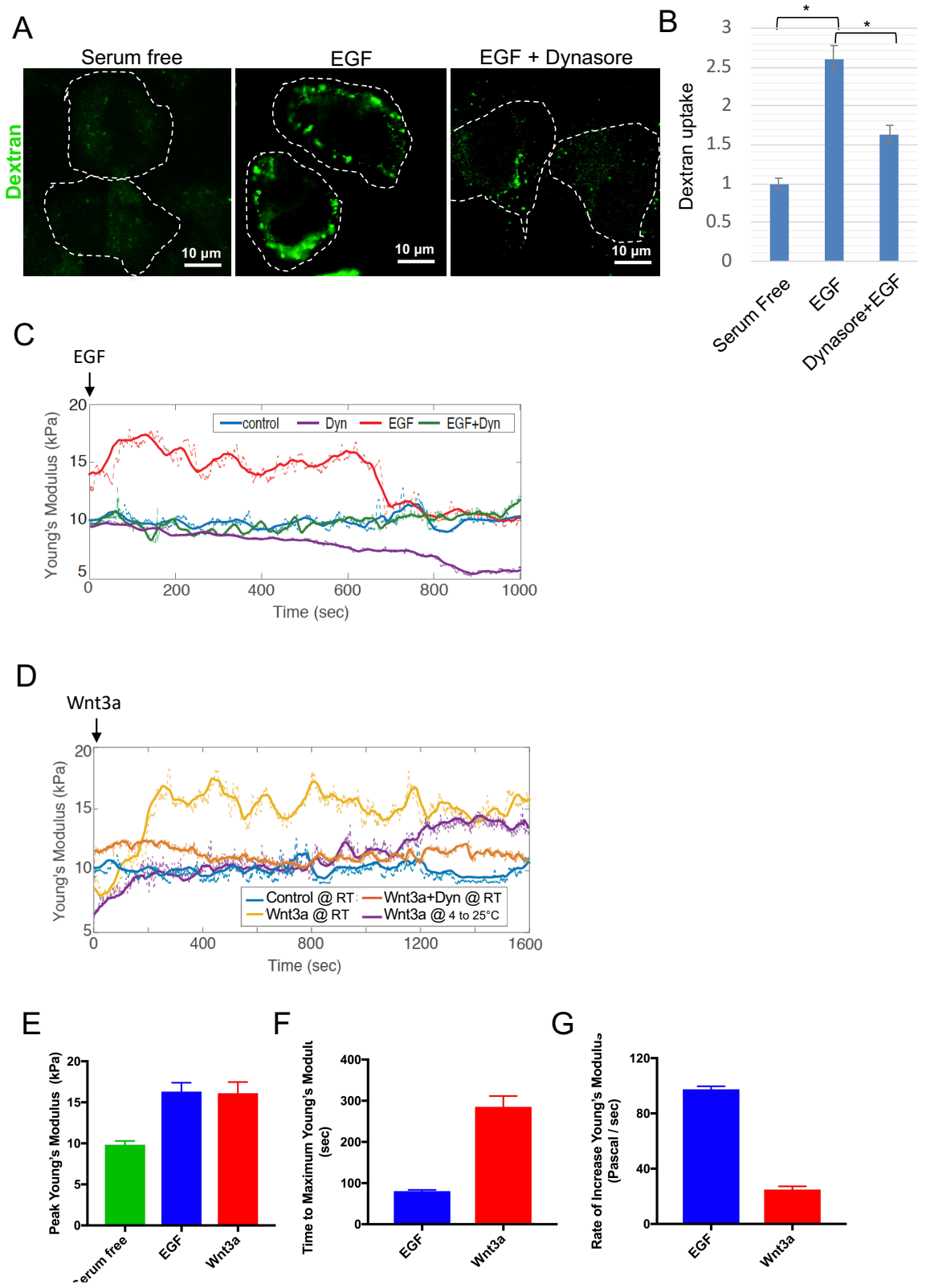
A
Serum free
EGF
EGF + Dynasore
Dextran
10 μm
10 μm
10 μm
B
Dextran uptake
3
2.5
2
1.5
1
0.5
0
*
*
Serum Free
EGF
Dynasore+EGF
C
EGF
Young's Modulus (kPa)
20
15
10
5
0
200
400
600
800
1000
Time (sec)
control
Dyn
EGF
EGF+Dyn
D
Wnt3a
Young's Modulus (kPa)
20
15
10
5
0
400
800
1200
1600
Time (sec)
Control @ RT
Wnt3a+Dyn @ RT
Wnt3a @ RT
Wnt3a @ 4 to 25°C
E
Peak Young's Modulus (kPa)
20
15
10
5
0
Serum free
EGF
Wnt3a
F
Time to Maximum Young's Modul
(sec)
400
300
200
100
0
EGF
Wnt3a
G
Rate of Increase Young's Modulu
(Pascal / sec)
120
80
40
0
EGF
Wnt3a

Figure 43. AFM detects ligand-dependent changes in elastic modulus during receptor-mediated endocytosis.

(A and B) Dextran uptake was stimulated in serum starved HeLa cells by EGF. This effect was blocked by dynasore. (C) Upon addition of EGF to the medium, AFM detected an immediate surge of Young's modulus (compare red to blue line). This effect of EGF was completely blocked by dynasore treatment (green line). Fresh addition of dynasore alone gradually decreased Young's modulus to 5 kPa during a time course of 800 s (purple line). (D) Similar effects were observed after addition of Wnt3a however the response was slower and the duration of response was longer (compare yellow to blue line). This Wnt3a-induced increase in Young's modulus was blocked by dynasore treatment (orange line) or by lowering the temperature (purple line). (E) The effect of EGF on the magnitude of Young's modulus was similar to the effect of Wnt3a. (F and G) EGF elicits a much rapid increase of Young's modulus than Wnt3a.

Single genetic manipulation changes membrane nanomechanics during receptor endocytosis

We next postulated whether the growth factor effects seen in HeLa cells could be reproduced in other cell lines. We chose the Caco2 cells, a colonic epithelial cell line, and performed EGF-stimulated endocytosis experiments. EGF elicited a largely similar change in the membrane elasticity in Caco2 cells **(Fig. 44A)**, suggesting that EGF induced similar nanoscale changes in plasma membranes of both cell types. We then sought to investigate whether our AFM measurement was capable of identifying the nanomechanical differences in receptor endocytosis profile from cells with a genetic alteration in the membrane trafficking machinery. For this purpose, we selectively depleted the small GTPase Cdc42, which plays critical roles in the organization of actin cytoskeleton and in the regulation of vesicular trafficking. We have recently shown that Cdc42 contributes to adult stem cell renewal (Sakamori et al., 2012a) and colonic tumor progression (Sakamori et al., 2014a). However, it was not clear whether Cdc42 is involved in EGF-stimulated receptor endocytosis. We first derived a stable Cdc42-deficient Caco2 cell line by knocking down the endogenous gene via lentiviral expression of Cdc42 specific siRNA **(Fig. 44B)**. Remarkably, when serum starved live *Cdc42*-deficient cells were stimulated with EGF, there was a drastic delay in the response to EGF stimulation by approximately 15 mins, compared to the control scramble knockdown cells, as reflected by the increase of Young's modulus **(Fig. 44A)**. Cdc42 deficiency diminished both the rate of increase in Young's modulus by 22-fold, and the amplitude of Young's modulus by over 3-fold (**Fig. 44A, C)**. The slow

increase of Young's modulus at a rate of 0.06 kPa/s to a maximum of 57.5 kPa in *Cdc42*-deficient Caco2 cells (as opposed to 1.3 kPa/s in control cells to a maximum of 219.4 kPa) suggested that there was some remaining but weak cellular response to EGF in the absence of Cdc42, even though the overall response was significantly dampened in the knockdown cells. Taken together, AFM-mediated real-time measurement of Young's modulus was capable to quantitatively assess the ligand-specific receptor endocytosis in genetically manipulated cells.

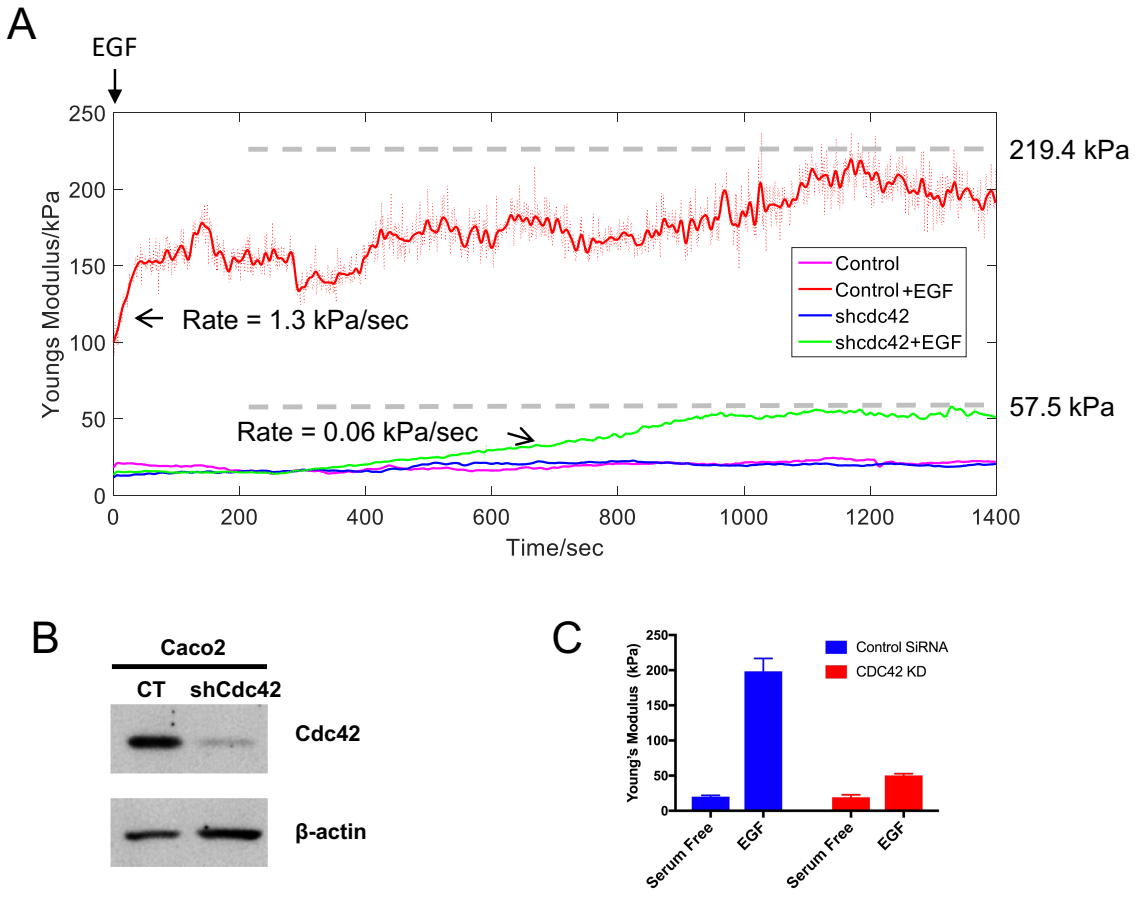

Figure 44. AFM detects changes in elastic modulus in cells with a genetic alteration.

(A) AFM detected EGF-stimulated Young's modulus increase, at a rate of 1.3 kPa/s, in control Caco2 cells (red line). In CDC42-knockdown (KD) cells, there was a rate of 0.06 kPa/s increase in Young's modulus. No significant difference between serum starved control and CDC42-KD cells was observed under unstimulated condition. (B) Western blot analysis for CDC42 confirmed stable knockdown of this gene in CDC42-KD cells. (C) AFM detected a nearly 5-time higher in the EGF-stimulated amplitude of Young's modulus in control cells than CDC42-KD cells

DISCUSSION

To our knowledge, this is the first study utilizing AFM to quantitatively assess nanomechanical property at plasma membrane during receptor endocytosis in live mammalian cells. Most of existing AFM studies of the endocytosis process have been focused on the morphological changes of live cells. For example, high-speed AFM has been used in combination with optical microscopy to elegantly capture the morphogenesis such as filopodia, membrane ruffles, pit formation, and endocytosis in COS-7, HeLa cells and hippocampal neurons (Shibata et al., 2015; Shibata et al., 2017). Time-resolved images of chemical-induced lamellar bodies of living alveolar type II cells was captured by low-force contact mode AFM, although with limited resolution on live specimens (Hecht et al., 2011). In addition, AFM imaging captured the uptake of liposomes on human coronary artery endothelial cells (HCAECs) (Zaske et al., 2013). Scanning raised domains at the inner cell plasma membrane and co-identifying of cargo-receptors and clathrin by using a combination of AFM and fluorescent microscopy predicted the potential occurrence of signaling and endocytosis in fixed RBL-2H3 mast cells (Frankel et al., 2006). Our work contrasted with above studies by revealing the mechanical evolution of cell membrane and the underneath biological pathways during endocytosis. By utilizing the control-based nanomechanical protocol developed by us (see Methods below) (Ren et al., 2013b) (Ren et al., 2013a), we were able to reliably quantify the nanomechanical properties (Young's modulus) of the cells over a large range of force spectrum, which allowed us to quantitatively monitor in real-time the nanomechanical evolution of the cell membrane during endocytosis,

with or without genetic alternations and/or biochemical modifications.

At a global scale, the rate of cellular endocytosis is influenced by environmental temperature and nutrient abundance (Etxeberria et al., 2005) (Grahammer et al., 2017) (Punnonen et al., 1998). During our early AFM instrumental development and study, we reported a decreased Young's modulus in serum-starved HeLa cells, which likely reflected a decreased endocytosis rate(Ren et al., 2013b). In this study, the dynamic changes in cellular plasma membrane, such as the alteration of basal rate of endocytosis at different temperatures, or the membrane compositions altered by various pharmacological molecules, were sensitively reflected in the elastic modules detected by AFM. It is important to note that despite of being inhibitory to endocytosis for various small chemical molecules, AFM was capable of revealing their distinct mechanistic actions on membrane properties. In general, our data suggest that higher membrane tension appears to be associated with enhanced endocytic rate induced by stimulative ligands at steady states. The enhanced tension could be a result from a reduction of plasma membrane from endocytosis or a cytoskeletal reorganization at the cortical membrane. For instance, the clathrin-dependent endocytosis requires reorganization of the cytoskeleton network at the membrane-cortex region. The reorganization of actin into comet-like tails is important for micropinocytosis (Merrifield, 1999) while remodeling of membrane-associated actin on endosomes may be generally important for membrane budding (Harder et al., 1997; Lamaze et al., 1997). Thus, in addition to a loss of surface membrane during endocytosis, cytoskeleton tension generated at plasma membrane is likely an important contributor to the detected

nanomechanical alteration and fluctuation. In addition, the potential alteration of membrane lipid composition following endocytosis may be another contributing factor to the elasticity change. This notion was supported by our results on CPZ or Filipin treated membranes, where anchoring of these amphipathic molecules to the phospholipid or cholesterol led to a stiffening of the membrane. At this moment, we do not have evidence to suggest that the observed elastic changes are predominantly determined by any single parameter of the above factors. We tentatively conclude that the plasma membrane elasticity change may result from multiple factors at steady states. Furthermore, change in cellular membrane tension can in turn affect cellular trafficking. It has been shown that high membrane tension tends to drive exocytotic membrane traffic to increase plasma membrane area and lower tension while low membrane tension favoring endocytosis; mitotic cells have high membrane tension and a nearly terminated endocytosis (Raucher and Sheetz, 1999). Overall, our AFM platform was sensitive enough to discern the changes in live cells, when their membrane homeostasis was perturbed by physiologic or chemical stimuli that affect endocytosis.

One of the most interesting findings from this study was the capability of our AFM to identify differences in mechanical force profiles from two different growth factors, namely EGF and Wnt3a, in terms of their demonstrated influences, e.g., rapidness, duration, and amplitude, on membrane elasticity. The observed rapid effect of EGF as well as the relatively slow but sustained effects of Wnt3a are in good agreement with cell biology studies that assessed the endocytic vesicle formation at plasma membrane (Carmon et al., 2012) (Sigismund et al., 2008). The

uncovering of a blunted EGF response in *Cdc42*-deficient cells by our AFM analysis is conceptually novel and important, which suggested that loss of Cdc42 may impair the cellular response to EGF, a critical growth factor that promotes cell growth and survival in the adult stem cell niche. We have previously reported that *Cdc42*-deficient mouse intestinal stem cells were outcompeted by wild type stem cells *in vivo* (Sakamori et al., 2012a), and Cdc42-deficient organoids failed to propagate *in vitro* (Sakamori et al., 2014a). These new AFM data pointed to a potentially important mechanism that may contribute to the reduced self-renewal capacity of *Cdc42*-deficient stem cells. The involvement of Cdc42 in EGF-induced endocytosis and signal transduction has not been formally examined and is important for further investigation at molecular levels. Overall, our study demonstrated the capacity of AFM in determining real-time alteration of mechanical properties at live cell plasma membrane. Future coupling of AFM nanomechanical analysis with morphological and molecular studies is anticipated to gain insights into membrane dynamics and cellular response to environmental signals.

SUMMARY OF CHAPTER 5

Whether environmental (thermal, chemical, and nutrient) signals generate quantifiable, nanoscale, mechanophysical changes in the cellular plasma membrane has not been well elucidated. Assessment of such mechanophysical properties of plasma membrane may shed lights on fundamental cellular process. Atomic force microscopic (AFM) measurement of the mechanical properties of live

cells was hampered by the difficulty in accounting for the effects of the cantilever motion and the associated hydrodynamic force on the mechanical measurement. These challenges have been addressed in our recently developed control-based AFM nanomechanical measurement protocol, which enables a fast, noninvasive, broadband measurement of the real-time changes in plasma membrane elasticity in live cells. Here we show using this newly developed AFM platform that the plasma membrane of live mammalian cells exhibits a constant and quantifiable nanomechanical property, the membrane elasticity. This mechanical property sensitively changes in response to environmental factors, such as the thermal, chemical, and growth factor stimuli. We demonstrate that different chemical inhibitors of endocytosis elicit distinct changes in plasma membrane elastic modulus reflecting their specific molecular actions on the lipid configuration or the endocytic machinery. Interestingly, two different growth factors, EGF and Wnt3a, elicited distinct elastic force profiles revealed by AFM at the plasma membrane during receptor-mediated endocytosis. By applying this platform to genetically modified cells, we uncovered a previously unknown contribution of Cdc42, a key component of the cellular trafficking network, to EGF-stimulated endocytosis at plasma membrane. Together, this nanomechanical AFM study establishes an important foundation that is expandable and adaptable for investigation of cellular membrane evolution in response to various key extracellular signals.

CHAPTER 6

FUTURE DIRECTIONS

Cdc42 regulated Paneth cell localization

Bulk RNA seq analysis the *Cdc42*^{iKO} mouse intestinal epithelium showed a loss of expression of Defensins and Sox9, signature genes of Paneth cells. GSEA analysis revealed the significant reduction of Paneth cell signature **(Fig. 45A)**. Consistently, lysozyme staining showed that *iKO* enteroids had diminished Paneth cells while *iKO;V2*^{Tg} enteroids developed Paneth cells **(Fig. 45B)**, suggesting that Paneth cell differentiation was dependent on Cdc42. As shown in Fig. 1 and Fig. 15A in CHAPTER 1, lysozyme-positive Paneth cells Cdc42-deficient epithelium delocalized from crypt bottom to villi. This phenotype persisted even in newly generated epithelia 7 days after irradiation in Cdc42-deficient mice **(Fig. 45C)**. Being another Rho subfamily member, Rac shared many functionalities of Cdc42. Constant activity of Rac led to precocious Paneth cell formation during late-stage embryogenesis (Stappenbeck and Gordon, 2000). These and our observations might shed light on some complementary and distinct roles of Cdc42 and Rac in regulating Paneth cell maturation and maintenance.

The function of EphrinB/EphB signaling in the intestines was proposed to enforce the precise positioning of proliferative and differentiated cells (Batlle et al., 2002). Ephrin-B1 and its receptors, EphB2 and EphB3, are involved in inter-cellular signaling. Usually when EphrinB on the membrane of one cell recognizes the EphB receptor on the other cell, signaling generated in both cells result in repulsive movement between these two cells. Rho GTPases are involved in these movements of the cell (Pitulescu and Adams, 2010). Paneth cell positioning were shown to depend on EphB3 signaling (Batlle et al., 2002). The Ephrin-The

expression of EphrinB1 and its receptors is negatively regulated by β-catenin /TCF (Batlle et al., 2002). Disruption of this signaling pathway led to delocalization of both proliferative cells and Paneth cells from the crypts.

Based on our bulk RNA-seq, EphB3 level in *Cdc42*^{iKO} mucosa was 25% less than in WT. In studies of neuronal dendritic spine formation, EphBs mediate actin reorganization through activation of Rho-GTPases including Cdc42. The Cdc42 specific GEFs, Intersectins associate with EphB by binding to the endocytosis adapter Numb, activating Cdc42 for neuronal spine growth. We postulated that EphB-Intersectin-Cdc42 signaling axis might be employed during Paneth cell positioning.

To test this hypothesis, we have investigated intestines of Intersectin1/2 double knockout (DKO) mice. Although Intersectin DKO intestines did not show overall abnormalities **(Fig. 46A)**, Paneth cells were mispositioned **(Fig. 46B)**, a phenotype similar to Cdc42 KO intestine. This suggested that Cdc42 activation by Intersectin is involved in Paneth cell positioning. Since EphB3 was found to be expressed by Paneth cells, future studies will test if deleting Cdc42 specifically in Paneth cells may cell-autonomously misposition Paneth cells. We have already established Paneth cell specific Cdc42 knockout mice. In terms of the mechanism of signaling, we specifically ask whether Intersectin and Cdc42 associate with EphB3 in IECs. We will test this by using co-immunoprecipitation assays using mouse intestinal tissues and human Caco2 cells.

A

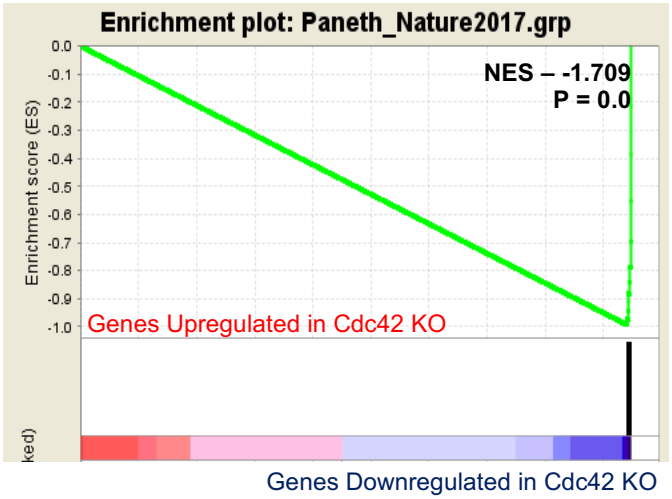
Enrichment plot: Paneth_Nature2017.grp
NES – -1.709
P = 0.0
Enrichment score (ES)
0.0
-0.1
-0.2
-0.3
-0.4
-0.5
-0.6
-0.7
-0.8
-0.9
-1.0
Genes Upregulated in Cdc42 KO
Genes Downregulated in Cdc42 KO

B

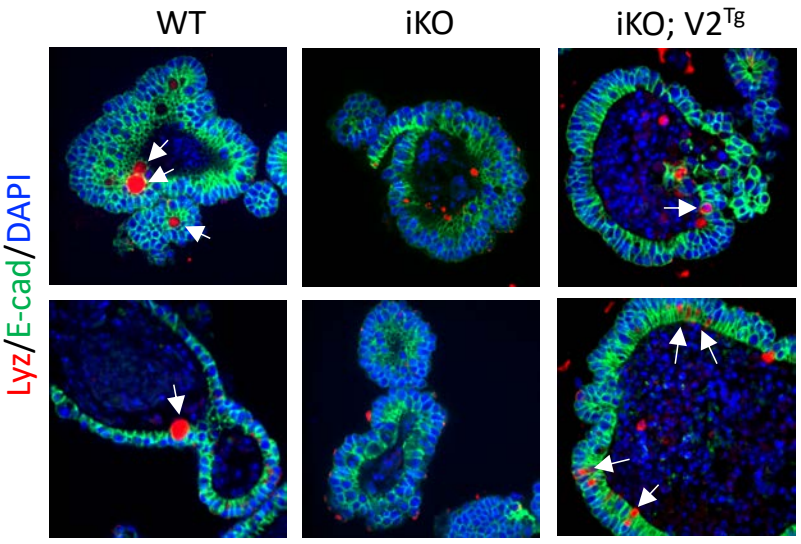
WT
iKO
iKO; V2Tg
Lyz/E-cad/DAPI

C

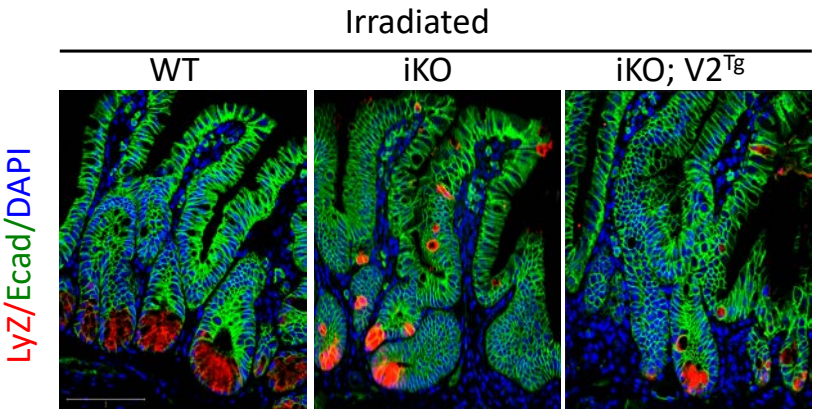
Irradiated
WT
iKO
iKO; V2Tg
LyZ/Ecad/DAPI

Figure 45. Differentiation and position of Paneth cells depend on Cdc42.

(A) Gene set enrichment analysis (GSEA) of bulk RNA-seq showed a significantly reduced Paneth cell gene signature (p=0.0) in *iKO* compared to WT IECs. (B) Immunofluorescence staining of Lysozyme (red), E-cad (green) and DAPI (Blue) in *WT, Cdc42iKO* and *iKO;V2*^{Tg} enteroids. (C) Immunofluorescence staining of Lysozyme (red), E-cad (green) and DAPI (Blue) in *WT, Cdc42iKO* and *iKO;V2*^{Tg} intestine 7 days after irradiation.

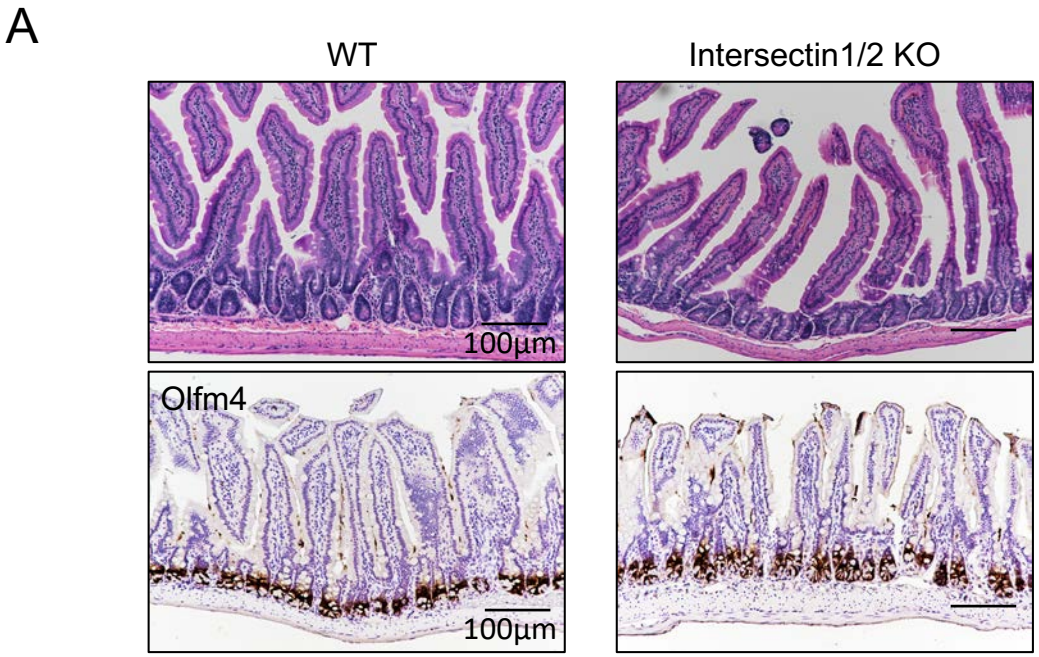
A
WT
Intersectin1/2 KO
100μm
Olfm4
100μm

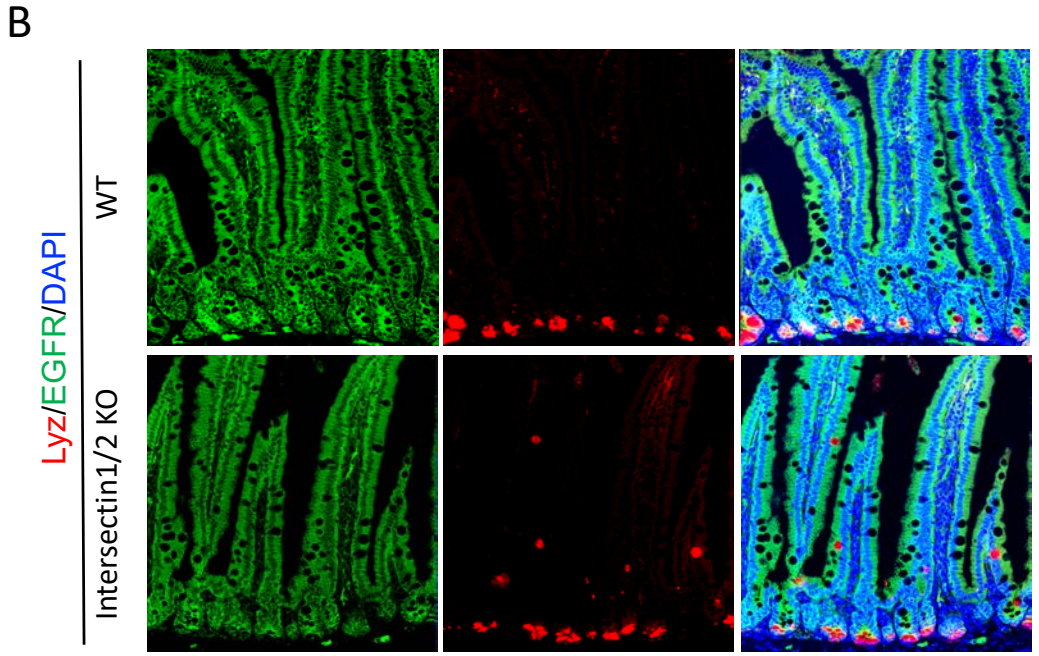
B
Lyz/EGFR/DAPI
WT
Intersectin1/2 KO

Figure 46. Intersectin1/2 DKO mice showed mispositioning of Paneth cells in intestines.

(A) H&E and Immunohistochemistry staining of Olfm4 of WT and Intersection1/2 KO intestine. (B) Immunofluorescence staining of Lysozyme (red), EGFR (green) and DAPI (Blue) in *WT, Cdc42iKO* and *iKO; V2*^{Tg} mice.

Cdc42 suppresses formation of microvillus inclusion

Intestinal epithelial cell specific ablation of Cdc42 also leads to typical microvillus inclusions in Cdc42-deficient enterocytes (Sakamori et al., 2012b), whose abnormalities highly resemble Rab8a-deficient intestinal microvillus phenotype (Sato et al., 2007). Previous studies were done in Cdc42 constitutive KO enterocytes. Here, we further characterized this phenotype by induced Cdc42 deletion in *iKO* mice using a time course **(Fig. 47A, B)**. Transmission electron microscopy showed that membranes are not well organized around the microvillus inclusion bodies **(Fig. 47C).**

We also analyzed *iKO;V2*^{Tg} mouse enterocytes **(Fig. 47D)**. Future studies will examine how Cdc42-V2 influences the formation of microvillus inclusion body.

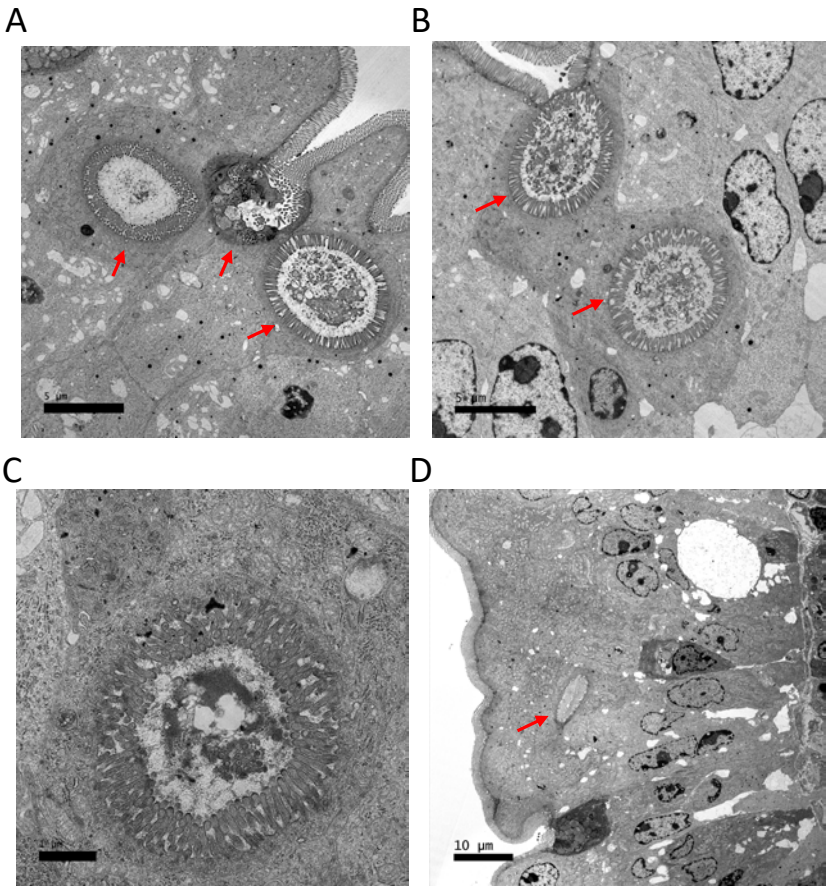

Figure 47. Electronic Microscopy showed microvillus inclusion bodies in *Cdc42^{iKO}* intestine 4days after tamoxifen injection.

(A-B) Formed and initiated microvillus inclusion bodies from the apical of the *iKO* epithelium. Rad arrows pointing at the microvillus inclusion bodies. (C) A microvillus inclusion body in higher magnification. (D) Fewer microvillus inclusion body was seen in *iKO;V2^{Tg}* mice.

Role of Cdc42 V2 in intestinal tumorigenesis

Cdc42 V2 was detected in developing mouse tissue **(Fig. 12B)**.and found to be elevated in human colorectal cancer tissues compared to adjacent normal tissues (Fig. 12C). We tested the role of Cdc42 V2 in intestinal tumorigenesis by generating $APC^{Min/+}; V2^{Tg}$ mice. We observed pronounced adenoma formations in $APC^{Min/+}; V2^{Tg}$ mice than in $APC^{Min/+}$ mice at 6-month of age **(Fig. 48).** This was in agreement with our previous report that Cdc42 deletion suppressed tumorigenesis in the intestines (Sakamori et al., 2014b). Future studies will carefully characterize the pathology of these tumors, identify signs of invasiveness, and investigate how Cdc42-V2 may enhance the cancer progression.

There are multiple possible mechanisms. First of all, direct or indirect interactions between Cdc42 and APC during directed cell migration were reported. Two pools of APC form complex with different interacting components: lower molecular weight APC complex contained beta-catenin degradation machinery; and the larger APC complex associated with cytoskeleton filaments at the cellular migrating fronts (Mahadevaiyer et al., 2007). Co-localization of activated Cdc42 and APC was observed at the front edge of polarized migrating cells (Osmani et al., 2006; Yamana et al., 2006) Thus, it is plausible that Cdc42-V2 had increased engagement with APC.

By yeast two-hybrid screening, FRET and GST pull-down assay, Cdc42 was found directly interacting with APC at the armadillo repeats (Sudhaharan et al., 2011). The Dbl family GEF of Cdc42, ASEF (Kawasaki et al., 2000) (Kawasaki et al., 2007), bind and is activated by APC. APC opens the closed auto-inhibitory

conformation of ASEF (Mitin et al., 2007; Zhang et al., 2012). Activated ASEF then increased cell motility by reducing the accumulation of E-cadherin and beta-catenin at cell-cell contacts. This migration promoting mechanism was especially utilized by CRC cells expressing truncated forms of APC, those that lost binding sites for microtubules, EB1, hDLG, beta-catenin, and Axin (Kawasaki et al., 2003). ASEF was confirmed to be required for adenoma formation in *APC*$^{Min/+}$ mice (Kawasaki et al., 2010). IQGAP1, the effector of Rac1 and Cdc42, also interacted with APC to regulate cytoskeleton dynamics (Mahadevaiyer et al., 2007; Noritake et al., 2005; Watanabe et al., 2005; Watanabe et al., 2004). ASEF was not only activated by APC but also by phosphorylation via tyrosine kinases such as Src under growth factor stimulation (Itoh et al., 2008). A study further explored the regulatory role of HGF-induced ASEF/IQGAP complex in endothelial cells (Tian et al., 2015). It is plausible that Cdc42-V2 was more susceptible to ASEF localization due to its uniquely palmitoylated C-terminal tail. These can be tested in future studies.

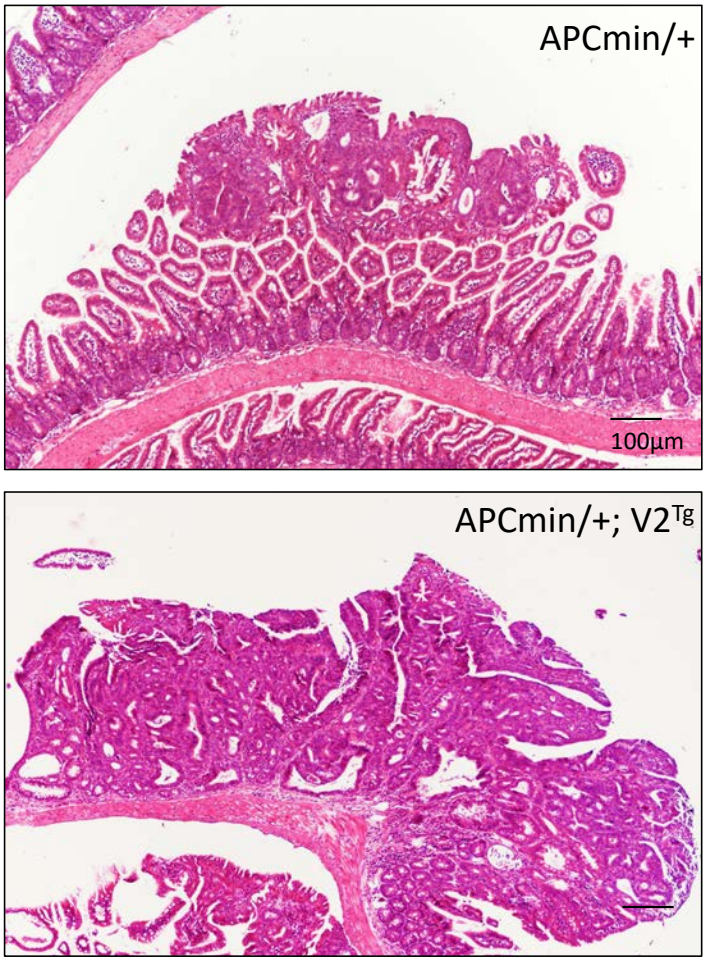

Figure 48. Cdc42-V2 overexpression in *APC*$^{Min/+}$ mice promoted tumorigenesis.

H&E staining of *APC*$^{Min/+}$ and *APC*$^{Min/+}$;*V2*^{Tg} intestine of mice at 6-month of age.

Microbiome and IL22 signaling in promoting Cdc42-deficient epithelial survival

A number of outstanding questions remained in this project including: (1) what are the lamina propria cell sources of IL22? (2) how this particular lamina propria IL22-producing cell population responded to Cdc42-deficiency in IECs? (3) what signals are used by Cdc42-deficient IECs to communicate to lamina propria to regulate cytokine production? (4) what epithelial cell type(s) produce 100-fold more of prolactin in Cdc42-deficient IECs? (5) how prolactin affects IL22 production at a mechanistic level? (6) how the altered gut microbiota influences the expression and production of cytokines (such as IL22) and prolactin?

Future studies will require single cell RNA-seq to identify the IL22-producing sources in KO ileal tissues. We will use enteroids, co-culture, cytokine/prolactin treatments to investigate the causalities described above and validate via qPCR the transcriptional regulation between IECs and lamina propria cell types. We will also use antibodies against prolactin and its receptors to identify the precise producers and receivers of this hormone and use ELISA to investigate how its production was regulated. We will use antibiotics and bacterial association studies to examine impacts of Cdc42 KO gut microbiota.

Ongoing investigation suggested that *Cdc42*$^{\Delta IEC}$ mice had an overrepresentation of *Lactobacillus* **(Fig. 49)**. Members of Clostridia have been shown to induce IL22 (Stefka et al., 2014), and *Lactobacillus* activates IL22 production from gut innate lymphoid cells (Nakamoto et al., 2017). Ablating microbiota by antibiotics or abrogating bacterial sensing in *Cdc42*-deficient IECs provoked further attenuation of ISC function, collectively suggesting that the

microbiota might be causal for the cytokine reprograming in *Cdc42*$^{\Delta IEC}$ gut. Microbe derived agonists and metabolites, including those from *Lactobacillus* have been shown to modulate ISC homeostasis (Ivanov and Honda, 2012; Kaiko et al., 2016; Lee et al., 2018b; Silva et al., 2015). Cdc42 was recently shown to mediate transcytosis of commensal bacterial antigens in enterocytes to regulate mucosal immune response (Ladinsky et al., 2019b). Future studies will identify microbial signals that elicit the signaling rewiring in *Cdc42*$^{\Delta IEC}$ gut mucosa.

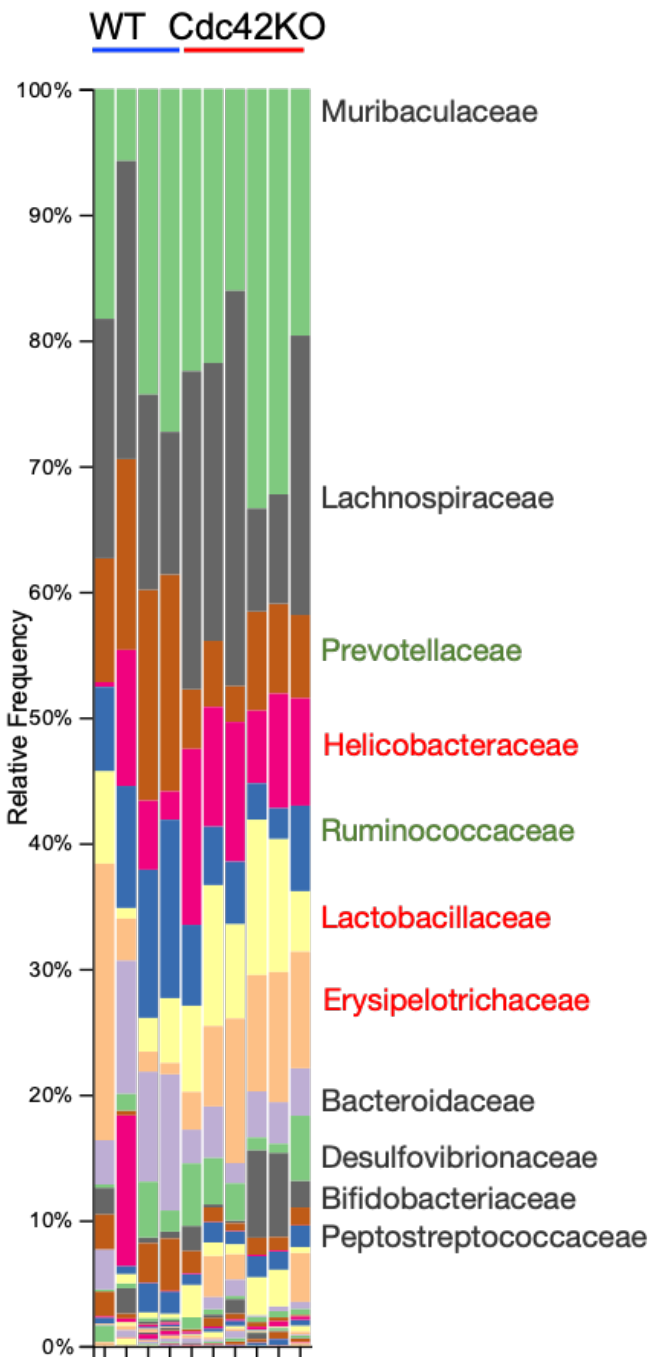

Figure 49. Changes in microbiota enrichment in *Cdc42*$^{\Delta IEC}$ intestine.

Enrichment of bacteria in *Cdc42*$^{\Delta IEC}$ vs. WT mouse stools ranking from most enriched to least enriched.

BIBLIOGRAPHY

Agudo, J., Park, E.S., Rose, S.A., Alibo, E., Sweeney, R., Dhainaut, M., Kobayashi, K.S., Sachidanandam, R., Baccarini, A., Merad, M.*, et al.* (2018). Quiescent Tissue Stem Cells Evade Immune Surveillance. Immunity *48*, 271-285 e275.

Akcora, D., Huynh, D., Lightowler, S., Germann, M., Robine, S., de May, J.R., Pollard, J.W., Stanley, E.R., Malaterre, J., and Ramsay, R.G. (2013). The CSF-1 receptor fashions the intestinal stem cell niche. Stem cell research *10*, 203-212.

Al-Tassan, N.A., Whiffin, N., Hosking, F.J., Palles, C., Farrington, S.M., Dobbins, S.E., Harris, R., Gorman, M., Tenesa, A., Meyer, B.F.*, et al.* (2015). A new GWAS and meta-analysis with 1000Genomes imputation identifies novel risk variants for colorectal cancer. Sci Rep *5*, 10442.

Allen, J.A., Yu, J.Z., Donati, R.J., and Rasenick, M.M. (2005). Beta-adrenergic receptor stimulation promotes G alpha s internalization through lipid rafts: a study in living cells. Molecular pharmacology *67*, 1493-1504.

Anderson, R.G. (1998). The caveolae membrane system (Annual Reviews 4139 El Camino Way, PO Box 10139, Palo Alto, CA 94303-0139, USA).

Andrews, C., McLean, M.H., and Durum, S.K. (2018). Cytokine Tuning of Intestinal Epithelial Function. Front Immunol *9*, 1270.

Aoki, R., Shoshkes-Carmel, M., Gao, N., Shin, S., May, C.L., Golson, M.L., Zahm, A.M., Ray, M., Wiser, C.L., Wright, C.V.*, et al.* (2016). Foxl1-expressing mesenchymal cells constitute the intestinal stem cell niche. Cell Mol Gastroenterol Hepatol *2*, 175-188.

Ares, G.R., and Ortiz, P.A. (2012). Dynamin2, Clathrin, and Lipid Rafts Mediate Endocytosis of the Apical Na/K/2Cl Cotransporter NKCC2 in Thick Ascending Limbs. The Journal of Biological Chemistry *287*, 37824-37834.

Auriac, A., Willemetz, A., and Canonne-Hergaux, F. (2010). Lipid raft-dependent endocytosis: a new route for hepcidin-mediated regulation of ferroportin in macrophages. Haematologica *95*, 1269-1277.

Barker, N., and Clevers, H. (2007). Tracking down the stem cells of the intestine: strategies to identify adult stem cells. Gastroenterology *133*, 1755-1760.

Barker, N., Huch, M., Kujala, P., van de Wetering, M., Snippert, H.J., van Es, J.H., Sato, T., Stange, D.E., Begthel, H., van den Born, M.*, et al.* (2010). Lgr5(+ve) stem cells drive self-renewal in the stomach and build long-lived gastric units in vitro. Cell Stem Cell *6*, 25-36.

Barker, N., Ridgway, R.A., van Es, J.H., van de Wetering, M., Begthel, H., van den Born, M., Danenberg, E., Clarke, A.R., Sansom, O.J., and Clevers, H. (2009). Crypt stem cells as the cells-of-origin of intestinal cancer. Nature *457*, 608-611.

Barkla, D.H., Whitehead, R.H., Foster, H., and Tutton, P.J. (1988). Tuft (caveolated) cells in two human colon carcinoma cell lines. Am J Pathol *132*, 521-525.

Basak, O., Beumer, J., Wiebrands, K., Seno, H., van Oudenaarden, A., and Clevers, H. (2017). Induced Quiescence of Lgr5+ Stem Cells in Intestinal Organoids Enables Differentiation of Hormone-Producing Enteroendocrine Cells. Cell Stem Cell *20*, 177-190 e174.

Bates, R.W., Garrison, M.M., and Cornfield, J. (1963). An Improved Bio-Assay for Prolactin Using Adult Pigeons. Endocrinology *73*, 217-223.

Batlle, E., Henderson, J.T., Beghtel, H., van den Born, M.M., Sancho, E., Huls, G., Meeldijk,

J., Robertson, J., van de Wetering, M., Pawson, T*., et al.* (2002). Beta-catenin and TCF mediate cell positioning in the intestinal epithelium by controlling the expression of EphB/ephrinB. Cell *111*, 251-263.
Batzer, A.G., Rotin, D., Urena, J.M., Skolnik, E.Y., and Schlessinger, J. (1994). Hierarchy of binding sites for Grb2 and Shc on the epidermal growth factor receptor. Mol Cell Biol *14*, 5192-5201.
Bäumler, A.J., and Sperandio, V. (2016). Interactions between the microbiota and pathogenic bacteria in the gut. Nature *535*, 85.
Ben-Jonathan, N., Mershon, J.L., Allen, D.L., and Steinmetz, R.W. (1996). Extrapituitary prolactin: distribution, regulation, functions, and clinical aspects. Endocr Rev *17*, 639-669.
Bernardino de la Serna, J., Schütz, G.J., Eggeling, C., and Cebecauer, M. (2016). There Is No Simple Model of the Plasma Membrane Organization. Frontiers in Cell and Developmental Biology *4*.
Bevins, C.L., and Salzman, N.H. (2011). Paneth cells, antimicrobial peptides and maintenance of intestinal homeostasis. Nat Rev Microbiol *9*, 356-368.
Bilic, J., Huang, Y.L., Davidson, G., Zimmermann, T., Cruciat, C.M., Bienz, M., and Niehrs, C. (2007). Wnt induces LRP6 signalosomes and promotes dishevelled-dependent LRP6 phosphorylation. Science *316*, 1619-1622.
Birchenough, G.M., Johansson, M.E., Gustafsson, J.K., Bergstrom, J.H., and Hansson, G.C. (2015). New developments in goblet cell mucus secretion and function. Mucosal Immunol *8*, 712-719.
Bishop, A.L., and Hall, A. (2000). Rho GTPases and their effector proteins. Biochem J *348 Pt 2*, 241-255.
Biteau, B., and Jasper, H. (2011). EGF signaling regulates the proliferation of intestinal stem cells in Drosophila. Development *138*, 1045-1055.
Biton, M., Haber, A.L., Rogel, N., Burgin, G., Beyaz, S., Schnell, A., Ashenberg, O., Su, C.-W., Smillie, C., Shekhar, K*., et al.* (2018a). T Helper Cell Cytokines Modulate Intestinal Stem Cell Renewal and Differentiation. Cell *175*, 1307-1320.e1322.
Biton, M., Haber, A.L., Rogel, N., Burgin, G., Beyaz, S., Schnell, A., Ashenberg, O., Su, C.W., Smillie, C., Shekhar, K*., et al.* (2018b). T Helper Cell Cytokines Modulate Intestinal Stem Cell Renewal and Differentiation. Cell *175*, 1307-1320 e1322.
Bjerknes, M., Khandanpour, C., Möröy, T., Fujiyama, T., Hoshino, M., Klisch, T.J., Ding, Q., Gan, L., Wang, J., Martín, M.G*., et al.* (2012). Origin of the brush cell lineage in the mouse intestinal epithelium. Developmental Biology *362*, 194-218.
Blasius, A.L., and Beutler, B. (2010). Intracellular toll-like receptors. Immunity *32*, 305-315.
Bogunovic, M., Dave, S.H., Tilstra, J.S., Chang, D.T., Harpaz, N., Xiong, H., Mayer, L.F., and Plevy, S.E. (2007). Enteroendocrine cells express functional Toll-like receptors. Am J Physiol Gastrointest Liver Physiol *292*, G1770-1783.
Bole-Feysot, C., Goffin, V., Edery, M., Binart, N., and Kelly, P.A. (1998). Prolactin (PRL) and its receptor: actions, signal transduction pathways and phenotypes observed in PRL receptor knockout mice. Endocr Rev *19*, 225-268.
Bos, J.L., Rehmann, H., and Wittinghofer, A. (2007). GEFs and GAPs: critical elements in the control of small G proteins. Cell *129*, 865-877.
Brodrick, B., Vidrich, A., Porter, E., Bradley, L., Buzan, J.M., and Cohn, S.M. (2011).

Fibroblast growth factor receptor-3 (FGFR-3) regulates expression of paneth cell lineage-specific genes in intestinal epithelial cells through both TCF4/beta-catenin-dependent and -independent signaling pathways. J Biol Chem *286*, 18515-18525.
Bruckner, K., Pablo Labrador, J., Scheiffele, P., Herb, A., Seeburg, P.H., and Klein, R. (1999). EphrinB ligands recruit GRIP family PDZ adaptor proteins into raft membrane microdomains. Neuron *22*, 511-524.
Buchon, N., Broderick, N.A., Chakrabarti, S., and Lemaitre, B. (2009). Invasive and indigenous microbiota impact intestinal stem cell activity through multiple pathways in Drosophila. Genes Dev *23*, 2333-2344.
Buchon, N., Broderick, N.A., Kuraishi, T., and Lemaitre, B. (2010). Drosophila EGFR pathway coordinates stem cell proliferation and gut remodeling following infection. BMC Biol *8*, 152.
Butt, H.-J., Cappella, B., and Kappl, M. (2005). Force measurements with the atomic force microscope: Technique, interpretation and applications. Surface Science Reports *59*, 1-152.
Calvo, F., Sanz-Moreno, V., Agudo-Ibanez, L., Wallberg, F., Sahai, E., Marshall, C.J., and Crespo, P. (2011). RasGRF suppresses Cdc42-mediated tumour cell movement, cytoskeletal dynamics and transformation. Nat Cell Biol *13*, 819-826.
Cardoso, A.P., Pinto, M.L., Pinto, A.T., Oliveira, M.I., Pinto, M.T., Goncalves, R., Relvas, J.B., Figueiredo, C., Seruca, R., Mantovani, A.*, et al.* (2014). Macrophages stimulate gastric and colorectal cancer invasion through EGFR Y(1086), c-Src, Erk1/2 and Akt phosphorylation and smallGTPase activity. Oncogene *33*, 2123-2133.
Carmon, K.S., Lin, Q., Gong, X., Thomas, A., and Liu, Q. (2012). LGR5 Interacts and Cointernalizes with Wnt Receptors To Modulate Wnt/β-Catenin Signaling. Molecular and Cellular Biology *32*, 2054-2064.
Carstens, P.H., Broghamer, W.L., Jr., and Hire, D. (1976). Malignant fibrillo-caveolated cell carcinoma of the human intestinal tract. Human pathology *7*, 505-517.
Carter, J.H., Douglass, L.E., Deddens, J.A., Colligan, B.M., Bhatt, T.R., Pemberton, J.O., Konicek, S., Hom, J., Marshall, M., and Graff, J.R. (2004). Pak-1 expression increases with progression of colorectal carcinomas to metastasis. Clin Cancer Res *10*, 3448-3456.
Carton-Garcia, F., Overeem, A.W., Nieto, R., Bazzocco, S., Dopeso, H., Macaya, I., Bilic, J., Landolfi, S., Hernandez-Losa, J., Schwartz, S., Jr.*, et al.* (2015). Myo5b knockout mice as a model of microvillus inclusion disease. Sci Rep *5*, 12312.
Charoenphandhu, N., and Krishnamra, N. (2007). Prolactin is an important regulator of intestinal calcium transport. Can J Physiol Pharmacol *85*, 569-581.
Chelakkot, C., Ghim, J., and Ryu, S.H. (2018). Mechanisms regulating intestinal barrier integrity and its pathological implications. Exp Mol Med *50*, 103.
Chen, W., Ju, S., Lu, T., Xu, Y., Zheng, X., Wang, H., Ge, Y., and Ju, S. (2017). Directional delivery of RSPO1 by mesenchymal stem cells ameliorates radiation-induced intestinal injury. Cytokine *95*, 27-34.
Cinar, E., and Sahin, F. (2014). New approach for nanoindentation using multiprobe AFM system. Paper presented at: 14th IEEE International Conference on Nanotechnology.
Clevers, H. (2006). Wnt/beta-catenin signaling in development and disease. Cell *127*, 469-480.

Clevers, H. (2013a). The intestinal crypt, a prototype stem cell compartment. Cell *154*, 274-284.
Clevers, H. (2013b). The Intestinal Crypt, A Prototype Stem Cell Compartment. Cell *154*, 274-284.
Clevers, H.C., and Bevins, C.L. (2013). Paneth cells: maestros of the small intestinal crypts. Annu Rev Physiol *75*, 289-311.
Commins, S., Steinke, J.W., and Borish, L. (2008). The extended IL-10 superfamily: IL-10, IL-19, IL-20, IL-22, IL-24, IL-26, IL-28, and IL-29. Journal of Allergy and Clinical Immunology *121*, 1108-1111.
Conner, S.D., and Schmid, S.L. (2003). Differential requirements for AP-2 in clathrin-mediated endocytosis. The Journal of cell biology *162*, 773.
Cordero, J.B., Ridgway, R.A., Valeri, N., Nixon, C., Frame, M.C., Muller, W.J., Vidal, M., and Sansom, O.J. (2014). c-Src drives intestinal regeneration and transformation. EMBO J *33*, 1474-1491.
Cordero, J.B., Stefanatos, R.K., Myant, K., Vidal, M., and Sansom, O.J. (2012). Non-autonomous crosstalk between the Jak/Stat and Egfr pathways mediates Apc1-driven intestinal stem cell hyperplasia in the Drosophila adult midgut. Development *139*, 4524-4535.
Crawley, S.W., Mooseker, M.S., and Tyska, M.J. (2014). Shaping the intestinal brush border. J Cell Biol *207*, 441-451.
Cutz, E., Rhoads, J.M., Drumm, B., Sherman, P.M., Durie, P.R., and Forstner, G.G. (1989). Microvillus inclusion disease: an inherited defect of brush-border assembly and differentiation. N Engl J Med *320*, 646-651.
Das, S., Yu, S., Sakamori, R., Vedula, P., Feng, Q., Flores, J., Hoffman, A., Fu, J., Stypulkowski, E., Rodriguez, A.*, et al.* (2015). Rab8a vesicles regulate Wnt ligand delivery and Paneth cell maturation at the intestinal stem cell niche. Development *142*, 2147-2162.
Davidson, G.P., Cutz, E., Hamilton, J.R., and Gall, D.G. (1978). Familial enteropathy: a syndrome of protracted diarrhea from birth, failure to thrive, and hypoplastic villus atrophy. Gastroenterology *75*, 783-790.
Davis, C.R., Richman, T.J., Deliduka, S.B., Blaisdell, J.O., Collins, C.C., and Johnson, D.I. (1998). Analysis of the mechanisms of action of the Saccharomyces cerevisiae dominant lethal cdc42G12V and dominant negative cdc42D118A mutations. J Biol Chem *273*, 849-858.
Day, C.A., Baetz, N.W., Copeland, C.A., Kraft, L.J., Han, B., Tiwari, A., Drake, K.R., De Luca, H., Chinnapen, D.J., Davidson, M.W.*, et al.* (2015). Microtubule motors power plasma membrane tubulation in clathrin-independent endocytosis. Traffic (Copenhagen, Denmark) *16*, 572-590.
Dufrene, Y.F., Ando, T., Garcia, R., Alsteens, D., Martinez-Martin, D., Engel, A., Gerber, C., and Muller, D.J. (2017). Imaging modes of atomic force microscopy for application in molecular and cell biology. Nat Nano *12*, 295-307.
Dumoutier, L., Louahed, J., and Renauld, J.C. (2000). Cloning and characterization of IL-10-related T cell-derived inducible factor (IL-TIF), a novel cytokine structurally related to IL-10 and inducible by IL-9. J Immunol *164*, 1814-1819.
Eberl, G., Colonna, M., Di Santo, J.P., and McKenzie, A.N. (2015). Innate lymphoid cells.

Innate lymphoid cells: a new paradigm in immunology. Science *348*, aaa6566.
El Marjou, F., Janssen, K.-P., Hung-Junn Chang, B., Li, M., Hindie, V., Chan, L., Louvard, D., Chambon, P., Metzger, D., and Robine, S. (2004). Tissue-specific and inducible Cre-mediated recombination in the gut epithelium. genesis *39*, 186-193.
Elias, E., and Dowling, R.H. (1976). The mechanism for small-bowel adaptation in lactating rats. Clin Sci Mol Med *51*, 427-433.
Erickson, R.P., Larson-Thome, K., Valenzuela, R.K., Whitaker, S.E., and Shub, M.D. (2008). Navajo microvillous inclusion disease is due to a mutation in MYO5B. Am J Med Genet A *146A*, 3117-3119.
Etxeberria, E., Baroja-Fernandez, E., Munoz, F.J., and Pozueta-Romero, J. (2005). Sucrose-inducible endocytosis as a mechanism for nutrient uptake in heterotrophic plant cells. Plant & cell physiology *46*, 474-481.
Feng, Q., and Gao, N. (2015). Keeping Wnt signalosome in check by vesicular traffic. J Cell Physiol *230*, 1170-1180.
Ferlazzo, A., Carvalho, E.S., Gregorio, S.F., Power, D.M., Canario, A.V., Trischitta, F., and Fuentes, J. (2012). Prolactin regulates luminal bicarbonate secretion in the intestine of the sea bream (Sparus aurata L.). J Exp Biol *215*, 3836-3844.
Firestone, A.J., Weinger, J.S., Maldonado, M., Barlan, K., Langston, L.D., O/'Donnell, M., Gelfand, V.I., Kapoor, T.M., and Chen, J.K. (2012). Small-molecule inhibitors of the AAA+ ATPase motor cytoplasmic dynein. Nature *484*, 125-129.
Florian, M.C., Dorr, K., Niebel, A., Daria, D., Schrezenmeier, H., Rojewski, M., Filippi, M.D., Hasenberg, A., Gunzer, M., Scharffetter-Kochanek, K.*, et al.* (2012). Cdc42 activity regulates hematopoietic stem cell aging and rejuvenation. Cell Stem Cell *10*, 520-530.
Frankel, D.J., Pfeiffer, J.R., Surviladze, Z., Johnson, A.E., Oliver, J.M., Wilson, B.S., and Burns, A.R. (2006). Revealing the Topography of Cellular Membrane Domains by Combined Atomic Force Microscopy/Fluorescence Imaging. Biophysical Journal *90*, 2404-2413.
Freeman, M.E., Kanyicska, B., Lerant, A., and Nagy, G. (2000). Prolactin: structure, function, and regulation of secretion. Physiol Rev *80*, 1523-1631.
Fukata, M., Vamadevan, A.S., and Abreu, M.T. (2009). Toll-like receptors (TLRs) and Nod-like receptors (NLRs) in inflammatory disorders. Seminars in Immunology *21*, 242-253.
Fukui, H., Zhang, X., Sun, C., Hara, K., Kikuchi, S., Yamasaki, T., Kondo, T., Tomita, T., Oshima, T., Watari, J.*, et al.* (2014). IL-22 produced by cancer-associated fibroblasts promotes gastric cancer cell invasion via STAT3 and ERK signaling. Br J Cancer *111*, 763-771.
Gao, L., Bai, L., and Nan, Q. (2013). Activation of Rho GTPase Cdc42 promotes adhesion and invasion in colorectal cancer cells. Med Sci Monit Basic Res *19*, 201-207.
Gao, X., Lowry, P.R., Zhou, X., Depry, C., Wei, Z., Wong, G.W., and Zhang, J. (2011). PI3K/Akt signaling requires spatial compartmentalization in plasma membrane microdomains. *108*, 14509-14514.
Gehart, H., and Clevers, H. (2019). Tales from the crypt: new insights into intestinal stem cells. Nature Reviews Gastroenterology & Hepatology *16*, 19-34.
Gerbe, F., Brulin, B., Makrini, L., Legraverend, C., and Jay, P. (2009). DCAMKL-1 expression identifies Tuft cells rather than stem cells in the adult mouse intestinal epithelium. Gastroenterology *137*, 2179-2180; author reply 2180-2171.
Gerbe, F., van Es, J.H., Makrini, L., Brulin, B., Mellitzer, G., Robine, S., Romagnolo, B.,

Shroyer, N.F., Bourgaux, J.F., Pignodel, C.*, et al.* (2011). Distinct ATOH1 and Neurog3 requirements define tuft cells as a new secretory cell type in the intestinal epithelium. J Cell Biol *192*, 767-780.
Geremia, A., and Arancibia-Carcamo, C.V. (2017). Innate Lymphoid Cells in Intestinal Inflammation. Front Immunol *8*, 1296.
Geske, M.J., Zhang, X., Patel, K.K., Ornitz, D.M., and Stappenbeck, T.S. (2008). Fgf9 signaling regulates small intestinal elongation and mesenchymal development. Development *135*, 2959.
Goh, L.K., Huang, F., Kim, W., Gygi, S., and Sorkin, A. (2010). Multiple mechanisms collectively regulate clathrin-mediated endocytosis of the epidermal growth factor receptor. The Journal of Cell Biology *189*, 871.
Gong, W., An, Z., Wang, Y., Pan, X., Fang, W., Jiang, B., and Zhang, H. (2009). P21-activated kinase 5 is overexpressed during colorectal cancer progression and regulates colorectal carcinoma cell adhesion and migration. Int J Cancer *125*, 548-555.
Gong, W., Guo, M., Han, Z., Wang, Y., Yang, P., Xu, C., Wang, Q., Du, L., Li, Q., Zhao, H.*, et al.* (2016). Mesenchymal stem cells stimulate intestinal stem cells to repair radiation-induced intestinal injury. Cell Death &Amp; Disease *7*, e2387.
Goodrich, J.K., Davenport, E.R., Clark, A.G., and Ley, R.E. (2017). The Relationship Between the Human Genome and Microbiome Comes into View. Annu Rev Genet *51*, 413-433.
Goodrich, J.K., Waters, J.L., Poole, A.C., Sutter, J.L., Koren, O., Blekhman, R., Beaumont, M., Van Treuren, W., Knight, R., Bell, J.T.*, et al.* (2014). Human genetics shape the gut microbiome. Cell *159*, 789-799.
Grahammer, F., Ramakrishnan, S.K., Rinschen, M.M., Larionov, A.A., Syed, M., Khatib, H., Roerden, M., Sass, J.O., Helmstaedter, M., Osenberg, D.*, et al.* (2017). mTOR Regulates Endocytosis and Nutrient Transport in Proximal Tubular Cells. J Am Soc Nephrol *28*, 230-241.
Gregorieff, A., and Clevers, H. (2005). Wnt signaling in the intestinal epithelium: from endoderm to cancer. *19*, 877-890.
Gregorieff, A., Liu, Y., Inanlou, M.R., Khomchuk, Y., and Wrana, J.L. (2015). Yap-dependent reprogramming of Lgr5(+) stem cells drives intestinal regeneration and cancer. Nature *526*, 715-718.
Gregorieff, A., Pinto, D., Begthel, H., Destree, O., Kielman, M., and Clevers, H. (2005). Expression pattern of Wnt signaling components in the adult intestine. Gastroenterology *129*, 626-638.
Gribble, F.M., and Reimann, F. (2019). Function and mechanisms of enteroendocrine cells and gut hormones in metabolism. Nat Rev Endocrinol *15*, 226-237.
Gronke, K., Hernández, P.P., Zimmermann, J., Klose, C.S.N., Kofoed-Branzk, M., Guendel, F., Witkowski, M., Tizian, C., Amann, L., Schumacher, F.*, et al.* (2019). Interleukin-22 protects intestinal stem cells against genotoxic stress. Nature *566*, 249-253.
Gupta, N., Wollscheid, B., Watts, J.D., Scheer, B., Aebersold, R., and DeFranco, A.L. (2006). Quantitative proteomic analysis of B cell lipid rafts reveals that ezrin regulates antigen receptor–mediated lipid raft dynamics. Nature immunology *7*, 625-633.
Hall, A. (2012). Rho family GTPases. Biochemical Society transactions *40*, 1378-1382.
Hallberg, B., Rayter, S.I., and Downward, J. (1994). Interaction of Ras and Raf in intact

mammalian cells upon extracellular stimulation. J Biol Chem *269*, 3913-3916.
Hasegawa, M., Yamazaki, T., Kamada, N., Tawaratsumida, K., Kim, Y.G., Nunez, G., and Inohara, N. (2011). Nucleotide-binding oligomerization domain 1 mediates recognition of Clostridium difficile and induces neutrophil recruitment and protection against the pathogen. J Immunol *186*, 4872-4880.
Hau, C.S., Kanda, N., Tada, Y., Shibata, S., Sato, S., and Watanabe, S. (2014). Prolactin induces the production of Th17 and Th1 cytokines/chemokines in murine Imiquimod-induced psoriasiform skin. J Eur Acad Dermatol Venereol *28*, 1370-1379.
He, D., Wu, H., Xiang, J., Ruan, X., Peng, P., Ruan, Y., Chen, Y.G., Wang, Y., Yu, Q., Zhang, H*., et al.* (2020). Gut stem cell aging is driven by mTORC1 via a p38 MAPK-p53 pathway. Nat Commun *11*, 37.
He, X.C., Zhang, J., Tong, W.-G., Tawfik, O., Ross, J., Scoville, D.H., Tian, Q., Zeng, X., He, X., Wiedemann, L.M*., et al.* (2004). BMP signaling inhibits intestinal stem cell self-renewal through suppression of Wnt–β-catenin signaling. Nature Genetics *36*, 1117.
Hecht, E., Usmani, S.M., Albrecht, S., Wittekindt, O.H., Dietl, P., Mizaikoff, B., and Kranz, C. (2011). Atomic force microscopy of microvillous cell surface dynamics at fixed and living alveolar type II cells. Analytical and Bioanalytical Chemistry *399*, 2369-2378.
Henley, J.R., Krueger, E.W.A., Oswald, B.J., and McNiven, M.A. (1998). Dynamin-mediated Internalization of Caveolae. The Journal of cell biology *141*, 85.
Henriksen, L., Grandal, M.V., Knudsen, S.L.J., van Deurs, B., and Grøvdal, L.M. (2013). Internalization Mechanisms of the Epidermal Growth Factor Receptor after Activation with Different Ligands. PLOS ONE *8*, e58148.
Heuberger, J., Kosel, F., Qi, J., Grossmann, K.S., Rajewsky, K., and Birchmeier, W. (2014a). Shp2/MAPK signaling controls goblet/paneth cell fate decisions in the intestine. Proc Natl Acad Sci U S A *111*, 3472-3477.
Heuberger, J., Kosel, F., Qi, J., Grossmann, K.S., Rajewsky, K., and Birchmeier, W. (2014b). Shp2/MAPK signaling controls goblet/paneth cell fate decisions in the intestine. Proceedings of the National Academy of Sciences *111*, 3472.
Hill, T., Odell, L.R., Edwards, J.K., Graham, M.E., McGeachie, A.B., Rusak, J., Quan, A., Abagyan, R., Scott, J.L., Robinson, P.J*., et al.* (2005). Small molecule inhibitors of dynamin I GTPase activity: development of dimeric tyrphostins. Journal of medicinal chemistry *48*, 7781-7788.
Hirsch, D., Barker, N., McNeil, N., Hu, Y., Camps, J., McKinnon, K., Clevers, H., Ried, T., and Gaiser, T. (2014). LGR5 positivity defines stem-like cells in colorectal cancer. Carcinogenesis *35*, 849-858.
Hofer, D., and Drenckhahn, D. (1996). Cytoskeletal markers allowing discrimination between brush cells and other epithelial cells of the gut including enteroendocrine cells. Histochemistry and cell biology *105*, 405-412.
Hofman, E.G., Ruonala, M.O., Bader, A.N., van den Heuvel, D., Voortman, J., Roovers, R.C., Verkleij, A.J., Gerritsen, H.C., and van Bergen en Henegouwen, P.M.P. (2008). EGF induces coalescence of different lipid rafts. Journal of Cell Science *121*, 2519.
Horiguchi, A., Asano, T., Kuroda, K., Sato, A., Asakuma, J., Ito, K., Hayakawa, M., Sumitomo, M., and Asano, T. (2010). STAT3 inhibitor WP1066 as a novel therapeutic agent for renal cell carcinoma. British Journal Of Cancer *102*, 1592.

Huang, F., Khvorova, A., Marshall, W., and Sorkin, A. (2004). Analysis of Clathrin-mediated Endocytosis of Epidermal Growth Factor Receptor by RNA Interference. *279*, 16657-16661.
Hubbard, S.R. (2005). EGF receptor inhibition: attacks on multiple fronts. Cancer Cell *7*, 287-288.
Humphreys, K.J., McKinnon, R.A., and Michael, M.Z. (2014). miR-18a inhibits CDC42 and plays a tumour suppressor role in colorectal cancer cells. PLoS One *9*, e112288.
Irwin, M.E., Mueller, K.L., Bohin, N., Ge, Y., and Boerner, J.L. (2011). Lipid raft localization of EGFR alters the response of cancer cells to the EGFR tyrosine kinase inhibitor gefitinib. *226*, 2316-2328.
Itoh, R., Kiyokawa, E., Aoki, K., Nishioka, T., Akiyama, T., and Matsuda, M. (2008). Phosphorylation and activation of the Rac1 and Cdc42 GEF Asef in A431 cells stimulated by EGF, Vol 121.
Ivanov, II, Atarashi, K., Manel, N., Brodie, E.L., Shima, T., Karaoz, U., Wei, D., Goldfarb, K.C., Santee, C.A., Lynch, S.V*., et al.* (2009). Induction of intestinal Th17 cells by segmented filamentous bacteria. Cell *139*, 485-498.
Ivanov, I.I., and Honda, K. (2012). Intestinal commensal microbes as immune modulators. Cell host & microbe *12*, 496-508.
Jenny, M., Uhl, C., Roche, C., Duluc, I., Guillermin, V., Guillemot, F., Jensen, J., Kedinger, M., and Gradwohl, G. (2002). Neurogenin3 is differentially required for endocrine cell fate specification in the intestinal and gastric epithelium. EMBO J *21*, 6338-6347.
Jiang, H., and Edgar, B.A. (2009). EGFR signaling regulates the proliferation of Drosophila adult midgut progenitors. Development *136*, 483-493.
Jiang, H., Grenley, M.O., Bravo, M.J., Blumhagen, R.Z., and Edgar, B.A. (2011). EGFR/Ras/MAPK signaling mediates adult midgut epithelial homeostasis and regeneration in Drosophila. Cell Stem Cell *8*, 84-95.
Jiang, H., Patel, P.H., Kohlmaier, A., Grenley, M.O., McEwen, D.G., and Edgar, B.A. (2009). Cytokine/Jak/Stat signaling mediates regeneration and homeostasis in the Drosophila midgut. Cell *137*, 1343-1355.
Jiang, H., Tian, A., and Jiang, J. (2016). Intestinal stem cell response to injury: lessons from Drosophila. Cell Mol Life Sci *73*, 3337-3349.
Jin, Y., Ha, N., Fores, M., Xiang, J., Glasser, C., Maldera, J., Jimenez, G., and Edgar, B.A. (2015). EGFR/Ras Signaling Controls Drosophila Intestinal Stem Cell Proliferation via Capicua-Regulated Genes. PLoS Genet *11*, e1005634.
Johnson, D.I. (1999a). Cdc42: An essential Rho-type GTPase controlling eukaryotic cell polarity. Microbiology and molecular biology reviews : MMBR *63*, 54-105.
Johnson, D.I. (1999b). Cdc42: An Essential Rho-Type GTPase Controlling Eukaryotic Cell Polarity. *63*, 54-105.
Johnson, D.I., and Pringle, J.R. (1990). Molecular characterization of CDC42, a Saccharomyces cerevisiae gene involved in the development of cell polarity. J Cell Biol *111*, 143-152.
Johnson, J.L., Erickson, J.W., and Cerione, R.A. (2012). C-terminal di-arginine motif of Cdc42 protein is essential for binding to phosphatidylinositol 4,5-bisphosphate-containing membranes and inducing cellular transformation. The Journal of biological chemistry *287*,

5764-5774.
Jones, R.M. (2016). The Influence of the Gut Microbiota on Host Physiology: In Pursuit of Mechanisms. Yale J Biol Med *89*, 285-297.
Kabiri, Z., Greicius, G., Madan, B., Biechele, S., Zhong, Z., Zaribafzadeh, H., Edison, Aliyev, J., Wu, Y., Bunte, R.*, et al.* (2014). Stroma provides an intestinal stem cell niche in the absence of epithelial Wnts. Development *141*, 2206-2215.
Kabiri, Z., Greicius, G., Zaribafzadeh, H., Hemmerich, A., Counter, C.M., and Virshup, D.M. (2018). Wnt signaling suppresses MAPK-driven proliferation of intestinal stem cells. J Clin Invest *128*, 3806-3812.
Kaiko, G.E., Ryu, S.H., Koues, O.I., Collins, P.L., Solnica-Krezel, L., Pearce, E.J., Pearce, E.L., Oltz, E.M., and Stappenbeck, T.S. (2016). The Colonic Crypt Protects Stem Cells from Microbiota-Derived Metabolites. Cell *165*, 1708-1720.
Kang, R., Wan, J., Arstikaitis, P., Takahashi, H., Huang, K., Bailey, A.O., Thompson, J.X., Roth, A.F., Drisdel, R.C., Mastro, R.*, et al.* (2008). Neural palmitoyl-proteomics reveals dynamic synaptic palmitoylation. Nature *456*, 904-909.
Karlsson, R., Pedersen, E.D., Wang, Z., and Brakebusch, C. (2009). Rho GTPase function in tumorigenesis. Biochimica et biophysica acta *1796*, 91-98.
Kasas, S., Stupar, P., and Dietler, G. (2017). AFM contribution to unveil pro- and eukaryotic cell mechanical properties. Seminars in Cell & Developmental Biology.
Kawasaki, Y., Jigami, T., Furukawa, S., Sagara, M., Echizen, K., Shibata, Y., Sato, R., and Akiyama, T. (2010). The adenomatous polyposis coli-associated guanine nucleotide exchange factor Asef is involved in angiogenesis. J Biol Chem *285*, 1199-1207.
Kawasaki, Y., Sagara, M., Shibata, Y., Shirouzu, M., Yokoyama, S., and Akiyama, T. (2007). Identification and characterization of Asef2, a guanine-nucleotide exchange factor specific for Rac1 and Cdc42. Oncogene *26*, 7620-7267.
Kawasaki, Y., Sato, R., and Akiyama, T. (2003). Mutated APC and Asef are involved in the migration of colorectal tumour cells. Nat Cell Biol *5*, 211-215.
Kawasaki, Y., Senda, T., Ishidate, T., Koyama, R., Morishita, T., Iwayama, Y., Higuchi, O., and Akiyama, T. (2000). Asef, a link between the tumor suppressor APC and G-protein signaling. Science *289*, 1194-1197.
Ke, T.W., Hsu, H.L., Wu, Y.H., Chen, W.T., Cheng, Y.W., and Cheng, C.W. (2014). MicroRNA-224 suppresses colorectal cancer cell migration by targeting Cdc42. Dis Markers *2014*, 617150.
Kim, C.-K., Yang, V.W., and Bialkowska, A.B. (2017a). The Role of Intestinal Stem Cells in Epithelial Regeneration Following Radiation-Induced Gut Injury. Current stem cell reports *3*, 320-332.
Kim, C.K., Yang, V.W., and Bialkowska, A.B. (2017b). The Role of Intestinal Stem Cells in Epithelial Regeneration Following Radiation-Induced Gut Injury. Curr Stem Cell Rep *3*, 320-332.
Kim, I.H., Wang, H., Soderling, S.H., and Yasuda, R. (2014). Loss of Cdc42 leads to defects in synaptic plasticity and remote memory recall. Elife *3*.
Kim, K.A., Kakitani, M., Zhao, J., Oshima, T., Tang, T., Binnerts, M., Liu, Y., Boyle, B., Park, E., Emtage, P.*, et al.* (2005). Mitogenic influence of human R-spondin1 on the intestinal epithelium. Science *309*, 1256-1259.

Kirchhausen, T., Macia, E., and Pelish, H.E. (2008). Use of dynasore, the small molecule inhibitor of dynamin, in the regulation of endocytosis. Methods in enzymology *438*, 77-93.
Kirchhausen, T., Owen, D., and Harrison, S.C. (2014). Molecular structure, function, and dynamics of clathrin-mediated membrane traffic. Cold Spring Harb Perspect Biol *6*, a016725.
Kishida, K., Pearce, S.C., Yu, S., Gao, N., and Ferraris, R.P. (2017). Nutrient sensing by absorptive and secretory progenies of small intestinal stem cells. American journal of physiology Gastrointestinal and liver physiology *312*, G592-G605.
Knowles, B.C., Roland, J.T., Krishnan, M., Tyska, M.J., Lapierre, L.A., Dickman, P.S., Goldenring, J.R., and Shub, M.D. (2014). Myosin Vb uncoupling from RAB8A and RAB11A elicits microvillus inclusion disease. J Clin Invest *124*, 2947-2962.
Knowles, B.C., Weis, V.G., Yu, S., Roland, J.T., Williams, J.A., Alvarado, G.S., Lapierre, L.A., Shub, M.D., Gao, N., and Goldenring, J.R. (2015). Rab11a regulates syntaxin 3 localization and microvillus assembly in enterocytes. J Cell Sci *128*, 1617-1626.
Knudsen, L.A., Petersen, N., Schwartz, T.W., and Egerod, K.L. (2015). The MicroRNA Repertoire in Enteroendocrine Cells: Identification of miR-375 as a Potential Regulator of the Enteroendocrine Lineage. Endocrinology *156*, 3971-3983.
Kobayashi, M., Kweon, M.-N., Kuwata, H., Schreiber, R.D., Kiyono, H., Takeda, K., and Akira, S. (2003). Toll-like receptor-dependent production of IL-12p40 causes chronic enterocolitis in myeloid cell-specific Stat3-deficient mice. The Journal of clinical investigation *111*, 1297-1308.
Korinek, V., Barker, N., Moerer, P., van Donselaar, E., Huls, G., Peters, P.J., and Clevers, H. (1998). Depletion of epithelial stem-cell compartments in the small intestine of mice lacking Tcf-4. Nat Genet *19*, 379-383.
Kotenko, S.V., Izotova, L.S., Mirochnitchenko, O.V., Esterova, E., Dickensheets, H., Donnelly, R.P., and Pestka, S. (2001). Identification, cloning, and characterization of a novel soluble receptor that binds IL-22 and neutralizes its activity. J Immunol *166*, 7096-7103.
Krausova, M., and Korinek, V. (2014). Wnt signaling in adult intestinal stem cells and cancer. Cellular Signalling *26*, 570-579.
Kumar, P., Thakar, M.S., Ouyang, W., and Malarkannan, S. (2013). IL-22 from conventional NK cells is epithelial regenerative and inflammation protective during influenza infection. Mucosal Immunol *6*, 69-82.
Kural, C., Tacheva-Grigorova, S.K., Boulant, S., Cocucci, E., Baust, T., Duarte, D., and Kirchhausen, T. (2012). Dynamics of intracellular clathrin/AP1-and clathrin/AP3-containing carriers. Cell reports *2*, 1111-1119.
Ladinsky, M.S., Araujo, L.P., Zhang, X., Veltri, J., Galan-Diez, M., Soualhi, S., Lee, C., Irie, K., Pinker, E.Y., Narushima, S.*, et al.* (2019a). Endocytosis of commensal antigens by intestinal epithelial cells regulates mucosal T cell homeostasis. Science *363*.
Ladinsky, M.S., Araujo, L.P., Zhang, X., Veltri, J., Galan-Diez, M., Soualhi, S., Lee, C., Irie, K., Pinker, E.Y., Narushima, S.*, et al.* (2019b). Endocytosis of commensal antigens by intestinal epithelial cells regulates mucosal T cell homeostasis. Science *363*, eaat4042.
Lajoie, P., and Nabi, I.R. (2010). Lipid rafts, caveolae, and their endocytosis. In International review of cell and molecular biology (Elsevier), pp. 135-163.

Le Droguen, P.-M., Claret, S., Guichet, A., and Brodu, V. (2015). Microtubule-dependent apical restriction of recycling endosomes sustains adherens junctions during morphogenesis of the Drosophila tracheal system. Development *142*, 363.
Ledesma-Colunga, M.G., Adan, N., Ortiz, G., Solis-Gutierrez, M., Lopez-Barrera, F., Martinez de la Escalera, G., and Clapp, C. (2017). Prolactin blocks the expression of receptor activator of nuclear factor kappaB ligand and reduces osteoclastogenesis and bone loss in murine inflammatory arthritis. Arthritis Res Ther *19*, 93.
Lee, S.J., Kar, A.N., Kawaguchi, R., Patel, P., Sahoo, P.K., Aguilar, B., Lanz, K.D., McCain, C., Coppola, G., Lu, Q*., et al.* (2018a). Selective axonal translation of prenylated Cdc42 mRNA isoform supports axon growth. bioRxiv.
Lee, Y.S., Kim, T.Y., Kim, Y., Lee, S.H., Kim, S., Kang, S.W., Yang, J.Y., Baek, I.J., Sung, Y.H., Park, Y.Y*., et al.* (2018b). Microbiota-Derived Lactate Accelerates Intestinal Stem-Cell-Mediated Epithelial Development. Cell Host Microbe *24*, 833-846.e836.
Lejeune, D., Dumoutier, L., Constantinescu, S., Kruijer, W., Schuringa, J.J., and Renauld, J.C. (2002). Interleukin-22 (IL-22) activates the JAK/STAT, ERK, JNK, and p38 MAP kinase pathways in a rat hepatoma cell line. Pathways that are shared with and distinct from IL-10. J Biol Chem *277*, 33676-33682.
Leppanen, J., Helminen, O., Huhta, H., Kauppila, J.H., Miinalainen, I., Ronkainen, V.P., Saarnio, J., Lehenkari, P.P., and Karttunen, T.J. (2016). Doublecortin-like kinase 1-positive enterocyte - a new cell type in human intestine. APMIS *124*, 958-965.
Levi, E., Misra, S., Du, J., Patel, B.B., and Majumdar, A.P. (2009). Combination of aging and dimethylhydrazine treatment causes an increase in cancer-stem cell population of rat colonic crypts. Biochem Biophys Res Commun *385*, 430-433.
Levin, T.G., Powell, A.E., Davies, P.S., Silk, A.D., Dismuke, A.D., Anderson, E.C., Swain, J.R., and Wong, M.H. (2010). Characterization of the intestinal cancer stem cell marker CD166 in the human and mouse gastrointestinal tract. Gastroenterology *139*, 2072-2082 e2075.
Li, Y., Liu, Y., Liu, B., Wang, J., Wei, S., Qi, Z., Wang, S., Fu, W., and Chen, Y.G. (2018). A growth factor-free culture system underscores the coordination between Wnt and BMP signaling in Lgr5(+) intestinal stem cell maintenance. Cell Discov *4*, 49.
Liang, J., Balachandra, S., Ngo, S., and O'Brien, L.E. (2017). Feedback regulation of steady-state epithelial turnover and organ size. Nature *548*, 588-591.
Liebau, S., Russ, H.A., and Kleger, A. (2019). Stem Cell Derived Organoids in Human Disease and Development. Stem Cells Int *2019*, 7919427.
Lin, Q., Fuji, R.N., Yang, W., and Cerione, R.A. (2003). RhoGDI is required for Cdc42-mediated cellular transformation. Curr Biol *13*, 1469-1479.
Lindemans, C.A., Calafiore, M., Mertelsmann, A.M., O'Connor, M.H., Dudakov, J.A., Jenq, R.R., Velardi, E., Young, L.F., Smith, O.M., Lawrence, G*., et al.* (2015). Interleukin-22 promotes intestinal-stem-cell-mediated epithelial regeneration. Nature *528*, 560-564.
Lipka, J., Kapitein, L.C., Jaworski, J., and Hoogenraad, C.C. (2016). Microtubule-binding protein doublecortin-like kinase 1 (DCLK1) guides kinesin-3-mediated cargo transport to dendrites. EMBO J *35*, 302-318.
Liu, L., Zhuang, R., Xiao, L., Chung, H.K., Luo, J., Turner, D.J., Rao, J.N., Gorospe, M., and Wang, J.Y. (2017). HuR Enhances Early Restitution of the Intestinal Epithelium by

Increasing Cdc42 Translation. Mol Cell Biol *37*.
Liu, Y., Yang, B., Ma, J., Wang, H., Huang, F., Zhang, J., Chen, H., and Wu, C. (2011). Interleukin-21 induces the differentiation of human Tc22 cells via phosphorylation of signal transducers and activators of transcription. Immunology *132*, 540-548.
Mabuchi, T., Takekoshi, T., and Hwang, S.T. (2011). Epidermal CCR6+ gammadelta T cells are major producers of IL-22 and IL-17 in a murine model of psoriasiform dermatitis. J Immunol *187*, 5026-5031.
Macia, E., Ehrlich, M., Massol, R., Boucrot, E., Brunner, C., and Kirchhausen, T. (2006). Dynasore, a Cell-Permeable Inhibitor of Dynamin. Developmental Cell *10*, 839-850.
Mahadevaiyer, S., Xu, C., and Gumbiner, B.M. (2007). Characterization of a 60S complex of the adenomatous polyposis coli tumor suppressor protein. Biochim Biophys Acta *1773*, 120-130.
Marillier, R.G., Michels, C., Smith, E.M., Fick, L.C., Leeto, M., Dewals, B., Horsnell, W.G., and Brombacher, F. (2008). IL-4/IL-13 independent goblet cell hyperplasia in experimental helminth infections. BMC Immunol *9*, 11.
Marsh, M., and McMahon, H. (1999). The structural era of endocytosis. Science *285*, 215-220.
Mashiko, S., Bouguermouh, S., Rubio, M., Baba, N., Bissonnette, R., and Sarfati, M. (2015). Human mast cells are major IL-22 producers in patients with psoriasis and atopic dermatitis. J Allergy Clin Immunol *136*, 351-359 e351.
Matthews, J.R., Sansom, O.J., and Clarke, A.R. (2011). Absolute requirement for STAT3 function in small-intestine crypt stem cell survival. Cell Death Differ *18*, 1934-1943.
May, R., Qu, D., Weygant, N., Chandrakesan, P., Ali, N., Lightfoot, S.A., Li, L., Sureban, S.M., and Houchen, C.W. (2014). Brief report: Dclk1 deletion in tuft cells results in impaired epithelial repair after radiation injury. Stem cells (Dayton, Ohio) *32*, 822-827.
May, R., Riehl, T.E., Hunt, C., Sureban, S.M., Anant, S., and Houchen, C.W. (2008). Identification of a novel putative gastrointestinal stem cell and adenoma stem cell marker, doublecortin and CaM kinase-like-1, following radiation injury and in adenomatous polyposis coli/multiple intestinal neoplasia mice. Stem Cells *26*, 630-637.
Melendez, J., Liu, M., Sampson, L., Akunuru, S., Han, X., Vallance, J., Witte, D., Shroyer, N., and Zheng, Y. (2013). Cdc42 coordinates proliferation, polarity, migration, and differentiation of small intestinal epithelial cells in mice. Gastroenterology *145*, 808-819.
Metcalfe, C., Kljavin, Noelyn M., Ybarra, R., and de Sauvage, Frederic J. (2014). Lgr5⁺ Stem Cells Are Indispensable for Radiation-Induced Intestinal Regeneration. Cell Stem Cell *14*, 149-159.
Michaux, G., Massey-Harroche, D., Nicolle, O., Rabant, M., Brousse, N., Goulet, O., Le Bivic, A., and Ruemmele, F.M. (2016). The localisation of the apical Par/Cdc42 polarity module is specifically affected in microvillus inclusion disease. Biol Cell *108*, 19-28.
Miguel, J.C., Maxwell, A.A., Hsieh, J.J., Harnisch, L.C., Al Alam, D., Polk, D.B., Lien, C.L., Watson, A.J., and Frey, M.R. (2017). Epidermal growth factor suppresses intestinal epithelial cell shedding through a MAPK-dependent pathway. J Cell Sci *130*, 90-96.
Min, S., Kim, S., and Cho, S.W. (2020). Gastrointestinal tract modeling using organoids engineered with cellular and microbiota niches. Exp Mol Med *52*, 227-237.
Mitin, N., Betts, L., Yohe, M.E., Der, C.J., Sondek, J., and Rossman, K.L. (2007). Release of

autoinhibition of ASEF by APC leads to CDC42 activation and tumor suppression. Nat Struct Mol Biol *14*, 814-823.
Montaldo, E., Teixeira-Alves, L.G., Glatzer, T., Durek, P., Stervbo, U., Hamann, W., Babic, M., Paclik, D., Stolzel, K., Grone, J.*, et al.* (2014). Human RORgammat(+)CD34(+) cells are lineage-specified progenitors of group 3 RORgammat(+) innate lymphoid cells. Immunity *41*, 988-1000.
Moossavi, S., Zhang, H., Sun, J., and Rezaei, N. (2013). Host-microbiota interaction and intestinal stem cells in chronic inflammation and colorectal cancer. Expert Rev Clin Immunol *9*, 409-422.
Moreira-Teixeira, L., Resende, M., Coffre, M., Devergne, O., Herbeuval, J.P., Hermine, O., Schneider, E., Rogge, L., Ruemmele, F.M., Dy, M.*, et al.* (2011). Proinflammatory environment dictates the IL-17-producing capacity of human invariant NKT cells. J Immunol *186*, 5758-5765.
Moutin, E., Nikonenko, I., Stefanelli, T., Wirth, A., Ponimaskin, E., De Roo, M., and Muller, D. (2017). Palmitoylation of cdc42 Promotes Spine Stabilization and Rescues Spine Density Deficit in a Mouse Model of 22q11.2 Deletion Syndrome. Cerebral cortex (New York, NY : 1991) *27*, 3618-3629.
Mukai, J., Dhilla, A., Drew, L.J., Stark, K.L., Cao, L., MacDermott, A.B., Karayiorgou, M., and Gogos, J.A. (2008). Palmitoylation-dependent neurodevelopmental deficits in a mouse model of 22q11 microdeletion. Nat Neurosci *11*, 1302-1310.
Mukai, J., Tamura, M., Fénelon, K., Rosen, Andrew M., Spellman, Timothy J., Kang, R., MacDermott, Amy B., Karayiorgou, M., Gordon, Joshua A., and Gogos, Joseph A. (2015). Molecular Substrates of Altered Axonal Growth and Brain Connectivity in a Mouse Model of Schizophrenia. Neuron *86*, 680-695.
Muller, E., and Dowling, R.H. (1981). Prolactin and the small intestine. Effect of hyperprolactinaemia on mucosal structure in the rat. Gut *22*, 558-565.
Muller, T., Hess, M.W., Schiefermeier, N., Pfaller, K., Ebner, H.L., Heinz-Erian, P., Ponstingl, H., Partsch, J., Rollinghoff, B., Kohler, H.*, et al.* (2008). MYO5B mutations cause microvillus inclusion disease and disrupt epithelial cell polarity. Nat Genet *40*, 1163-1165.
Munneke, J.M., Bjorklund, A.T., Mjosberg, J.M., Garming-Legert, K., Bernink, J.H., Blom, B., Huisman, C., van Oers, M.H., Spits, H., Malmberg, K.J.*, et al.* (2014). Activated innate lymphoid cells are associated with a reduced susceptibility to graft-versus-host disease. Blood *124*, 812-821.
Musteanu, M., Blaas, L., Mair, M., Schlederer, M., Bilban, M., Tauber, S., Esterbauer, H., Mueller, M., Casanova, E., Kenner, L.*, et al.* (2010). Stat3 is a negative regulator of intestinal tumor progression in Apc(Min) mice. Gastroenterology *138*, 1003-1011 e1001-1005.
Mytych, J., Satora, L., and Koziol, K. (2018). Confirmation of the immunoreactivity of monoclonal anti-human C-terminal EGFR antibodies in bronze Corydoras Corydoras aeneus (Callichthyidae Teleostei) by Western Blot method. Acta Histochem *120*, 151-153.
Nagalakshmi, M.L., Rascle, A., Zurawski, S., Menon, S., and de Waal Malefyt, R. (2004). Interleukin-22 activates STAT3 and induces IL-10 by colon epithelial cells. Int Immunopharmacol *4*, 679-691.
Nagano, K. (2019). R-spondin signaling as a pivotal regulator of tissue development and homeostasis. Jpn Dent Sci Rev *55*, 80-87.

Nagy, E., and Berczi, I. (1991). Hypophysectomized rats depend on residual prolactin for survival. Endocrinology *128*, 2776-2784.
Nakamoto, N., Amiya, T., Aoki, R., Taniki, N., Koda, Y., Miyamoto, K., Teratani, T., Suzuki, T., Chiba, S., Chu, P.-S*., et al.* (2017). Commensal Lactobacillus Controls Immune Tolerance during Acute Liver Injury in Mice. Cell Reports *21*, 1215-1226.
Nautiyal, J., Du, J., Yu, Y., Kanwar, S.S., Levi, E., and Majumdar, A.P. (2012). EGFR regulation of colon cancer stem-like cells during aging and in response to the colonic carcinogen dimethylhydrazine. Am J Physiol Gastrointest Liver Physiol *302*, G655-663.
Ness-Schwickerath, K.J., and Morita, C.T. (2011). Regulation and function of IL-17A- and IL-22-producing gammadelta T cells. Cell Mol Life Sci *68*, 2371-2390.
Nigro, G., Hanson, M., Fevre, C., Lecuit, M., and Sansonetti, P.J. (2019). Intestinal Organoids as a Novel Tool to Study Microbes-Epithelium Interactions. Methods Mol Biol *1576*, 183-194.
Nigro, G., Rossi, R., Commere, P.H., Jay, P., and Sansonetti, P.J. (2014). The cytosolic bacterial peptidoglycan sensor Nod2 affords stem cell protection and links microbes to gut epithelial regeneration. Cell Host Microbe *15*, 792-798.
Nishimura, A., and Linder, M.E. (2013). Identification of a novel prenyl and palmitoyl modification at the CaaX motif of Cdc42 that regulates RhoGDI binding. Mol Cell Biol *33*, 1417-1429.
Nomanbhoy, T.K., Erickson, J.W., and Cerione, R.A. (1999). Kinetics of Cdc42 membrane extraction by Rho-GDI monitored by real-time fluorescence resonance energy transfer. Biochemistry *38*, 1744-1750.
Noritake, J., Watanabe, T., Sato, K., Wang, S., and Kaibuchi, K. (2005). IQGAP1: a key regulator of adhesion and migration. J Cell Sci *118*, 2085-2092.
O'Brien, C.A., Pollett, A., Gallinger, S., and Dick, J.E. (2007). A human colon cancer cell capable of initiating tumour growth in immunodeficient mice. Nature *445*, 106-110.
Oeser, K., Schwartz, C., and Voehringer, D. (2015). Conditional IL-4/IL-13-deficient mice reveal a critical role of innate immune cells for protective immunity against gastrointestinal helminths. Mucosal Immunol *8*, 672-682.
Okumura, R., and Takeda, K. (2017). Roles of intestinal epithelial cells in the maintenance of gut homeostasis. Exp Mol Med *49*, e338.
Onyiah, J.C., and Colgan, S.P. (2016). Cytokine responses and epithelial function in the intestinal mucosa. Cell Mol Life Sci *73*, 4203-4212.
Oshima, H., Kok, S.Y., Nakayama, M., Murakami, K., Voon, D.C., Kimura, T., and Oshima, M. (2019). Stat3 is indispensable for damage-induced crypt regeneration but not for Wnt-driven intestinal tumorigenesis. FASEB J *33*, 1873-1886.
Osmani, N., Vitale, N., Borg, J.P., and Etienne-Manneville, S. (2006). Scrib controls Cdc42 localization and activity to promote cell polarization during astrocyte migration. Curr Biol *16*, 2395-2405.
Otte, J.M., Rosenberg, I.M., and Podolsky, D.K. (2003). Intestinal myofibroblasts in innate immune responses of the intestine. Gastroenterology *124*, 1866-1878.
Ouhtit, A., Kelly, P.A., and Morel, G. (1994). Visualization of gene expression of short and long forms of prolactin receptor in rat digestive tissues. Am J Physiol *266*, G807-815.
Owen, D.J., Collins, B.M., and Evans, P.R. (2004). Adaptors for clathrin coats: structure and

function. Annu Rev Cell Dev Biol *20*, 153-191.
Palazzo, M., Balsari, A., Rossini, A., Selleri, S., Calcaterra, C., Gariboldi, S., Zanobbio, L., Arnaboldi, F., Shirai, Y.F., Serrao, G.*, et al.* (2007). Activation of enteroendocrine cells via TLRs induces hormone, chemokine, and defensin secretion. J Immunol *178*, 4296-4303.
Park, J.S., Kim, Y.S., and Yoo, M.A. (2009). The role of p38b MAPK in age-related modulation of intestinal stem cell proliferation and differentiation in Drosophila. Aging (Albany NY) *1*, 637-651.
Parks, O.B., Pociask, D.A., Hodzic, Z., Kolls, J.K., and Good, M. (2016). Interleukin-22 Signaling in the Regulation of Intestinal Health and Disease. Frontiers in cell and developmental biology *3*, 85-85.
Parton, R.G., and Simons, K. (2007). The multiple faces of caveolae. Nature reviews Molecular cell biology *8*, 185-194.
Patel, B.B., Yu, Y., Du, J., Levi, E., Phillip, P.A., and Majumdar, A.P. (2009). Age-related increase in colorectal cancer stem cells in macroscopically normal mucosa of patients with adenomas: a risk factor for colon cancer. Biochem Biophys Res Commun *378*, 344-347.
Patra, S.K. (2008). Dissecting lipid raft facilitated cell signaling pathways in cancer. Biochimica et Biophysica Acta (BBA) - Reviews on Cancer *1785*, 182-206.
Peng, W.C., de Lau, W., Forneris, F., Granneman, J.C., Huch, M., Clevers, H., and Gros, P. (2013). Structure of stem cell growth factor R-spondin 1 in complex with the ectodomain of its receptor LGR5. Cell Rep *3*, 1885-1892.
Pereira, D.B., and Chao, M.V. (2007). The tyrosine kinase Fyn determines the localization of TrkB receptors in lipid rafts. J Neurosci *27*, 4859-4869.
Peterson, L.W., and Artis, D. (2014). Intestinal epithelial cells: regulators of barrier function and immune homeostasis. Nat Rev Immunol *14*, 141-153.
Pickert, G., Neufert, C., Leppkes, M., Zheng, Y., Wittkopf, N., Warntjen, M., Lehr, H.-A., Hirth, S., Weigmann, B., Wirtz, S.*, et al.* (2009). STAT3 links IL-22 signaling in intestinal epithelial cells to mucosal wound healing. The Journal of Experimental Medicine *206*, 1465.
Pike, L.J., Han, X., and Gross, R.W. (2005). Epidermal Growth Factor Receptors Are Localized to Lipid Rafts That Contain a Balance of Inner and Outer Leaflet Lipids: A SHOTGUN LIPIDOMICS STUDY. *280*, 26796-26804.
Pinchuk, I.V., Beswick, E.J., Saada, J.I., Suarez, G., Winston, J., Mifflin, R.C., Di Mari, J.F., Powell, D.W., and Reyes, V.E. (2007). Monocyte chemoattractant protein-1 production by intestinal myofibroblasts in response to staphylococcal enterotoxin a: relevance to staphylococcal enterotoxigenic disease. J Immunol *178*, 8097-8106.
Pinto, D., Gregorieff, A., Begthel, H., and Clevers, H. (2003). Canonical Wnt signals are essential for homeostasis of the intestinal epithelium. Genes Dev *17*, 1709-1713.
Pitulescu, M.E., and Adams, R.H. (2010). Eph/ephrin molecules--a hub for signaling and endocytosis. Genes Dev *24*, 2480-2492.
Potten, C.S. (1977). Extreme sensitivity of some intestinal crypt cells to X and γ irradiation. Nature *269*, 518.
Powell, A.E., Wang, Y., Li, Y., Poulin, E.J., Means, A.L., Washington, M.K., Higginbotham, J.N., Juchheim, A., Prasad, N., Levy, S.E.*, et al.* (2012). The pan-ErbB negative regulator Lrig1 is an intestinal stem cell marker that functions as a tumor suppressor. Cell *149*, 146-158.

Powell, D.W., Pinchuk, I.V., Saada, J.I., Chen, X., and Mifflin, R.C. (2011). Mesenchymal cells of the intestinal lamina propria. Annu Rev Physiol *73*, 213-237.
Praefcke, G.J., and McMahon, H.T. (2004). The dynamin superfamily: universal membrane tubulation and fission molecules? Nature reviews Molecular cell biology *5*, 133-147.
Punnonen, E.L., Ryhanen, K., and Marjomaki, V.S. (1998). At reduced temperature, endocytic membrane traffic is blocked in multivesicular carrier endosomes in rat cardiac myocytes. European journal of cell biology *75*, 344-352.
Puri, C., Tosoni, D., Comai, R., Rabellino, A., Segat, D., Caneva, F., Luzzi, P., Di Fiore, P.P., and Tacchetti, C. (2005). Relationships between EGFR Signaling–competent and Endocytosis-competent Membrane Microdomains. Molecular Biology of the Cell *16*, 2704-2718.
Pyo, J.H., Jeon, H.J., Park, J.S., Lee, J.S., Chung, H.Y., and Yoo, M.A. (2018). Drosophila PEBP1 inhibits intestinal stem cell aging via suppression of ERK pathway. Oncotarget *9*, 17980-17993.
Qi, Z., Li, Y., Zhao, B., Xu, C., Liu, Y., Li, H., Zhang, B., Wang, X., Yang, X., Xie, W*., et al.* (2017). BMP restricts stemness of intestinal Lgr5+ stem cells by directly suppressing their signature genes. Nature Communications *8*, 13824.
Radaeva, S., Sun, R., Pan, H.N., Hong, F., and Gao, B. (2004). Interleukin 22 (IL-22) plays a protective role in T cell-mediated murine hepatitis: IL-22 is a survival factor for hepatocytes via STAT3 activation. Hepatology *39*, 1332-1342.
Radhakrishnan, A., Raju, R., Tuladhar, N., Subbannayya, T., Thomas, J.K., Goel, R., Telikicherla, D., Palapetta, S.M., Rahiman, B.A., Venkatesh, D.D*., et al.* (2012). A pathway map of prolactin signaling. J Cell Commun Signal *6*, 169-173.
Radtke, F., and Clevers, H. (2005). Self-Renewal and Cancer of the Gut: Two Sides of a Coin. *307*, 1904-1909.
Raifer, H., Mahiny, A.J., Bollig, N., Petermann, F., Hellhund, A., Kellner, K., Guralnik, A., Reinhard, K., Bothur, E., Huber, M*., et al.* (2012). Unlike alphabeta T cells, gammadelta T cells, LTi cells and NKT cells do not require IRF4 for the production of IL-17A and IL-22. Eur J Immunol *42*, 3189-3201.
Rakoff-Nahoum, S., Paglino, J., Eslami-Varzaneh, F., Edberg, S., and Medzhitov, R. (2004). Recognition of commensal microflora by toll-like receptors is required for intestinal homeostasis. Cell *118*, 229-241.
Rappoport, J.Z. (2008). Focusing on clathrin-mediated endocytosis. Biochemical Journal *412*, 415-423.
Raucher, D., and Sheetz, M.P. (1999). Membrane expansion increases endocytosis rate during mitosis. The Journal of cell biology *144*, 497-506.
Razani, B., Woodman, S.E., and Lisanti, M.P. (2002). Caveolae: from cell biology to animal physiology. Pharmacological reviews *54*, 431-467.
Ren, F., Wang, B., Yue, T., Yun, E.Y., Ip, Y.T., and Jiang, J. (2010). Hippo signaling regulates Drosophila intestine stem cell proliferation through multiple pathways. Proc Natl Acad Sci U S A *107*, 21064-21069.
Ren, J., Yu, S., Gao, N., and Zou, Q. (2013a). A control-based approach to quantification of rate-dependent elastic modulus of living cell using atomic force microscope. Paper presented at: 2013 American Control Conference.
Ren, J., Yu, S., Gao, N., and Zou, Q. (2013b). Indentation quantification for in-liquid

nanomechanical measurement of soft material using an atomic force microscope: Rate-dependent elastic modulus of live cells. Physical Review E *88*, 052711.
Rey, K., Manku, S., Enns, W., Van Rossum, T., Bushell, K., Morin, R.D., Brinkman, F.S.L., and Choy, J.C. (2018). Disruption of the Gut Microbiota With Antibiotics Exacerbates Acute Vascular Rejection. Transplantation *102*, 1085-1095.
Riehl, T.E., Ee, X., and Stenson, W.F. (2012). Hyaluronic acid regulates normal intestinal and colonic growth in mice. American Journal of Physiology-Gastrointestinal and Liver Physiology *303*, G377-G388.
Rigby, R.J., Knight, S.C., Kamm, M.A., and Stagg, A.J. (2005). Production of interleukin (IL)-10 and IL-12 by murine colonic dendritic cells in response to microbial stimuli. Clin Exp Immunol *139*, 245-256.
Roland, J.T., Bryant, D.M., Datta, A., Itzen, A., Mostov, K.E., and Goldenring, J.R. (2011). Rab GTPase-Myo5B complexes control membrane recycling and epithelial polarization. Proc Natl Acad Sci U S A *108*, 2789-2794.
Roossien, D., Miller, K., and Gallo, G. (2015). Ciliobrevins as tools for studying dynein motor function. Frontiers in Cellular Neuroscience *9*.
Ros-Baro, A., Lopez-Iglesias, C., Peiro, S., Bellido, D., Palacin, M., Zorzano, A., and Camps, M. (2001). Lipid rafts are required for GLUT4 internalization in adipose cells. Proceedings of the National Academy of Sciences of the United States of America *98*, 12050-12055.
Rothberg, K.G., Heuser, J.E., Donzell, W.C., Ying, Y.S., Glenney, J.R., and Anderson, R.G. (1992). Caveolin, a protein component of caveolae membrane coats. Cell *68*, 673-682.
Ruemmele, F.M., Schmitz, J., and Goulet, O. (2006). Microvillous inclusion disease (microvillous atrophy). Orphanet J Rare Dis *1*, 22.
Saha, S., Aranda, E., Hayakawa, Y., Bhanja, P., Atay, S., Brodin, N.P., Li, J., Asfaha, S., Liu, L., Tailor, Y.*, et al.* (2016). Macrophage-derived extracellular vesicle-packaged WNTs rescue intestinal stem cells and enhance survival after radiation injury. Nat Commun *7*, 13096.
Sahu, U., Choudhury, A., Parvez, S., Biswas, S., and Kar, S. (2017). Induction of intestinal stemness and tumorigenicity by aberrant internalization of commensal non-pathogenic E. coli. Cell Death &Amp; Disease *8*, e2667.
Sakamori, R., Das, S., Yu, S., Feng, S., Stypulkowski, E., Guan, Y., Douard, V., Tang, W., Ferraris, R.P., Harada, A.*, et al.* (2012a). Cdc42 and Rab8a are critical for intestinal stem cell division, survival, and differentiation in mice. The Journal of Clinical Investigation *122*, 1052-1065.
Sakamori, R., Das, S., Yu, S., Feng, S., Stypulkowski, E., Guan, Y., Douard, V., Tang, W., Ferraris, R.P., Harada, A.*, et al.* (2012b). Cdc42 and Rab8a are critical for intestinal stem cell division, survival, and differentiation in mice. J Clin Invest *122*, 1052-1065.
Sakamori, R., Yu, S., Zhang, X., Hoffman, A., Sun, J., Das, S., Vedula, P., Li, G., Fu, J., Walker, F.*, et al.* (2014a). CDC42 Inhibition Suppresses Progression of Incipient Intestinal Tumors. Cancer Research *74*, 5480.
Sakamori, R., Yu, S., Zhang, X., Hoffman, A., Sun, J., Das, S., Vedula, P., Li, G., Fu, J., Walker, F.*, et al.* (2014b). CDC42 inhibition suppresses progression of incipient intestinal tumors. Cancer Res *74*, 5480-5492.
Salzer, U., and Prohaska, R. (2001). Stomatin, flotillin-1, and flotillin-2 are major integral proteins of erythrocyte lipid rafts. Blood *97*, 1141-1143.

Sarnataro, D., Caputo, A., Casanova, P., Puri, C., Paladino, S., Tivodar, S.S., Campana, V., Tacchetti, C., and Zurzolo, C. (2009). Lipid Rafts and Clathrin Cooperate in the Internalization of PrPC in Epithelial FRT Cells. PLOS ONE *4*, e5829.
Sato, A. (2007). Tuft cells. Anat Sci Int *82*, 187-199.
Sato, T., Mushiake, S., Kato, Y., Sato, K., Sato, M., Takeda, N., Ozono, K., Miki, K., Kubo, Y., Tsuji, A.*, et al.* (2007). The Rab8 GTPase regulates apical protein localization in intestinal cells. Nature *448*, 366-369.
Sato, T., Stange, D.E., Ferrante, M., Vries, R.G., Van Es, J.H., Van den Brink, S., Van Houdt, W.J., Pronk, A., Van Gorp, J., Siersema, P.D.*, et al.* (2011a). Long-term expansion of epithelial organoids from human colon, adenoma, adenocarcinoma, and Barrett's epithelium. Gastroenterology *141*, 1762-1772.
Sato, T., van Es, J.H., Snippert, H.J., Stange, D.E., Vries, R.G., van den Born, M., Barker, N., Shroyer, N.F., van de Wetering, M., and Clevers, H. (2011b). Paneth cells constitute the niche for Lgr5 stem cells in intestinal crypts. Nature *469*, 415-418.
Sato, T., Vries, R.G., Snippert, H.J., van de Wetering, M., Barker, N., Stange, D.E., van Es, J.H., Abo, A., Kujala, P., Peters, P.J.*, et al.* (2009a). Single Lgr5 stem cells build crypt-villus structures in vitro without a mesenchymal niche. Nature *459*, 262-265.
Sato, T., Vries, R.G., Snippert, H.J., van de Wetering, M., Barker, N., Stange, D.E., van Es, J.H., Abo, A., Kujala, P., Peters, P.J.*, et al.* (2009b). Single Lgr5 stem cells build crypt□villus structures in vitro without a mesenchymal niche. Nature *459*, 262.
Satora, L., Mytych, J., and Bilska-Kos, A. (2018). The presence and expression of the HIF-1alpha in the respiratory intestine of the bronze Corydoras Corydoras aeneus (Callichthyidae Teleostei). Fish Physiol Biochem *44*, 1291-1297.
Sbarbati, A., and Osculati, F. (2005). A new fate for old cells: brush cells and related elements. J Anat *206*, 349-358.
Schepers, A., and Clevers, H. (2012). Wnt Signaling, Stem Cells, and Cancer of the Gastrointestinal Tract. *4*.
Schindelin, J., Arganda-Carreras, I., Frise, E., Kaynig, V., Longair, M., Pietzsch, T., Preibisch, S., Rueden, C., Saalfeld, S., Schmid, B.*, et al.* (2012). Fiji: an open-source platform for biological-image analysis. Nature methods *9*, 676-682.
Schindler, C., and Darnell, J.E., Jr. (1995). Transcriptional responses to polypeptide ligands: the JAK-STAT pathway. Annu Rev Biochem *64*, 621-651.
Schmechel, S., Konrad, A., Diegelmann, J., Glas, J., Wetzke, M., Paschos, E., Lohse, P., Goke, B., and Brand, S. (2008). Linking genetic susceptibility to Crohn's disease with Th17 cell function: IL-22 serum levels are increased in Crohn's disease and correlate with disease activity and IL23R genotype status. Inflamm Bowel Dis *14*, 204-212.
Schmitt, M., Schewe, M., Sacchetti, A., Feijtel, D., van de Geer, W.S., Teeuwssen, M., Sleddens, H.F., Joosten, R., van Royen, M.E., van de Werken, H.J.G.*, et al.* (2018). Paneth Cells Respond to Inflammation and Contribute to Tissue Regeneration by Acquiring Stem-like Features through SCF/c-Kit Signaling. Cell Reports *24*, 2312-2328.e2317.
Schneeberger, K., Vogel, G.F., Teunissen, H., van Ommen, D.D., Begthel, H., El Bouazzaoui, L., van Vugt, A.H., Beekman, J.M., Klumperman, J., Muller, T.*, et al.* (2015). An inducible mouse model for microvillus inclusion disease reveals a role for myosin Vb in apical and basolateral trafficking. Proc Natl Acad Sci U S A *112*, 12408-12413.

Schoenborn, A.A., von Furstenberg, R.J., Valsaraj, S., Hussain, F.S., Stein, M., Shanahan, M.T., Henning, S.J., and Gulati, A.S. (2018). The enteric microbiota regulates jejunal Paneth cell number and function without impacting intestinal stem cells. Gut Microbes, 1-14.
Schuijers, J., and Clevers, H. (2012). Adult mammalian stem cells: the role of Wnt, Lgr5 and R-spondins. EMBO J *31*, 2685-2696.
Schuijers, J., Junker, J.P., Mokry, M., Hatzis, P., Koo, B.K., Sasselli, V., van der Flier, L.G., Cuppen, E., van Oudenaarden, A., and Clevers, H. (2015). Ascl2 acts as an R-spondin/Wnt-responsive switch to control stemness in intestinal crypts. Cell Stem Cell *16*, 158-170.
Schuijers, J., Mokry, M., Hatzis, P., Cuppen, E., and Clevers, H. (2014). Wnt-induced transcriptional activation is exclusively mediated by TCF/LEF. EMBO J *33*, 146-156.
Schulte, L., Hohwieler, M., Muller, M., and Klaus, J. (2019). Intestinal Organoids as a Novel Complementary Model to Dissect Inflammatory Bowel Disease. Stem Cells Int *2019*, 8010645.
Schust, J., Sperl, B., Hollis, A., Mayer, T.U., and Berg, T. (2006). Stattic: a small-molecule inhibitor of STAT3 activation and dimerization. Chem Biol *13*, 1235-1242.
Seale, A.P., Stagg, J.J., Yamaguchi, Y., Breves, J.P., Soma, S., Watanabe, S., Kaneko, T., Cnaani, A., Harpaz, S., Lerner, D.T*., et al.* (2014). Effects of salinity and prolactin on gene transcript levels of ion transporters, ion pumps and prolactin receptors in Mozambique tilapia intestine. Gen Comp Endocrinol *206*, 146-154.
Sei, Y., Feng, J., Samsel, L., White, A., Zhao, X., Yun, S., Citrin, D., McCoy, J.P., Sundaresan, S., Hayes, M.M*., et al.* (2018). Mature enteroendocrine cells contribute to basal and pathological stem cell dynamics in the small intestine. *315*, G495-G510.
Sekikawa, A., Fukui, H., Suzuki, K., Karibe, T., Fujii, S., Ichikawa, K., Tomita, S., Imura, J., Shiratori, K., Chiba, T*., et al.* (2010). Involvement of the IL-22/REG Ialpha axis in ulcerative colitis. Lab Invest *90*, 496-505.
Selleri, S., Palazzo, M., Deola, S., Wang, E., Balsari, A., Marincola, F.M., and Rumio, C. (2008). Induction of pro-inflammatory programs in enteroendocrine cells by the Toll-like receptor agonists flagellin and bacterial LPS. Int Immunol *20*, 961-970.
Shaker, A., Swietlicki, E.A., Wang, L., Jiang, S., Onal, B., Bala, S., DeSchryver, K., Newberry, R., Levin, M.S., and Rubin, D.C. (2010). Epimorphin deletion protects mice from inflammation-induced colon carcinogenesis and alters stem cell niche myofibroblast secretion. J Clin Invest *120*, 2081-2093.
Shibata, M., Uchihashi, T., Ando, T., and Yasuda, R. (2015). Long-tip high-speed atomic force microscopy for nanometer-scale imaging in live cells. *5*, 8724.
Shibata, M., Watanabe, H., Uchihashi, T., Ando, T., and Yasuda, R. (2017). High-speed atomic force microscopy imaging of live mammalian cells. Biophysics and Physicobiology *14*, 127-135.
Shoshkes-Carmel, M., Wang, Y.J., Wangensteen, K.J., Toth, B., Kondo, A., Massasa, E.E., Itzkovitz, S., and Kaestner, K.H. (2018). Subepithelial telocytes are an important source of Wnts that supports intestinal crypts. Nature *557*, 242-246.
Shreiner, A.B., Kao, J.Y., and Young, V.B. (2015). The gut microbiome in health and in disease. Curr Opin Gastroenterol *31*, 69-75.
Shroyer, N.F., Helmrath, M.A., Wang, V.Y., Antalffy, B., Henning, S.J., and Zoghbi, H.Y. (2007). Intestine-specific ablation of mouse atonal homolog 1 (Math1) reveals a role in cellular

homeostasis. Gastroenterology *132*, 2478-2488.
Sigismund, S., Argenzio, E., Tosoni, D., Cavallaro, E., Polo, S., and Di Fiore, P.P. (2008). Clathrin-Mediated Internalization Is Essential for Sustained EGFR Signaling but Dispensable for Degradation. Developmental Cell *15*, 209-219.
Silva, M.J.B., Carneiro, M.B.H., dos Anjos Pultz, B., Pereira Silva, D., Lopes, M.E.d.M., and dos Santos, L.M. (2015). The multifaceted role of commensal microbiota in homeostasis and gastrointestinal diseases. J Immunol Res *2015*, 321241-321241.
Simons, K., and Ehehalt, R. (2002). Cholesterol, lipid rafts, and disease. The Journal of clinical investigation *110*, 597-603.
Simons, K., and Toomre, D. (2000). Lipid rafts and signal transduction. Nature reviews Molecular cell biology *1*, 31-39.
Sinha, S., and Yang, W. (2008). Cellular signaling for activation of Rho GTPase Cdc42. Cell Signal *20*, 1927-1934.
Snippert, H.J., van der Flier, L.G., Sato, T., van Es, J.H., van den Born, M., Kroon-Veenboer, C., Barker, N., Klein, A.M., van Rheenen, J., Simons, B.D.*, et al.* (2010). Intestinal crypt homeostasis results from neutral competition between symmetrically dividing Lgr5 stem cells. Cell *143*, 134-144.
Snoeck, V., Goddeeris, B., and Cox, E. (2005). The role of enterocytes in the intestinal barrier function and antigen uptake. Microbes Infect *7*, 997-1004.
Sobajima, T., Yoshimura, S., Iwano, T., Kunii, M., Watanabe, M., Atik, N., Mushiake, S., Morii, E., Koyama, Y., Miyoshi, E.*, et al.* (2014). Rab11a is required for apical protein localisation in the intestine. Biol Open *4*, 86-94.
Sorkin, A., and Von Zastrow, M. (2009). Endocytosis and signalling: intertwining molecular networks. Nature reviews Molecular cell biology *10*, 609-622.
Spits, H., and Cupedo, T. (2012). Innate lymphoid cells: emerging insights in development, lineage relationships, and function. Annu Rev Immunol *30*, 647-675.
Stappenbeck, T.S., and Gordon, J.I. (2000). Rac1 mutations produce aberrant epithelial differentiation in the developing and adult mouse small intestine. Development *127*, 2629-2642.
Steenwinckel, V., Louahed, J., Lemaire, M.M., Sommereyns, C., Warnier, G., McKenzie, A., Brombacher, F., Van Snick, J., and Renauld, J.C. (2009). IL-9 promotes IL-13-dependent paneth cell hyperplasia and up-regulation of innate immunity mediators in intestinal mucosa. J Immunol *182*, 4737-4743.
Stefka, A.T., Feehley, T., Tripathi, P., Qiu, J., McCoy, K., Mazmanian, S.K., Tjota, M.Y., Seo, G.-Y., Cao, S., and Theriault, B.R.J.P.o.t.N.A.o.S. (2014). Commensal bacteria protect against food allergen sensitization. *111*, 13145-13150.
Stengel, K., and Zheng, Y. (2011). Cdc42 in oncogenic transformation, invasion, and tumorigenesis. Cell Signal *23*, 1415-1423.
Sudhaharan, T., Goh, W.I., Sem, K.P., Lim, K.B., Bu, W., and Ahmed, S. (2011). Rho GTPase Cdc42 is a direct interacting partner of Adenomatous Polyposis Coli protein and can alter its cellular localization. PLoS One *6*, e16603.
Sugimoto, K., Ogawa, A., Mizoguchi, E., Shimomura, Y., Andoh, A., Bhan, A.K., Blumberg, R.S., Xavier, R.J., and Mizoguchi, A. (2008). IL-22 ameliorates intestinal inflammation in a mouse model of ulcerative colitis. J Clin Invest *118*, 534-544.

Suh, H.N., Kim, M.J., Jung, Y.S., Lien, E.M., Jun, S., and Park, J.I. (2017). Quiescence Exit of Tert(+) Stem Cells by Wnt/beta-Catenin Is Indispensable for Intestinal Regeneration. Cell Rep *21*, 2571-2584.

Sun, J., Yu, S., Zhang, X., Capac, C., Aligbe, O., Daudelin, T., Bonder, E.M., and Gao, N. (2017). A Wntless-SEC12 complex on the ER membrane regulates early Wnt secretory vesicle assembly and mature ligand export. J Cell Sci *130*, 2159-2171.

Suzuki, A., Sekiya, S., Gunshima, E., Fujii, S., and Taniguchi, H. (2010). EGF signaling activates proliferation and blocks apoptosis of mouse and human intestinal stem/progenitor cells in long-term monolayer cell culture. Lab Invest *90*, 1425-1436.

Takeda, H., and Kiyokawa, E. (2017). Activation of Erk in ileal epithelial cells engaged in ischemic-injury repair. Sci Rep *7*, 16469.

Takeda, N., Jain, R., LeBoeuf, M.R., Wang, Q., Lu, M.M., and Epstein, J.A. (2011). Interconversion between intestinal stem cell populations in distinct niches. Science *334*, 1420-1424.

Tetteh, Paul W., Basak, O., Farin, Henner F., Wiebrands, K., Kretzschmar, K., Begthel, H., van den Born, M., Korving, J., de Sauvage, F., van Es, Johan H.*, et al.* (2016). Replacement of Lost Lgr5-Positive Stem Cells through Plasticity of Their Enterocyte-Lineage Daughters. Cell Stem Cell *18*, 203-213.

Tian, Y., Gawlak, G., Shah, A.S., Higginbotham, K., Tian, X., Kawasaki, Y., Akiyama, T., Sacks, D.B., and Birukova, A.A. (2015). Hepatocyte growth factor-induced Asef-IQGAP1 complex controls cytoskeletal remodeling and endothelial barrier. J Biol Chem *290*, 4097-4109.

Tierney, B.T., Yang, Z., Luber, J.M., Beaudin, M., Wibowo, M.C., Baek, C., Mehlenbacher, E., Patel, C.J., and Kostic, A.D. (2019). The Landscape of Genetic Content in the Gut and Oral Human Microbiome. Cell Host Microbe *26*, 283-295 e288.

Tominaga, A., Konishi, Y., Taguchi, T., Fukuoka, S., Kawaguchi, T., Noda, T., and Shimizu, K. (2013). Autonomous cure of damaged human intestinal epithelial cells by TLR2 and TLR4-dependent production of IL-22 in response to Spirulina polysaccharides. International Immunopharmacology *17*, 1009-1019.

Tomoda, H., Kishimoto, Y., and Lee, Y.C. (1989). Temperature effect on endocytosis and exocytosis by rabbit alveolar macrophages. Journal of Biological Chemistry *264*, 15445-15450.

Tong, K., Pellon-Cardenas, O., Sirihorachai, V.R., Warder, B.N., Kothari, O.A., Perekatt, A.O., Fokas, E.E., Fullem, R.L., Zhou, A., Thackray, J.K.*, et al.* (2017). Degree of Tissue Differentiation Dictates Susceptibility to BRAF-Driven Colorectal Cancer. Cell Rep *21*, 3833-3845.

Touz, M.C., Kulakova, L., and Nash, T.E. (2004). Adaptor Protein Complex 1 Mediates the Transport of Lysosomal Proteins from a Golgi-like Organelle to Peripheral Vacuoles in the Primitive Eukaryote Giardia lamblia. Molecular Biology of the Cell *15*, 3053-3060.

Traub, L.M., and Bonifacino, J.S. (2013). Cargo recognition in clathrin-mediated endocytosis. Cold Spring Harbor perspectives in biology *5*, a016790.

Trifari, S., Kaplan, C.D., Tran, E.H., Crellin, N.K., and Spits, H. (2009). Identification of a human helper T cell population that has abundant production of interleukin 22 and is distinct from T(H)-17, T(H)1 and T(H)2 cells. Nat Immunol *10*, 864-871.

Turner, J.E., Stockinger, B., and Helmby, H. (2013). IL-22 mediates goblet cell hyperplasia

and worm expulsion in intestinal helminth infection. PLoS Pathog *9*, e1003698.
Ungewiss, H., Rotzer, V., Meir, M., Fey, C., Diefenbacher, M., Schlegel, N., and Waschke, J. (2018). Dsg2 via Src-mediated transactivation shapes EGFR signaling towards cell adhesion. Cell Mol Life Sci *75*, 4251-4268.
van der Flier, L.G., and Clevers, H. (2009). Stem cells, self-renewal, and differentiation in the intestinal epithelium. Annu Rev Physiol *71*, 241-260.
van der Flier, L.G., Haegebarth, A., Stange, D.E., van de Wetering, M., and Clevers, H. (2009). OLFM4 is a robust marker for stem cells in human intestine and marks a subset of colorectal cancer cells. Gastroenterology *137*, 15-17.
Van der Flier, L.G., Sabates-Bellver, J., Oving, I., Haegebarth, A., De Palo, M., Anti, M., Van Gijn, M.E., Suijkerbuijk, S., Van de Wetering, M., Marra, G.*, et al.* (2007). The Intestinal Wnt/TCF Signature. Gastroenterology *132*, 628-632.
van der Heijden, M., and Vermeulen, L. (2019). Stem cells in homeostasis and cancer of the gut. Mol Cancer *18*, 66.
van Es, J.H., Haegebarth, A., Kujala, P., Itzkovitz, S., Koo, B.K., Boj, S.F., Korving, J., van den Born, M., van Oudenaarden, A., Robine, S.*, et al.* (2012). A critical role for the Wnt effector Tcf4 in adult intestinal homeostatic self-renewal. Mol Cell Biol *32*, 1918-1927.
VanDussen, K.L., Carulli, A.J., Keeley, T.M., Patel, S.R., Puthoff, B.J., Magness, S.T., Tran, I.T., Maillard, I., Siebel, C., Kolterud, A.*, et al.* (2012). Notch signaling modulates proliferation and differentiation of intestinal crypt base columnar stem cells. Development *139*, 488-497.
Vehlow, A., Soong, D., Vizcay-Barrena, G., Bodo, C., Law, A.-L., Perera, U., and Krause, M. (2013). Endophilin, Lamellipodin, and Mena cooperate to regulate F-actin-dependent EGF-receptor endocytosis. The EMBO journal *32*, 2722-2734.
Vieira, A.V., Lamaze, C., and Schmid, S.L. (1996). Control of EGF Receptor Signaling by Clathrin-Mediated Endocytosis. Science *274*, 2086.
Vogel, G.F., Klee, K.M., Janecke, A.R., Muller, T., Hess, M.W., and Huber, L.A. (2015). Cargo-selective apical exocytosis in epithelial cells is conducted by Myo5B, Slp4a, Vamp7, and Syntaxin 3. J Cell Biol *211*, 587-604.
Vogel, J.D., West, G.A., Danese, S., De La Motte, C., Phillips, M.H., Strong, S.A., Willis, J., and Fiocchi, C. (2004). CD40-mediated immune-nonimmune cell interactions induce mucosal fibroblast chemokines leading to T-cell transmigration. Gastroenterology *126*, 63-80.
von Kleist, L., Stahlschmidt, W., Bulut, H., Gromova, K., Puchkov, D., Robertson, M.J., MacGregor, K.A., Tomilin, N., Pechstein, A., Chau, N.*, et al.* (2011). Role of the clathrin terminal domain in regulating coated pit dynamics revealed by small molecule inhibition. Cell *146*, 471-484.
Walton, K.L., Holt, L., and Sartor, R.B. (2009). Lipopolysaccharide activates innate immune responses in murine intestinal myofibroblasts through multiple signaling pathways. Am J Physiol Gastrointest Liver Physiol *296*, G601-611.
Wang, X., and Huycke, M.M. (2015). Colorectal cancer: role of commensal bacteria and bystander effects. Gut Microbes *6*, 370-376.
Wang, Y., Jiang, C.Q., and Fan, L.F. (2015a). Correlation of Musashi-1, Lgr5, and pEGFR expressions in human small intestinal adenocarcinomas. Tumour Biol *36*, 6075-6082.

Wang, Y., Shi, C., Lu, Y., Poulin, E.J., Franklin, J.L., and Coffey, R.J. (2015b). Loss of Lrig1 leads to expansion of Brunner glands followed by duodenal adenomas with gastric metaplasia. Am J Pathol *185*, 1123-1134.
Watanabe, T., Noritake, J., and Kaibuchi, K. (2005). Roles of IQGAP1 in cell polarization and migration. Novartis Found Symp *269*, 92-101; discussion 101-105, 223-130.
Watanabe, T., Wang, S., Noritake, J., Sato, K., Fukata, M., Takefuji, M., Nakagawa, M., Izumi, N., Akiyama, T., and Kaibuchi, K. (2004). Interaction with IQGAP1 links APC to Rac1, Cdc42, and actin filaments during cell polarization and migration. Dev Cell *7*, 871-883.
Weaver, L.T., Austin, S., and Cole, T.J. (1991). Small intestinal length: a factor essential for gut adaptation. Gut *32*, 1321-1323.
Weber, G.F., Schlautkotter, S., Kaiser-Moore, S., Altmayr, F., Holzmann, B., and Weighardt, H. (2007). Inhibition of interleukin-22 attenuates bacterial load and organ failure during acute polymicrobial sepsis. Infect Immun *75*, 1690-1697.
Weigel, P.H., and Oka, J.A. (1981). Temperature dependence of endocytosis mediated by the asialoglycoprotein receptor in isolated rat hepatocytes. Evidence for two potentially rate-limiting steps. Journal of Biological Chemistry *256*, 2615-2617.
Wells, J.A., and de Vos, A.M. (1996). Hematopoietic receptor complexes. Annu Rev Biochem *65*, 609-634.
Wentworth, C.C., Alam, A., Jones, R.M., Nusrat, A., and Neish, A.S. (2011). Enteric Commensal Bacteria Induce Extracellular Signal-regulated Kinase Pathway Signaling via Formyl Peptide Receptor-dependent Redox Modulation of Dual Specific Phosphatase 3. The Journal of Biological Chemistry *286*, 38448-38455.
Wentworth, C.C., Jones, R.M., Kwon, Y.M., Nusrat, A., and Neish, A.S. (2010). Commensal-epithelial signaling mediated via formyl peptide receptors. The American journal of pathology *177*, 2782-2790.
Westphalen, C.B., Asfaha, S., Hayakawa, Y., Takemoto, Y., Lukin, D.J., Nuber, A.H., Brandtner, A., Setlik, W., Remotti, H., Muley, A.*, et al.* (2014). Long-lived intestinal tuft cells serve as colon cancer–initiating cells. The Journal of Clinical Investigation *124*, 1283-1295.
White, C.D., Brown, M.D., and Sacks, D.B. (2009). IQGAPs in cancer: a family of scaffold proteins underlying tumorigenesis. FEBS Lett *583*, 1817-1824.
Wiegerinck, C.L., Janecke, A.R., Schneeberger, K., Vogel, G.F., van Haaften-Visser, D.Y., Escher, J.C., Adam, R., Thoni, C.E., Pfaller, K., Jordan, A.J.*, et al.* (2014a). Loss of syntaxin 3 causes variant microvillus inclusion disease. Gastroenterology *147*, 65-68 e10.
Wiegerinck, C.L., Janecke, A.R., Schneeberger, K., Vogel, G.F., van Haaften-Visser, D.Y., Escher, J.C., Adam, R., Thoni, C.E., Pfaller, K., Jordan, A.J.*, et al.* (2014b). Loss of syntaxin 3 causes variant microvillus inclusion disease. Gastroenterology *147*, 65-68.e10.
Wirth, A., Chen-Wacker, C., Wu, Y.-W., Gorinski, N., Filippov, Mikhail A., Pandey, G., and Ponimaskin, E. (2013a). Dual lipidation of the brain-specific Cdc42 isoform regulates its functional properties. Biochemical Journal *456*, 311-322.
Wirth, A., Chen-Wacker, C., Wu, Y.W., Gorinski, N., Filippov, M.A., Pandey, G., and Ponimaskin, E. (2013b). Dual lipidation of the brain-specific Cdc42 isoform regulates its functional properties. Biochem J *456*, 311-322.
Wolfe, B.L., and Trejo, J. (2007). Clathrin-dependent mechanisms of G protein-coupled receptor endocytosis. Traffic *8*, 462-470.

Wolk, K., Kunz, S., Asadullah, K., and Sabat, R. (2002). Cutting edge: immune cells as sources and targets of the IL-10 family members? J Immunol *168*, 5397-5402.
Wolk, K., Kunz, S., Witte, E., Friedrich, M., Asadullah, K., and Sabat, R. (2004). IL-22 increases the innate immunity of tissues. Immunity *21*, 241-254.
Worthington, J.J., Reimann, F., and Gribble, F.M. (2018). Enteroendocrine cells-sensory sentinels of the intestinal environment and orchestrators of mucosal immunity. Mucosal Immunol *11*, 3-20.
Wouters, M.M., Lambrechts, D., Knapp, M., Cleynen, I., Whorwell, P., Agreus, L., Dlugosz, A., Schmidt, P.T., Halfvarson, J., Simren, M.*, et al.* (2014). Genetic variants in CDC42 and NXPH1 as susceptibility factors for constipation and diarrhoea predominant irritable bowel syndrome. Gut *63*, 1103-1111.
Wu, X., Quondamatteo, F., Lefever, T., Czuchra, A., Meyer, H., Chrostek, A., Paus, R., Langbein, L., and Brakebusch, C. (2006). Cdc42 controls progenitor cell differentiation and β-catenin turnover in skin. Genes & Development *20*, 571-585.
Xu, N., Wang, S.Q., Tan, D., Gao, Y., Lin, G., and Xi, R. (2011). EGFR, Wingless and JAK/STAT signaling cooperatively maintain Drosophila intestinal stem cells. Dev Biol *354*, 31-43.
Yamamoto, H., Komekado, H., and Kikuchi, A. (2006). Caveolin is necessary for Wnt-3a-dependent internalization of LRP6 and accumulation of beta-catenin. Dev Cell *11*, 213-223.
Yamana, N., Arakawa, Y., Nishino, T., Kurokawa, K., Tanji, M., Itoh, R.E., Monypenny, J., Ishizaki, T., Bito, H., Nozaki, K.*, et al.* (2006). The Rho-mDia1 pathway regulates cell polarity and focal adhesion turnover in migrating cells through mobilizing Apc and c-Src. Mol Cell Biol *26*, 6844-6858.
Yan, K.S., Chia, L.A., Li, X., Ootani, A., Su, J., Lee, J.Y., Su, N., Luo, Y., Heilshorn, S.C., Amieva, M.R.*, et al.* (2012). The intestinal stem cell markers Bmi1 and Lgr5 identify two functionally distinct populations. Proc Natl Acad Sci U S A *109*, 466-471.
Yan, K.S., Gevaert, O., Zheng, G.X.Y., Anchang, B., Probert, C.S., Larkin, K.A., Davies, P.S., Cheng, Z.-f., Kaddis, J.S., Han, A.*, et al.* (2017). Intestinal Enteroendocrine Lineage Cells Possess Homeostatic and Injury-Inducible Stem Cell Activity. Cell Stem Cell *21*, 78-90.e76.
Yang, Y.P., Ma, H., Starchenko, A., Huh, W.J., Li, W., Hickman, F.E., Zhang, Q., Franklin, J.L., Mortlock, D.P., Fuhrmann, S.*, et al.* (2017). A Chimeric Egfr Protein Reporter Mouse Reveals Egfr Localization and Trafficking In Vivo. Cell Rep *19*, 1257-1267.
Yap, K., Xiao, Y., Friedman, Brad A., Je, H.S., and Makeyev, Eugene V. (2016). Polarizing the Neuron through Sustained Co-expression of Alternatively Spliced Isoforms. Cell Reports *15*, 1316-1328.
Yarden, Y., and Sliwkowski, M.X. (2001). Untangling the ErbB signalling network. Nat Rev Mol Cell Biol *2*, 127-137.
Yi, J., Bergstrom, K., Fu, J., Shan, X., McDaniel, J.M., McGee, S., Qu, D., Houchen, C.W., Liu, X., and Xia, L. (2018). Dclk1 in tuft cells promotes inflammation-driven epithelial restitution and mitigates chronic colitis. Cell Death Differ.
Yin, X., Farin, H.F., van Es, J.H., Clevers, H., Langer, R., and Karp, J.M. (2014). Niche-independent high-purity cultures of Lgr5+ intestinal stem cells and their progeny. Nature methods *11*, 106-112.
Yu, F., Liu, J., Yu, S., Yang, Z., Pan, Y., Gao, N., Zou, Q., and Jeon, J. (2015). Soft polymer-based cantilever probe for AFM nanoindentation of live mammalian cells in liquid. Paper

presented at: 2015 Transducers - 2015 18th International Conference on Solid-State Sensors, Actuators and Microsystems (TRANSDUCERS).
Yu, F., Liu, J., Zhang, X., Lin, A.-L., Khan, N., Pan, Y., Gao, N., Zou, Q., and Jeon, J. (2016). Design, fabrication, and characterization of polymer-based cantilever probes for atomic force microscopes. Journal of Vacuum Science & Technology B, Nanotechnology and Microelectronics: Materials, Processing, Measurement, and Phenomena *34*, 06KI01.
Yu, J. (2013). Intestinal stem cell injury and protection during cancer therapy. Translational cancer research *2*, 384-396.
Yu, S., Douard, V., Edelblum, K.L., Laubitz, D., Zhao, Y., Kiela, P.R., Yap, G.S., and Gao, N. (2017). Paneth Cell Specific Lysozyme Regulates Intestinal Mucosal Immune Response by Shaping Gut Microbiota Landscape. The Journal of Immunology *198*, 218.213-218.213.
Yu, S., Nie, Y., Knowles, B., Sakamori, R., Stypulkowski, E., Patel, C., Das, S., Douard, V., Ferraris, R.P., Bonder, E.M.*, et al.* (2014a). TLR sorting by Rab11 endosomes maintains intestinal epithelial-microbial homeostasis. EMBO J *33*, 1882-1895.
Yu, S., Tong, K., Zhao, Y., Balasubramanian, I., Yap, G.S., Ferraris, R.P., Bonder, E.M., Verzi, M.P., and Gao, N. (2018). Paneth Cell Multipotency Induced by Notch Activation following Injury. Cell Stem Cell *23*, 46-59.e45.
Yu, S., Yehia, G., Wang, J., Stypulkowski, E., Sakamori, R., Jiang, P., Hernandez-Enriquez, B., Tran, T.S., Bonder, E.M., Guo, W.*, et al.* (2014b). Global ablation of the mouse Rab11a gene impairs early embryogenesis and matrix metalloproteinase secretion. J Biol Chem *289*, 32030-32043.
Yun, M.-S., Kim, S.-E., Jeon, S.H., Lee, J.-S., and Choi, K.-Y. (2005). Both ERK and Wnt/β-catenin pathways are involved in Wnt3a-induced proliferation. Journal of Cell Science *118*, 313.
Zaske, A.-M., #xed, Danila, D., Queen, M.C., Golunski, E., and Conyers, J.L. (2013). Biological Atomic Force Microscopy for Imaging Gold-Labeled Liposomes on Human Coronary Artery Endothelial Cells. Journal of Pharmaceutics *2013*, 8.
Zhang, J., and Li, L. (2005). BMP signaling and stem cell regulation. Dev Biol *284*, 1-11.
Zhang, X., and Gao, N. (2016). RAB and RHO GTPases regulate intestinal crypt cell homeostasis and enterocyte function. Small GTPases *7*, 59-64.
Zhang, X., Ren, J., Wang, J., Li, S., Zou, Q., and Gao, N. (2018). Receptor-mediated endocytosis generates nanomechanical force reflective of ligand identity and cellular property. *233*, 5908-5919.
Zhang, Z., Chen, L., Gao, L., Lin, K., Zhu, L., Lu, Y., Shi, X., Gao, Y., Zhou, J., Xu, P.*, et al.* (2012). Structural basis for the recognition of Asef by adenomatous polyposis coli. Cell Res *22*, 372-386.
Zhong, Z., Wen, Z., and Darnell, J.E., Jr. (1994). Stat3: a STAT family member activated by tyrosine phosphorylation in response to epidermal growth factor and interleukin-6. Science *264*, 95-98.
Zhou, X., Geng, L., Wang, D., Yi, H., Talmon, G., and Wang, J. (2017). R-Spondin1/LGR5 Activates TGFbeta Signaling and Suppresses Colon Cancer Metastasis. Cancer Res *77*, 6589-6602.
Zindl, C.L., Lai, J.F., Lee, Y.K., Maynard, C.L., Harbour, S.N., Ouyang, W., Chaplin, D.D., and Weaver, C.T. (2013). IL-22-producing neutrophils contribute to antimicrobial defense and

restitution of colonic epithelial integrity during colitis. Proc Natl Acad Sci U S A *110*, 12768-12773.

Zwarycz, B., Gracz, A.D., Rivera, K.R., Williamson, I.A., Samsa, L.A., Starmer, J., Daniele, M.A., Salter-Cid, L., Zhao, Q., and Magness, S.T. (2019). IL22 Inhibits Epithelial Stem Cell Expansion in an Ileal Organoid Model. Cell Mol Gastroenterol Hepatol *7*, 1-17.

APPENDIX

List of proteins in Cdc42 proteomics that involve in clathrin-mediated trafficking.

Identified Proteins (38)	Spectra counts (Cdc42V1)	Spectra counts (Cdc42V2)	Unique Peptide (Cdc42V1)	Unique Peptide (Cdc42V2)
Actin, cytoplasmic 1	89	49	1	1
Actin, cytoplasmic 2	89	49	19	16
Actin, alpha skeletal muscle	41	0	1	0
Myosin-9	32	13	27	12
Mitogen-activated protein kinase kinase kinase 7	17	8	11	6
Clathrin heavy chain 1	14	7	12	7
Myosin light polypeptide 6	10	3	6	2
Myosin-10	8	2	6	2
Mitogen-activated protein kinase 1	7	3	5	3
Myosin-4	5	0	2	0
Myosin-6	5	0	1	0
Ras-related protein Rab-5C	5	1	3	1
Myosin regulatory light chain 12A	4	1	4	3
Dynactin subunit 2	4	3	2	1
Serine/threonine-protein kinase PAK 4	4	1	3	1
Growth factor receptor-bound protein 2	4	1	4	1
AP-2 complex subunit alpha-1	3	1	3	1
EH domain-containing protein 4	3	0	3	1
Actin-related protein 2/3 complex subunit 2	3	1	3	1
Actin-related protein 2/3 complex subunit 4	3	1	3	0
Mitogen-activated protein kinase 3	3	0	2	0
AP-2 complex subunit beta	2	1	2	1
Phosphatidylinositol 5-phosphate 4-kinase type-2 alpha	2	0	2	2
Endophilin-B1	2	0	2	0
Myosin light chain 1/3, skeletal muscle isoform	2	0	1	0
Dynactin subunit 1	2	2	1	0
Mitogen-activated protein kinase 9	2	0	2	0
Dynamin-1-like protein	1	0	1	1
Dynamin-3	1	0	1	1
AP-2 complex subunit sigma	1	0	1	0
Clathrin interactor 1	1	0	1	1
ADP-ribosylation factor 6	1	1	1	0
Endophilin-A2	1	0	1	0
Myosin regulatory light chain 2, skeletal muscle isoform	1	0	1	0
Actin-related protein 2/3 complex subunit 3	1	1	1	0
Actin-related protein 3	1	1	1	0
Actin-related protein 6	1	0	1	0
Dynein light chain 1, cytoplasmic	1	0	1	0

ShinyGo analysis of upregulated genes in Cdc42-iKO mucosa.

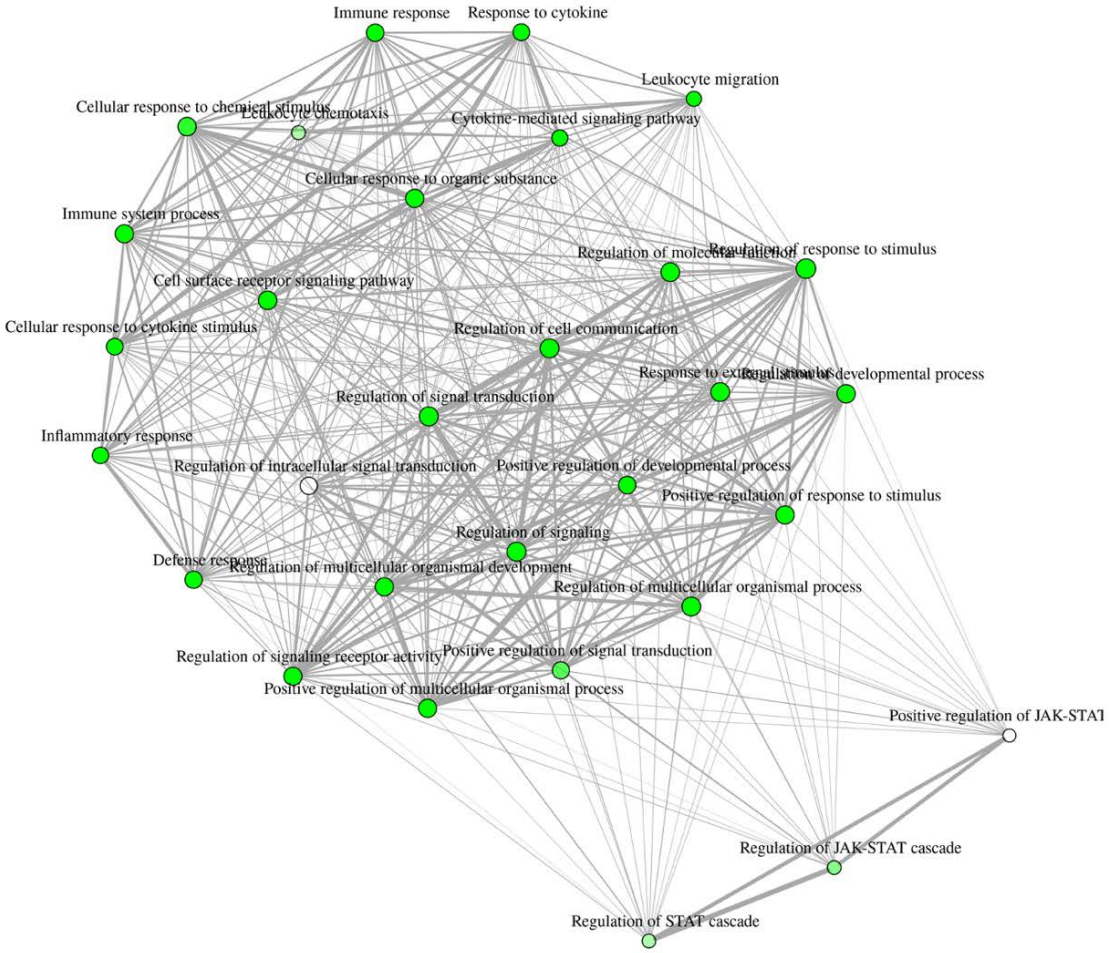

Reagents and resources

REAGENT or RESOURCE	SOURCE	IDENTIFIER
Antibodies		
Rabbit anti-p-ERK	Cell Signaling	9101s
Rabbit anti-ERK	Cell Signaling	4695s
Mouse anti-β-Catenin	BD Biosciences	610153
Rabbit anti-p-Lrp6	Cell Signaling	2568s
Rabbit anti-Lrp6	Cell Signaling	3395S
Mouse anti-β-actin	Santa Cruz	sc-4778
Rabbit anti-Clathrin	Cell Signaling	4796p
Mouse anti-α-Tubulin	Sigma-Aldrich	T6199
Rabbit anti-EGFR	Santa Cruz	sc-03
Rabbit anti-Cdc42	abcam	ab64533
Rabbit anti-p-EGFR^{Y1068}	Cell Signaling	2234s
Rabbit anti-PAK1	Cell Signaling	2602s
Rabbit anti-Fyn	Cell Signaling	4023
Mouse anti-Flotillin1	BD Biosciences	610820
Rabbit anti-Caveolin1	Cell Signaling	3267s
Rabbit anti-Calnexin	cell signaling	2433
Rabbit anti-PI3K-P110	Cell Signaling	4255
Rabbit anti-p-ERBB2$^{Y1221/1222}$	Cell Signaling	2243T
Rabbit anti-ERBB2	Cell Signaling	4290T
Goat Anti-DDDDK tag	abcam	ab95045
Mouse anti-pHH3	Cell Signaling	9706s
Rabbit anti-Cdc42V2	El-Husseini, A.	(Kang et al., 2008)
Rabbit anti-Cdc42V2	LifeSpan BioSciences	LS-C153281
Rabbit anti-EEA1	Cell Signaling	3288s
Rabbit anti-EGFR	Cell Signaling	4267p
Mouse anti-Flag	Sigma-Aldrich	f1804
Rabbit anti-Ki67	abcam	ab16637
Goat anti-Lysozyme C	Santa Cruz	sc-27958
Goat anti-GFP	abcam	ab6673
Rabbit anti-Cleaved Caspase3	Cell Signaling	9664s
Mouse anti-E-Cadherin (clone 36)	BD Biosciences	610182
Rabbit anti-Olfm4 (clone D6Y5A)	Cell Signaling	39141
Rabbit anti-lysozyme	Biogenex	AR024-10R

Rat anti-BrdU	Accurate Chemical	OBT0030G
Rabbit anti-pStat3^{Y705}	Cell Signaling	9145
Donkey anti-Rabbit, Alexa Fluor 488	Thermo Fisher Scientific	A-21206
Donkey anti-Rabbit, Alexa Fluor 546	Thermo Fisher Scientific	A10040
Donkey anti-Goat, Alexa Fluor 488	Thermo Fisher Scientific	A-11055
Donkey anti-Goat, Alexa Fluor 555	Thermo Fisher Scientific	A-21432
Donkey anti-Rat, Alexa Fluor 488	Thermo Fisher Scientific	A-21208
Donkey anti-Mouse, Alexa Fluor 555	Thermo Fisher Scientific	A-31570
Donkey anti-Mouse, Alexa Fluor 647	Thermo Fisher Scientific	A-31571
Biotinylated Horse Anti-Rabbit IgG	Vector Laboratories	BA-1100
Chemicals and Recombinant Proteins		
propidium iodide	Sigma-Aldrich	P4170
Corn oil	Sigma-Aldrich	C8267
Tamoxifen	Sigma-Aldrich	T5648
Citric acid	Sigma-Aldrich	251275
Ampicillin sodium salt	Sigma-Aldrich	A9518
Alfa Aesar™ Vancomycin hydrochloride, Molecular Biology Grade	Thermo Fisher Scientific	AAJ6279006SDS
Neomycin Sulfate	Life Technologies	21810-031
Cefoperazone sodium salt	Sigma-Aldrich	C4292-5G
Metronidazole	Sigma-Aldrich	M3761-25G
STAT3 inhibitor V, stattic	Santa Cruz	sc-202818
WP-1066	Santa Cruz	sc-203282
Donkey serum	Sigma-Aldrich	D9663
Bovine Serum	Sigma-Aldrich	A3294
EdU (5-ethynyl-20-deoxyuridine)	Thermo Fisher Scientific	A10044
CHIR99021	Sigma-Aldrich	SML1046-5MG
BrdU	Invitrogen	00-0103
Recombinant Murine Wnt-3a	Peprotech	315-20
Recombinant Murine EGF	Peprotech	315-09 B
Recombinant Murine Noggin	Peprotech	250-38
Recombinant Murine R-spondin	R&D	3474-RS-050
Recombinant Murine HGF	Sigma-Aldrich	H5791-10UG
Recombinant Murine TGFα	Sigma-Aldrich	T7924-.1MG

Recombinant Murine IL22	Peprotech	212-12
Recombinant Murine IL-12 p70	Peprotech	210-12
Recombinant Murine MIP-2 (CXCL2)	Peprotech	250-15
Recombinant Murine KC (CXCL1)	Peprotech	250-11
Recombinant Murine LIX (CXCL6)	Peprotech	250-17
Recombinant Murine IL-33	Peprotech	210-33
Recombinant Mouse Prolactin Protein	Novus Biologicals	NBP2-35120-10ug
Recombinant Mouse IL-1ra/IL-1F3/ IL1RN Protein	Novus Biologicals	NBP2-35105-20ug
Critical Commercial Assays		
CDC42-specific GLISA assay	Cytoskeleton	BK127
Maxima Universal First Strand cDNA Synthesis Kit	Thermo Fisher Scientific	K1671
Cell Titer-Glo 3D Cell Viability Assay	Promega	G9681
Flag Immunoprecipitation Kit	Sigma-Aldrich	FLAGIPT1
GoTaq Probe qPCR Master Mix	Promega	A6101/2
Advanced DMEM/F12 medium	Thermo Fisher Scientific	12634028
Corning Recovery Solution	Corning	354253
4',6-Diamidino-2-Phenylindole (DAPI)	Thermo Fisher Scientific	D1306
SignalStain EDTA Unmasking Solution	Cell Signaling	14747
DAKO Target Retrieval Solution	Agilent	S1699
Prolong Gold antifade medium	Thermo Fisher Scientific	P36930
VECTASTAIN Elite ABC HRP Kit (Peroxidase, Standard)	Vector Laboratories	PK-6100
RNeasy Plus Micro kit	QIAGEN	74034
DAB Peroxidase (HRP) Substrate Kit (with Nickel), 3,30 -diaminobenzidine	Vector Laboratories	SK-4100
Click-iT EdU Alexa Fluor 555 Imaging Kit	Thermo Fisher Scientific	C10338
Experimental Models, Cell lines		
Cdc42 flox	Brakebusch, C.	(Wu et al., 2006)
Cdc42 $V2^{Tg}$	This study	
Villin-CreER	Robine, S.	(El Marjou et al., 2004)
Rosa-ZsGreen	Jackson Lab	007906
C57BL/6-$^{IL22tm1.1(icre)Stck}$/J	Jackson Lab	027524
emEGFR	Coffey, R.	(Yang et al., 2017)
Myd88 flox	Jackson Lab	008888
B6.129P2-$Lgr5^{tm1(cre/ERT2)Cle}$/J	Jackson Lab	008875
Human HEK293	ATCC	CRL-1573

Human Caco2	ATCC	HTB-37
Software and Algorithms		
Prism	GraphPad	https://www.graphpad.com/scientific-software/prism/
Fiji software	(Schindelin et al., 2012)	https://fiji.sc
Recombinant DNAs		
pcDNA6A-EGFR WT	Addgene	#42665
pcDNA6A-EGFR ICD (645-1186)	Addgene	#42667
pcDNA6A-EGFR ECD (1-644)	Addgene	#42666
CAG-3×Flag-Cdc42 V2	This study	
PQCXIP-3×Flag-Cdc42V2-K185R	This study	
PQCXIP-3×Flag-Cdc42V1	This study	
PQCXIP-3×Flag-Cdc42V2	This study	
CAG-lox-CAT-lox-unique Bam cloning site-hGH polyA (Clone 17)	Addgene	#53959
PQCXIP-3×Flag	This study	

PCR and RT-PCR primers used in this study.

Primer	Sequence
PCR--mouse cdc42 V1-F	TATGTATAGTCAGCGCGTGCCCCTGT
PCR--mouse cdc42 V1-R	CCACAGGCTGTCCTATGGTT
PCR--mouse cdc42 V2-F	GCGGAGAAGCTGAGGACAAGAT
PCR--mouse cdc42 V2-R	AAGAAGACGCAGAGGCTTTCA
Realtime PCR--mouse cdc42 V1/2-F	CACTCCAGAGACTGCTGAAAAGC
Realtime PCR--mouse cdc42 V1-R	TCATAGCAGCACACACCTGCG
Realtime PCR--mouse cdc42 V2-R	TGGGTTGAGTTTCCGGAGGC
Realtime PCR--mouse ZDHHC8-F	GTGCCCTATCAGTACAGAGGAC
Realtime PCR--mouse ZDHHC8-R	GGTGCTGTCATCTGCCAGAGTA
Realtime PCR--mouse LRIG1-F	AAGGGAACTCAACTTGGCGAG
Realtime PCR--mouse LRIG1-R	ACGTGAGGCCTTCAATCAGC
Realtime PCR--mouse LGR5-F	ACCCGCCAGTCTCCTACATC
Realtime PCR--mouse LGR5-R	GCATCTAGGCGCAGGGATTG
Realtime PCR--mouse Bmi1-F	GGAGAAGAAATGGCCCACTACC
Realtime PCR--mouse Bmi1-R	TTGGCCTTGTCACTCCCAGA
Realtime PCR--mouse HopX-F	CATCCTTAGTCAGACGCGCA
Realtime PCR--mouse HopX-R	AGGCAAGCCTTCTGACCGC
Realtime PCR--mouse Olfm4-F	TGGCCCTTGGAAGCTGTAGT
Realtime PCR--mouse Olfm4-R	ACCTCCTTGGCCATAGCGAA
Realtime PCR--mouse IL22-F	GTGACGACCAGAACATCCAGA
Realtime PCR--mouse IL22-R	AAACAGCAGGTCCAGTTCCC
Realtime PCR--mouse BCL2-F	GTCCCGCCTCTTCACCTTTCAG
Realtime PCR--mouse BCL2-R	GATTCTGGTGTTTCCCCGTTGG
Realtime PCR--mouse Survivin-F	TCATCCACTGCCCTACCGAGAAC
Realtime PCR--mouse Survivin-R	TCTATCGGGTTGTCATCGGGTTC
Realtime PCR--mouse cMyc-F	GTGCTGCATGAGGAGACACC
Realtime PCR--mouse cMyc-R	CAGGGGTTTGCCTCTTCTCC
Realtime PCR--mouse Hprt-F	TCCCTGGTTAAGCAGTACAGC
Realtime PCR—mouse Hprt-R	TCCAACAAAGTCTGGCCTGT
Realtime PCR—mouse PRL2C2 F	CAGGCTCACACACTATTCAG
Realtime PCR—mouse PRL2C2 R	CTGTGGCTTTGGAGATGATTA
Realtime PCR—mouse CXCL3 F	TGAGACCATCCAGAGCTTGAGG
Realtime PCR—mouse CXCL3 R	CCTTGGGGGTTGAGGCAAACTT
Realtime PCR—mouse TNFrsf11b F	CGGAAACAGAGAAGCCACGCAA

Realtime PCR—mouse NFrsf11b R	CTGTCCACCAAAACACTCAGCC
Realtime PCR—mouse IL1rn F	GCTCATTGCTGGGTACTTACAA
Realtime PCR—mouse IL1rn R	CCAGACTTGGCACAAGACAGG
Realtime PCR—mouse CXCL5 F	GCATTTCTGTTGCTGTTCACGCTG
Realtime PCR—mouse CXCL5 R	CCTCCTTCTGGTTTTTCAGTTTAGC
Realtime PCR—mouse CXCL1 F	TGAGCTGCGCTGTCAGTGCCT
Realtime PCR—mouse CXCL1 R	AGAAGCCAGCGTTCACCAGA
Realtime PCR—mouse CXCL2 F	GAGCTTGAGTGTGACGCCCCCAGG
Realtime PCR—mouse CXCL2 R	GTTAGCCTTGCCTTTGTTCAGTATC